

Electronic Thesis and Dissertation Repository

11-9-2017 11:00 AM

Coordination and Organometallic Chemistry of Novel Gallium Complexes: Synthesis, Reactivity and Spectroscopy

Jeremy L. Bourque
The University of Western Ontario

Supervisor
Kim M. Baines
The University of Western Ontario

Graduate Program in Chemistry
A thesis submitted in partial fulfillment of the requirements for the degree in Doctor of Philosophy
© Jeremy L. Bourque 2017

Follow this and additional works at: <https://ir.lib.uwo.ca/etd>

 Part of the [Inorganic Chemistry Commons](#)

Recommended Citation

Bourque, Jeremy L., "Coordination and Organometallic Chemistry of Novel Gallium Complexes: Synthesis, Reactivity and Spectroscopy" (2017). *Electronic Thesis and Dissertation Repository*. 5026.
<https://ir.lib.uwo.ca/etd/5026>

This Dissertation/Thesis is brought to you for free and open access by Scholarship@Western. It has been accepted for inclusion in Electronic Thesis and Dissertation Repository by an authorized administrator of Scholarship@Western. For more information, please contact wlsadmin@uwo.ca.

Abstract

The work described in this thesis incorporates three main themes: the synthesis and reactivity of new coordination and organometallic gallium compounds, and the chemical state determination of molecular gallium complexes using XPS and XAS. The coordination chemistry of low valent gallium cations was explored using macrocyclic ethers as ligands. The experimental oxidation number, or chemical state, of newly synthesized low valent gallium cationic complexes was compared to known compounds to allow for the assessment of the electronic environment at gallium. The organometallic chemistry of gallium was examined using donor ligands to stabilize monomeric organogallium(III) compounds, demonstrating the ability to substitute the ligands on gallium and to generate a compound containing a gallium-carbon double bond.

Two multinuclear low valent gallium cations were synthesized using cryptand[2.2.2] as a stabilizing ligand and $\text{Ga}_2\text{Cl}_4(\text{THF})_2$ as a starting material. Conventional characterization techniques and computational methods were used to examine the structure and bonding of the cationic gallium cores contained within the cryptand ligand. These compounds are the first examples of binuclear cryptand[2.2.2] complexes, where two metal centres are located within the cryptand cavity.

The experimental chemical states, namely the experimentally determined electronic environments or partial charges, of the gallium centres in two gallium-cryptand[2.2.2] complexes were evaluated using X-ray photoelectron spectroscopy (XPS) and X-ray absorption spectroscopy (XAS) as a means of probing the electronic environment of the gallium centres. The experimental XPS data of the gallium-cryptand complexes were compared to known gallium compounds with unambiguously assigned oxidation numbers to determine the electron density at the gallium centres and to allow for an assessment of their potential reactivity. To overcome the instrumental limitations of the XPS experiments, XAS studies of the synthesized gallium-cryptand[2.2.2] complexes and other low valent gallium compounds with multiple gallium atoms were performed to separate the signals originating from the individual gallium centres. The higher resolution of the XAS data allowed for the observation of multiple signals from gallium centres with different assigned oxidation

numbers within a single complex and gave additional information on the electronic structure and bonding of the cryptand complexes in conjunction with computational studies.

The synthesis and reactivity of a gallium(I) cationic complex using 12-crown-4 as a stabilizing ligand was explored. The synthesis of $[\text{Ga}(12\text{-crown-4})][\text{GaCl}_4]$ was achieved in one step from commercially available starting materials. Anion exchange reactions to replace the reactive tetrachlorogallate anion for the perfluorophenylborate were performed. $[\text{Ga}(12\text{-crown-4})][\text{B}(\text{C}_6\text{F}_5)_4]$ was analyzed using XPS, which allowed for the classification of the gallium(I)-crown ether complex as electron deficient. Reactions of the gallium(I)-crown ether complex with Cp^*K , cryptand[2.2.2], and DMAP demonstrated the facile synthesis of known gallium(I) compounds as well as the generation of novel gallium(I) cations, highlighting the use of the gallium(I)-crown ether complex as an effective starting material for new gallium(I) compounds.

The synthesis of a compound with a gallium-carbon double bond, a gallene, was explored. The synthetic route utilized was inspired by strategies reported for the synthesis of compounds containing main group element-carbon double bonds with the key step being a dehydrohalogenation of a gallium(III) fluoride. The precursor organogallium(III) fluorides were synthesized using an NHC and DMAP as donor ligands to stabilize neutral species. Dehydrohalogenation of the gallium(III) fluoride was examined in an attempt to generate a gallene. Toluinaldehyde was used as a trapping agent *in situ*, resulting in the formation of a 2:1 cycloadduct, giving evidence for the generation of an intermediate gallene. The synthetic route presented highlights the use of donor stabilization to facilitate ligand substitution and exchange reactions for neutral organogallium compounds.

Keywords

Gallium • Coordination Chemistry • Macrocyclic Ligands • X-ray Spectroscopy • Chemical State • Organometallic Chemistry • Donor Stabilization • Structure and Bonding • Group 13 Chemistry • Multiple Bonds

Co-Authorship Statement

This thesis includes work from 3 previously published manuscripts in Chapters 2 and 3.

The article presented in Chapter 2 was coauthored by: J.L. Bourque, P.D. Boyle, and K.M. Baines, *Chem. Eur. J.*, **2015**, *21*, 9790-9796. JLB performed all of the synthetic and characterization work as well as the theoretical calculations. JLB also collected and solved the X-ray crystallographic data, with significant input and assistance from PDB. The manuscript was prepared by JLB and edited by KMB.

The articles presented in Chapter 3 were coauthored by: J.L. Bourque, M.C. Biesinger, and K.M. Baines, *Dalton Trans.*, **2016**, *45*, 7678-7696; L. Yang, J.L. Bourque, J.A. McLeod, P. Shen, K.M. Baines, and L. Liu, *Inorg. Chem.*, **2017**, *56*, 2985-2991. JLB was responsible for all of the synthetic work for the first article. X-ray photoelectron spectroscopic data were collected and processed by MCB. JLB prepared the manuscript, including all data interpretation and analysis. For the latter article, JLB was responsible for the majority of synthetic work and the X-ray crystallographic data, with assistance from LY. XAS data were collected, processed and analyzed by LY, JAM, PS and LL, and computational work was performed by JAM. JLB contributed significantly to the interpretation and analysis of the processed XAS data.

J.L. Bourque, R.A. Nanni, M.C. Biesinger, and K.M. Baines contributed to the research presented in Chapter 4. RAN was an undergraduate honours specialization student who was supervised by JLB. He synthesized complexes **4.1**, **4.2**, and **4.3** and performed preliminary reactivity studies; the remaining synthetic and characterization work was carried out by JLB. JLB was responsible for the X-ray crystallographic data collection and analysis. MCB collected and processed the X-ray photoelectron spectroscopic data. JLB was responsible for the interpretation and analysis of the XPS data. The chapter was prepared by JLB with input from RAN and edited by KMB.

Acknowledgments

First and foremost, I thank my supervisor, Kim Baines, for her continual guidance throughout my PhD and for allowing me the freedom to work on projects independently that were not always directly related to other research in the group. She has undoubtedly helped me become a well-rounded scientist, improved my ability to critically think, communicate scientific ideas, and to look above and beyond the narrow goals of a project. Her editing and commitment to publishing throughout my years in her group have been extremely valuable. We have enjoyed in depth discussions about chemistry and, of course, a few beers, talking about what makes the Maritimes great.

Second, the Baines' group members over the years have helped make every day in lab enjoyable. Thank you to Nada Tashkandi, for giving me tons of great and sometimes not so great crystals, it was always fun to see what solution we would get. Also thanks for inspiring me to try and make a gallene; it was a difficult but great project that stands out in my thesis. Thanks to Bahar Farhadpour for always bringing the best treats to the office, some crystals and for Persian music days. Thanks to Mike Krause for being a great fume hood neighbour and glass blower. Thank you to the current members, Andrew Henry, Sarah McOnie and Maissa Belcina for listening to me rant and rave in the last few months of this thesis and good luck to you all in the future. I am also very grateful to Robert Nanni, who did as much as could be asked from a 4th year student. Thanks for working so hard and being so interested in learning about this crazy chemistry. I am grateful to had have the opportunity to work with you. I know you will make a stand out lawyer and will have a lot of success in the future.

Third, I have to thank all of the other graduate students who have been great friends over the years. Thanks to all who played softball as those nights were great to look forward to and always a lot of fun. Thanks to the Blacquiere and Ragogna groups for being good friends and, to the latter, tolerating me knocking on the office door to get coffee. Special thanks to Matt McCready, JP Bow, Richard Hazelhurst, James Stubbs, Ryan Maar, Jeff Binns, and especially to Barista Cam Graham, for always hearing me out when it came to chemistry ideas, sports or anything else. I have lost count of the number of conversations we

have had throwing hair-brained ideas around or trying to solve each other's problems. It is something I will definitely miss.

Thanks to many of the staff for always being helpful when it came to equipment, chemicals or gas cylinders and dewars. A thank you goes to Mat Willans for all of his NMR expertise, some football knowledge, and for fruitful conversations about life. Thanks to Doug Hairsine for getting mass spectral data, even out of samples that completely contaminated the ESI instrument for months. Thank you to Paul Boyle for training me to run my own X-ray diffraction samples for which I am indebted for. Thank you also for dealing with my early morning/late evening messages asking whether I could use a diffractometer.

A great deal of gratitude goes to my parents, as they have been supported throughout all of my education. Thanks for listening to me when I needed to talk about things that you didn't really know much about, but it definitely helped me a lot. Thank you also for encouraging me from an early age to have an interest in learning new things, as the curiosity that you instilled in me has allowed me to complete this thesis. I also want to thank my friends far and wide. Thank you for your continued friendship and support.

Lastly, and most importantly, I have to thank my wife, Vanessa, for everything that she has tolerated while I finished my PhD. I know getting married to a graduate student means putting off the real world for an extra few years and I am glad that you accepted that without hesitation. I am so grateful that we met and stayed together throughout the many trials, tribulations and long distance periods of our relationship. The support that we have shown each other through this journey called life is invaluable and means so much to me. I am excited to see what the future holds for us.

Table of Contents

Abstract.....	i
Acknowledgments.....	iv
Table of Contents.....	vi
List of Tables.....	xi
List of Figures.....	xiii
List of Schemes.....	xxiii
List of Charts.....	xxv
List of Abbreviations.....	xxvi
The 25 Man Roster: List of Compounds Reported.....	xxxii
Chapter 1.....	1
1 Introduction.....	1
1.1 Classification and Analysis of Novel Complexes.....	4
1.1.1 Conventional Characterization Techniques.....	4
1.1.2 Oxidation Numbers as a Tool.....	5
1.2 Ligand Types for the Stabilization of Low Valent Group 13 Complexes.....	7
1.2.1 Sterically Demanding (Bulky) Ligands.....	8
1.2.2 Strong Electron Donating Ligands.....	9
1.2.3 Macrocyclic Ethers as Ligands.....	11
1.3 Low Valent Gallium Chemistry.....	12
1.4 Reactivity of Low Valent Gallium Complexes.....	16
1.5 Scope of Thesis.....	18
1.6 References.....	19
Chapter 2.....	28
2 Synthesis and Characterization of Cationic Gallium Complexes of Cryptand[2.2.2].....	28

2.1	Introduction.....	28
2.2	Results and Discussion	29
2.3	Conclusions.....	40
2.4	Experimental.....	40
2.4.1	General Considerations.....	40
2.4.2	Synthesis of 2.1	41
2.4.3	Synthesis of 2.2	42
2.4.4	Synthesis of 2.2a	43
2.4.5	X-ray Crystallography – General Procedures	43
2.4.6	Computational Details	46
2.5	References.....	46
Chapter 3.....		51
3	Resolution of the Chemical State of Molecular Gallium Compounds Using XPS and XAS.....	51
3.1	Introduction.....	51
3.1.1	Oxidation Number, Valence Number and Main Group Compounds	51
3.1.2	Experimental Techniques for Chemical State Elucidation	56
3.2	Results and Discussion	62
3.2.1	X-ray Photoelectron Spectroscopy	62
3.2.2	X-ray Absorption Spectroscopy.....	86
3.3	Conclusions.....	96
3.4	Experimental.....	98
3.4.1	General Considerations.....	98
3.4.2	Syntheses.....	99
3.4.3	XPS Analysis	100
3.4.4	XAS Analysis	101

3.5	References.....	102
Chapter 4.....		109
4	Synthesis and Reactivity of Cationic Gallium(I) Crown Ether Complexes.....	109
4.1	Introduction.....	109
4.2	Results and Discussion	114
4.2.1	Synthesis and Characterization.....	114
4.2.2	XPS Analysis of [Ga(12-crown-4)][B(C ₆ F ₅) ₄], 4.3	118
4.2.3	Computational Analysis of [Ga(12-crown-4)] ⁺	120
4.2.4	Reactivity of [Ga(12-crown-4)][B(C ₆ F ₅) ₄], 4.3	122
4.3	Conclusions.....	130
4.4	Experimental.....	130
4.4.1	General Considerations.....	130
4.4.2	Synthesis of [Ga(12-crown-4)][GaCl ₄], 4.1	131
4.4.3	Synthesis of [Ga(12-crown-4)][B(C ₆ F ₅) ₄], 4.3	132
4.4.4	[Ga(crypt-222)][B(C ₆ F ₅) ₄], 4.4	133
4.4.5	Synthesis of [Ga(DMAP) ₃][B(C ₆ F ₅) ₄], 4.5	134
4.4.6	Synthesis of Cp [*] Ga	134
4.4.7	X-ray Crystallographic Details	135
4.4.8	Computational Details	135
4.5	References.....	136
Chapter 5.....		141
5	Synthesis of Donor-Stabilized Organogallium Complexes and a Compound with a Gallium-Carbon Double Bond.....	141
5.1	Introduction.....	141
5.2	Results and Discussion	146
5.2.1	Synthesis of Gallene Precursors.....	146

5.2.2	Generation and Trapping of a Gallene.....	158
5.3	Conclusions.....	162
5.4	Experimental.....	162
5.4.1	General Considerations.....	162
5.4.2	Synthesis of Lithium Dichlorofluorenylmesitylgallate, [Li(Et ₂ O)][GaCl ₂ FIMes], 5.1	163
5.4.3	Synthesis of Chloro(1,3-diisopropyl-4,5-dimethylimidazol-2- ylidene)fluorenylmesitylgallane, ^{Me} IiPr→GaClFIMes, 5.3	164
5.4.4	Synthesis of Chloro(4-dimethylaminopyridine)fluorenylmesitylgallane, DMAP→GaClFIMes, 5.4	165
5.4.5	Synthesis of Butyl(1,3-diisopropyl-4,5-dimethylimidazol-2- ylidene)fluorenylmesitylgallane, ^{Me} IiPr→GaBuFIMes, 5.5	166
5.4.6	Synthesis of (1,3-diisopropyl-4,5-dimethylimidazol-2- ylidene)fluorenylmesityltrifluoromethanesulfonatogallane, ^{Me} IiPr→GaOTfFIMes, 5.7	168
5.4.7	Synthesis of (1,3-diisopropyl-4,5-dimethylimidazol-2- ylidene)fluorenylfluoromesitylgallane, ^{Me} IiPr→GaFFIMes, 5.8	169
5.4.8	Synthesis of (4- dimethylaminopyridine)fluorenylmesityltrifluoromethanesulfonatogallane, DMAP→GaOTfFIMes, 5.9	170
5.4.9	Synthesis of (4-dimethylaminopyridine)fluorenylfluoromesitylgallane, DMAP→GaFFIMes, 5.10	172
5.4.10	Synthesis of 5.11	173
5.4.11	X-ray Crystallography.....	175
5.4.12	Additional Details.....	179
5.5	References.....	179
Chapter 6	185
6	Summary, Conclusions and Future Work.....	185
6.1	Summary and Conclusions.....	185
6.2	Future Work.....	188

6.2.1 Utilizing XPS for Other Main Group Elements.....	188
6.2.2 The Use of [Ga(12-crown-4)] ⁺ as a Widely Applicable Source of Gallium(I)	189
6.2.3 The Use of Bulkier Ligands for the Synthesis of Gallenes.....	191
6.3 References.....	193
Appendices.....	195
Appendix A: Supplementary Information for Chapter 2	195
Appendix B: Supplementary Information for Chapter 3	200
Appendix C: Supplementary Information for Chapter 4	212
Appendix D: Supplementary Information for Chapter 5	226
Appendix E: Copyrighted Material and Permissions.....	245
Appendix F: Curriculum Vitae	253

List of Tables

Table 2.1: Bond lengths and angles around the gallium centres of 2.1.	32
Table 2.2: Bond lengths and angles around the gallium centres of 2.2.	34
Table 2.3: Crystallographic details for 2.1 and 2.2.....	36
Table 2.4: Wiberg bond indices and atom-atom overlap-weighted NAO bond orders for 2.1.	38
Table 2.5: Wiberg bond indices and overlap-weighted NAO bond orders for 2.2.....	39
Table 3.1: Gallium compounds studied by XPS. Valence numbers are given in parentheses following the compound names.....	63
Table 3.2: Photoelectron binding and Auger electron kinetic energies and full-width at half- maxima for high-resolution XPS spectra. Note: Ga L ₃ M ₄₅ M ₄₅ signals are kinetic energy values, which have opposite trends to binding energies (Equation 3.1).....	68
Table 3.3: Auger parameters and relevant shifts for compounds analyzed using Ga 3d _{5/2} binding energy.	74
Table 4.1: Crystallographic data for 4.1, 4.3, and 4.4.....	125
Table 4.2: Summary of XPS data for standard compounds and 4.3, 4.4, and 4.5.	129
Table 5.1: Selected crystallographic details for compounds 5.1, 5.3, 5.5 and 5.7.....	175
Table 5.2: Selected crystallographic details for compounds 5.2, 5.4, 5.6 and 5.9.....	176
Table 5.3: Selected crystallographic details for compounds 5.8, 5.10 and 5.11.....	178
Table A.1: Bond lengths, angles and torsions around the gallium centres in 2.2a.	195
Table A.2: Crystallographic details for 2.2a.	196
Table A.3: Tabulated survey scans for all compounds studied by XPS.	200

Table A.4: Auger parameters and relevant shifts for compounds analyzed using Ga 2p _{3/2} binding energy.	201
Table A.5: Crystallographic details for Ga ₂ Cl ₄ (1,4-dioxane) ₂	209
Table A.6: Selected crystallographic data for 4.2, [GaCl ₂ (15-crown-5)][GaCl ₄], [Ga ₂ Cl ₃ (15-crown-5)(CH ₃ CN)][Ga ₂ Cl ₆].....	215
Table A.7: Selected crystallographic data for [NMe ₄][GaClMes ₃].....	230

List of Figures

Figure 1.1: Ambiphilic nature of coordinatively unsaturated gallium(I) compounds.	3
Figure 1.2: Illustration of how oxidation and valence numbers may differ.....	6
Figure 1.3: Demonstration of the prediction of reactivity for PX_5 and PR_3 compounds based on their oxidation numbers.	7
Figure 1.4: A tetrameric aluminum(I) compound (IV) with a bulky silicon ligand.	9
Figure 1.5: The reaction of $[GaDAB^{Dipp}]^-$ with ditetrelenes (A); and the reaction of $GaNacNac^{Dipp}$ with $B(C_6F_5)_3$, followed by the addition of benzaldehyde (B) (TMEDA = tetramethylethylenediamine).....	15
Figure 1.6: Reaction with H_2 and fixation of CO_2 by Ga(III)-NacNac' complex (A), and catalytic carbon-carbon bond formation using Ga(0) activated by Ag(I) (B) (pin = pinacolato).....	17
Figure 2.1: Displacement ellipsoid plot of the cation of 2.1. Ellipsoids are at the 50% probability level and hydrogen atoms were omitted for clarity.....	31
Figure 2.2: $Ga_3I_5(PEt_3)_3$	32
Figure 2.3: Displacement ellipsoid plot of the cation of 2.2. Ellipsoids are at the 50% probability level and the disordered backbone and hydrogen atoms were omitted for clarity.	33
Figure 2.4: HOMO and HOMO-7 of the cation of 2.1.	38
Figure 2.5: Proposed bonding models for the $[Ga_3Cl_4]^+$ core of 2.1.	38
Figure 2.6: HOMO and LUMO of the cation of 2.2.	40
Figure 3.1: Differences in oxidation and valence numbers for BF_3 and B_2F_4	52
Figure 3.2: Oxidation and valence numbers of a digallene and a disilene.	53

Figure 3.3: Two possible structures of Ga ₂ Cl ₄	55
Figure 3.4: Two bonding models for the [Ga ₅ I ₄] ³⁺ core of [Ga ₅ I ₄ (^t BuNacNac ^{Mes}) ₃], with the NacNac ligands removed for clarity.	55
Figure 3.5: A generic Wagner plot.	59
Figure 3.6: Ga 3d signal for GaNacNac ^{Dipp} . The experimental (black), simulated (red), component Ga 3d _{3/2} (blue) and Ga 3d _{5/2} (green) and background spectra (dashes) are shown.	66
Figure 3.7: Ga 2p _{3/2} signal for GaNacNac ^{Dipp} . The experimental (black), simulated Ga 2p _{3/2} (red) and background spectra (dashes) are shown.	66
Figure 3.8: Ga L ₃ M ₄₅ M ₄₅ signal for GaNacNac ^{Dipp} . The experimental (black) and simulated Ga L ₃ M ₄₅ M ₄₅ (red) spectra are shown.	67
Figure 3.9: Ga 3d (left), Ga 2p _{3/2} (centre) and Ga L ₃ M ₄₅ M ₄₅ (right) XPS spectra of GaCl ₃ (bottom), GaBr ₃ (middle) and GaI ₃ (top).	68
Figure 3.10: Ga 3d (left), Ga 2p _{3/2} (centre) and Ga L ₃ M ₄₅ M ₄₅ (right) XPS spectra of Ga _(m) (bottom), GaNacNac ^{Dipp} (lower middle), Ga ₂ Cl ₄ (diox) ₂ (upper middle) and GaCl ₃ (top).	71
Figure 3.11: Wagner plot of gallium halides using Ga 3d _{5/2} binding energy. Symbol legend: diamond = chloride ligands; square = bromide ligands; triangle = iodide ligands.	73
Figure 3.12: Wagner plot of Ga-Ga compounds using Ga 3d _{5/2} binding energy. Symbol legend: diamond = synthesized gallium-cryptand complexes; square = chloride and iodide ligands and O/N donors; triangle = iodide and terphenyl ligands.	76
Figure 3.13: Wagner plot of Ga(I) compounds using Ga 3d _{5/2} binding energy. Symbol legend: diamond = halide ligands; square = chloride ligands and O/N donors; triangle = organic ligands.	78
Figure 3.14: Wagner plot of gallium-chloride and gallium-nitrogen compounds using Ga 3d _{5/2} binding energy. Symbol legend: diamond = Ga(III); square = Ga(II); triangle = Ga(I).	80

Figure 3.15: Wagner plot of gallium-iodide compounds using Ga 3d _{5/2} binding energy. Symbol legend: diamond = Ga(III); square = Ga(II).....	81
Figure 3.16: Wagner plot of gallium materials using Ga 3d _{5/2} binding energy. Symbol legend: square = Group 15 elements; diamond = Group 16 elements.....	85
Figure 3.17: Ga K-edge XAS spectra of [Ga(prismand)][GaCl ₄] and Ga[GaCl ₄] in comparison with Na[GaCl ₄].....	87
Figure 3.18: Calculated Ga K-edge XAS spectra of [Ga(prismand)][GaCl ₄] and Ga[GaCl ₄], showing the influence of the chemical environment on the spectra.	88
Figure 3.19: Measured and calculated (with and without self-absorption) Ga K-edge XAS of NaGaCl ₄ , Ga[GaCl ₄], and [Ga(prismand)][GaCl ₄].....	89
Figure 3.20: Local structures of <i>pseudo</i> -five coordinate Ga sites in [Ga ₂ Cl ₂ (crypt-222)][OTf] ₂ (only the cation is shown, the OTf is omitted) and Ga ₂ Cl ₄ (1,4-dioxane) ₂	90
Figure 3.21: Experimental and calculated Ga K-edge XAS of Ga ₂ Cl ₄ (1,4-dioxane) ₂ and [Ga ₂ Cl ₂ (crypt-222)][OTf] ₂ . The dashed lines A and B mark the energy position of the Ga(I) and Ga(III) features of [Ga(prismand)][GaCl ₄] and Na[GaCl ₄] (see Figure 3.19).	92
Figure 3.22: Experimental and calculated Ga K-edge XAS of [Ga ₃ Cl ₄ (crypt-222)][GaCl ₄] shown at the top. Below that, the calculated contribution from the sum of the Ga sites within the cryptand (labeled Ga ₃ Cl ₄ (crypt-222), solid orange line) is directly compared to the calculated spectrum of [Ga ₂ Cl ₂ (crypt-222)][OTf] ₂ (dotted brown line). Finally, the calculated spectrum from each Ga site in [Ga ₃ Cl ₄ (crypt-222)][GaCl ₄] is shown independently. The calculated spectrum from the [GaCl ₄] ⁻ in Ga[GaCl ₄] is shown at the bottom (dotted purple line) in direct comparison with the [GaCl ₄] ⁻ site in the cryptand. The dashed lines A and B mark the energy position of the Ga(I) and Ga(III) features of [Ga(prismand)][GaCl ₄] and Na[GaCl ₄] (see Figure 3.19).	93
Figure 3.23: The first derivatives of the measured Ga K-edge XAS are shown in (a). The features that correlate with oxidation numbers are marked with *. A plot of the energies of these features (relative to the metallic Ga onset of 10367 eV) in comparison with the	

calculated atomic charge is shown in (b). The colour of the data markers in (b) matches the colour of the spectra in (a). 95

Figure 4.1: Displacement ellipsoid plot of 4.1. Ellipsoids are drawn at the 50% probability level and hydrogen atoms are omitted for clarity. Selected bond lengths and angles (Å, °): Ga1-O1 2.3599(11), Ga1-O2 2.5041(13), Ga1-O3 2.3789(11), Ga1-O4 2.5008(13), Ga1•••C11 3.5937(9); O1-Ga1-O2 68.12(3), O1-Ga1-O3 102.21(3). 115

Figure 4.2: Displacement ellipsoid plot of 4.3. Ellipsoids are drawn at the 50% probability level and hydrogen atoms are omitted for clarity. Selected bond lengths and angles (Å, °): Ga1-O1 2.4122(9), B1-C3 1.6617(11), Ga1•••F2 3.4923(8), Ga1•••F3 3.8518(10), Ga1•••C5 3.9747(11), Ga1•••C6 4.1431(12); O1-Ga1-O1A 106.50(4), O1-Ga1-O1B 69.02(2). 117

Figure 4.3: Wagner plot of representative Ga(I), Ga(II) and Ga(III) compounds and [Ga(12-crown-4)][B(C₆F₅)₄], 4.3. 119

Figure 4.4: Calculated frontier molecular orbitals for [Ga(12-crown-4)]⁺ at the UM062X/6-311+G(2d,p) level of theory (isovalue = 0.03). 121

Figure 4.5: Displacement ellipsoid plot of 4.4. Ellipsoids are drawn at the 50% probability level, hydrogen atoms and the second formula unit are omitted for clarity. Selected bond lengths and angles (Å, °): Ga1-N1 2.9218(14), Ga1-N2 3.1242(14), Ga1-O1 2.8418(15), Ga1-O2 2.9081(12), Ga1-O3 2.7709(14), Ga1-O4 2.9177(14), Ga1-O5 2.8037(14), Ga1-O6 2.8510(13); N1-Ga1-N2 179.53(3). 124

Figure 4.6: Calculated frontier molecular orbitals for [Ga(crypt-222)]⁺ at the UM062X/6-311+G(2d,p) level of theory (isovalue = 0.03). 127

Figure 5.1: Three strategies for the synthesis of gallenes and gallene precursors. 146

Figure 5.2: Displacement ellipsoid plot of 5.1•Et₂O. Ellipsoids are drawn at the 50% probability level. Hydrogen atoms and disorder about the ether molecules are omitted for clarity. Selected parameters (bond lengths in Å; bond angles in °): Ga1-C1 2.003(4), Ga1-C14 1.986(4), Ga1-Cl1 2.3080(13), Ga1-Cl2 2.3052(13), Li1-Cl1 2.369(9), Li1-Cl2 2.402(8);

C1-Ga1-C14 124.51(17), C1-Ga1-Cl1 103.32(13), C1-Ga1-Cl2 104.17(14), C14-Ga1-Cl1 114.59(12), C14-Ga1-Cl2 112.20(14), Cl1-Ga1-Cl2 92.12(5)..... 147

Figure 5.3: Displacement ellipsoid plot of 5.2. Ellipsoids are drawn at the 50% probability level. Hydrogen atoms are omitted for clarity. Selected parameters (bond lengths in Å; bond angles in °): Ga1-C1 1.979(3), Ga1-O1 1.9584(18), Ga1-Cl1 2.1809(8), Ga1-Cl2 2.1657(8); Cl1-Ga1-Cl2 110.93(3), C1-Ga1-O1 105.10(9), Ga1-C1-C2 107.43(18)..... 148

Figure 5.4: Displacement ellipsoid plot of 5.3. Ellipsoids are drawn at the 50% probability level. Hydrogen atoms are omitted for clarity. Selected parameters (bond lengths in Å; bond angles in °): Ga1-C1 2.0254(12), Ga1-C14 2.0031(12), Ga1-C23 2.0551(13), Ga1-Cl1 2.2888(6); C14-Ga1-C1 113.63(5), C14-Ga1-C23 109.85(5), C1-Ga1-C23 120.12(4), C1-Ga1-Cl1 102.29(4), C23-Ga1-Cl1 98.99(3)..... 150

Figure 5.5: Displacement ellipsoid plot of 5.4. Ellipsoids are drawn at the 50% probability level. Hydrogen atoms are omitted for clarity. Selected parameters (bond lengths in Å; bond angles in °): Ga1-C1 2.034(2), Ga1-C14 1.991(3), Ga1-N1 2.011(2), Ga1-Cl1 2.2325(7); C1-Ga1-C14 123.30(10), C1-Ga1-N1 99.09(9), C1-Ga1-Cl1 110.57(7), N1-Ga1-Cl1 100.74(6), C14-Ga1-Cl1 112.18(8)..... 150

Figure 5.6: Displacement ellipsoid plot of 5.5. Ellipsoids are drawn at the 50% probability level. Hydrogen atoms are omitted for clarity. Selected parameters (bond lengths in Å; bond angles in °): Ga1-C1 2.099(3), Ga1-C14 2.025(3), Ga1-C23 2.089(3), Ga1-C34 2.013(3); C23-Ga1-C1 119.87(11), C14-Ga1-C1 102.84(11), C34-Ga1-C1 108.47(12), C34-Ga1-C14 119.76(11), C34-Ga1-C23 100.79(11)..... 152

Figure 5.7: Displacement ellipsoid plot of 5.6. Ellipsoids are drawn at the 50% probability level. Hydrogen atoms and the toluene solvent molecule are omitted for clarity. Selected parameters (bond lengths in Å; bond angles in °): Ga1-C1 2.0072(9), Ga1-C14 2.0422(8), Ga1-Cl1 2.2221(4), Ga1-Cl2 2.2234(5); Cl1-Ga1-Cl2 102.083(12), C1-Ga1-C14 113.75(3), Ga1-C1-C2 109.55(5)..... 153

Figure 5.8: Displacement ellipsoid plot of 5.7. Ellipsoids are drawn at the 50% probability level. Hydrogen atoms are omitted for clarity. Selected parameters (bond lengths in Å; bond angles in °): Ga1-C1 2.028(2), Ga1-C14 1.994(2), Ga1-C23 2.056(2), Ga1-O1 2.0004(17);

O1-Ga1-C14 98.58(8), C1-Ga1-C14 128.48(10), O1-Ga1-C1 104.62(9), O1-Ga1-C23 100.05(8), C14-Ga1-C23 112.80(10), C1-Ga1-C23 107.54(10). 154

Figure 5.9: Displacement ellipsoid plot of 5.8. Ellipsoids are drawn at the 50% probability level. Hydrogen atoms are omitted for clarity. Selected parameters (bond lengths in Å; bond angles in °): Ga1-C1 2.012(2), Ga1-C14 1.997(2), Ga1-C23 2.051(2), Ga1-F1 1.8443(14); C1-Ga1-C23 118.91(8), C14-Ga1-C23 110.57(9), C14-Ga1-C1 116.21(9), F1-Ga1-C1 101.35(8), F1-Ga1-C14 108.65(8), F1-Ga1-C23 98.51(7). 155

Figure 5.10: Displacement ellipsoid plot of 5.9. Ellipsoids are drawn at the 50% probability level. Hydrogen atoms, the second formula unit and the dichloromethane solvent molecule are omitted for clarity. Selected parameters (bond lengths in Å; bond angles in °): Ga1-C1 2.005(5), Ga1-C14 1.978(6), Ga1-N1 1.993(5), Ga1-O1 2.004(4); C1-Ga1-C14 128.8(2), C1-Ga1-O1 100.8(2), C1-Ga1-N1 108.9(2), N1-Ga1-O1 97.3(2), N1-Ga1-C14 106.9(2); Ga2-C31 1.960(6), Ga2-C44 1.982(5), Ga2-N3 1.991(5), Ga2-O4 1.982(5); C31-Ga2-C44 130.9(2), C31-Ga2-O4 99.1(2), C31-Ga2-N3 108.8(4), N3-Ga2-O4 95.10(19), N3-Ga2-C44 107.7(2). 156

Figure 5.11: Displacement ellipsoid plot of 5.10. Ellipsoids are drawn at the 50% probability level. Hydrogen atoms and the dichloromethane solvent molecule are omitted for clarity. Selected parameters (bond lengths in Å; bond angles in °): Ga1-C1 2.0139(19), Ga1-C14 1.9735(19), Ga1-F1 1.8226(12), Ga1-N1 2.0128(15); C1-Ga1-C14 124.19(7), C1-Ga1-F1 101.82(7), C1-Ga1-N1 108.50(7), N1-Ga1-F1 94.86(6), N1-Ga1-C14 109.37(7), C14-Ga1-F1 114.03(7). 157

Figure 5.12: Displacement ellipsoid plot of 5.11. Ellipsoids are drawn at the 50% probability level. Hydrogen atoms are omitted for clarity. Selected parameters (bond lengths in Å; bond angles in °): Ga1-O1 1.8677(15), Ga1-O2 1.8650(15), Ga1-C30 1.980(2), Ga1-C39 2.045(2), O1-C1 1.418(3), O2-C2 1.408 (3), C1-C3 1.569(3), C2-C31.593(3); O1-Ga1-O2 96.83(7), C1-O1-Ga1 106.22(12), C2-O2-Ga1 108.48(12), O1-C1-C3 111.19(17), O2-C2-C3 110.21(17), C1-C3-C2 107.26(17). 160

Figure A.1: Displacement ellipsoid plot of 2.2a. Ellipsoids are drawn at 50% probability level and anion disorder, solvent, and hydrogen atoms are omitted for clarity 195

Figure A.2: ^1H NMR spectrum of 2.1 in CD_3CN at 600 MHz.	197
Figure A.3: $^{13}\text{C}\{^1\text{H}\}$ NMR spectrum of 2.1 in CD_3CN at 151 MHz.	197
Figure A.4: $^{71}\text{Ga}\{^1\text{H}\}$ NMR spectrum of 2.1 in CD_3CN at 183 MHz.	198
Figure A.5: ^1H NMR spectrum of 2.2 in CD_3CN at 600 MHz.	198
Figure A.6: $^{13}\text{C}\{^1\text{H}\}$ NMR spectrum of 2.2 in CD_3CN at 151 MHz. The triflate signal was omitted for clarity.	199
Figure A.7: ^{19}F NMR spectrum of 2.2 in CD_3CN at 376 MHz.	199
Figure A.8: Wagner plot of gallium halides using Ga $2p_{3/2}$ binding energy. Symbol legend: diamond = chloride ligands; square = bromide ligands; triangle = iodide ligands.	203
Figure A.9: Wagner plot of Ga-Ga compounds using Ga $2p_{3/2}$ binding energy. Symbol legend: diamond = synthesized gallium-cryptand complexes; square = chloride and iodide ligands and O/N donors; triangle = iodide and terphenyl ligands.	204
Figure A.10: Wagner plot of Ga(I) compounds using Ga $2p_{3/2}$ binding energy. Symbol legend: diamond = halide ligands; square = chloride ligands and O/N donors; triangle = organic ligands.	205
Figure A.11: Wagner plot of gallium-chloride and gallium-nitrogen compounds using Ga $2p_{3/2}$ binding energy. Symbol legend: diamond = Ga(III); square = Ga(II); triangle = Ga(I).	206
Figure A.12: Wagner plot of gallium-iodide compounds using Ga $2p_{3/2}$ binding energy. Symbol legend: diamond = Ga(III); square = Ga(II).	207
Figure A.13: Displacement ellipsoid plot of $\text{Ga}_2\text{Cl}_4(1,4\text{-dioxane})_2$ showing naming and numbering scheme. Ellipsoids are drawn at the 50% probability level and hydrogen atoms are omitted for clarity. Selected parameters (bond lengths in Å, angles in °): Ga1-Cl1 2.1837(9), Ga-Cl2 2.1937(9), Ga1-O1 2.1432(9), Ga1-Ga1 2.3911(17), Ga1-O2B 2.631(1); O1-Ga1-Cl1 95.23(4), O1-Ga1-Cl2 94.50(4), O1-Ga1-Ga1-98.52(4), Cl1-Ga1-Cl2 111.44(4), O1-Ga1-O2B 179.86(4).	208

Figure A.14: Displacement ellipsoid plot of $\text{Ga}_2\text{Cl}_4(1,4\text{-dioxane})_2$ showing naming and numbering scheme and the bridging structure between formula units. Ellipsoids are drawn at the 50% probability level and hydrogen atoms are omitted for clarity.....	208
Figure A.15: Displacement ellipsoid plot of 4.2. Ellipsoids are drawn at the 50% probability level and hydrogen atoms are omitted for clarity. Selected bond lengths and angles (\AA , $^\circ$): Ga1-C1 1.9445(11), Ga1-C11 2.2188(5), Ga1-C12 2.2068(5), Ga1-C13 2.2438(6), Na1-C11 2.8108(8), Na1-C12 3.2106(10); C11-Ga1-C12 102.91(2), C11-Ga1-C13 100.45(2).	213
Figure A.16: Displacement ellipsoid plot of $[\text{GaCl}_2(15\text{-crown-5})][\text{GaCl}_4]$. Ellipsoids are drawn at the 50% probability level and hydrogen atoms are omitted for clarity.....	214
Figure A.17: Displacement ellipsoid plot of $[\text{Ga}_2\text{Cl}_3(15\text{-crown-5})(\text{CH}_3\text{CN})]_2[\text{Ga}_2\text{Cl}_6]$. Ellipsoids are drawn at the 50% probability level and hydrogen atoms are omitted for clarity.	214
Figure A.18 : ^1H NMR spectrum of 4.1 in CD_3CN at 600 MHz.	217
Figure A.19: $^{13}\text{C}\{^1\text{H}\}$ NMR spectrum of 4.1 in CD_3CN at 151 MHz.	217
Figure A.20: $^{71}\text{Ga}\{^1\text{H}\}$ NMR spectrum of 4.1 in CD_3CN at 183 MHz.	218
Figure A.21: $^{71}\text{Ga}\{^1\text{H}\}$ NMR spectrum of 4.1 in CD_3CN at 183 MHz.	218
Figure A.22: ^1H NMR spectrum of 4.3 in CD_3CN at 600 MHz.	219
Figure A.23: $^{13}\text{C}\{^1\text{H}\}$ NMR spectrum of 4.3 in CD_3CN at 151 MHz.	219
Figure A.24: $^{11}\text{B}\{^1\text{H}\}$ NMR spectrum of 4.3 in CD_3CN at 193 MHz.	220
Figure A.25: ^{19}F NMR spectrum of 4.3 in CD_3CN at 564 MHz.	220
Figure A.26: ^1H NMR spectrum of 4.4 in CD_3CN at 600 MHz.	221
Figure A.27: $^{13}\text{C}\{^1\text{H}\}$ NMR spectrum of 4.4 in CD_3CN at 151 MHz.	221
Figure A.28: $^{11}\text{B}\{^1\text{H}\}$ NMR spectrum of 4.4 in CD_3CN at 193 MHz.	222

Figure A.29: ^{19}F NMR spectrum of 4.4 in CD_3CN at 564 MHz.	222
Figure A.30: $^{71}\text{Ga}\{^1\text{H}\}$ NMR spectrum of 4.4 in CD_3CN at 183 MHz.	223
Figure A.31: ^1H NMR spectrum of 4.5 in CD_3CN at 600 MHz.	223
Figure A.32: $^{13}\text{C}\{^1\text{H}\}$ NMR spectrum of 4.5 in CD_3CN at 151 MHz.	224
Figure A.33: $^{11}\text{B}\{^1\text{H}\}$ NMR spectrum of 4.5 in CD_3CN at 193 MHz.	224
Figure A.34: ^{19}F NMR spectrum of 4.5 in CD_3CN at 564 MHz.	225
Figure A.35: Displacement ellipsoid plot of $[\text{NMe}_4][\text{GaClMes}_3]$. Ellipsoids are drawn at the 50% probability level and hydrogen atoms are omitted for clarity. Selected bond lengths and angles (\AA , $^\circ$): Ga1-C1 2.0360(18), Ga1-C10 2.0361(18), Ga1-C19 2.0371(18), Ga1-Cl1 2.3536(6); Cl1-Ga1-C1 104.56(5), Cl1-Ga1-C10 102.05(5), Cl1-Ga1-C19 99.38(5).	229
Figure A.36: Displacement ellipsoid plot of Ar^*GaCl_2 . Ellipsoids are drawn at the 50% probability level and hydrogen atoms are omitted for clarity. Selected bond lengths and angles (\AA , $^\circ$): Ga1-C1 1.946(2), Ga1-Cl1 2.1571(7), Ga1-Cl2 2.3142(6), Ga1A-Cl2 2.3146(7); C1-Ga1-Cl1 126.93(6), C1-Ga1-Cl2 112.38(6), Cl1-Ga1-Cl2 103.61(3), Cl2-Ga1-Cl2A 87.95(2), Ga1-Cl2-Ga1A 92.05(2).	229
Figure A.37: ^1H NMR spectrum of 5.1 in $\text{THF-}d_8$ at 600 MHz.	233
Figure A.38: $^{13}\text{C}\{^1\text{H}\}$ NMR spectrum of 5.1 in $\text{THF-}d_8$ at 151 MHz.	234
Figure A.39: ^1H NMR spectrum of 5.3 in C_6D_6 at 600 MHz.	234
Figure A.40: $^{13}\text{C}\{^1\text{H}\}$ NMR spectrum of 5.3 in C_6D_6 at 151 MHz.	235
Figure A.41: ^1H NMR spectrum of 5.4 in CDCl_3 at 600 MHz.	235
Figure A.42: $^{13}\text{C}\{^1\text{H}\}$ NMR spectrum of 5.4 in CDCl_3 at 151 MHz.	236
Figure A.43: ^1H NMR spectrum of 5.5 in C_6D_6 at 600 MHz.	236
Figure A.44: $^{13}\text{C}\{^1\text{H}\}$ NMR spectrum of 5.5 in C_6D_6 at 151 MHz.	237

Figure A.45: ^1H NMR spectrum of 5.7 in C_6D_6 at 600 MHz.	237
Figure A.46: $^{13}\text{C}\{^1\text{H}\}$ NMR spectrum of 5.7 in C_6D_6 at 151 MHz.	238
Figure A.47: ^{19}F NMR spectrum of 5.7 in C_6D_6 at 564 MHz.	238
Figure A.48: ^1H NMR spectrum of 5.8 in C_6D_6 at 600 MHz.	239
Figure A.49: $^{13}\text{C}\{^1\text{H}\}$ NMR spectrum of 5.8 in C_6D_6 at 151 MHz.	239
Figure A.50: ^{19}F NMR spectrum of 5.8 in C_6D_6 at 564 MHz.	240
Figure A.51: ^1H NMR spectrum of 5.9 in CDCl_3 at 600 MHz.	240
Figure A.52: $^{13}\text{C}\{^1\text{H}\}$ NMR spectrum of 5.9 in CDCl_3 at 151 MHz.	241
Figure A.53: ^{19}F NMR spectrum of 5.9 in CDCl_3 at 564 MHz.	241
Figure A.54: ^1H NMR spectrum of 5.10 in CDCl_3 at 600 MHz.	242
Figure A.55: $^{13}\text{C}\{^1\text{H}\}$ NMR spectrum of 5.10 in CDCl_3 at 151 MHz.	242
Figure A.56: ^{19}F NMR spectrum of 5.10 in CDCl_3 at 564 MHz.	243
Figure A.57: ^1H NMR spectrum of 5.11 in C_6D_6 at 600 MHz.	243
Figure A.58: $^{13}\text{C}\{^1\text{H}\}$ NMR spectrum of 5.11 in C_6D_6 at 151 MHz.	244

List of Schemes

Scheme 1.1: The first example of frustrated Lewis pair (FLP) activation of H ₂ .	3
Scheme 1.2: Reduction of a diborane to a diborane dianion stabilized by Eind ligands (Naph = naphthalenide).	9
Scheme 1.3: Monomer-dimer equilibrium of gallium-(<i>m</i> -terphenyl) complexes and their alternate reactivities.	14
Scheme 1.4: Selective redistribution of gallium-based ligands in gallium(III)-NHC complexes (Mes = 2,4,6-trimethylphenyl).	16
Scheme 2.1: Various gallium(I) cations.	29
Scheme 2.2: Synthesis of gallium-cryptand[2.2.2] complexes.	30
Scheme 2.3: Gallium-gallium bond lengths in complexes similar to 2.2.	35
Scheme 3.1: Example of how the valence number can fail to accurately predict reactivity.	52
Scheme 3.2: Synthesis of gallium-cryptand[2.2.2] complexes, 2.1 and 2.2.	63
Scheme 4.1: Synthesis of previously reported multinuclear gallium cations stabilized by cryptand[2.2.2].	123
Scheme 4.2: Summary of the reactivity of 4.1 and 4.3.	128
Scheme 5.1: Structure of a digallene, its reactivity with H ₂ and ethylene, and its dimer-monomer equilibrium.	142
Scheme 5.2: Synthesis and reactivity of a boron-carbon doubly bonded compound, a borene (I).	143
Scheme 5.3: Modified synthesis of the germene precursor Mes ₂ GeFFI (V).	144

Scheme 5.4: Dehydrohalogenation of Mes_2GeFFl (V) to give $\text{Mes}_2\text{Ge=Fl}$, a germene (VII).	145
Scheme 5.5: Synthesis of 5.1 from GaCl_2Mes	147
Scheme 5.6: Synthesis of donor-stabilized organogallium compounds 5.1 to 5.8.	151
Scheme 5.7: Synthesis of DMAP-stabilized organogallium compounds 5.4, 5.9 and 5.10.	157
Scheme 5.8: Dehydrohalogenation of 5.8 to give gallene and subsequent trapping reactions products.....	158
Scheme 5.9: Two possible mechanisms for the formation of 5.11.....	161
Scheme 6.1: Reactivity of 4.3 with donor and organic ligands.....	190
Scheme 6.2: Synthesis of Ar^*GaCl_2 and its reaction with LiFl	192
Scheme 6.3: Synthesis of substituted phenyl gallium dichlorides and the pathway to two sterically stabilized gallenes.	192

List of Charts

Chart 1.1: Examples of transient (I) and isolated (II, III) Group 13 dimetallenes (Dipp = 2,6-diisopropylphenyl).	8
Chart 1.2: An aluminum(I) AlNacNac complex (V), a boron(I)-lithium compound (VI) (THF = tetrahydrofuran), and Group 13 centres with an oxidation number of +1 stabilized by a bulky amide ligand (VII).	10
Chart 1.3: An NHC-stabilized boron-boron triple bond (VIII) and a CAAC-stabilized boron(I) HB centre (IX).	11
Chart 1.4: Crown ether complexes of indium(I) showing mono- and sandwich-type complexes (X and XI, respectively) (OTf = trifluoromethanesulfonate).	12
Chart 1.5: Coordination complexes of GaCp* (XII, XIII) and the structure of gallium-(<i>m</i> -terphenyl) complexes (XIV - XVI).	14
Chart 1.6: Structures of gallium(I) (XVII) and gallium(II) (XVIII) NHC complexes (Mes = 2,4,6-trimethylphenyl).	16
Chart 4.1: Examples of gallium(I) compounds (Cp* = pentamethylcyclopentadienyl, Dipp = 2,6-diisopropylphenyl).	110
Chart 4.2: Germanium(II) complexes of 12-crown-4 and 15-crown-5 (X = [OTf] ⁻ or [GeCl ₃] ⁻).	111
Chart 4.3: Gallium(I) cations complexed by macrocyclic ligands.	112

List of Abbreviations

°	degrees
α	Auger parameter
α'	modified Auger parameter
A	product of fluorescence rate and other experimental factors (XAS)
Å	angstrom, 10^{-10} m
Ar	aryl group
Ar*	2,6-bis(2,4,6-trimethylphenyl)phenyl, 2,6-dimesitylphenyl
Ar'	2,6-bis(2,4,6-triisopropylphenyl)phenyl
B	sum of background absorption at fluorescence energy E_F (XAS)
BCF	tris(pentafluorophenyl)borane, $B(C_6F_5)_3$
br	broad
Bu	butyl
CAAC	cyclic alkylaminocarbenes
calcd	calculated
CCDC	Cambridge Crystallographic Data Centre
CM5	Charge Method 5
coord	coordinated
Cp*	pentamethylcyclopentadienyl
C_Q	quadrupolar coupling constant
crypt-222	cryptand[2.2.2]
Δ	difference (X-ray crystallography), reflux
$\Delta\alpha'$	relaxation shift
$\Delta\varepsilon$	initial state shift
ΔR	final state shift
δ	chemical shift
d	doublet
DAB	diazabutadiene
DCM	dichloromethane
decomp	decomposition
diox	1,4-dioxane

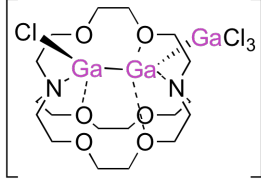
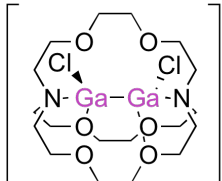
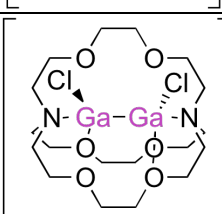
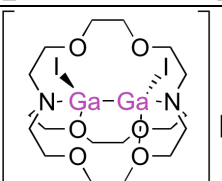
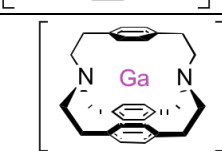
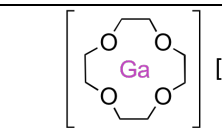
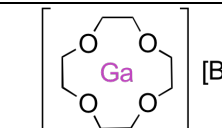
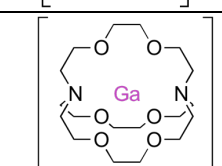
Dipp	2,6-diisopropylphenyl
DFT	density functional theory
DMAP	4-dimethylaminopyridine
E	Group 13, 14, 15 or 16 element
E_B	binding energy
E_{hv}	energy of photons (XPS instrument)
Eind	1,1,3,3,5,5,7,7-octaethyl-s-hydrindacen-4-yl
E_K	kinetic energy of photoelectron
$E_{K(Auger)}$	kinetic energy of Auger electron
eq	molar equivalents
eqn	equation
ESI	electrospray ionization
Et	ethyl
Et ₂ O	diethyl ether
eV	electron volts
ϕ_{XPS}	work function, XPS instrument
FDMNES	finite difference method near edge structures, theoretical model for XAS analysis
FEFF	software package for the analysis of XAS spectra
Fl	fluorenyl
FLP	frustrated Lewis pair
FT	Fourier transform
FWHM	full width at half maximum
gCOSY	gradient homonuclear correlation spectroscopy
gHSQC	gradient heteronuclear single-quantum correlation spectroscopy
gHMBC	gradient heteronuclear multiple-bond correlation spectroscopy
GOF	goodness of fit
h	hour
HOMO	highest occupied molecular orbital
HR	high resolution
HXMA	hard X-ray microanalysis beamline
I(E)	measured absorption intensity at excitation energy E

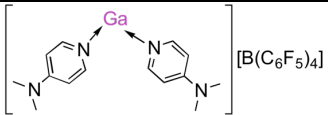
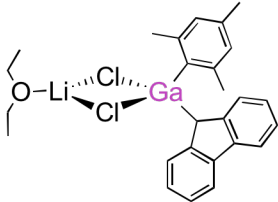
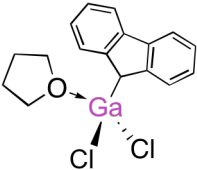
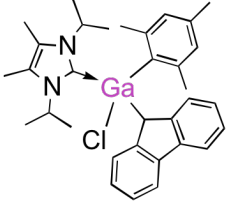
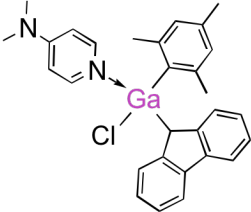
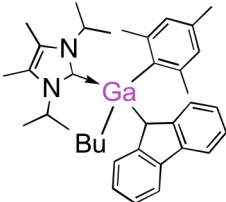
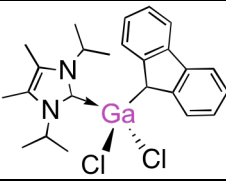
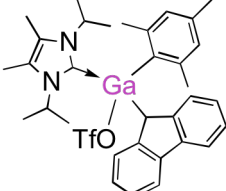
<i>i</i> Pr	<i>iso</i> -propyl
IR	infrared
<i>J</i>	coupling constant
K	kelvin
kV	kilovolts
λ	wavelength, Å or nanometres
LR	low resolution
LUMO	lowest unoccupied molecular orbital
μ	bridging (molecular formula)
$\mu_{\text{Ga}}(\text{E})$	true absorption of gallium at excitation energy E
μm	micrometre
M06	Minnesota 2006 exchange-correlation functional
M06-2X	Minnesota 2006 exchange-correlation functional with double non-local exchange
<i>m/z</i>	mass to charge ratio
<i>m</i>	multiplet
M	metal
^(m)	metal
<i>m</i>	meta
mA	milliamp
Me	methyl
^{Me} <i>i</i> Pr	1,3-diisopropyl-4,5-dimethyl-imidazol-2-ylidene
meas.	measured
Mes	mesityl, 2,4,6-trimethylphenyl
mg	milligram
MHz	megahertz
mL	millilitre
MO	molecular orbital
mol	moles
mp	melting point
MS	mass spectroscopy, mass spectrum
m_s	electron spin quantum number

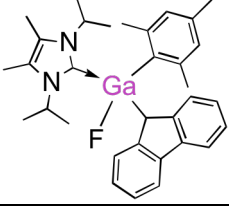
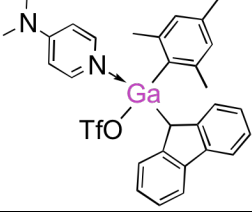
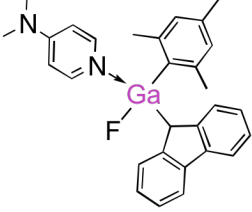
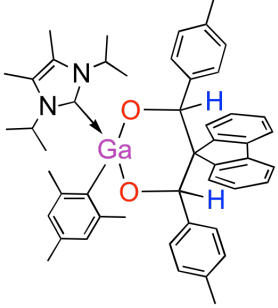
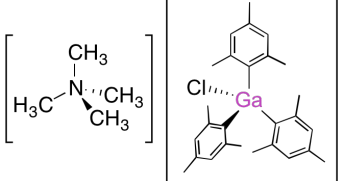
NacNac	1,3-diketimine
NAO	natural atomic orbital
Naph	naphthalenide
NBO	natural bond orbital
NHC	<i>N</i> -heterocyclic carbene
NIMAG	number of imaginary frequencies
nm	nanometre
NMR	nuclear magnetic resonance
NQR	nuclear quadrupole resonance
<i>o</i>	ortho
OTf	triflate, trifluoromethanesulfonate
ov	overlapping
<i>p</i>	para
params	parameters
PBE1PBE	Perdew-Burke-Ernzerhof exchange-correlation functional
Ph	phenyl
pin	pinacolato
ppm	parts per million
prisman	π -prisman, 4,10,15-(1,4)tribenzena-1,7-diazabicyclo[5.5.5]heptadecaphane
q	quartet
R	organic ligand/substituent
refinm	refinement
refl	reflections
RT	room temperature
σ	standard deviation
s	singlet
SIESTA	Spanish Initiative for Electronic Simulations with Thousands of Atoms
SSNMR	solid-state nuclear magnetic resonance
StoBe	Stockholm-Berlin, density functional theory package
t	triplet
<i>t</i> Bu	<i>tert</i> -butyl

TD	time-dependent
THF	tetrahydrofuran
TMEDA	tetramethylethylenediamine
TMS	trimethylsilyl, Me ₃ Si
TOF	time of flight
tol	toluene
Trip	2,4,6-triisopropylphenyl
WBI	Wiberg bond indices
X	halide, or halogen; anion
XANES	X-ray absorption near edge structures
XAS	X-ray absorption spectroscopy
XPS	X-ray photoelectron spectroscopy
XRD	X-ray diffraction

The 25 Man Roster: List of Compounds Reported

Structure	Compound Code	X-ray Structure	CCDC Code
 $[GaCl_4]$	2.1	Yes	1055145
 $[O_3SCF_3]_2$	2.2	Yes	1055146
 $[O_3SCF_3]$ $[GaCl_4]$	2.2a	Yes	1055147
 $[GaI_4]_{1.75}$ $[O_3SCF_3]_{0.25}$	3.1	-	-
 $[OTf]$	3.4	-	-
$Ga_2Cl_4(1,4-dioxane)_2$	-	Yes	1487710
 $[GaCl_4]$	4.1	Yes	
$[Na][GaCl_3Ph]$	4.2	Yes	
 $[B(C_6F_5)_4]$	4.3	Yes	
 $[B(C_6F_5)_4]$	4.4	Yes	

	4.5	Poor Quality	
[GaCl ₂ (15-crown-5)] [GaCl ₄]	-	Yes	
[Ga ₂ Cl ₃ (15-crown-5)(CH ₃ CN)] ₂ [Ga ₂ Cl ₆]	-	Yes	
	5.1	Yes	
	5.2	Yes	
	5.3	Yes	
	5.4	Yes	
	5.5	Yes	
	5.6	Yes	
	5.7	Yes	

	5.8	Yes	
	5.9	Yes	
	5.10	Yes	
	5.11	Yes	
	-	Yes	
$\text{Ar}^* \text{GaCl}_2$	-	Yes	

Chapter 1

1 Introduction

The study of new compounds of *p* block elements featuring unique structures and bonding, although often the subject of fundamental research, has led to many important discoveries which have been recognized by Nobel Prizes in Chemistry. The 1976 Nobel Prize in Chemistry was awarded to William N. Lipscomb for elucidating the structures of complex borane clusters and the evaluation of their chemical bonding.¹ The 1979 Nobel Prize in Chemistry was awarded jointly to Herbert C. Brown and Georg Wittig for their work utilizing boron and phosphorus compounds for organic synthesis.² When considering the elements of Group 13, boron, aluminum, gallium, indium and thallium, significant advances and applications have been realized, including the use of boronic acids in palladium cross-coupling reactions pioneered by Akira Suzuki, who received the 2010 Nobel Prize in Chemistry,³ and Karl Ziegler and Giulio Natta's use of organometallic aluminum catalysts in the polymerization of terminal alkenes, which was similarly recognized in 1963.⁴

Recently, the study of low valent main group compounds has experienced a shift in focus from fundamental investigations of structure and bonding to the application of main group element-containing compounds in the activation of small molecules and catalysis. A desire to expand the scope of chemical transformations pushes development of low valent main group chemistry.⁵ As industrially important transition metals such as platinum, palladium, iridium, rhodium and ruthenium are classified as Class 1 metals with significant safety concerns⁶ and have low natural abundances, there is a desire to generate less harmful and cheaper catalysts from less toxic and earth-abundant main group elements. Although some examples of main group catalysis have already been reported in the literature, the potential to use earth abundant and non-toxic elements for industrial applications continues to motivate further research in this field.

Of the groups in the *p* block, Group 13 chemistry has shown to be, arguably, the most promising in terms of main group element-based catalysis. Neutral compounds containing Group 13 elements are electron poor, as they possess only three valence electrons. Another key characteristic of the Group 13 elements is that several oxidation numbers are accessible, from 0 to +3. Normally, Group 13 compounds that undergo small molecule activation are low valent (meaning they have an assigned oxidation number lower than +3), often having an oxidation number of +1. The heavier elements of the group have a greater affinity for the +1 oxidation number, due to the relativistic inert pair effect. Thus, compounds of thallium(I) are, in general, more stable than those of thallium(III), and are easily isolated under ambient conditions. In contrast, compounds of boron, aluminum, and gallium require suitable ligands to facilitate the isolation of complexes where the Group 13 element has an assigned oxidation number of +1. Group 13 centres in compounds with an oxidation number of +1 are nominally ambiphilic, meaning that they are capable of acting as a Lewis acid, due to the presence of at least one empty *p*-type orbital, and as a Lewis base, as a result of the lone pair of electrons on the metal centre (Figure 1.1).⁷ The electronic structure of a Group 13 element with an oxidation number of +1 is comparable to transition metals that are used in catalysis, such as palladium(0), which possesses both an empty orbital required for substrate coordination and an electron pair to undergo bond activation/oxidative addition.⁸ As a consequence, the activity of Group 13 complexes with an oxidation number of +1 is such that they are capable of reacting with traditionally difficult, but important substrates, such as H₂, giving rise to the high level of interest in low valent Group 13 chemistry.⁹

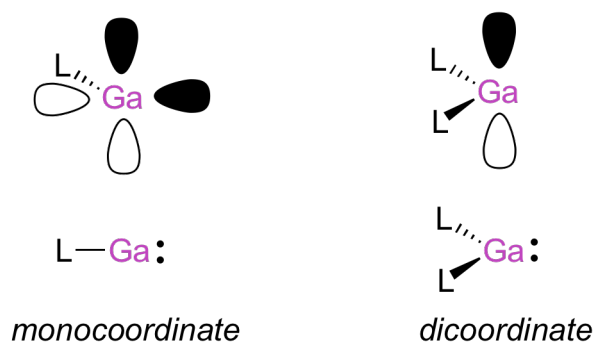
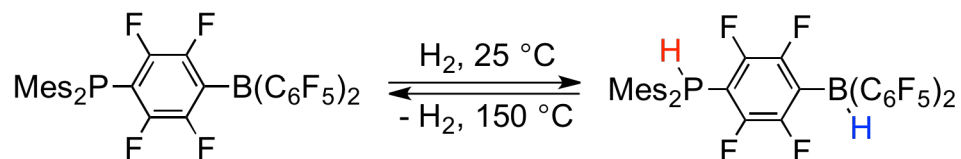


Figure 1.1: Ambiphilic nature of coordinatively unsaturated gallium(I) compounds.

While initial reports of small molecule activation using Group 13 elements frequently featured low valent Group 13 elements,¹⁰ more recently small molecule activation has also been achieved with compounds containing a Group 13 element with an oxidation number of +3. The most prominent example involves sterically hindered and electrophilic boranes, where the inability to form a Lewis acid-base pair with bulky Lewis bases has led to the reversible activation of H₂. This type of reactivity has been termed ‘frustrated Lewis pair’ (FLP) chemistry (Scheme 1.1).¹¹ In more recent work, FLPs have been used as non-transition metal catalysts for the hydrogenation of imines,¹² terminal alkenes,¹³ and other unsaturated organic functional groups.



Scheme 1.1: The first example of frustrated Lewis pair (FLP) activation of H₂.^{11a}

Research focused on the synthesis and isolation of low valent Group 13 compounds aims not only to broaden the scope of possible reactions and chemical transformations, but also to synthesize new reagents with catalytic efficiencies approaching those exhibited by transition metals. The overall goal of this research is to synthesize reactive Group 13 compounds that are chemically robust, derived from cheap and commercially-available starting materials, and that can be made in a minimal number

of synthetic steps to mitigate the amount of unwanted waste and to lower costs. Although potential reactivity or catalytic activity can be predicted using chemical intuition, an understanding of the electronic structure of new compounds using both experimental and computational tools is invaluable to be able to anticipate reactivity and to aid in the understanding of observed transformations. The synthesis of new low valent Group 13 compounds, the initial assessment of their reactivity and the development of experimental techniques to predict the reactivity of novel complexes are the overall goals of the work described in this thesis.

1.1 Classification and Analysis of Novel Complexes

1.1.1 Conventional Characterization Techniques

Upon the isolation of a new compound, several standard analytical methods are used to determine its purity, chemical formula and molecular structure. These include multinuclear nuclear magnetic resonance (NMR) spectroscopy (^1H , $^{13}\text{C}\{^1\text{H}\}$, and other NMR spectroscopies of active nuclei, if present), mass spectrometry, and vibrational spectroscopies, as well as melting point determination and elemental analysis. Although these techniques are capable of giving the chemical formula, structure, an assessment of purity and the physical properties of a novel complex through detailed data interpretation and elucidation, single crystal X-ray diffraction is frequently used to unequivocally determine the detailed structure of the compound. X-ray diffraction methods not only give the general connectivity of a chemical system, as accurate bond lengths, bond angles and torsion angles can also be determined for a compound in the solid-state. Despite the extensive structural information available using this technique, the detailed electronic structure, particularly at the reactive centre of a complex, may not be discernable using the aforementioned techniques; a direct probe of the electron density of an element, and therefore, its electronic environment, is required. Ultraviolet-visible (UV-Vis) spectroscopy may be used for this purpose. However, the lowest energy electronic transitions of main group compounds are commonly of too high an energy to be accessed

using the wavelengths of light generated by conventional UV-Vis instruments. In addition, the observed signals are often broad, leading to ambiguity in the interpretation of the data. As such, the use of theoretical or computational methods can be a useful tool to interpret the UV-Vis data.

Two additional spectroscopic techniques that are often used to probe the electronic environment of a given element are electron paramagnetic resonance (EPR) and NMR spectroscopy, including solid-state NMR (SSNMR) spectroscopy. Some drawbacks do exist for these techniques: a species with one or more unpaired electrons is required to detect a signal in EPR spectroscopy, and the signals in NMR and SSNMR spectroscopy may suffer from broadness, especially when quadrupolar nuclei are involved. In some instances, significant computational analysis is required to interpret the NMR data.

Computational techniques are utilized to gain an understanding of the electronic environment of a given element in a complex. They are performed using a variety of methods, for example, atomic charge determinations using natural bond orbital (NBO) or atoms in molecules (AIM) calculations, to visualizing frontier molecular orbitals generated from population analysis computations. The utilization of computational methods in main group chemistry to understand electronic structure has risen sharply over the past decade, as a result of improvements in computing technology and the increased accessibility of programs to perform quantum chemical calculations. Although progressively more available, care must be taken when performing such calculations, as expertise is required to avoid misinterpretations and false conclusions from the data obtained.

1.1.2 Oxidation Numbers as a Tool

Oxidation numbers are extensively used to give a qualitative indication of the electronic structure of a given element in a chemical system. They are calculated by examining the number of electrons remaining on a central element after heterolytically

cleaving all bonds, and assigning the bonding electrons to the element originally involved in the bond with the higher electronegativity. The charge remaining on the central atom is its assigned oxidation number. Oxidation numbers allow for the classification or grouping of compounds; as an example, boron trihalides (BX_3 , where $\text{X} = \text{F}, \text{Cl},$ and Br) are all classified as boron(III) compounds. Alternatively, valence numbers can be utilized as a descriptor; they are determined by simply counting the number of electrons from the central element involved in bonding.¹⁴ While oxidation and valence numbers are often used interchangeably, they can be significantly different in many systems (Figure 1.2). In this thesis, oxidation numbers will be utilized.

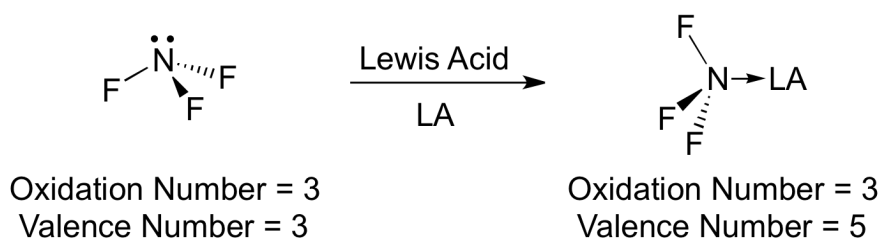


Figure 1.2: Illustration of how oxidation and valence numbers may differ.

In addition to the classification of compounds, oxidation numbers can be used to predict and rationalize observed reactivity. To demonstrate how oxidation numbers can help in the general understanding of the reactivity of main group compounds, consider a Group 15 element such as phosphorus (Figure 1.3). A P(V) centre can be considered to have no valence electrons associated with itself. This allows for the classification of PX_5 compounds as Lewis acids. Lewis acidity is a trait common to phosphorus(V) compounds with a variety of substituents, such as halide ligands. For example, reactions of P(V) compounds often involve the addition of another halide substituent to the phosphorus centre, giving $[\text{PX}_6]^-$ anions (Figure 1.3, **A**). Conversely, P(III) compounds have two valence electrons that are not involved in bonding, and thus, PX_3 or PR_3 compounds are classified as Lewis bases.¹⁵ As a consequence, P(III) compounds commonly act as ligands to transition metals (i.e. $\text{Pt}(\text{PPh}_3)_4$) or in the formation of Lewis acid-base adducts (Figure 1.3, **B**). The use of oxidation numbers to predict reactivity is well known and can

help identify the reactivity of a given compound with a specific reagent (Figure 1.2, Figure 1.3).¹⁶ However, in many instances, oxidation numbers fail to properly predict reactivity and to describe the electronic environment of a central element in main group complexes. As an example, $F_3N \rightarrow LA$ (Figure 1.2) has an assigned oxidation number of +3 at nitrogen, however, as its lone pair is engaged in a dative bond, this compound will not act as a Lewis base.

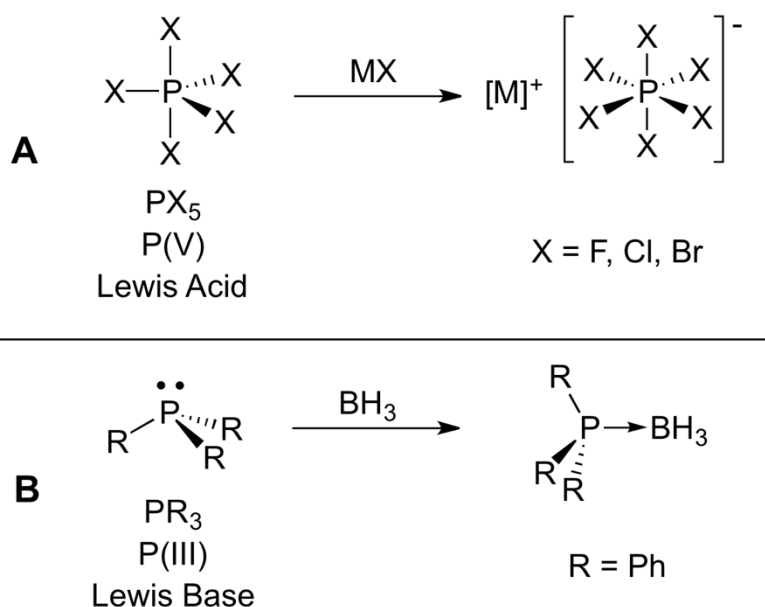


Figure 1.3: Demonstration of the prediction of reactivity for PX_5 and PR_3 compounds based on their oxidation numbers.

1.2 Ligand Types for the Stabilization of Low Valent Group 13 Complexes

The stabilization of low valent or low oxidation number main group compounds of elements from the first four rows of the periodic table relies on the electronic or steric protection of the metal centre. While many ligands stabilize a metal centre using both modalities, in most instances, the steric or electronic effect dominates and the classification of ligands is often based on how the ligand stabilizes a reactive main group

centre. Sterically demanding ligands prevent reagents from reacting with the main group centre or prevent the reactive main group centre from reacting with itself. Strongly electron donating ligands generally provide the reactive main group element with sufficient electron density to moderate its reactivity. The development of new ligands for low valent main group compounds is a well-explored area of research, and the following discussion will describe common ligands utilized in Group 13 chemistry.

1.2.1 Sterically Demanding (Bulky) Ligands

Sterically hindering alkyl groups, such as *t*Bu, are capable of stabilizing reactive main group species; for example, $\text{Al}(t\text{Bu})_3$ exists as a monomer in the solid state,¹⁷ whereas AlMe_3 exhibits a dimeric structure in the solid state.¹⁸ However, they are, in general, not sufficiently shielding to stabilize main group complexes with a lower oxidation number, although some examples have been reported, i.e. the tetrameric aluminum(I) compound $[\text{Al}(\text{CH}_2\text{C}(\text{CH}_3)_3)_4]$.¹⁹ Sterically encumbered aryl groups such as 2,4,6-*tert*-butylphenyl and *m*-terphenyls have been utilized extensively to synthesize dimeric main group species, termed dimetallenes, with a double bond between two main group centres (Chart 1.1).²⁰ Bulky aryl ligands have had a significant influence on multiply-bonded main group chemistry, as dimetallene and dimetallyne (compounds with a homoatomic triple bond) derivatives of almost every Group 13, 14 and 15 element have been isolated using this type of ligand, including dialumenes, digallenes and diindenes (Chart 1.1; **I**, **II**, and **III**, respectively).^{21,22,23,24} These complexes exhibit reactivity that is traditionally associated with transition metals.^{23a,b,25}

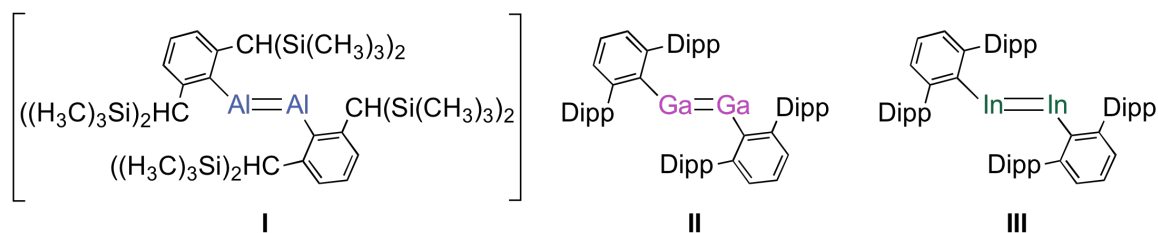
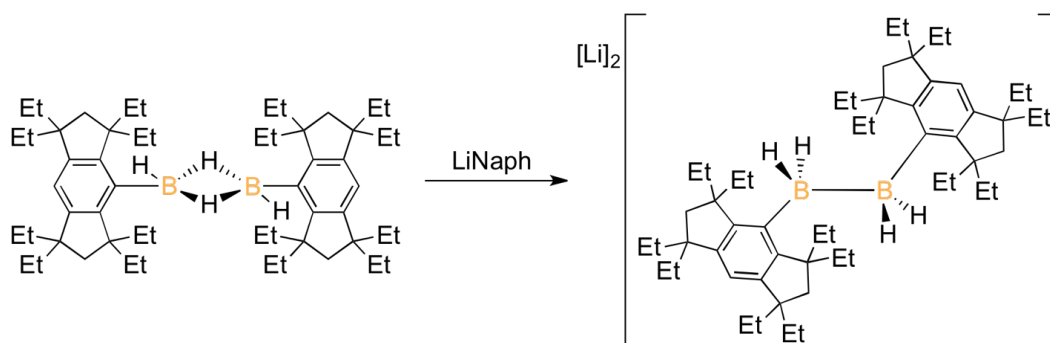


Chart 1.1: Examples of transient (**I**) and isolated (**II**, **III**) Group 13 dimetallenes^{21;23b,c}
(Dipp = 2,6-diisopropylphenyl).

Recently, uniquely tuned ligands in terms of size and donor strength have been synthesized and applied in main group chemistry. Examples include the Eind ligand (1,1,3,3,5,5,7,7-octaethyl-*s*-hydrindacen-4-yl) which has been used to stabilize a novel germanone,²⁶ as well as various hydroboranes and their reduction products (Scheme 1.2).²⁷ Bulky silicon containing ligands such as $-\text{Si}(t\text{Bu})_3$, $-\text{C}(\text{Si}(\text{CH}_3)_3)_3$ and $-\text{Si}(\text{Si}(\text{CH}_3)_3)_3$, have also been utilized in main group chemistry, and have been used to stabilize Group 13 elements in the +1 oxidation state (Figure 1.4, **IV**).²⁸ Many other examples of bulky ligands exist, however, few ligand types have been as widely utilized as the bulky alkyl and *m*-terphenyl ligand groups.



Scheme 1.2: Reduction of a diborane to a diborane dianion stabilized by Eind ligands²⁷
(Naph = naphthalenide).

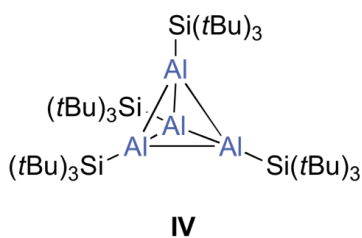


Figure 1.4: A tetrameric aluminum(I) compound (**IV**) with a bulky silicon ligand.^{28a}

1.2.2 Strong Electron Donating Ligands

Another approach for the stabilization of low valent main group compounds involves the use of strong electron donating ligands. Although some low valent Group 13

centres are capable of being stabilized by halide ligands, (for example, InCl, which is commercially available), the use of donor ligands is needed for Group 13 elements from the first three rows (B, Al and Ga). Early examples of strongly donating ligands were electron-rich organic groups, such as cyclopentadienyl (Cp),²⁹ and pentamethylcyclopentadienyl (Cp*^{*}).³⁰ Alternative ligands employ heteroatoms as donors; these include simple cyclic ethers, such as in GeCl₂•dioxane,³¹ or amines.³² Chelating diimines such as diazabutadiene (DAB^X, where X is the substituent on nitrogen) derivatives,³³ 1,3-diketimines (NacNac^X, where X is the substituent on nitrogen)³⁴ and guanidinate ligands³⁵ have been widely used in Group 13 chemistry.³⁶ The synthesis of an aluminum(I) complex using the NacNac diimine ligand system (Chart 1.2, **V**) and its reactivity with various types of σ bonds is an interesting example.^{34c} In addition, boryl anions have been synthesized using DAB ligands, demonstrating the ability of strong electron donating ligands to stabilize so-called ‘umpolung’ Group 13 systems (Chart 1.2, **VI**).³⁷ Group 13 species with an oxidation number of +1 have been stabilized in their monomeric form using bulky amide ligands (Chart 1.2, **VII**); most of the stabilization can be attributed to the electron rich nitrogen atom, as not only is covalently bound to the metal centre, its lone pair also donates electron density to the Group 13 element.⁷

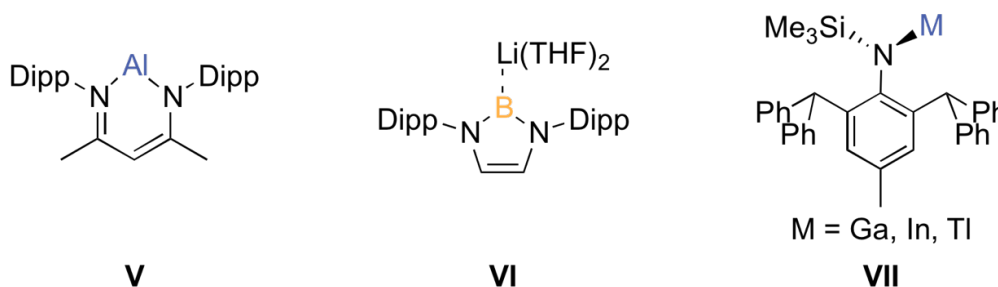


Chart 1.2: An aluminum(I) AlNacNac complex (**V**),³⁶ a boron(I)-lithium compound (**VI**)³⁷ (THF = tetrahydrofuran), and Group 13 centres with an oxidation number of +1 stabilized by a bulky amide ligand (**VII**).⁷

The advent of stable *N*-heterocyclic carbenes (NHCs)³⁸ as strong σ donor ligands has helped expand the library of isolable low valent main group compounds. The strongly

donating properties of NHCs are a result of their structure; with two electron rich nitrogen atoms bonded to the carbenic carbon, the p orbital at the carbon atom has significant electron density from the nitrogen atoms, stabilizing the electron deficient carbon.³⁹ NHCs have been used to stabilize low valent species of many main group elements, however, few examples exist for Group 13 compounds. The synthesis of a boron-boron triple bond stabilized by NHCs (Chart 1.3, **VIII**) has recently been reported.⁴⁰ In the past decade, new types of carbenes have been developed, namely cyclic alkylaminocarbenes (CAACs),⁴¹ which have been successfully used to isolate $\text{HB}(\text{CAAC})_2$, which contains a borylene, a boron(I) centre with a lone pair of electrons (Chart 1.3, **IX**).⁴² The σ donor strength of CAACs in comparison to NHCs is markedly increased as a result of the replacement of a directly-bound σ withdrawing nitrogen with a carbon atom. Conversely, CAACs are capable of accepting π electron density from the bound metal centre.⁴³ These factors have a significant effect on the bond strength between a CAAC and a main group centre.

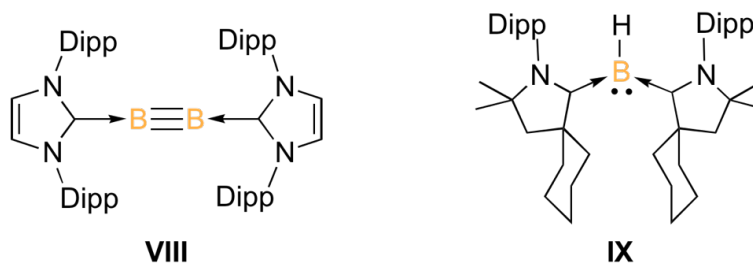


Chart 1.3: An NHC-stabilized boron-boron triple bond (**VIII**)⁴⁰ and a CAAC-stabilized boron(I) HB centre (**IX**).⁴²

1.2.3 Macrocyclic Ethers as Ligands

Although research into the development of new ligand systems is relatively widespread, the use of simple, commercially available ligands to minimize overall costs and reduce the number of synthetic steps required to generate low valent main group complexes is desirable particularly if the complexes are to be used in further applications. Crown ethers and other macrocycles, used primarily as chelating agents or as a means to

improve the solubility characteristics of metal cations,⁴⁴ have recently received attention by facilitating the isolation of low valent Group 14 cations. Initial reports demonstrated the use of paracyclophane macrocycles as ligands for the stabilization of germanium(II) and tin(II) cations.⁴⁵ Other new cationic species were synthesized using commercially available macrocyclic ethers and amines: aza-crown ether,⁴⁶ crown ether,⁴⁷ and cryptand[2.2.2]⁴⁸ complexes of germanium(II) and tin(II) have been reported. The use of macrocyclic ligands for the synthesis of low valent Group 13 complexes has been demonstrated as well: the complexation of indium(I) has been reported using crown ethers of various sizes, giving several bonding motifs (Chart 1.4).⁴⁹ The choice of macrocyclic ether and the counteranion can influence the number of bound donor atoms and cause significant differences in the coordination environment at the metal centre. The utilization of macrocyclic ethers as ligands can also have a large impact on the reactivity of novel low valent main group complexes in comparison to bulky or strongly donating ligands.

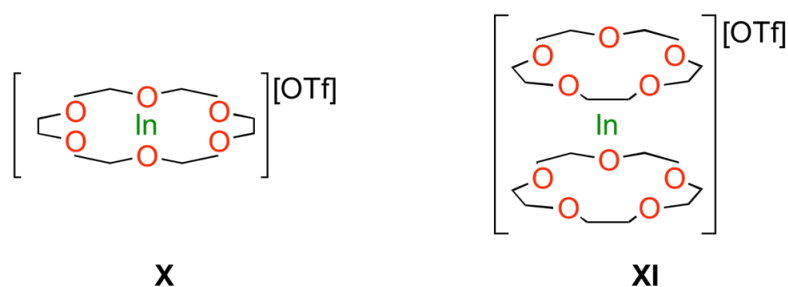


Chart 1.4: Crown ether complexes of indium(I) showing mono- and sandwich-type complexes (**X** and **XI**, respectively)^{49a,c} (OTf = trifluoromethanesulfonate).

1.3 Low Valent Gallium Chemistry

While boron and aluminum are rarely found with an oxidation number other than +3, the position of gallium in the group allows for stable, but reactive, compounds to be synthesized containing gallium(I) or gallium(II) using a wide range of ligand types. The first example of a gallium(I) compound was described in the 1950's; the crystal structure

of the mixed valent halide salt Ga_2Cl_4 ($[\text{Ga}][\text{GaCl}_4]$, where the oxidation numbers for the gallium centres are +1 and +3, respectively) was reported.⁵⁰ Following this discovery, the synthesis of gallium(II) complexes with Ga-Ga single bonds, containing neutral donors as stabilizing ligands, such as in $\text{Ga}_2\text{Cl}_4(1,4\text{-dioxane})_2$ ⁵¹ or $\text{Ga}_2\text{Cl}_4(\text{pyridine})_2$,⁵² and without donor ligands, for example when bulkier silicon containing ligands were employed, as in $\text{Ga}_2[\text{CH}(\text{SiMe}_3)_2]_4$, were reported.⁵³ A wide range of binding motifs and ligands for gallium(II) compounds have been explored, and have been reviewed in detail.⁵⁴ Although gallium(II) complexes have an assigned oxidation number lower than +3, such compounds often lack the reactivity potential that is required for subsequent applications, as all of their electrons are being used in bonding, and the metal centres are often coordinatively saturated.

Other than the mixed valent halide salts Ga_2X_4 , very few examples of gallium(I) compounds were known until the discovery of functionalized gallium(I) complexes using Cp and Cp* ligands. Due to the minimal steric protection provided by the Cp ligand, the gallium(I) centre undergoes a wide range of reactions.⁵⁵ Cp*Ga has been widely used as a Lewis base and a two electron donor ligand in transition metal and coordination chemistry (Chart 1.5, **XII** and **XIII**).⁵⁶ The solid state structure of Cp*Ga was found to be hexameric,⁵⁷ indicating that the Cp* ligand is not sufficiently bulky to stabilize monomeric gallium(I) compounds in the solid state.⁵⁸ The synthesis of monomeric gallium(I) complexes was ultimately achieved using the enhanced steric protection provided by *m*-terphenyl ligands. Initially, anionic digallynes (Chart 1.5, **XIV**)⁵⁹ containing a purported Ga-Ga triple bond were synthesized. Increasing the steric bulk of the *m*-terphenyl ligand allowed for the isolation of a monomeric gallium(I) compound, both in solution and in the solid state (Chart 1.5, **XV**).^{21b,60,61} When a less bulky ligand was used, the isolated gallium(I) complex exhibited a dimeric structure in the solid state (Chart 1.5, **XVI**) and a monomer-dimer equilibrium in solution. With an oxidation number of +1, the *m*-terphenyl-stabilized gallium species exhibited reactivity with small molecules, Lewis acids and various alkenes and alkynes, demonstrating how multiply

bonded gallium(I) systems can display different reactivity compared to their monomeric analogues (Scheme 1.3).⁶²

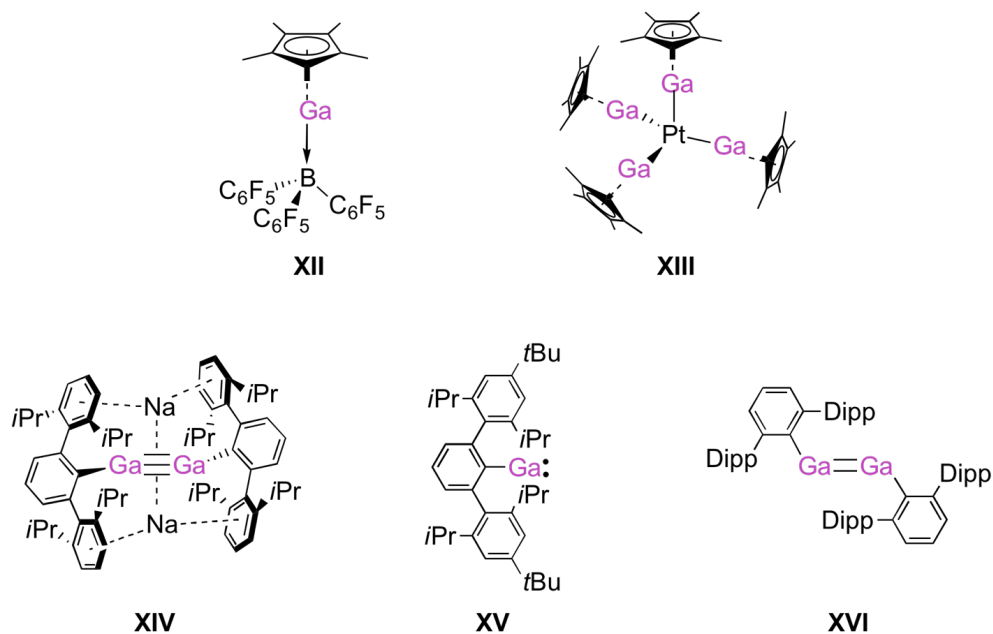
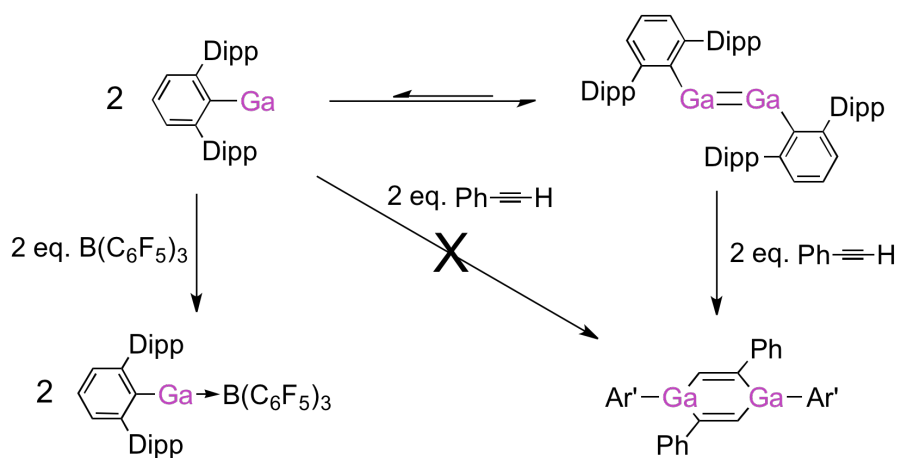


Chart 1.5: Coordination complexes of GaCp^* (XII, XIII) and the structure of gallium-*(m*-terphenyl) complexes (XIV - XVI).



Scheme 1.3: Monomer-dimer equilibrium of gallium-*(m*-terphenyl) complexes and their alternate reactivities.^{60a,61,62a}

Similar to other low valent main group elements, strong electron donating ligands are able to stabilize gallium(I) species; NacNac and DAB ligands have been used for the synthesis of gallium(I) compounds.⁶³ $\text{GaNacNac}^{\text{Dipp}}$ and $[\text{GaDAB}^{\text{Dipp}}]^-$ react as two-electron donor ligands and can stabilize standard Lewis acids,⁶⁴ germynes and stannylenes (Figure 1.5, **A**),⁶⁵ be used as ligands in transition metal chemistry,⁶⁶ and be utilized in FLP-type reagents (Figure 1.5, **B**),⁶⁷ among other examples.⁶⁸

NHCs have been sparingly used in gallium chemistry and have almost exclusively been used to stabilize gallium(III) alkyl, halide and hydride complexes.⁶⁹ The controlled and selective substitution of the halide ligands in NHC-stabilized gallium halides for hydrides and other halides has been demonstrated (Scheme 1.4)^{70,71} An NHC/tris(alkyl)gallium system has been shown to activate aldehydes, where the aldehyde is inserted between the gallium centre and the carbene.⁷² A few examples of low valent gallium-NHC complexes have been described; NHCs have been utilized as neutral donors to stabilize a gallium(I) cation (Chart 1.6, **XVII**),⁷³ gallium(II) Ga_2Cl_4 fragments (Chart 1.6, **XVIII**),⁷⁰ in addition to acting as stabilizing ligands for low valent gallium clusters.⁷⁴

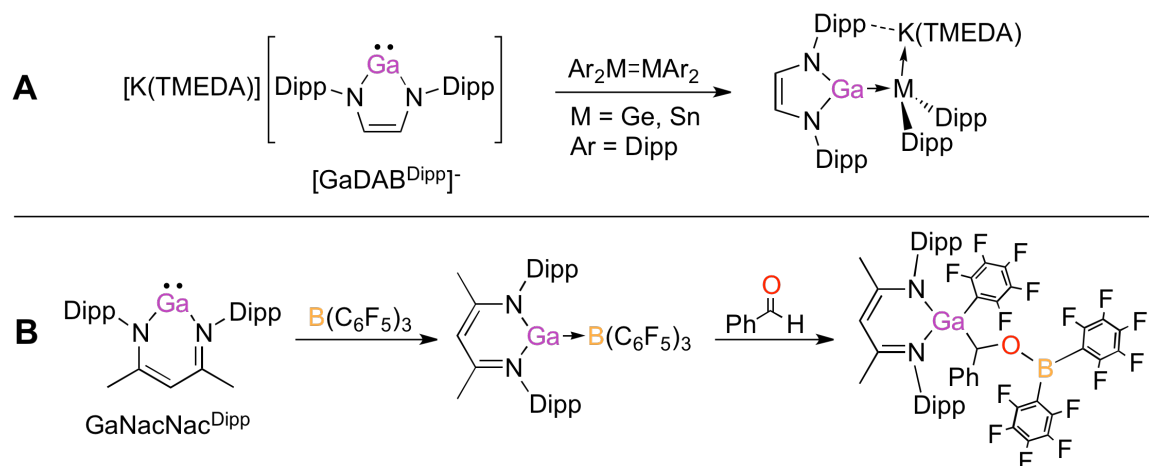
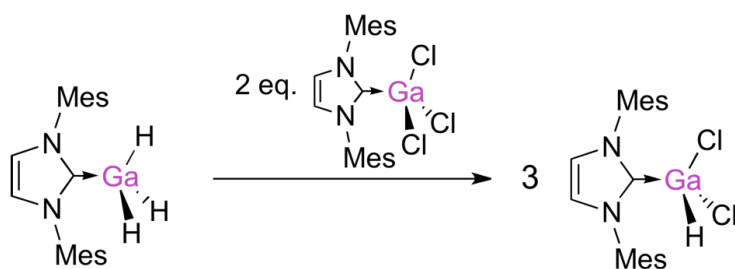


Figure 1.5: The reaction of $[\text{GaDAB}^{\text{Dipp}}]^-$ with ditetrelenes (**A**);^{65a} and the reaction of $\text{GaNacNac}^{\text{Dipp}}$ with $\text{B}(\text{C}_6\text{F}_5)_3$, followed by the addition of benzaldehyde (**B**)⁶⁷ (TMEDA = tetramethylethylenediamine).



Scheme 1.4: Selective redistribution of gallium-based ligands in gallium(III)-NHC complexes⁷¹ (Mes = 2,4,6-trimethylphenyl).

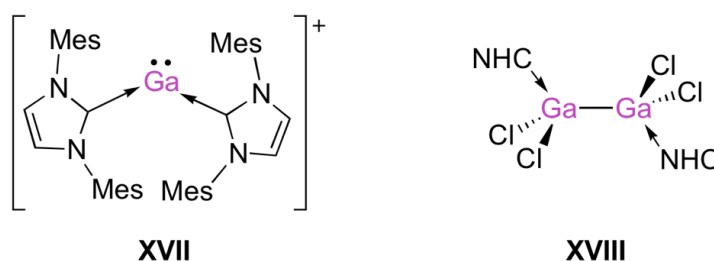


Chart 1.6: Structures of gallium(I) (XVII) and gallium(II) (XVIII) NHC complexes^{70,73} (Mes = 2,4,6-trimethylphenyl).

1.4 Reactivity of Low Valent Gallium Complexes

The use of gallium(I) complexes in small molecule activation and catalysis has greatly increased in recent years. Although some gallium compounds are difficult to synthesize and manipulate, low valent and coordinatively unsaturated gallium complexes have been shown to be viable catalysts for several chemical processes. The reactions of (*m*-terphenyl)-gallium compounds with H₂ and NH₃ were early examples of small molecule activation using Ga(I) centres.⁶² Other examples followed this report, where GaNacNac^{Dipp} demonstrated the ability to oxidatively add main group element hydrides⁷⁵ and the fixation and conversion of H₂ and carbon dioxide was performed using unsaturated gallium(III) centres stabilized by a [NacNac']²⁻ ligand (Figure 1.6, A).⁷⁶ Gallium(II) complexes with strongly donating bis(imide) ligands undergo addition reactions with alkynes, such as phenylacetylene. When phenylacetylene was added to

gallium(II)-bis(imide) complexes, cooperative reactivity is observed, as the ligand is involved in the activation of the substrate.⁷⁷ Only recently have full catalytic cycles using gallium(I) complexes been reported. As an example, gallium(I) cations stabilized by fluorinated arenes and weakly coordinating perfluorinated aluminate anions have been shown to catalyze the polymerization of isobutylene, an important reaction in the production of industrial plastics.⁷⁸ An unidentified gallium(I) species, generated *in situ* from the ultrasonic activation of gallium metal using silver(I) salts is effective as a catalyst for the formation of carbon-carbon bonds (Figure 1.6, **B**).⁷⁹ The reports of the catalytic activity of gallium(I) complexes is demonstrative of the significant strides that have been achieved to generate new Group 13 element catalysts that could have potential applications in industrial chemistry.

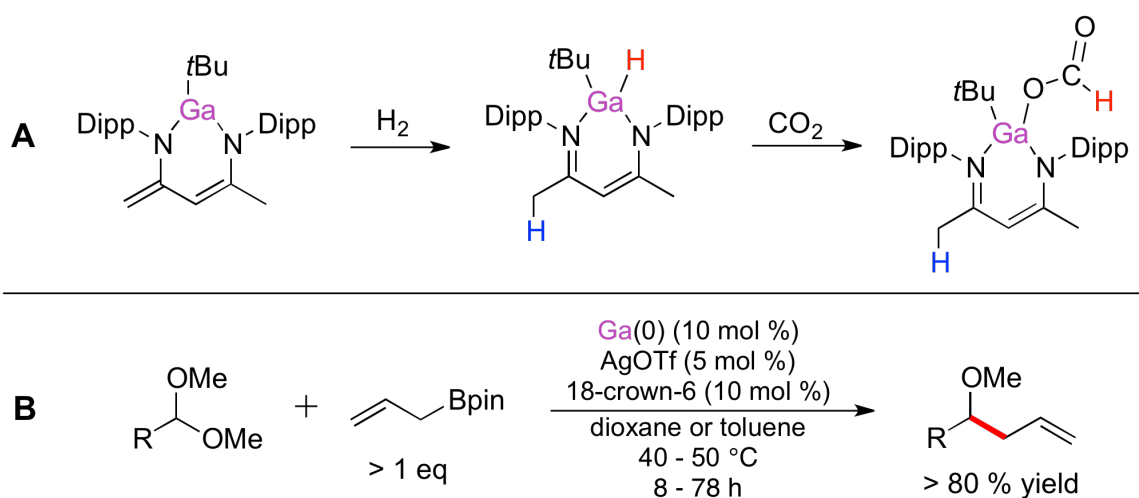


Figure 1.6: Reaction with H₂ and fixation of CO₂ by Ga(III)-NacNac' complex (**A**),⁷⁶ and catalytic carbon-carbon bond formation using Ga(0) activated by Ag(I) (**B**)⁷⁹ (pin = pinacolato).

The study of new gallium complexes with a multitude of chemical and electronic environments has led to many important advances in chemistry. The synthesis of low valent gallium complexes has contributed to the realization that main group elements can undergo small molecule activation and act as catalysts, which was previously thought to

be only the domain of transition metals. While low valent gallium compounds often require specialized ligands to stabilize reactive species, the desire for easy synthetic methodologies and an appropriate balance of reactivity and stability are motivations for the study of the synthesis of new low valent gallium complexes.

1.5 Scope of Thesis

The thesis herein has three main themes, all centred around the goal of synthesizing novel gallium compounds in new bonding motifs to be used directly in the activation of small molecules, in catalysis or to be versatile reagents for the synthesis of such complexes. The goal was to use commercially available ligands and gallium halides as starting materials.

Chapter 2 describes the synthesis and characterization of cationic gallium-cryptand complexes from Ga_2Cl_4 and the commercially available cryptand[2.2.2], in the presence and absence of a halide abstraction agent. The mixed valent halide salt Ga_2Cl_4 ($[\text{Ga}][\text{GaCl}_4]$) can be purchased from various suppliers, but was synthesized in one step from GaCl_3 and gallium metal. Full characterization of the newly synthesized complexes using traditional experimental techniques and computational analyses was performed.

A study of the chemical state of numerous molecular gallium compounds with a range of assigned oxidation numbers using two X-ray spectroscopies, X-ray photoelectron spectroscopy (XPS) and X-ray absorption spectroscopy (XAS), is described in Chapter 3. The goals were to experimentally evaluate the electronic environment of the gallium centres of the new gallium-cryptand[2.2.2] complexes synthesized in Chapter 2, to compare the results to the assigned oxidation numbers, and to distinguish the electronic environments of different gallium centres in compounds with multiple gallium centres.

Chapter 4 revisits the complexation of gallium using macrocyclic ethers as ligands. The commercially available 12-crown-4 was reacted with Ga_2Cl_4 ($[\text{Ga}][\text{GaCl}_4]$).

The resulting complexes were analyzed by traditional characterization methods, XPS and computational techniques in an effort to describe the electronic environment of the novel complexes and to predict their subsequent reactivity.

Chapter 5 diverges from the themes of the first three experimental chapters. The synthesis of a compound containing a gallium-carbon double bond was targeted. Several synthetic routes were explored. The use of donor ligands gave easily manipulated organogallium compounds with halide ligands. Reactions of a gallene precursor with a strong base gave an intermediate doubly-bonded gallium-carbon species that was trapped *in situ*.

1.6 References

- [1] Nobel Media AB. Press Release: The 1976 Nobel Prize in Chemistry. https://www.nobelprize.org/nobel_prizes/chemistry/laureates/1976/press.html (accessed Jan 2, 2017).
- [2] Nobel Media AB. Press Release: The 1979 Nobel Prize in Chemistry. https://www.nobelprize.org/nobel_prizes/chemistry/laureates/1979/press.html (accessed Jan 2, 2017).
- [3] Nobel Media AB. Press Release: The 2010 Nobel Prize in Chemistry. https://www.nobelprize.org/nobel_prizes/chemistry/laureates/2010/press.html (accessed Jan 2, 2017).
- [4] Nobel Media AB. Nobelprize.org. https://www.nobelprize.org/nobel_prizes/chemistry/laureates/1963/press.html (accessed Jan 2, 2017).
- [5] Power, P.P. *Nature* **2010**, *463*, 171-177.
- [6] a) European Medicines Agency Residual Metals Limits. http://www.ema.europa.eu/docs/en_GB/document_library/Scientific_guideline/2009/09/WC500003586.pdf (accessed June 13, 2017). b) Egorova, K.S.; Ananikov, V.P. *Angew. Chem., Int. Ed.* **2016**, *55*, 12150-12162; *Angew. Chem.* **2016**, *128*, 12334-12347.

- [7] Dange, D.; Li, J.; Schenk, C.; Schnöckel, H.; Jones, C. *Inorg. Chem.* **2012**, *51*, 13050-13059.
- [8] Prabusankar, G.; Gemel, C.; Parameswaran, P.; Flener, C.; Frenking, G.; Fischer, R.A. *Angew. Chem., Int. Ed.* **2009**, *48*, 5526-5529.
- [9] As an example, see: Chu, T.; Korobkov, I.; Nikonov, G.I. *J. Am. Chem. Soc.* **2014**, *136*, 9195-9202.
- [10] a) Schulz, S.; Häming, L.; Herbst-Irmer, R.; Roesky, H.W.; Sheldrick, G.M. *Angew. Chem., Int. Ed. Engl.* **1994**, *33*, 969-970; b) Zhu, H.; Chai, J.; Fan, H.; Roesky, H.W.; He, C.; Jancik, V.; Schmidt, H.-G.; Noltemeyer, M.; Merrill, W.A.; Power, P.P. *Angew. Chem., Int. Ed.* **2005**, *44*, 5090-5093; c) Uhl, W.; Benter, M. *J. Chem. Soc., Dalton Trans.* **2000**, 3133-3135; d) Uhl, W.; Keimling, S.U.; Pohl, S.; Saak, W.; Wartchow, R. *Chem. Ber.* **1997**, *130*, 1269-1272.
- [11] a) Welch, G.C.; San Juan, R.R.; Masuda, J.D.; Stephan, D.W. *Science* **2006**, *314*, 1124-1126; b) For a review of FLP systems: Stephan, D.W. *J. Am. Chem. Soc.* **2015**, *137*, 10018-10032.
- [12] Chase, P.A.; Welch, G.C.; Jurca, T.; Stephan, D.W. *Angew. Chem., Int. Ed.* **2007**, *46*, 8050-8053.
- [13] Greb, L.; Oña-Burgos, P.; Schirmer, B.; Grimme, S.; Stephan, D.W.; Paradies, J. *Angew. Chem., Int. Ed.* **2012**, *51*, 10164-10168.
- [14] Parkin, G. *J. Chem. Educ.* **2006**, *83*, 791-799.
- [15] Housecroft, C.E.; Sharpe, A.G. *Inorganic Chemistry*, 3rd ed.; Pearson Prentice Hall: Harlow, Essex, England, 2008.
- [16] a) Russell, D.R.; Sharp, D.W.A. *J. Chem. Soc.* **1961**, 4689-4690; b) Nainan, K.C.; Ryschkewitsch, G.E. *Inorg. Chem.* **1969**, *8*, 2671-2674.
- [17] Woski, M.; Mitzel, N.W. *Z. Naturforsch.* **2004**, *59b*, 269-273.
- [18] a) Lewis, P.H.; Rundle, R.E. *J. Chem. Phys.* **1953**, *21*, 986-992; b) Vranka, R.G.; Amma, E.L. *J. Am. Chem. Soc.* **1967**, *89*, 3121-3126; c) McGrady, G.S.; Turner, J.F.C.; Ibberson, R.M.; Prager, M. *Organometallics* **2000**, *19*, 4398-4401.

- [19] Schram, E.P.; Sudha, N. *Inorg. Chim. Acta* **1991**, *183*, 213-216.
- [20] The first report of a dimetallene system, a diphosphene: Yoshifuji, M.; Shima, I.; Inamoto, N.; Hirotsu, K.; Higushi, T. *J. Am. Chem. Soc.* **1981**, *103*, 4587-4589.
- [21] As examples: a) Stender, M.; Phillips, A.D.; Wright, R.J.; Power, P.P. *Angew. Chem., Int. Ed.* **2002**, *41*, 1785-1787; b) Hardman, N.J.; Wright, R.J.; Phillips, A.D.; Power, P.P. *Angew. Chem., Int. Ed.* **2002**, *41*, 2842-2844.
- [22] A review of dimetallene and dimetallyne chemistry: Rivard, E.; Power, P.P. *Inorg. Chem.* **2007**, *46*, 10047-10064.
- [23] Dialumene: a) Wright, R.J.; Phillips, A.D.; Power, P.P. *J. Am. Chem. Soc.* **2003**, *125*, 10784-10785; b) Agou, T.; Nagata, K.; Sasamori, T.; Tokitoh, N. *Phosphorus, Sulfur Silicon Relat. Elem.* **2016**, *191*, 588-590; Diindene: c) Wright, R.J.; Phillips, A.D.; Hardman, N.J.; Power, P.P. *J. Am. Chem. Soc.* **2002**, *124*, 8538-8539.
- [24] Although a solid-state distannene was reported in 1976, the distannene, along with its germanium analogue, behaved as a monomeric stannylene in solution: Goldberg, D.E.; Harris, D.H.; Lappert, M.F.; Thomas, K.M. *J. Chem. Soc., Chem Commun.* **1976**, 261-262.
- [25] Nagata, K.; Murosaki, T.; Agou, T.; Sasamori, T.; Matsuo, T.; Tokitoh, N. *Angew. Chem., Int. Ed.* **2016**, *55*, 12877-12880.
- [26] Li, L.; Fukawa, T.; Matsuo, T.; Hashizume, D.; Fueno, H.; Tanaka, K.; Tamao, K. *Nat. Chem.* **2012**, *4*, 361-365.
- [27] Shoji, Y.; Matsuo, T.; Hashizume, D.; Gutmann, M.J.; Fueno, H.; Tanaka, K.; Tamao, K. *J. Am. Chem. Soc.* **2011**, *133*, 11058-11061.
- [28] A selection: a) Purath, A.; Dohmeier, C.; Ecker, A.; Schnöckel, H.; Amelunxen, K.; Passler, T.; Wiberg, N. *Organometallics* **1998**, *17*, 1894-1896; b) Purath, A.; Schnöckel, H. *J. Organomet. Chem.* **1999**, *579*, 373-375; c) Uhl, W.; Hiller, W.; Layh, M.; Schwarz, W. *Angew. Chem., Int. Ed.* **1992**, *31*, 1364-1366; d) Linti, G.; Çoban, S.; Dutta, D. *Z. Anorg. Allg. Chem.* **2004**, *630*, 319-323.
- [29] First report: Fischer, E.O.; Hofmann, H.P. *Angew. Chem.* **1957**, *69*, 639-640.

- [30] Initial reports for Al(I), In(I), Si(II), Ge(II), and Sn(II) : a) Dohmeier, C.; Robl, C.; Tacke, M.; Schnöckel, H. *Angew. Chem., Int. Ed. Engl.* **1991**, *30*, 564-565; b) Beachley, Jr., O.T.; Blom, R.; Churchill, M.R.; Faegri, Jr., K.; Fettinger, J.C.; Pazik, J.C.; Victoriano, L. *Organometallics* **1989**, *8*, 346-356; c) Jutzi, P.; Kanne, D.; Krüger, C. *Angew. Chem., Int. Ed. Engl.* **1986**, *25*, 164; d) Jutzi, P.; Kohl, F.; Hofmann, P.; Krüger, C.; Tsay, Y.-H. *Chem. Ber.* **1980**, *113*, 757-769; e) Schöpfer, A.; Saak, W.; Weidenbruch, M. *J. Organomet. Chem.* **2006**, *691*, 809-810; f) Atwood, J.L.; Hunter, W.E.; Cowley, A.H.; Jones, R.A.; Stewart, C.A. *J. Chem. Soc., Chem. Comm.* **1981**, 925-927; g) Jutzi, P.; Mix, A.; Rummel, B.; Schoeller, W.W.; Neumann, B.; Stammler, H.-G. *Science* **2004**, *305*, 849-851; h) Winter, J.G.; Portius, P.; Kociok-Köhn, G.; Steck, R.; Filippou, A.C. *Organometallics* **1998**, *17*, 4176-4182; i) Jutzi, P.; Kohl, F.; Krüger, C. *Angew. Chem., Int. Ed. Engl.* **1979**, *18*, 59-60.
- [31] a) Kolesnikov, S.P.; Rogozhin, I.S.; Nefedov, O.M. *Izv. Akad. Nauk. SSSR. Ser. Khim.* **1974**, 2379-2380; b) Fjeldberg, T.; Haaland, A.; Schilling, B.E.R.; Lappert, M.F.; Thorne, A.J. *J. Chem. Soc., Dalton Trans.* **1986**, 1551-1556.
- [32] Mocker, M.; Robl, C.; Schnöckel, H. *Angew. Chem., Int. Ed. Engl.* **1994**, *33*, 1754-1755.
- [33] Denk, M.; Lennon, R.; Hayashi, R.; West, R.; Belyakov, A.V.; Verne, H.P.; Haaland, A.; Wagner, M.; Metzler, N. *J. Am. Chem. Soc.* **1994**, *116*, 2691-2692.
- [34] First report of ligand: a) Feldman, J.; McLain, S.J.; Parthasarathy, A.; Marshall, W.J.; Calabrese, J.C.; Arthur, S.D. *Organometallics* **1997**, *16*, 1514-1516; Early use for stabilization of main group element: b) Qian, B.; Ward, D.L.; Smith, III, M.R. *Organometallics* **1998**, *17*, 3070-3076; Early report of low valent Group 13 element stabilization: c) Cui, C.; Roesky, H.W.; Schmidt, H.-G.; Noltemeyer, M.; Hao, H.; Cimpoesu, F. *Angew. Chem., Int. Ed.* **2000**, *39*, 4274-4276.
- [35] Jones, C.; Junk, P.C.; Platts, J.A.; Rathmann, D.; Stasch, A. *Dalton Trans.* **2005**, 2497-2499.

- [36] a) Gorden, J.D.; Voigt, A.; Macdonald, C.L.B.; Silverman, J.S.; Cowley, A.H. *J. Am. Chem. Soc.* **2000**, *122*, 950-951; b) Yang, Z.; Ma, X.; Oswald, R.B.; Roesky, H.W.; Zhu, H.; Schulzke, C.; Starke, K.; Baldus, M.; Schmidt, H.-G.; Noltemeyer, M. *Angew. Chem., Int. Ed.* **2005**, *44*, 7072-7074.
- [37] Segawa, Y.; Suzuki, Y.; Yamashita, M.; Nozaki, K. *J. Am. Chem. Soc.* **2008**, *130*, 16069-16079.
- [38] Arduengo, III, A.J.; Harlow, R.L.; Kline, M. *J. Am. Chem. Soc.* **1991**, *113*, 361-363.
- [39] Arduengo, III, A.J.; Rasika Dias, H.V.; Harlow, R.L.; Kline, M. *J. Am. Chem. Soc.* **1992**, *114*, 5530-5534.
- [40] Braunschweig, H.; Dewhurst, R.D.; Hammond, K.; Mies, J.; Radacki, K.; Vargas, A. *Science* **2012**, *336*, 1420-1422.
- [41] Lavallo, V.; Canac, Y.; Präsang, C.; Donnadiou, B.; Bertrand, G. *Angew. Chem., Int. Ed.* **2005**, *44*, 5705-5709.
- [42] Kinjo, R.; Donnadiou, B.; Celik, M.A.; Frenking, G.; Bertrand, G. *Science* **2011**, *333*, 610-613.
- [43] a) Lavallo, V.; Canac, Y.; Donnadiou, B.; Schoeller, W.W.; Bertrand, G. *Angew. Chem., Int. Ed.* **2006**, *45*, 3488-3491; b) Martin, D.; Melaimi, M.; Soleilhavoup, M.; Bertrand, G. *Organometallics* **2011**, *30*, 5304-5313.
- [44] Izatt, R.M.; Bradshaw, J.S.; Nielsen, S.A.; Lamb, J.D.; Christensen, J.J.; Sen, D. *Chem. Rev.* **1985**, *85*, 271-339.
- [45] Probst, T.; Steigelmann, O.; Riede, J.; Schmidbaur, H. *Angew. Chem., Int. Ed. Engl.* **1990**, *29*, 1397-1398.
- [46] a) Cheng, F.; Hector, A.L.; Levason, W.; Reid, G.; Webster, M.; Zhang, W. *Angew. Chem., Int. Ed.* **2009**, *48*, 5152-5154; b) Everett, M.; Jolleys, A.; Levason, W.; Light, M.E.; Pugh, D.; Reid, G. *Dalton Trans.* **2015**, *44*, 20898-20905.
- [47] a) Rupar, P.A.; Bandyopadhyay, R.; Cooper, B.F.T.; Stinchcombe, M.R.; Ragona, P.J.; Macdonald, C.L.B.; Baines, K.M. *Angew. Chem., Int. Ed.* **2009**, *48*,

5155-5158; b) Herber, R.H.; Smelkinson, A.E. *Inorg. Chem.* **1978**, *17*, 1023-1029; c) Drew, M.G.B.; Nicholson, D.G. *J. Chem. Soc., Dalton Trans.* **1986**, 1543-1549; d) Bandyopadhyay, R.; Cooper, B.F.T.; Rossini, A.J.; Schurko, R.W.; Macdonald, C.L.B. *J. Organomet. Chem.* **2010**, *695*, 1012-1018.

[48] a) Rupar, P.A.; Staroverov, V.N.; Baines, K.M. *Science* **2008**, *322*, 1360-1363; b) Avery, J.C.; Hanson, M.A.; Herber, R.H.; Bladek, K.J.; Rupar, P.A.; Nowik, I.; Huang, Y.; Baines, K.M. *Inorg. Chem.* **2011**, *51*, 7306-7316.

[49] a) Andrews, C.G.; Macdonald, C.L.B. *Angew. Chem., Int. Ed.* **2005**, *44*, 7453-7456; b) Cooper, B.F.T.; Andrews, C.G.; Macdonald, C.L.B. *J. Organomet. Chem.* **2007**, *692*, 2843-2848; c) Cooper, B.F.T.; Macdonald, C.L.B. *J. Organomet. Chem.* **2008**, *693*, 1707-1711; d) Cooper, B.F.T.; Macdonald, C.L.B. *New J. Chem.* **2010**, *34*, 1551-1555; e) Cooper, B.F.T.; Hamaed, H.; Friedl, W.W.; Stinchcombe, M.R.; Schurko, R.W.; Macdonald, C.L.B. *Chem. Eur. J.* **2011**, *17*, 6148-6161.

[50] Garton, G.; Powell, H.M. *J. Inorg. Nucl. Chem.* **1957**, *4*, 84-89.

[51] Beamish, J.C.; Small, R.W.H.; Worrall, I.J. *Inorg. Chem.* **1979**, *18*, 220-223.

[52] Beamish, J.C.; Boardman, A.; Small, R.W.H.; Worrall, I.J. *Polyhedron* **1985**, *4*, 983-987.

[53] Uhl, W.; Layh, M.; Hildenbrand, T. *J. Organomet. Chem.* **1989**, *364*, 289-300.

[54] Uhl, W.; Layh, M. Formal Oxidation State +2: Metal-Metal Bonded versus Homonuclear Derivatives. In *The Group 13 Metals Aluminum, Gallium, Indium and Thallium: Chemical Patterns and Peculiarities*; Aldridge, S.; Downs, A.J., Eds., John Wiley & Sons: Chichester, West Sussex, England, 2011; pp. 246-284.

[55] a) Loos, D.; Schnöckel, H.; Gauss, J.; Schneider, U. *Angew. Chem., Int. Ed. Engl.* **1992**, *31*, 1362-1364; b) Loos, D.; Schnöckel, H. *J. Organomet. Chem.* **1993**, *463*, 37-40; c) Jutzi, P.; Schebaum, L.O. *J. Organomet. Chem.* **2002**, *654*, 176-179.

[56] a) Jutzi, P.; Neumann, B.; Reumann, G.; Schebaum, L.O.; Stammler, H.-G. *Organometallics* **2001**, *20*, 2854-2858; b) Gemel, C.; Steinke, T.; Cokoja, M.; Kemper, A.; Fischer, R.A. *Eur. J. Inorg. Chem.* **2004**, 4161-4176, and references therein.

- [57] Loos, D.; Baum, E.; Ecker, A.; Schnöckel, H.; Downs, A.J. *Angew. Chem., Int. Ed. Engl.* **1997**, *36*, 860-862.
- [58] a) Uhl, W.; Hiller, W.; Layh, M.; Schwarz, W. *Angew. Chem., Int. Ed. Engl.* **1992**, *31*, 1364-1366; b) Linti, G. *J. Organomet. Chem.* **1996**, *520*, 107-113.
- [59] The synthesis of such a compound is reported, as well as a summary of other known multiply bonded gallium complexes: Twamley, B.; Power, P.P. *Angew. Chem. Int. Ed.* **2000**, *39*, 3500-3503.
- [60] a) Hardman, N.J.; Wright, R.J.; Phillips, A.D.; Power, P.P. *J. Am. Chem. Soc.* **2003**, *125*, 2667-2679; b) Zhu, Z.; Fisher, R.C.; Ellis, B.D.; Rivard, E.; Merrill, W.A.; Olmstead, M.M.; Power, P.P.; Guo, J.D.; Nagase, S.; Pu, L. *Chem. Eur. J.* **2009**, *15*, 5263-5272.
- [61] Caputo, C.A.; Koivistoinen, J.; Moilanen, J.; Boynton, J.N.; Tuononen, H.M.; Power, P.P. *J. Am. Chem. Soc.* **2013**, *135*, 1952-1960.
- [62] a) Zhu, Z.; Wang, X.; Olmstead, M.M.; Power, P.P. *Angew. Chem., Int. Ed.* **2009**, *48*, 2027-2030; b) Zhu, Z.; Wang, X.; Peng, Y.; Lei, H.; Fettinger, J.C.; Rivard, E.; Power, P.P. *Angew. Chem., Int. Ed.* **2009**, *48*, 2031-2034; c) Caputo, C.A.; Zhu, Z.; Brown, Z.D.; Fettinger, J.C.; Power, P.P. *Chem. Commun.* **2011**, *47*, 7506-7508; d) Caputo, C.A.; Guo, J.-D.; Nagase, S.; Fettinger, J.C.; Power, P.P. *J. Am. Chem. Soc.* **2012**, *134*, 7155-7164.
- [63] a) Hardman, N.J.; Eichler, B.E.; Power, P.P. *Chem. Commun.* **2000**, 1991-1992; b) Schmidt, E.S.; Jockisch, A.; Schmidbaur, H. *J. Am. Chem. Soc.* **1999**, *121*, 9758-9759; c) Schmidt, E.S.; Schier, A.; Schmidbaur, H. *J. Chem. Soc., Dalton Trans.* **2001**, 505-507; d) Baker, R.J.; Farley, R.D.; Jones, C.; Kloth, M.; Murphy, D.M. *J. Chem. Soc., Dalton Trans.* **2002**, 3844-3850; e) Jones, C.; Junk, P.C.; Platts, J.A.; Stasch, A. *J. Am. Chem. Soc.* **2006**, *128*, 2006-2207; f) Liu, Y.; Li, S.; Yang, X.-J.; Li, Q.-S.; Xie, Y.; Schaefer, H.F.; Wu, B. *J. Organomet. Chem.* **2011**, *696*, 1450-1455; g) Fedushkin, I.L.; Lukoyanov, A.N.; Fukin, G.K.; Ketkov, S.Y.; Hummert, M.; Schumann, H. *Chem. Eur. J.* **2008**, *14*, 8465-8468.

- [64] Hardman, N.J.; Power, P.P.; Gorden, J.D.; Macdonald, C.L.B.; Cowley, A.H. *Chem. Commun.* **2001**, 1866-1867.
- [65] a) Green, S.P.; Jones, C.; Lippert, K.-A.; Mills, D.P.; Stasch, A. *Inorg. Chem.* **2006**, *45*, 7242-7251; b) Rugar, P.A.; Jennings, M.C.; Baines, K.M. *Can. J. Chem.* **2007**, *85*, 141-147.
- [66] Baker, R.J.; Jones, C.; Platts, J.A. *Dalton Trans.* **2003**, 3673-3674.
- [67] Ganesamoorthy, C.; Matthias, M.; Bläser, D.; Wölper, C.; Schulz, S. *Dalton Trans.* **2016**, *45*, 11437-11444.
- [68] Asay, M.; Jones, C.; Driess, M. *Chem. Rev.* **2011**, *111*, 354-396.
- [69] a) Li, X.-W.; Su, J.; Robinson, G.H. *Chem. Commun.* **1996**, 2683-2684; b) Stasch, A.; Singh, S.; Roesky, H.W.; Noltemeyer, M.; Schmidt, H.-G. *Eur. J. Inorg. Chem.* **2004**, 4052-4055; c) Marion, N.; Escudero-Adán, E.C.; Benet-Buchholz, J.; Stevens, E.D.; Fensterbank, L.; Malacria, M.; Nolan, S.P. *Organometallics* **2007**, *26*, 3256-3259; d) Cole, M.L.; Furfari, S.K.; Kloth, M. *J. Organomet. Chem.* **2009**, *694*, 2934-2940.
- [70] Ball, G.E.; Cole, M.L.; McKay, A.I. *Dalton Trans.* **2012**, *41*, 946-952.
- [71] Bour, C.; Monot, J.; Tang, S.; Guillot, R.; Farjon, J.; Gandon, V. *Organometallics* **2014**, *33*, 594-599.
- [72] Uzelac, M.; Armstrong, D.R.; Kennedy, A.R.; Hevia, A. *Chem. Eur. J.* **2016**, *22*, 15826-15833.
- [73] Higelin, A.; Keller, S.; Göhringer, C.; Jones, C.; Krossing, I. *Angew. Chem., Int. Ed.* **2013**, *52*, 4941-4944.
- [74] Quillian, B.; Wei, P.; Wannere, C.S.; Schleyer, P.v.R.; Robinson, G.H. *J. Am. Chem. Soc.* **2009**, *131*, 3168-3169.
- [75] a) Kempter, A.; Gemel, C.; Fischer, R.A. *Inorg. Chem.* **2008**, *47*, 7279-7285; b) Jones, C.; Mills, D.P.; Rose, R.P. *J. Organomet. Chem.* **2006**, *691*, 3060-3064; c) Seifert, A.; Scheid, D.; Linti, G.; Zessin, T. *Chem. Eur. J.* **2009**, *15*, 12114-12120; d)

Ganesamoorthy, C.; Bläser, D.; Wölper, C.; Schulz, S. *Organometallics* **2015**, *34*, 2991-2996.

[76] Abdalla, J.A.B.; Riddlestone, I.M.; Tirfoin, R.; Aldridge, S. *Angew. Chem., Int. Ed.* **2015**, *54*, 5098-5102.

[77] Fedushkin, I.L.; Nikipelov, A.S.; Lyssenko, K.A. *J. Am. Chem. Soc.* **2010**, *132*, 7874-7875.

[78] Lichtenthaler, M.R.; Higelin, A.; Kraft, A.; Hughes, S.; Steffani, A.; Plattner, D.A.; Slattery, J.M.; Krossing, I. *Organometallics* **2013**, *32*, 6725-6735.

[79] Qin, B.; Schneider, U. *J. Am. Chem. Soc.* **2016**, *138*, 13119-13122.

Chapter 2

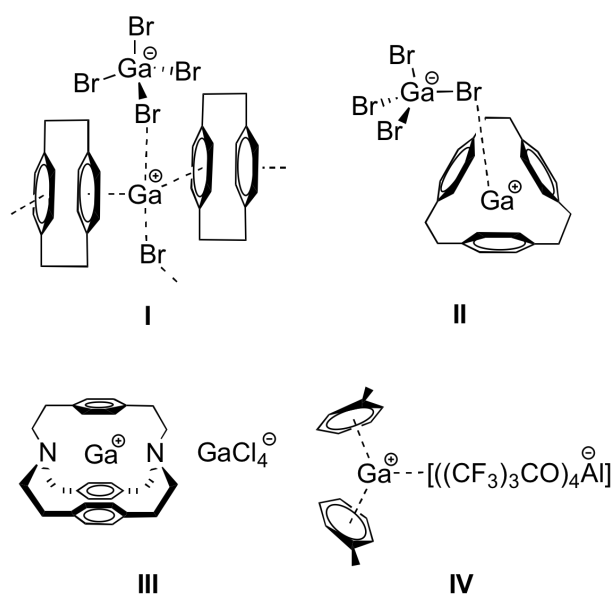
2 Synthesis and Characterization of Cationic Gallium Complexes of Cryptand[2.2.2]*

2.1 Introduction

Gallium(I) chemistry has received significant interest in recent years. Possessing a lone pair of electrons capable of donating to electron deficient centres¹ and orthogonal *p* orbitals able to accept pairs of electrons, a wide array of bonding environments and reaction pathways exist for such complexes.² For example, gallium(I) compounds undergo the addition of H₂, NH₃ and olefins³ highlighting the unusual reactivity of these complexes and demonstrating the use of gallium(I) complexes as alternatives to transition metals in the activation of small molecules.² Gallium(I) compounds have also been shown to catalyze the polymerization of isobutylene.⁴

Gallium(I) cations were first isolated as stabilized cations from the dissolution of Ga₂Cl₄, which exists as a mixed valent halide salt [Ga][GaCl₄]⁵ in aromatic solvents.⁶ Paracyclophanes have been utilized to complex gallium(I) cations (Scheme 2.1; **I**, **II**)⁷ leading to the development of a π -prismand, which was used to successfully encapsulate a free gallium(I) cation (Scheme 2.1; **III**) without contacts to the counter-anion.⁸ Weakly coordinating aluminate anions have been utilized as counter-ions, allowing for the synthesis of gallium(I) cations coordinated only to aromatic solvents molecules with weak contacts to the counter-anion (Scheme 2.1; **IV**).⁹ These [Ga(arene)₂][Al(OR^F)₄] complexes are reactive toward a wide range of Lewis bases¹⁰ and serve as catalysts for the polymerization of isobutylene.⁴ Additionally, cooperative reactivity has been shown with a gallium(III) centre, demonstrating the ability of gallium compounds with differing oxidation states to act similar to transition metals.¹¹

* Reproduced with permission from “Synthesis and Characterization of Cationic Low-Valent Gallium Complexes of Cryptand[2.2.2].” J. L. Bourque, P. D. Boyle, K. M. Baines, *Chem. Eur. J.*, **2015**, *21*, 9790-9796, Copyright 2015 John Wiley and Sons.



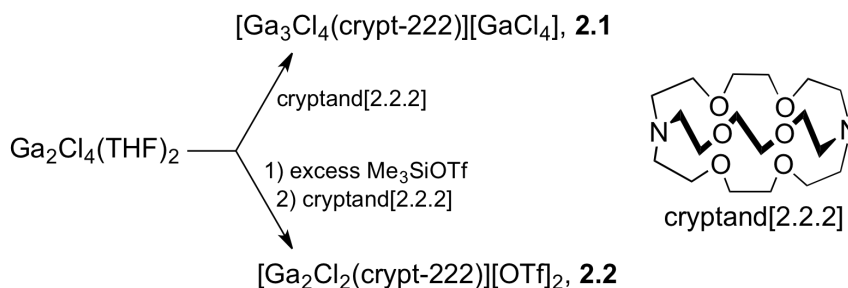
Scheme 2.1: Various gallium(I) cations.

We have used macrocyclic ethers, including cryptand[2.2.2] (Scheme 2.2), as stabilizing ligands for low valent main group cations. A germanium(II) dication was encapsulated within cryptand[2.2.2],¹² and several germanium(II) complexes of crown ethers have been isolated.¹³ Cryptand[2.2.2] has also been used in the complexation of tin(II) cations.¹⁴ The encapsulation of low valent gallium cations in cryptand[2.2.2] was therefore targeted, with the long term goal of comparing the reactivity of synthesized derivatives with other low valent gallium complexes, and Group 14-cryptand[2.2.2] complexes.

2.2 Results and Discussion

Cryptand[2.2.2] was added to $\text{Ga}_2\text{Cl}_4(\text{THF})_2$,¹⁵ both with and without Me_3SiOTf as a co-reagent (Scheme 2.2). The addition of $\text{Ga}_2\text{Cl}_4(\text{THF})_2$ to cryptand[2.2.2] in THF resulted in the precipitation of an off-white solid, **2.1**. The ^1H and $^{13}\text{C}\{^1\text{H}\}$ NMR spectroscopic data of **2.1** indicated that one asymmetric product was present; the $^{13}\text{C}\{^1\text{H}\}$ spectrum revealed 18 signals, corresponding to the number of carbon atoms in cryptand[2.2.2]. The ^{71}Ga NMR spectrum of **2.1** exhibited one signal at 251.2 ppm,

consistent with the tetrachlorogallate anion¹⁶ and the ESI-MS of **2.1** revealed two clusters of signals, one corresponding to $[\text{Ga}(\text{crypt-222})]^+$ and another corresponding to $[\text{Ga}_3\text{Cl}_4(\text{crypt-222})]^+$.



Scheme 2.2: Synthesis of gallium-cryptand[2.2.2] complexes.

The molecular structure of **2.1** was determined to be $[\text{Ga}_3\text{Cl}_4(\text{crypt-222})][\text{GaCl}_4] \cdot \text{CH}_3\text{CN}$, with a molecule of acetonitrile incorporated into the structure resulting from its use as the recrystallization solvent. The solid-state structure of the cation is shown in Figure 2.1 (**Table 2.3**). The trigallium-cryptand[2.2.2] complex with its $[\text{Ga}_2\text{Cl}]^+$ core represents the first example of a salt containing multiple metal ions within the cryptand[2.2.2] cavity. Three gallium centres are present in the cation: Ga(1) is located outside the cavity of the cryptand, has three chlorides attached and a bond to Ga(2); Ga(2) is coordinated by an oxygen and a nitrogen atom of the cryptand and is bound to both Ga(1) and Ga(3); and Ga(3), which has one chloride ligand and an interaction with a nitrogen and oxygen of the cryptand. The closest gallium-anion and -solvent contacts are 4.9098(9) Å and 6.344(3) Å, respectively, indicating that the compound is an isolated ionic pair with no unusually close interactions between the cation and other species present in the asymmetric unit.

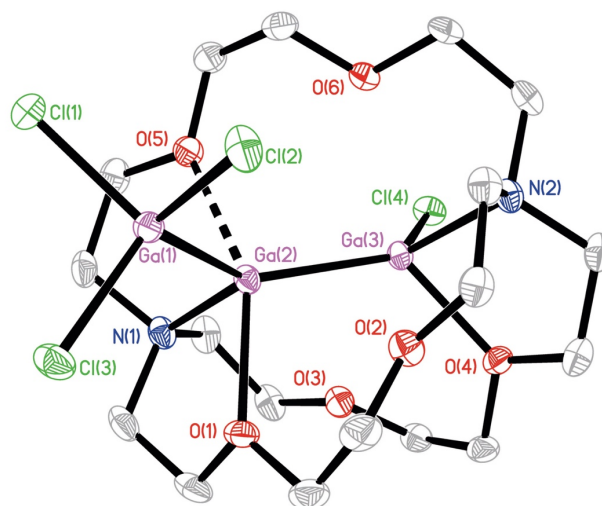


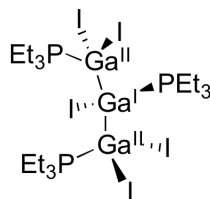
Figure 2.1: Displacement ellipsoid plot of the cation of **2.1**. Ellipsoids are at the 50% probability level and hydrogen atoms were omitted for clarity.

The crystallographic data are listed in Table 2.1. Both the Ga(1)-Ga(2) (2.4232(5) Å) and Ga(2)-Ga(3) (2.4087(5) Å) bond lengths are shorter than the sum of the covalent radii (covalent radius of Ga = 1.24 Å)¹⁷ and fall within the range observed in related donor-stabilized gallium complexes (2.390(2) to 2.4467(4) Å).¹⁸ For example, the Ga-Ga bond length of Ga₂Cl₄(1,4-dioxane)₂ is 2.406(1) Å.¹⁹ The bond angles between the nitrogen and oxygen atoms at Ga(2) and Ga(3) are less than 90° (N(1)-Ga(2)-O(1) 79.38(9)°, N(2)-Ga(3)-O(4) 80.43(9)°) and most of the remaining angles (N-Ga-X, X = Ga, Cl) are larger than 110° (i.e. N(1)-Ga(2)-Ga(3) 111.69(7)°, N(2)-Ga(3)-Ga(2) 117.41(7)°). While Ga(1) is in a tetrahedral environment and sp³ hybridized, Ga(2) is distorted trigonal bipyramidal in geometry. Ga(2) lies in a plane containing Ga(1), Ga(3) and N(1) (sum of the angles around Ga(2) = 358.8°, displacement from plane = 0.1429(8) Å); O(1) and O(5) occupy the axial positions and coordinate to Ga(2). Ga(3) is in distorted trigonal monopyramidal geometry and lies in a distorted plane containing Ga(2), N(2) and Cl(4) (sum of the angles = 350.4°, displacement from plane = 0.4005(9) Å) and is coordinated by O(4).

Table 2.1: Bond lengths (Å) and angles (°) around the gallium centres of **2.1**.

Parameter	Ga(1)	Ga(2)	Ga(3)
Ga-Ga		2.4232(5)	2.4087(5)
Ga-Cl	2.2349(9)		2.2150(8)
Ga-N		2.100(2)	2.104(2)
Ga-O		2.2153(19)	2.1053(19)
Ga...O		2.391(2)	
Ga-Ga-Ga		136.667(18)	
O-Ga-N		79.38(9)	80.43(9)
N-Ga-Ga	110.45(7)		111.69(7)
Cl-Ga-Ga			128.51(3)
N-Ga-Ga-N			179.2(1)

Upon a survey of the literature, very few structures are similar to **2.1**. One compound, $\text{Ga}_3\text{I}_5(\text{PEt}_3)_3$, has a trigallium fragment stabilized by neutral phosphine ligands, however, the bonding in this structure is more obvious than in **2.1**. The gallium-gallium bond lengths in $\text{Ga}_3\text{I}_5(\text{PEt}_3)_3$ are similar to those in **2.1** at 2.451(1) Å and 2.460(1) Å. In $\text{Ga}_3\text{I}_5(\text{PEt}_3)_3$, the terminal gallium atoms are in the +2 oxidation state each with two iodide ligands and the central gallium is in the +1 oxidation state with covalent bonds to an iodide ligand and to the other gallium atoms (Figure 2.2).²⁰ This contrasts the $[\text{Ga}_3\text{Cl}_4]^+$ fragment in **2.1**, as the terminal atoms appear to be in different oxidation states, and Ga(2) does not possess any halide ligands. Furthermore, the presence of the GaCl_3 fragment in **2.1** allows for much variability in terms of its bonding description.

**Figure 2.2:** $\text{Ga}_3\text{I}_5(\text{PEt}_3)_3$.

The reaction of $\text{Ga}_2\text{Cl}_4(\text{THF})_2$ with a large excess of Me_3SiOTf , followed by the addition of cryptand[2.2.2] yielded an off-white precipitate, **2.2**, that was purified by

recrystallization. **2.2** was characterized using multinuclear NMR spectroscopy, ESI-MS and elemental analysis. The ^1H NMR spectrum of **2.2** revealed numerous overlapping complex multiplets, however, the $^{13}\text{C}\{^1\text{H}\}$ NMR spectrum exhibited only nine signals, indicating that **2.2** possessed 2-fold symmetry. The ^{19}F NMR spectrum of **2.2** revealed the presence of triflate as the counter-anion.^{13a,21} The ESI-MS of **2.2** revealed a cationic fragment corresponding to $([\text{Ga}_2\text{Cl}_2(\text{crypt-222})][\text{OTf})]^+$.

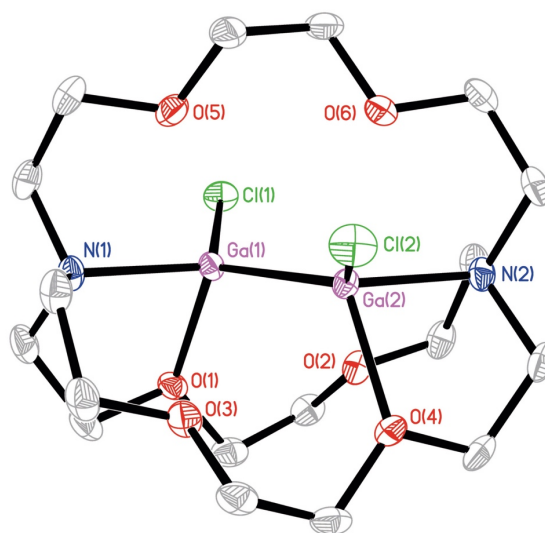


Figure 2.3: Displacement ellipsoid plot of the cation of **2.2**. Ellipsoids are at the 50% probability level and the disordered backbone and hydrogen atoms were omitted for clarity.

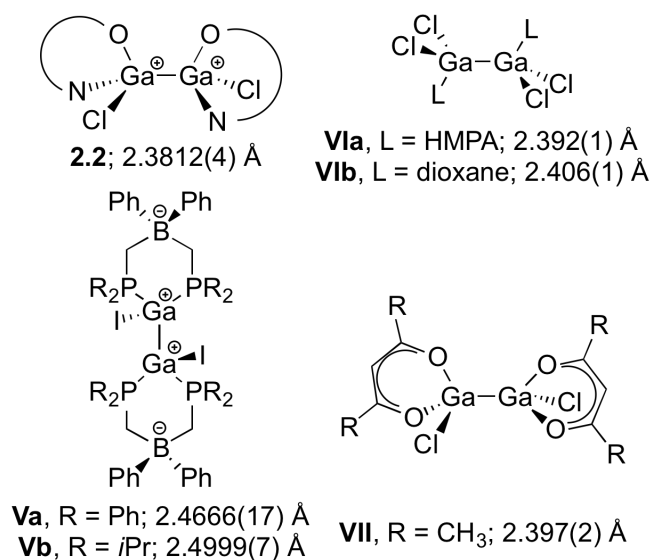
The solid-state structure of the cation of $[\text{Ga}_2\text{Cl}_2(\text{crypt-222})][\text{OTf}]_2\cdot\text{CH}_3\text{CN}$ (**2.2**) is shown in Figure 2.3 (Table 2.3). As with **2.1**, a molecule of acetonitrile was incorporated into the structure from its use as the solvent. The molecule contains a $[\text{Ga}_2\text{Cl}_2]^{2+}$ fragment encapsulated within the cryptand cavity. While **2.2** has 2-fold symmetry in the solution state, the gallium centres are not crystallographically equivalent as the cation crystallizes on a general position (Table 2.2). The $[\text{Ga}_2\text{Cl}_2]^{2+}$ fragment is partially eclipsed, with a torsion angle between O(1) and O(4) of $-10.70(6)^\circ$. As with **2.1**, angles of approximately 90° were observed for the nitrogen- and chlorine-gallium-oxygen

angles. The remaining angles were obtuse ($\sim 120^\circ$ for Cl-Ga-X, X = Ga, N) (Table 2.2). The gallium centres are in distorted trigonal monopyramidal environments with each gallium lying in a plane consisting of the attached gallium, nitrogen and chlorine atoms (sum of the angles at Ga(1) = 356.0° , displacement from plane = $0.2542(6)$ Å; Ga(2) = 355.0° , $0.2850(6)$ Å). An oxygen atom of the cryptand coordinates nearly perpendicular to the aforementioned plane at each gallium. As with **2.1**, the cation of **2.2** did not have any interactions with the anions or the solvent present in the asymmetric unit, as the closest contacts were found to be $4.230(2)$ Å and $5.180(3)$ Å, respectively.

Table 2.2: Bond lengths and angles around the gallium centres of **2.2**.

Parameter	Ga(1)	Ga(2)
Ga-Ga	2.3812(4) Å	
Ga-Cl	2.1889(6) Å	2.1867(6) Å
Ga-N	2.0599(17) Å	2.0584(17) Å
Ga-O	2.1272(14) Å	2.0894(13) Å
O-Ga-N	80.61(6)°	81.78(6)°
O-Ga-Cl	91.47(4)°	91.45(4)°
O-Ga-Ga	114.91(4)°	115.60(4)°
N-Ga-Cl	110.07(5)°	108.30(5)°
N-Ga-Ga	122.78(4)°	121.96(5)°
Cl-Ga-Ga	123.19(2)°	124.76(2)°

Complex **2.2** has a Ga-Ga bond length of $2.3812(4)$ Å. The Ga-Ga bond lengths of structurally similar complexes are shown in Scheme 2.3. Complexes with a $[\text{Ga}_2\text{I}_2]^{2+}$ core stabilized by bidentate phosphine ligands (Scheme 2.3; **Va**, **Vb**),²² coordinating solvent molecules (Scheme 2.3; **Via**, **Vib**),^{18b,c,e,f,h,19,23} and with anionic acetylacetonato ligands (Scheme 2.3; **VII**)²⁴ have Ga-Ga bond lengths that were significantly longer than that found in **2.2** ($2.3812(4)$ Å for **2.2** versus $2.392(1)$ Å and longer for **V** - **VII**). Most gallium complexes with similar bond lengths contain bulky organic ligands,²⁵ or multidentate anionic nitrogen ligands, highlighting the novelty of compound **2.2**.²⁶ The short gallium-gallium bond length is postulated to arise from the steric constraints imposed by the cryptand moiety.



Scheme 2.3: Gallium-gallium bond lengths in complexes similar to **2.2**.

The number of equivalents of Me₃SiOTf was varied to determine its effect on the outcome of the reaction. When one equivalent of Me₃SiOTf was used, the digallium-cryptand[2.2.2] dication was obtained with one of the triflate counter-anions replaced by a tetrachlorogallate, giving [Ga₂Cl₂(crypt-222)][OTf][GaCl₄]•C₆H₆ (Figure A.1, **2.2a**) from recrystallization in benzene. Similar metrical parameters to **2.2** were observed (Table A.1). Another crystal from the same reaction mixture was identified as [Ga₃Cl₄(crypt-222)][OTf]•CH₃CN (**2.1a**) by X-ray diffraction using acetonitrile as the crystallization solvent, although the structure was not fully refined due to the compositionally disordered nature of the crystal. When four equivalents of Me₃SiOTf were used in the reaction, an off-white solid was isolated. While the single crystals obtained corresponded to **2.2**, the ⁷¹Ga NMR spectrum revealed a signal corresponding to [GaCl₄]⁻. This was corroborated by negative ion ESI-MS, as both triflate and tetrachlorogallate anions were detected (*m/z* 149 and *m/z* 211, respectively). The composition of the bulk material was confirmed by elemental analysis and ¹⁹F NMR spectroscopy, giving an approximate composition of [Ga₂Cl₂(crypt-222)][OTf]_{1.5}[GaCl₄]_{0.5} for the bulk material.

Table 2.3: Crystallographic details for **2.1** and **2.2**.

	2.1•CH₃CN	2.2•CH₃CN
Formula	C ₁₈ H ₃₆ Cl ₈ Ga ₄ N ₂ O ₆ •CH ₃ CN	C ₂₀ H ₃₆ Cl ₂ F ₆ Ga ₂ N ₂ O ₁₂ S ₂ •CH ₃ CN
M _r (g mol ⁻¹)	980.02	926.02
Crystal Size (mm)	0.124 × 0.114 × 0.043	0.223 × 0.190 × 0.151
Crystal Colour/Habit	colourless plate	colourless prism
Crystal System	orthorhombic	monoclinic
Space Group	P b c a	P 2 ₁ /n
Temperature, K	110	110
a, Å	15.0894(19)	12.472(2)
b, Å	14.0250(19)	14.155(3)
c, Å	34.032(6)	20.098(4)
α, °	90	90
β, °	90	97.481(7)
γ, °	90	90
V, Å ³	7202.2(18)	3517.9(11)
Z	8	4
F(000)	3904	1880
ρ (g/cm ³)	1.808	1.748
λ, Å	1.54178 (CuKα)	0.71073 (MoKα)
μ, cm ⁻¹	9.202	1.894
Diffractometer Type	Nonius KappaCCD Apex2	Bruker Kappa Axis Apex2
Max 2θ for Data Collection, °	136.664	72.718
Measd Fraction of Data	0.992	0.997
No. Rflns Measd	68936	55091
Unique Rflns Measd	6485	42012
R _{merge}	0.0807	0.0590
No. Rflns in Refinement	6485	42012
R ₁	0.0271	0.0469
wR ₂	0.0548	0.0973
R ₁ (all data)	0.414	0.0993
wR ₂ (all data)	0.0595	0.1142
GOF	1.024	1.040
Min, Max Peak Heights on final ΔF map (e/Å)	-0.347, 0.445	-1.022, 1.183

Where: $R_1 = \Sigma(|F_o| - |F_c|) / \Sigma F_o$; $wR_2 = [\Sigma(w(F_o^2 - F_c^2)^2) / \Sigma(wF_o^4)]^{1/2}$; $GOF = [\Sigma(w(F_o^2 - F_c^2)^2) / (\text{No. of reflns.} - \text{No. of params.})]^{1/2}$

Computational studies were undertaken to explore the electronic structures of **2.1** and **2.2**. Atomic charge methods were used to determine the best description of the bonding in both cations. Natural bond orbital (NBO)²⁷ methods have been used previously in our group¹² and to ensure consistency, CM5²⁸ methods were also employed.

The highest atomic charge for **2.1** is located on Ga(3) (NBO 1.00; CM5 0.27), however, significant residual charges are present on Ga(1) (NBO 0.50; CM5 0.20) and Ga(2) (NBO 0.78; CM5 0.13) (Figure 2.5). The coefficients of the significant bonding pairs for the $[\text{Ga}_3\text{Cl}_4]^+$ fragment were also located and suggested that the Ga-Ga bonds are slightly polarized and the gallium-heteroatom bonds are Lewis donor-acceptor interactions. Interestingly, a bonding electron pair was not found between Ga(2) and O(1). A comparison of the Ga(2)-O(1) bond length to the Ga(3)-O(4) bond length (2.215(2) Å and 2.105(2) Å, respectively) suggested that the NBO was not identified due to the greater distance between Ga(2) and O(1).

Bond orders were also obtained from the NBO analysis (Table 2.4). The Wiberg bond indices (WBI) for the Ga-Ga bonds of **2.1** are slightly below 1 (0.80, 0.84), however, the values suggest that the interactions are on the order of two-centre-two-electron bonds. This is also reflected in the atom-atom overlap-weighted natural atomic orbital (NAO) bond orders (0.84, 0.99). The bond orders between the cryptand heteroatoms and the gallium centres (Wiberg: 0.13 – 0.20; NAO: 0.06 – 0.21) were, for the most part, slightly higher than those calculated for $[\text{Ge}(\text{crypt-222})][\text{OTf}]_2$ which ranged from 0.10 to 0.11. The higher bond orders can be rationalized given that the single germanium cation is stabilized by all eight heteroatoms in $[\text{Ge}(\text{crypt-222})][\text{OTf}]_2$, whereas in **2.1**, only two heteroatoms are contributing electron density to each gallium.¹² Additionally, the lower bond order value for the Ga(2)-O(1) interaction is consistent with the absence of an NBO bonding pair. The frontier molecular orbitals of **2.1** were calculated and plotted (Figure 2.4). The lowest lying unoccupied orbitals were not located on the gallium core. The HOMO and HOMO-7 were delocalized on the core with the HOMO having a node at Ga(2), with significant contributions from the chlorine atoms of the cation, and minimal interactions from the nitrogen and oxygen atoms of the cryptand.

Table 2.4: Wiberg bond indices and atom-atom overlap-weighted NAO bond orders for **2.1**.

Bond	Wiberg Bond Index	Atom-Atom Overlap-Weighted NAO Bond Order
Ga1-Ga2	0.80	0.84
Ga2-Ga3	0.84	0.99
Ga2-N1	0.18	0.16
Ga2-O1	0.13	0.06
Ga3-N2	0.20	0.21
Ga3-O4	0.16	0.14

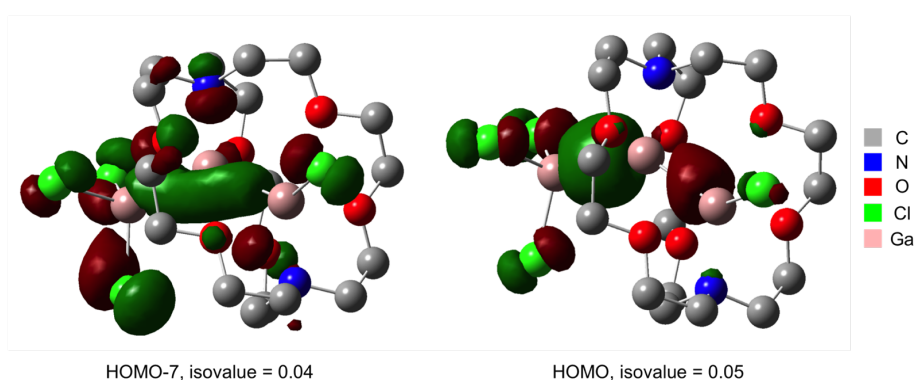


Figure 2.4: HOMO and HOMO-7 of the cation of **2.1**.

On the basis of the experimental and computational data for **2.1**, we put forward three possible and reasonable bonding descriptors for the $[\text{Ga}_3\text{Cl}_4]^+$ core of **2.1** (Figure 2.5).²⁹ The available data suggest that model **C** most accurately reflects the bonding of **2.1**; however, additional calculations and reactivity studies may reveal that descriptor **B** provides better insight into the electronic structure of **2.1**.³⁰

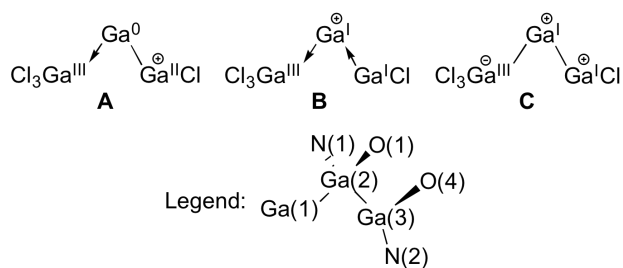


Figure 2.5: Proposed bonding models for the $[\text{Ga}_3\text{Cl}_4]^+$ core of **2.1**.

The NBO- and CM5-calculated atomic charges of **2.2** are approximately +1 on each gallium (Ga(1): NBO, + 1.02; CM5, + 0.31; Ga(2): NBO, + 1.03; CM5, + 0.31) and the gallium-gallium bond has a bond order approaching 1, suggesting the presence of a two-centre-two-electron bond (Table 2.5). The magnitude of the bond orders for the gallium-cryptand[2.2.2] interactions were larger in **2.2** compared to those in **2.1**, possibly due to the higher electron deficiency of the gallium core, or the core being less sterically congested, allowing for stronger interactions. The frontier molecular orbitals of **2.2** were calculated and plotted (Figure 2.6). The HOMO of **2.2** corresponds to a bonding interaction between the two gallium atoms of the core, whereas the LUMO corresponds to the anti-bonding interaction. As with **2.1**, while the chlorine atoms of the $[\text{Ga}_2\text{Cl}_2]^{2+}$ core are involved in both the HOMO and LUMO, the heteroatoms of the cryptand are not contributing to the frontier molecular orbitals. Time-dependent density functional theory (TD-DFT) calculations demonstrated that the HOMO-LUMO gap is 5.81 eV (213 nm), which is larger than other main group systems that have demonstrated reactivity toward small molecules.³¹ From the computational data obtained for **2.2**, a single bonding description is proposed, with two equivalent gallium centres, both formally cationic and in the +2 oxidation state. The bonding in **2.2** can, therefore, be interpreted as a dicationic digallane.

Table 2.5: Wiberg bond indices and overlap-weighted NAO bond orders for **2.2**.

Bond	Wiberg Bond Index	Atom-Atom Overlap-Weighted NAO Bond Order
Ga1-Ga2	0.89	1.00
Ga1-N1	0.26	0.27
Ga1-O1	0.20	0.19
Ga2-N2	0.26	0.27
Ga2-O4	0.20	0.19

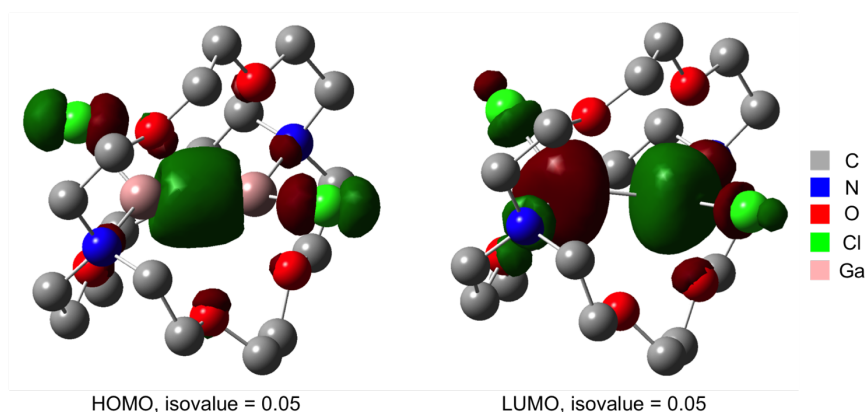


Figure 2.6: HOMO and LUMO of the cation of **2.2**.

2.3 Conclusions

In conclusion, we have demonstrated the synthesis and characterization of the first low valent gallium-cryptand[2.2.2] complexes which are also the first bimetallic cationic cryptand[2.2.2] complexes. The complexes were analyzed using computational methods to evaluate the electronic structures of both cations. Experimental studies, including X-ray photoelectron spectroscopy (XPS), will be employed to assess the proposed oxidation states for the gallium atoms of **2.1** and **2.2**. Complexes **2.1** and **2.2** possess unique, low valent Ga₂ fragments with weak interactions to the cryptand ligand; the mechanism for the formation and the reactivity of these novel species will be the subject of further studies.

2.4 Experimental

2.4.1 General Considerations

All manipulations were performed under an inert atmosphere of argon using Schlenk techniques or under an atmosphere of nitrogen in an MBraun glovebox unless otherwise stated. All solvents were purified using an Innovative Technologies 400-5 Solvent Purification System and were stored over activated 3 or 4 Å molecular sieves, unless otherwise stated. CD₃CN was dried over activated 3 Å molecular sieves. All

reagents were used as received from Sigma-Aldrich, Alfa Aesar, Strem Chemicals or Gelest. Ga₂Cl₄³² was synthesized according to the literature procedures. NMR spectra were recorded on a Varian INOVA I600 (¹H 600 MHz; ¹³C 151 MHz; ⁷¹Ga 183 MHz) or a Varian INOVA I400 FT-NMR (¹⁹F 376 MHz) spectrometer. Chemical shifts (δ) are reported in ppm and were internally referenced to the residual protonated solvent peaks for ¹H spectra (1.94 ppm for CD₂H₂CN), and the deuterated solvent for ¹³C (118.69 ppm for CD₃CN). ¹⁹F NMR spectra were referenced to CFCl₃ (0.0 ppm) using the internal lock signal from the deuterated solvent and to Ga(NO₃)₃ (0.0 ppm) in D₂O for ⁷¹Ga spectra. Coupling constants (J) are reported in Hz and multiplicities are reported as singlet (s), doublet (d), triplet (t), quartet (q), multiplet (m), broad (br) and overlapping (ov). ¹H and ¹³C NMR assignments were confirmed using two-dimensional techniques (gCOSY, gHSQC, gHMBC). Electrospray ionization mass spectra were collected using a Bruker micrOTOF II spectrometer. Mass spectral data are reported in mass-to-charge units (m/z). Elemental analyses were performed by Laboratoire d'Analyse Élémentaire de l'Université de Montréal (Montréal, QC). X-ray crystallographic data were collected by Dr. Paul Boyle, and by JLB under the supervision of Dr. Boyle.

2.4.2 Synthesis of **2.1**

A solution of cryptand[2.2.2] (0.12 g, 0.32 mmol) dissolved in THF (1 mL) was added dropwise to a solution of Ga₂Cl₄ (0.090 g, 0.32 mmol) dissolved in THF (2 mL). The mixture was allowed to stir for 18 hours, at which point a yellow precipitate had formed. The solution was centrifuged and decanted, the precipitate was washed with THF (5 mL), and dried under reduced pressure, yielding an off-white solid. Purification was unsuccessful due to the low solubility of **2.1** in various solvents. X-ray quality single crystals were grown from a supersaturated solution of **2.1** in CD₃CN in an NMR tube.

Yield : 0.065 g (43 %); mp: 274 – 276 °C (decomposition); ¹H NMR (600 MHz, CD₃CN, 298 K; poorly soluble) δ : 4.32 (td, J = 2 Hz, 11 Hz, 1H, CHO), 4.28 (td, J = 4 Hz, 7 Hz, 1H, CHO), 4.18 – 4.00 (m, 6H, CHO, CHN), 3.99 – 3.61 (m, 20H, CHO, CHN), 3.44 – 3.25 (m, 4H, CHN), 3.09 (dd, J = 4 Hz, 12 Hz, 1H, CHN), 2.99 – 2.95 (m, 1H, CHN),

2.79 (dt, $J = 3$ Hz, 13 Hz, 1H, CHN), 2.77 – 2.72 (m, 1H, CHN); $^{13}\text{C}\{^1\text{H}\}$ NMR (151 MHz, CD_3CN , 298 K) δ : 73.65 (CH_2O), 73.45 (CH_2O), 72.61 (CH_2O), 71.63 (CH_2O), 70.78 (CH_2O), 70.03 (CH_2O), 68.78 (CH_2O), 67.62 (CH_2O), 67.01 (CH_2O), 66.95 (CH_2O), 66.86 (CH_2O), 66.56 (CH_2O), 62.78 (CH_2N), 60.85 (CH_2N), 57.68 (CH_2N), 56.52 (CH_2N), 56.45 (CH_2N), 55.70 (CH_2N); $^{71}\text{Ga}\{^1\text{H}\}$ (183 MHz, CD_3CN , 298 K) δ : 251.6 ($[\text{GaCl}_4]$); LR ESI-TOF MS (m/z ; positive ion): 445 ($[\text{Ga}(\text{crypt-222})]^+$); 723 ($[\text{Ga}_3^{35}\text{Cl}_4(\text{crypt-222})]^+$); HR ESI-TOF MS (m/z ; positive ion): Calcd. for $\text{C}_{18}\text{H}_{36}\text{N}_2\text{O}_6\text{Ga}_3^{35}\text{Cl}_4^+$ ($[\text{Ga}_3\text{Cl}_4(\text{crypt-222})]^+$): 722.9095, Found: 722.9123; Elemental analysis data calcd. (%) for $[\text{Ga}_3\text{Cl}_4(\text{crypt-222})][\text{GaCl}_4]$ ($\text{C}_{18}\text{H}_{36}\text{Cl}_8\text{Ga}_4\text{O}_6\text{N}_2$): C, 23.02; H, 3.86; N, 2.98; found C, 22.68; H, 3.78; N, 2.76.

2.4.3 Synthesis of **2.2**

Solid Ga_2Cl_4 (0.141 g, 0.500 mmol) was dissolved in THF (4 mL). The solution turned yellow, and was allowed to stir for 1 hour, at which point the solvent was removed under reduced pressure. Toluene (4 mL) was added to the reaction flask, along with THF (1 drop), followed by a solution of Me_3SiOTf (0.889 g, 4.00 mmol) dissolved in toluene (2 mL). The mixture was allowed to stir for 2 hours, at which point a solution of cryptand[2.2.2] (0.188 g, 0.500 mmol) dissolved in toluene (2 mL) was added, leading to the immediate formation of a white precipitate. The mixture was allowed to stir for 36 hours, after which a green-grey oil had separated in the vessel. The supernatant was decanted, and the oil was triturated in CH_3CN (3 mL). A metallic-like solid was removed by filtration, and the filtrate was concentrated under reduced pressure. The concentrated solution was then placed in a vapour diffusion system with THF, which was kept at room temperature for several days, after which the $\text{CH}_3\text{CN}/\text{THF}$ mixture was cooled to -20 °C. X-ray diffraction quality crystals of **2.2** were obtained, as an off-white solid. Both the bulk product and the crystalline material demonstrated identical spectroscopic characteristics.

Yield: 0.17 g (38 %); mp: 279 – 282 °C (decomposition); ^1H NMR (600 MHz, CD_3CN , 298 K)³³ δ : 4.17 – 4.14 (m, 2H, $[\text{O}-\text{CH}_2-\text{CH}_2-\text{O}]_{\text{coord}}$), 4.13 – 4.12 (m, 4H, $[\text{O}-\text{CH}_2-\text{CH}_2-\text{O}]_{\text{free}}$), 4.11 – 4.08 (m, 2H, $[\text{O}-\text{CH}_2-\text{CH}_2-\text{N}]_{\text{coord}}$), 4.07 – 4.06 (m, 2H, $[\text{O}-\text{CH}_2-\text{CH}_2-$

$N]_{\text{free}}$), 4.05 – 4.03 (m, 2H, $[O-CH_2-CH_2-N]_{\text{free}}$), 4.03 – 4.00 (m, 2H, $[O-CH_2-CH_2-O]_{\text{coord}}$), 3.99 – 3.94 (m, 2H, $[O-CH_2-CH_2-N]_{\text{coord}}$), 3.83 – 3.81 (m, 2H, $[O-CH_2-CH_2-N]_{\text{coord}}$), 3.80 – 3.78 (m, 4H, $[O-CH_2-CH_2-O]_{\text{coord}}$), 3.77 – 3.75 (m, 2H, $[O-CH_2-CH_2-N]_{\text{coord}}$), 3.69 (td, $J = 6$ Hz, 13 Hz, 2H, $[O-CH_2-CH_2-N]_{\text{coord}}$), 3.65 – 3.59 (m, 2H, $[O-CH_2-CH_2-N]_{\text{coord}}$), 3.49 (ddd, $J = 2$ Hz, 4 Hz, 14 Hz, 2H, $[O-CH_2-CH_2-N]_{\text{free}}$), 3.34 (dddd, $J = 1$ Hz, 7 Hz, 12 Hz, 16 Hz, 2H, $[O-CH_2-CH_2-N]_{\text{free}}$), 3.17 (dd, $J = 3$ Hz, 13 Hz, 2H, $[O-CH_2-CH_2-N]_{\text{coord}}$), 2.97 (dt, $J = 3$ Hz, 14 Hz, 2H, $[O-CH_2-CH_2-N]_{\text{coord}}$); $^{13}\text{C}\{^1\text{H}\}$ NMR (151 MHz, CD_3CN , 298 K) δ : 122.52 (q, $J = 321$ Hz, $[\text{F}_3\text{CSO}_3]^-$), 74.44 ($[O-CH_2-CH_2-O]_{\text{free}}$), 72.34 ($[O-CH_2-CH_2-O]_{\text{coord}}$), 70.55 ($[O-CH_2-CH_2-N]_{\text{free}}$), 68.20 ($[O-CH_2-CH_2-O]_{\text{coord}}$), 66.60 ($[O-CH_2-CH_2-N]_{\text{coord}}$), 66.55 ($[O-CH_2-CH_2-N]_{\text{coord}}$), 60.54 ($[O-CH_2-CH_2-N]_{\text{coord}}$), 56.53 ($[O-CH_2-CH_2-N]_{\text{coord}}$), 55.50 ($[O-CH_2-CH_2-N]_{\text{free}}$); ^{19}F NMR (376 MHz, CD_3CN , 298 K) δ : -79.4 ($^-\text{O}_3\text{SCF}_3$); $^{71}\text{Ga}\{^1\text{H}\}$ (183 MHz, CD_3CN , 298 K) δ : no signal observed; LR ESI-TOF MS (m/z ; positive ions): 629 $[[^{69}\text{Ga}^{35}\text{Cl}(\text{crypt-222})][\text{OTf}]^+]$; 733 $[[^{69}\text{Ga}_2^{35}\text{Cl}_2(\text{crypt-222})][\text{OTf}]^+]$; LR ESI-TOF MS (m/z ; negative ion): 149 ($[\text{OTf}]^-$); HR ESI-TOF MS (m/z ; positive ion): Calcd. for $\text{C}_{19}\text{H}_{36}\text{F}_3\text{N}_2\text{O}_9\text{S}^{35}\text{Cl}_2^{69}\text{Ga}_2$ $[[\text{Ga}_2\text{Cl}_2(\text{crypt-222})][\text{OTf}]^+]$: 732.9982, Found: 732.9981; Elemental analysis data calcd. (%) for $[\text{Ga}_2\text{Cl}_2(\text{crypt-222})][\text{OTf}]_2 \cdot \text{CH}_3\text{CN}$ ($\text{C}_{20}\text{H}_{39}\text{Cl}_2\text{F}_6\text{Ga}_2\text{O}_{12}\text{N}_3\text{S}_2$): C, 28.53; H, 4.24; N, 4.54; S, 6.93; found C, 28.41; H, 4.17; N, 4.41; S, 7.10.

2.4.4 Synthesis of **2.2a**

X-ray quality crystals of **2.2a** were obtained from the reaction mixture of $\text{Ga}_2\text{Cl}_4(\text{THF})_2$ with 1 equivalent of Me_3SiOTf and 0.5 equivalents of cryptand[2.2.2]. Bulk isolation of **2.2a** was not possible, as different batches of crystals also yielded the trigallium cation found in **2.1**, and did not represent the bulk composition of the crystalline material.

2.4.5 X-ray Crystallography – General Procedures

Data Collection and Processing: The samples were mounted on a MiTeGen polyimide micromount with a small amount of Paratone N oil. All X-ray measurements were made

on either a Bruker Kappa Axis Apex2 or a Nonius KappaCCD Apex2 diffractometer at a temperature of 110 K.

Structure Solution and Refinement: The structures were solved by using a dual space methodology using the SHELXT program.³⁴ All non-hydrogen atoms were obtained from the initial solution. The hydrogen atoms were introduced at idealized positions and were allowed to ride on the parent atom. The structural model was fit to the data using full matrix least-squares based on F^2 . The calculated structure factors included corrections for anomalous dispersion from the usual tabulation. The structures were refined using the SHELXL-2014 program from the Shelx suite of crystallographic software.³⁵ Graphic plots were produced using the XP program from the SHELXTL suite.³⁶ Additional details may be found in Appendix A.

2.4.5.1 X-ray Crystallographic Details for 2.1

Data Collection and Processing: The unit cell dimensions were determined from a symmetry constrained fit of 9952 reflections with $11.62^\circ < 2\theta < 135.32^\circ$. The data collection strategy was a number of ω and ϕ scans which collected data up to 136.664° (2θ). The frame integration was performed using SAINT.³⁷ The resulting raw data were scaled and absorption corrected using a multi-scan averaging of symmetry equivalent data using SADABS.³⁸

2.4.5.2 X-ray Crystallographic Details for 2.2

Data Collection and Processing: The initial indexing indicated the sample crystal was a non-merohedral twin. The twin law was determined to be:

```
Twin Law, Sample 1 of 1
Transforms h1.1(1)->h1.2(2)
  -0.99781  0.00228  0.00983
   0.01175  0.99860  0.03753
  -0.02497  0.07395 -1.00054
```

which corresponds to an approximately 179.1° rotation about [010]. The twin fraction was included in the refinement model, *vide infra*. The unit cell dimensions were

determined from a symmetry constrained fit of 9853 reflections with $5.0^\circ < 2\theta < 67.6^\circ$. The data collection strategy was a number of ω and ϕ scans which collected data up to 72.718° (2θ). The frame integration was performed using SAINT.³⁷ The resulting raw data were scaled and absorption corrected using a multi-scan averaging of symmetry equivalent data using TWINABS.³⁹

Structure Solution and Refinement: There were several disorders present in the structure. The C(15)-C(16) ethylene backbone was disordered over two positions. The normalized occupancy factor for the dominant conformer refined to a value of 0.905(7). The second disorder involved the triflate anion containing atom S(1). This disorder arose from the reorientation of the anion giving rise to alternative atom position for all atoms except O(7) and F(2). The normalized occupancy factor for the dominant orientation refined to a value of 0.790(3). The twin fraction refined to a value of 0.07768(19).

2.4.5.3 X-ray Crystallographic Details for **2.2a**

Data Collection and Processing: The unit cell dimensions were determined from a symmetry constrained fit of 9852 reflections with $5.4^\circ < 2\theta < 54.78^\circ$. The data collection strategy was a number of ω and ϕ scans which collected data up to 63.216° (2θ). The frame integration was performed using SAINT.³⁷ The resulting raw data were scaled and absorption corrected using a multi-scan averaging of symmetry equivalent data using SADABS.³⁸

Structure Solution and Refinement: The structure exhibited two disorders, one in the $[\text{GaCl}_4]^-$ anion, and the other in the triflate anion. The $[\text{GaCl}_4]^-$ anion was disordered over two orientations related by a rotation about the Ga(3)-Cl(4) bond by approximately 8.2° . The normalized occupancy for the major component of this disorder refined to a value of 0.57(3). The triflate anion was disordered giving rise to two distinct CF_3 groups and two distinct O(9) atoms. These were related by a pivot of approximately 27.2° between each CF_3 group and O(9) atom. The normalized occupancy for the major component of this disorder refined to a value of 0.535(9). The asymmetric unit demonstrated a region of disorder, postulated to be a molecule of acetonitrile. Attempts at modeling the electron

density using several restraints were unsuccessful. The data were then subject to the SQUEEZE procedure⁴⁰ as implemented in the PLATON program.⁴¹

2.4.6 Computational Details

All calculations were performed using Gaussian 09⁴² on the Shared Hierarchical Academic Research Computing Network (SHARCNET, www.sharcnet.ca). Computations were run using a single AMD Opteron 2.2 GHz 24 core CPU with 32 GB of memory. All data were obtained using crystallographically determined atomic coordinates. Natural bond orbital calculations were performed using the PBE1PBE functional,⁴³ and the 6-311+G* basis set using NBO Version 3.1,⁴⁴ as implemented in Gaussian 09. Molecular orbital calculations were performed using normal population method, using the M06 functional,⁴⁵ and the 6-311+G* basis set. Cube files were generated using the cubegen utility included in Gaussian 09, and visualized in GaussView 3.09. The HOMO-LUMO gap was calculated using the time-dependent DFT method,⁴⁶ using the same functional and basis set as used for the population analysis.

2.5 References

- [1] Hardman, N.J.; Power, P.P.; Gordon, J.D.; Macdonald, C.L.B.; Cowley, A.H. *Chem. Commun.* **2001**, 1866-1867.
- [2] Power, P.P. *Nature* **2010**, *463*, 171-177.
- [3] a) Caputo, C.A.; Zhu, Z.; Brown, Z.D.; Fettingner, J.C.; Power, P.P. *Chem. Commun.* **2011**, *47*, 7506-7508; b) Zhu, Z.; Wang, X.; Peng, Y.; Lei, H.; Fettingner, J.C.; Rivard, E.; Power, P.P. *Angew. Chem., Int. Ed.* **2009**, *48*, 2031-2034.
- [4] a) Lichtenthaler, M.R.; Higelin, A.; Kraft, A.; Hughes, S.; Steffani, A.; Plattner, D.A.; Slattery, J.M.; Krossing, I. *Organometallics* **2013**, *32*, 6725-6735; b) Lichtenthaler, M.R.; Maurer, S.; Mangan, R.J.; Stahl, F.; Monkemeyer, F.; Hamann, J.; Krossing, I. *Chem. Eur. J.* **2015**, *21*, 157-165.
- [5] Garton, G.; Powell, H.M. *J. Inorg. Nucl. Chem.* **1957**, *4*, 84-89.

- [6] a) Schmidbaur, H.; Nowak, R.; Huber, B.; Müller, G. *Polyhedron* **1990**, *9*, 283-287; b) Schmidbaur, H.; Thewalt, U.; Zafiropoulos, T. *Organometallics* **1983**, *2*, 1550-1554; c) Schmidbaur, H.; Thewalt, U.; Zafiropoulos, T. *Angew. Chem., Int. Ed. Engl.* **1984**, *23*, 76-77.
- [7] a) Schmidbaur, H.; Bublak, W.; Huber, B.; Müller, G. *Organometallics* **1986**, *5*, 1647-1651; b) Schmidbaur, H.; Hager, R.; Huber, B.; Müller, G. *Angew. Chem., Int. Ed. Engl.* **1987**, *26*, 338-340.
- [8] Kunze, A.; Gleiter, R.; Bethke, S.; Rominger, F. *Organometallics* **2006**, *25*, 4787-4791.
- [9] Slattery, J.M.; Higelin, A.; Bayer, T.; Krossing, I. *Angew. Chem., Int. Ed.* **2010**, *49*, 3228-3231.
- [10] a) Higelin, A.; Haber, C.; Meier, S.; Krossing, I. *Dalton Trans.* **2012**, *41*, 12011-12015; b) Higelin, A.; Keller, S.; Gohringer, C.; Jones, C.; Krossing, I. *Angew. Chem., Int. Ed.* **2013**, *52*, 4941-4944; c) Higelin, A.; Sachs, U.; Keller, S.; Krossing, I. *Chem. Eur. J.* **2012**, *18*, 10029-10034; d) Lichtenthaler, M.R.; Stahl, F.; Kratzert, D.; Benkml, B.; Wegner, H.A.; Krossing, I. *Eur. J. Inorg. Chem.* **2014**, 4335-4341.
- [11] Abdalla, J.A.B.; Riddlestone, I.M.; Tirfoin, R.; Aldridge, S. *Angew. Chem., Int. Ed.* **2015**, *54*, 5098-5102.
- [12] Rupar, P.A.; Staroverov, V.N.; Baines, K.M. *Science* **2008**, *322*, 1360-1363.
- [13] a) Rupar, P.A.; Bandyopadhyay, R.; Cooper, B.F.T.; Stinchcombe, M.R.; Ragogna, P.J.; Macdonald, C.L.B.; Baines, K.M. *Angew. Chem., Int. Ed.* **2009**, *48*, 5155-5158; b) Bandyopadhyay, R.; Nguyen, J.H.; Swidan, A.; Macdonald, C.L.B. *Angew. Chem., Int. Ed.* **2013**, *52*, 3469-3472.
- [14] Avery, J.C.; Hanson, M.A.; Herber, R.H.; Bladec, K.J.; Rupar, P.A.; Nowik, I.; Huang, Y.; Baines, K.M. *Inorg. Chem.* **2012**, *51*, 7306-7316.
- [15] Schmidt, E.S.; Schier, A.; Mitzel, N.W.; Schmidbaur, H. *Z. Naturforsch., B: Chem. Sci.* **2001**, *56b*, 337-341.
- [16] Harris, R.K.; Mann, B.E. *NMR and the periodic table*, Academic Press, **1978**.

- [17] Pyykko, P.; Atsumi, M. *Chem. Eur. J.* **2009**, *15*, 186-197.
- [18] a) Brown, K.L.; Hall, D. *J. Chem. Soc., Dalton Trans.* **1973**, 1843; b) Duan, T.; Schnöckel, H. *Z. Anorg. Allg. Chem.* **2004**, *630*, 2622-2626; c) Beamish, J.C.; Boardman, A.; Small, R.W.H.; Worrall, I.J. *Polyhedron* **1985**, *4*, 983-987; d) Khan, M.A.; Tuck, D.G.; Taylor, M.J.; Rogers, D.A. *J. Crystallogr. Spectrosc. Res.* **1986**, *16*, 895-905; e) Pashkov, A.Y.; Belsky, V.K.; Butychev, M.; Zvukova, T.M. *Russ. Chem. Bull.* **1996**, *45*, 1973-1976; f) Gordon, E.M.; Hepp, A.F.; Duraj, S.A.; Habash, T.S.; Fanwick, P.E.; Schupp, J.D.; Eckles, W.E.; Long, S. *Inorg. Chim. Acta* **1997**, *257*, 247-251; g) Uhl, W.; Cuypers, L.; Schüler, K.; Spies, T.; Strohmann, C.; Lehmen, K. *Z. Anorg. Allg. Chem.* **2000**, *626*, 1526-1534; h) Nogai, S.D.; Schmidbaur, H. *Organometallics* **2004**, *23*, 5877-5880.
- [19] Beamish, J.C.; Small, R.W.H.; Worrall, I.J. *Inorg. Chem.* **1979**, *18*, 220-223.
- [20] Schnepf, A.; Doriat, C.; Möllhausen, E.; Schnöckel, H. *Chem. Commun.* **1997**, 2111-2112.
- [21] a) Boersma, A.D.; Goff, H.M. *Inorg. Chem.* **1982**, *21*, 581-586; b) Dolbier, W.R. *Guide to Fluorine NMR for Organic Chemists*, Wiley, **2009**.
- [22] Malbrecht, B.J.; Dube, J.W.; Willans, M.J.; Ragona, P.J. *Inorg. Chem.* **2014**, *53*, 9644-9656.
- [23] a) Rickard, C.E.F.; Taylor, M.J.; Kilner, M. *Acta Crystallogr., Sect. C: Cryst. Struct. Commun.* **1999**, *55*, 1215-1216; b) Nogai, S.; Schmidbaur, H. *Inorg. Chem.* **2002**, *41*, 4770-4774; c) Ball, G.E.; Cole, M.L.; McKay, A.I. *Dalton Trans.* **2012**, *41*, 946-952.
- [24] Beachley, Jr., O.T.; Gardinier, J.R.; Churchill, M.R. *Organometallics* **2000**, *19*, 4544-4549.
- [25] Twamley, B.; Power, P.P. *Angew. Chem., Int. Ed.* **2000**, *39*, 3500-3503.
- [26] a) Brown, D.S.; Decken, A.; Cowley, A.H. *J. Am. Chem. Soc.* **1995**, *117*, 5421-5422; b) Yurkerwich, K.; Parkin, G. *J. Cluster Sci.* **2010**, *21*, 225-234.
- [27] a) Foster, J.P.; Weinhold, F. *J. Am. Chem. Soc.* **1980**, *102*, 7211-7218; b) Reed, A.E.; Curtiss, L.A.; Weinhold, F. *Chem. Rev.* **1988**, *88*, 899-926.

- [28] a) Hirshfeld, F.L. *Theor. Chim. Acta* **1977**, *44*, 129-138; b) Marenich, A.V.; Jerome, S.V.; Cramer, C.J.; Truhlar, D.G. *J. Chem. Theory Comput.* **2012**, *8*, 527-541.
- [29] a) Himmel, D.; Krossing, I.; Schnepf, A. *Angew. Chem., Int. Ed.* **2014**, *53*, 370-374; b) Frenking, G. *Angew. Chem., Int. Ed.* **2014**, *53*, 6040-6046; c) Himmel, D.; Krossing, I.; Schnepf, A. *Angew. Chem., Int. Ed.* **2014**, *53*, 6047-6048.
- [30] Minkin, V.I. *Pure Appl. Chem.* **1999**, *71*, 1919-1981.
- [31] Zhu, Z.; Fischer, R.C.; Ellis, B.D.; Rivard, E.; Merrill, W.A.; Olmstead, M.M.; Power, P.P.; Guo, J.D.; Nagase, S.; Pu, L. *Chem. Eur. J.* **2009**, *15*, 5263-5272.
- [32] a) Beamish, J.C.; Wilkinson, M.; Worrall, I.J. *Inorg. Chem.* **1978**, *17*, 2026-2027; b) Schmidt, E.S.; Schier, A.; Schmidbaur, H. *J. Chem. Soc., Dalton Trans.* **2001**, 505-507.
- [33] The subscript "coord" refers to the two arms of cryptand[2.2.2] coordinated to the gallium centres; the subscript "free" refers to the arm of cryptand[2.2.2] that is not coordinated to a gallium centre.
- [34] Sheldrick, G.M. SHELXT, University of Göttingen, 2014.
- [35] Sheldrick, G.M. *Acta Cryst.* **2008**, *A64*, 112-122.
- [36] Bruker-AXS, XP version 2013.1, **2013**, Bruker-AXS, Madison, WI, 53711, USA.
- [37] Bruker-AXS, SAINT version 2013.8, **2013**, Bruker-AXS, Madison, WI, 53711, USA.
- [38] Bruker-AXS, SADABS version 2012.1, **2012**, Bruker-AXS, Madison, WI, 53711, USA.
- [39] Bruker-AXS, TWINABS version 2012.1, **2012**, Bruker-AXS, Madison, WI, 53711, USA.
- [40] van der Sluis, P.; Spek, A.L. *Acta Cryst.* **1990**, *A46*, 194-201.
- [41] Spek, A.L. *J. Appl. Crystallogr.* **2003**, *36*, 7-13.
- [42] Frisch, M.J.; Trucks, G.W.; Schlegel, H.B.; Scuseria, G.; Robb, M.A.; Cheeseman, J.R.; Scalmani, G.; Barone, V.; Mennucci, B.; Petersson, G.A.; Nakatsuji, H.; Caricato, M.; Li, X.; Hratchian, H.P.; Izmaylov, A.F.; Bloino, J.; Zheng, G.;

Sonnenberg, J.L.; Hada, M.; Ehara, M.; Toyota, K.; Fukuda, R.; Hasegawa, J.; Ishida, M.; Nakajima, T.; Honda, Y.; Kitao, O.; Nakai, H.; Vreven, T.; Montgomery, Jr., J.A.; Peralta, J.E.; Ogliaro, F.; Bearpark, M.; Heyd, J.J.; Brothers, E.; Kudin, K.N.; Staroverov, V.N.; Kobayashi, R.; Normand, J.; Raghavachari, K.; Rendell, A.; Burant, J.C.; Iyengar, S.S.; Tomasi, J.; Cossi, M.; Rega, N.; Millam, M.J.; Klene, M.; Knox, J.E.; Cross, J.B.; Bakken, V.; Adamo, C.; Jaramillo, J.; Comperts, R.; Stratmann, R.E.; Yazyev, O.; Austin, A.J.; Cammi, R.; Pomelli, C.; Ochterski, J.W.; Martin, R.L.; K. Morokuma, K.; Zakrzewski, V.G.; Voth, G.A.; Salvador, P.; Dannenberg, J.J.; Dapprich, S.; Daniels, A.D.; Farkas, Ö.; Foresman, J.B.; Ortiz, J.V.; Cioslowski, J.; Fox, D.J.; Gaussian 09, Revision D.01, **2009**, Gaussian, Inc., Wallingford, CT.

[43] Ernzerhof, M.; Perdew, J.P. *J. Chem. Phys.* **1998**, *109*, 3313.

[44] Glendening, E.D.; Reed, A.E.; Carpenter, J.E.; Weinhold, F. NBO Version 3.1.

[45] Zhao, Y.; Truhlar, D.G. *Theor. Chem. Acc.* **2008**, *120*, 215-241.

[46] Bauernschmitt, R.; Ahlrichs, R. *Chem. Phys. Lett.* **1996**, *256*, 454-464.

Chapter 3

3 Resolution of the Chemical State of Molecular Gallium Compounds Using XPS and XAS[†]

3.1 Introduction

3.1.1 Oxidation Number, Valence Number and Main Group Compounds

The chemical state of the key atoms in novel inorganic complexes is a vital piece of information for understanding reactivity. The concept of chemical states can have several meanings but for our discussion, we define the chemical state as the experimentally determined electronic environment or partial charge of an atom of interest in a molecular complex. Two common formalisms exist for classifying the atoms of interest in a new compound: oxidation or valence numbers.¹ As put forth by Parkin, the oxidation number can be described as "...the charge remaining on an atom when all ligands are removed heterolytically,..." with the electron pairs involved in bonding given to the atom with the larger electronegativity. Conversely, valence indicates the "number of electrons that an atom uses in bonding."² While the oxidation and valence numbers are sometimes equal, many examples exist for main group compounds where this is not the case. As an example, Group 13 halides in their monomeric forms are assigned an oxidation and valence number of +3, illustrated using BF_3 in Figure 3.1. In B_2F_4 , each boron atom is assigned an oxidation number of +2, and a valence number of 3.² Both compounds react primarily as Lewis acids, despite their different oxidation numbers,^{3,4}

[†] Reproduced from "Chemical state determination of molecular gallium compounds using XPS" J. L. Bourque, M. C. Biesinger and K. M. Baines, *Dalton Trans.*, **2016**, 45, 7678, DOI: 10.1039/C6DT00771F with permission from The Royal Society of Chemistry. Reproduced with permission from "Beyond Oxidation States: Distinguishing Chemical States of Gallium in Compounds with Multiple Gallium Centers." L. Yang, J. L. Bourque, J. A. McLeod, P. Shen, K. M. Baines, and L. Liu, *Inorg. Chem.*, **2017**, 56, 2985-2991, Copyright 2017 American Chemical Society.

and demonstrate that one measure alone cannot be used to predict the reactivity of main group compounds.

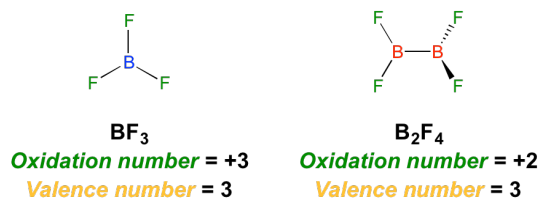
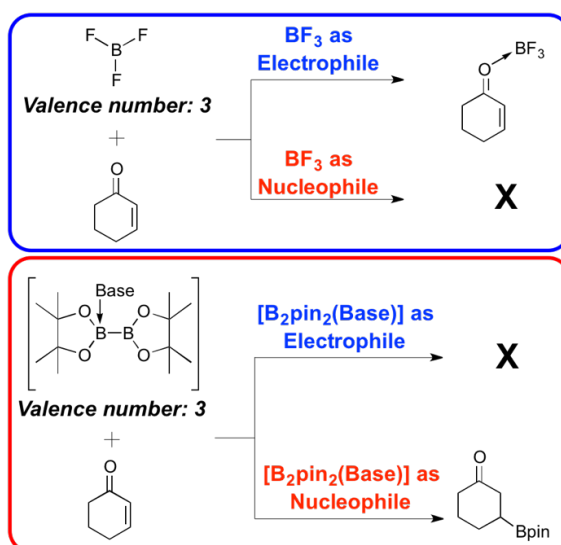


Figure 3.1: Differences in oxidation and valence numbers for BF_3 and B_2F_4 .

Although Parkin argues that the valence number of an atom is more reflective of its chemical state, several main group complexes do not follow this narrative. For example, in Scheme 3.1, although both compounds have valence numbers of 3, BF_3 reacts as a Lewis acid and an electrophile, coordinating to the oxygen atom of 1-cyclohex-2-enone.⁵ Conversely, if a base such as a phosphine or methoxide is added to B_2pin_2 (pin = pinacolato), the boron fragment acts as a nucleophile, resulting in addition to the alkene, demonstrating that the construct of valence numbers can fail when attempting to predict reactivity.⁶



Scheme 3.1: Example of how the valence number can fail to accurately predict reactivity.

Another example where valence numbers do not properly predict reactivity is observed for unsaturated main group compounds, examples of which are shown in Figure 3.2. Here, a multiply bonded digallene⁷ and disilene⁸ are shown, along with their assigned oxidation and valence numbers. While the valence numbers depict main group centres that are using all of their available electrons for bonding, their oxidation numbers demonstrate that these two complexes are reactive toward a variety of organic and inorganic substrates.^{9,10} It is evident that while chemically intuitive qualitative descriptors can aid in the prediction of reactivity, experimentally determined measures of the chemical state of a given atom in a compound are needed.

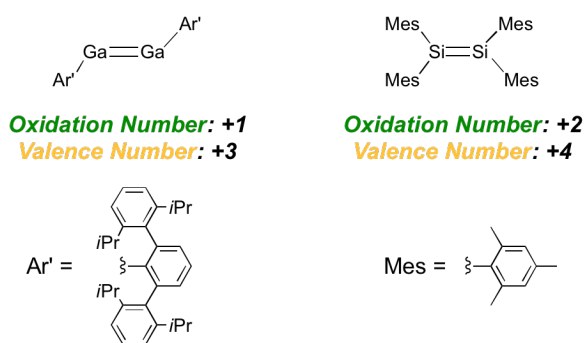


Figure 3.2: Oxidation and valence numbers of a digallene and a disilene.

As with its lighter congeners, gallium chemistry has many examples where the assigned oxidation number and reactivity of a given complex may not correlate. Often, the oxidation numbers of individual atoms may not be immediately evident upon initial scrutiny, and depending on the compound, the formalism of oxidation numbers may not accurately represent the reactivity of the molecule. It is, therefore, important to use a measure that has an experimental basis that can correctly give indications as to what types of reactivity can be expected. As examples, the structural and bonding characteristics of two common “low valent” gallium starting materials, ‘GaI’ and Ga_2Cl_4 , have required extensive studies to firmly establish the compositions of both compounds and to understand their reactivity.

As the crystal structure of ‘GaI’ could not be determined due to its insolubility, susceptibility to disproportionation in donor solvents, variable composition, and amorphous nature, only spectroscopic and diffraction methods have been used to determine the composition of ‘GaI’.¹¹ A recent study utilizing Raman, ⁷¹Ga solid-state NMR, and ¹²⁷I NQR spectroscopies and powder X-ray diffraction has revealed that, depending on the reaction time, ‘GaI’ can have vastly different compositions; its chemical formula was found to be either $[\text{Ga}^0]_2[\text{Ga}^+][\text{GaI}_4^-]$ or $[\text{Ga}^0]_2[\text{Ga}^+]_2[\text{Ga}_2\text{I}_6^{2-}]$.¹¹ The formulae were elucidated using the chemical shift values and quadrupolar coupling constants of the ⁷¹Ga solid-state NMR signals, and the unique frequencies of the ¹²⁷I NQR signals of the multiple iodide environments present in the ‘GaI’ samples. Despite its variable composition and the presence of higher oxidation numbers within the sample, the reactivity of ‘GaI’ can mostly be attributed to the gallium(I) centres, but the occurrence of gallium(II) and gallium(III) products can be attributed to the ease with which Lewis bases can cause disproportionation of the gallium(I) cation or the existing gallium centres with higher oxidation numbers in the starting material.

Similarly, the structure of Ga₂Cl₄ was initially unknown, and it was uncertain as to whether Ga₂Cl₄ was a gallium(II) compound containing a gallium-gallium bond with equivalent gallium centres, or a mixed valent salt with a gallium(I) cation and a tetrachlorogallate(III) anion (Figure 3.3). Following successful crystallization, it was determined that the latter description was the most accurate.¹² As an added complexity, comproportionation of Ga₂Cl₄ from $[\text{Ga}][\text{GaCl}_4]$ to $\text{Cl}_2\text{GaGaCl}_2$ readily occurs upon the addition of a Lewis base to the complex.¹³ ³⁵Cl and ^{69/71}Ga solid-state NMR spectroscopy have also been utilized to characterize $[\text{Ga}][\text{GaCl}_4]$. Two gallium environments exist: the gallium(I) signal was centred around -610 ppm, and the tetrachlorogallate(III) signal was located at 231 ppm.^{14,15} While the significant difference in the electronic nature between the two sites allows for easy characterization and assignment in this salt, in more complex species, it may be more difficult to assign an oxidation number based on chemical shifts or quadrupolar coupling constants.

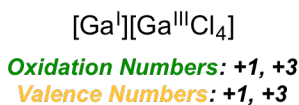
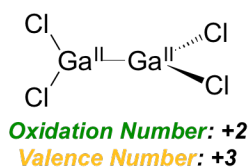


Figure 3.3: Two possible structures of Ga_2Cl_4 .

Examples where the oxidation number of gallium in a given complex is ambiguous despite knowing the molecular structure often arise when multiple atoms of a given element are bound together, or when a gallium centre is bound by ligands that are capable of hosting electron delocalization or a negative charge. An example is shown in Figure 3.4. Here, a $[\text{Ga}_5\text{I}_4]^{3+}$ fragment stabilized by NacNac ligands can be described by multiple bonding descriptors, two of which are shown. The ambiguity of the bonding in this compound cannot be confirmed through structural or traditional spectroscopic methods typically employed by synthetic chemists, highlighting the need for alternative techniques for chemical state determination.¹⁶

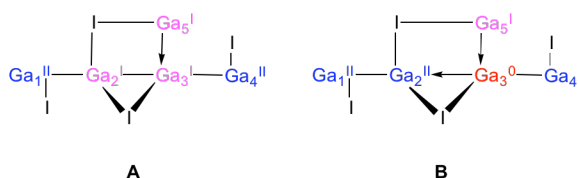


Figure 3.4: Two bonding models for the $[\text{Ga}_5\text{I}_4]^{3+}$ core of $[\text{Ga}_5\text{I}_4(\text{tBuNacNac}^{\text{Mes}})_3]$, with the NacNac ligands removed for clarity.

We have recently reported the synthesis of novel cationic multinuclear gallium-cryptand[2.2.2] complexes, **2.1** and **2.2**. Despite extensive characterization using the standard spectroscopic techniques and analysis of the bonding using computational methods, the oxidation numbers of the gallium centres were ambiguous.¹⁷ Thus, we

sought out a means to assess the chemical state of the gallium in these complexes to aid in the prediction and rationalization of their reactivity.

3.1.2 Experimental Techniques for Chemical State Elucidation

Very few analytical methods for the evaluation of the chemical states of main group elements exist. One well-known technique is Mössbauer spectroscopy. This method uses γ -irradiation to induce a nuclear transition in the sample. Although Mössbauer spectroscopy is extremely sensitive and is very effective at distinguishing chemical states of certain elements, the technique is somewhat limited since few elements of the periodic table have adequate γ -ray sources and γ -ray sources are subject to decay.^{18,19} Although Mössbauer spectroscopy has been used for many years as an effective technique to probe the bonding and chemical states of molecular tin and iron compounds,^{20,21,22} more widely accessible techniques for chemical state determination are desired for those elements which do not possess a suitable Mössbauer source.

Solid-state NMR spectroscopy has been utilized for the assessment of the chemical state of main group compounds. Our group has used ^{35}Cl solid-state NMR spectroscopy as an indirect probe for evaluating the chemical state of a range of chlorogermanes. The magnitude of the quadrupolar coupling constant (C_Q) of the ^{35}Cl signal was found to correlate to the assigned oxidation number of the germanium centre.²³ While this has been shown to be effective, methods which probe the element of interest directly and are more generally applicable are desired.

3.1.2.1 X-ray Photoelectron Spectroscopy

Another technique that has been used for chemical state elucidation is X-ray photoelectron spectroscopy (XPS). Unlike the aforementioned ^{35}Cl solid-state NMR spectroscopic study for germanium compounds, the presence of an indirect probe, in this case a chloride ligand, is not required, as the data obtained pertain directly to the element being examined. XPS provides information on the chemical state of the atom using X-ray radiation. XPS can be used to analyze most solid samples and can detect all elements

except for hydrogen and helium. Although XPS has been utilized primarily for surface analysis and speciation, it may be applied to molecular compounds as well, despite the rarity of such reports in the literature. The dearth of XPS studies on molecular compounds may arise from the potential for surface contamination, as often contaminants remain in the analysis chamber, which, despite the ultra-high vacuum, and may deposit on the surface of the sample. In some cases, when the contaminant contains the primary element of focus for a particular study, the data obtained may be affected. However, this is not the case for many main group elements, as they are rarely observed as contaminants. While contamination of the sample may result in a decrease in the desired signal intensity, this is not a significant problem if the signal of interest is of a sufficient strength.²⁴

The initial process of performing XPS is straightforward. A sample is placed inside an observation chamber that has been put under ultra-high vacuum ($\sim 10^{-9}$ Torr). The sample, which is spread onto a sample holder, forming a surface, is bombarded by high-energy X-ray photons (E_{hv}) (typically monochromatic Al K(α) radiation at 1486.71 eV or Mg K(α) at 1253.6 eV). This causes the expulsion of core electrons from the atoms present in the sample, termed photoelectron emission. The kinetic energy of the photoelectrons is measured, and is related to the binding energy of the electrons by Equation 1:

$$E_K = E_{hv} - E_B - \phi_{XPS} \quad (1)$$

where E_K is the kinetic energy of the photoelectron, ϕ_{XPS} is the work function of the XPS spectrometer, and E_B is the binding energy of the photoelectron. The binding energy is specific to each orbital for each element of the periodic table. The usefulness of XPS relies on the fact that the binding energies shift depending on the chemical state of the atom. The chemical state can be thought of as any variable that can affect the nature of the atom being observed, or as a measure of the experimental partial charge located at the atom of interest in a given environment. For example, changes in oxidation or valence number, ligand type, and charge can affect the chemical state of an atom and the binding

energies of its photoelectrons. While using only binding energies to probe the chemical state of certain elements can be somewhat inaccurate, the use of the Auger parameter can improve the accuracy of these measurements.²⁴

The original definition of the Auger parameter is shown in Equation 2:

$$\alpha = E_K(\text{Auger}) - E_k \quad (2)$$

$$\alpha' = E_B + E_K(\text{Auger}) \quad (3)$$

where E_K is the kinetic energy of the photoelectron, and $E_K(\text{Auger})$ is the kinetic energy of the Auger electron.²⁵ Auger electron emission results from a relaxation mechanism, whereby an atom, which has emitted a photoelectron, fills its core hole, resulting in the simultaneous emission of an Auger electron from a higher orbital, and the repopulation of the core hole by an electron from the same orbital. The Auger electron kinetic energy is dependent on the valence electron richness of the atom being analyzed: as the electron richness increases, the kinetic energy also increases. Although the original Auger parameter was defined as the difference of the kinetic energies of the photo- and Auger electrons, the modified Auger parameter (Equation 3), which is the sum of the photoelectron binding energy and the Auger electron kinetic energy, is independent of the X-ray energy used. The reasoning behind using the Auger parameter in determining differences in chemical states arises from the stronger influence of the environment of the atom on the Auger electron energies for some elements, as well as combining the influence of both the photo- and Auger electron energies. This is an important consideration for insulators and semi-conductors, as the accumulation of charge on the sample can result in significant deviations in electron energies. Additionally, any surface charging shifts will be of the same magnitude, but of the opposite direction in each of the components, and any associated error will be eliminated.²⁶ The modified Auger parameter has been extensively studied and utilized, and therefore, is now the accepted definition.²⁷ Several reviews have been published in recent years, outlining the mathematical and theoretical background to using the Auger parameter for the differentiation of chemical states.^{26,28}

The Auger parameter has been used for many elements of the periodic table and its effectiveness is maximized when the data are presented in a graphical plot. These are known as chemical speciation or Wagner plots. An example is shown in Figure 3.5. Wagner plots contain three axes: on the left axis, the Auger electron kinetic energy ($E_K(\text{Auger})$, or $E_K(\text{C}'\text{C}''\text{C}''')$); these are expressed in X-ray notation, i.e. LMM^{24}); on the bottom, the photoelectron binding energy (E_B , or $E_B(\text{C})$); this is presented in spectroscopic notation, i.e. $2p_{3/2}$); and on the right axis, the modified Auger parameter (α). The definition of the Auger parameter leads to the generation of lines with a slope of 1, which are equal to the value of the Auger parameter, with the intercepts being equal to the photoelectron binding energy and the Auger electron kinetic energy for the x and y axes, respectively. Wagner plots are known to be effective in chemical state determination, allowing the differences in photoelectron binding energy and the Auger electron kinetic energy to be visualized. Although the use of the Auger parameter and Wagner plots aids in the determination of chemical states, the Auger parameter itself is not a measure of the electron deficiency or richness of a given element, as compounds with vastly different electronic environments may have similar Auger parameter values.

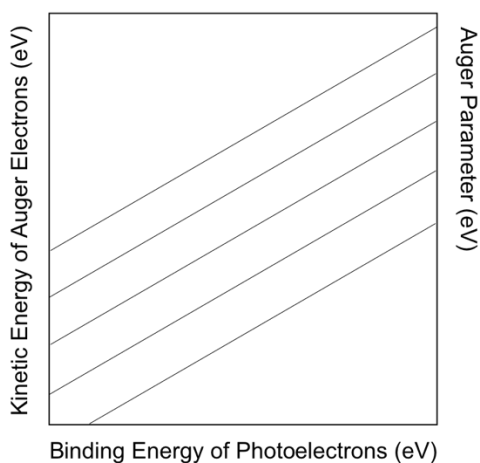


Figure 3.5: A generic Wagner plot.

An additional aspect of chemical state differentiation that can be extracted from the Auger parameter and Wagner plots are whether the differences between compounds

are more strongly influenced by initial or final state effects. Initial state effects are shifts in the orbital energies of an atom before it is subject to X-ray radiation. These effects are highly dependent on the nature of the ligands bound to the element of interest. In essence, the partial charge induced at the atom by the attached ligands gives rise to significant deviations in the binding energy observed. These deviations can be thought of as a type of chemical shift. An example is the change in binding energy as halide ligands are varied down Group 17, as the binding energy is expected to decrease due to increased electron density at the central atom. Final state effects result from differences in polarization within the electron cloud of the atom after it has been ionized by X-ray irradiation. Final state effects are often dominant when dealing with compounds that have the potential for significant polarization or electron motility.^{29,30} From Wagner plots, a series of compounds that follow a straight line with a slope equal to 1, meaning they have similar Auger parameter values, have similar final state characteristics, whereas samples that follow a line with a slope of 3, have similar initial state effects.^{26,29} These trends, in some cases, can help discern between differing chemical states of a given element. As an example, when two lines, one with a slope of 1 and one with a slope of 3, are plotted on a Wagner plot for copper compounds and intersect at the data point for copper metal, compounds with a +2 oxidation number generally follow the line with a slope of 3, whereas those with a +1 oxidation number are closer to the line with a slope of 1. These results would indicate that copper compounds with a +2 oxidation number have similar initial state effects but different final state effects. Alternatively, copper compounds with a +1 oxidation number have similar final state effects but different initial state effects.²⁹

Although many elements of the periodic table have been extensively studied using XPS and chemical speciation plots, few studies have involved gallium. Despite reports of the binding energies of several molecular gallium(III) compounds,³¹ most studies have utilized XPS to characterize surfaces and study reactivity and structural features of gallium-containing materials.^{32,33,34,35,36,37,38,39,40} Only one example of a Wagner plot for gallium compounds has been reported in the literature,²⁸ and while more data exist for other main group elements, these studies generally focus on the characterization of materials and minerals.^{28,41,42} It is therefore of interest to not only demonstrate the

applicability of XPS and Wagner plots to elucidate the chemical state of a variety of gallium compounds, but to apply this technique to molecular compounds of other heavier *p*-block elements. The goal of this study is to analyze a range of standard gallium compounds in a variety of assigned oxidation numbers, electronic and bonding environments using XPS, and to generate a Wagner plot to determine the chemical states of these compounds. Distinctions between the assigned oxidation numbers of the known complexes and the experimental chemical states will be made in examples where these quantities differ. Subsequently, three gallium-cryptand[2.2.2] complexes will be studied by XPS and following the determination of their chemical states, reactivities will be predicted.

3.1.2.2 X-ray Absorption Spectroscopy

XPS is a straightforward, readily accessible technique which can be used to assess the Ga chemical state for compounds possessing single Ga centres. For multivalent Ga complexes, the technique lacks the resolution to distinguish between different Ga environments due to the instrumental resolution limit. In addition, XPS probes shifts in the core level electron binding energy, and this is only indirectly related to the change in valency of the element. Alternatively, XAS is a non-destructive, direct probe of the electron density of unoccupied states. XAS and X-ray absorption near edge structures (XANES) has been commonly employed to evaluate the local geometry and chemical state of a given atom in a molecular compound or material.^{43,44,45} There are, however, many disadvantages to using XANES or XAS to probe the chemical state of a given element; a synchrotron is required to perform such experiments, and significant expertise in this field is required for data acquisition and interpretation limiting the use of XANES. Nonetheless, XAS has much promise in this endeavor.⁴⁶ During an XAS measurement, a core electron of Ga is excited to a previously unoccupied electronic state. The spectral profile is dependent on the binding energy of the core electron, as well as the energy and density of the unoccupied molecular orbitals local to the absorption site. In addition, the theory of XAS is reasonably well-established, and experimental XAS can be rationalized using theoretical models that are readily available, such as FEFF,⁴⁷ StoBe,⁴⁸ or

FDMNES.⁴⁹ Although XAS is widely applied to solid-state materials, the use of XAS to study the chemical nature of organometallic or coordination compounds is still underexplored. However, this valuable technique can provide information that other techniques cannot. For example, we have reported an XAS study on a series of Ge-based coordination complexes.⁴⁶ By measuring the XAS in combination with FEFF calculations, Ge compounds with assigned oxidation numbers of +2 and +4 can be distinguished, and the degree of ionicity of the compounds can be obtained. The preliminary study demonstrated the feasibility of XAS in analyzing the chemical nature of coordination compounds of main group elements with different oxidation numbers.

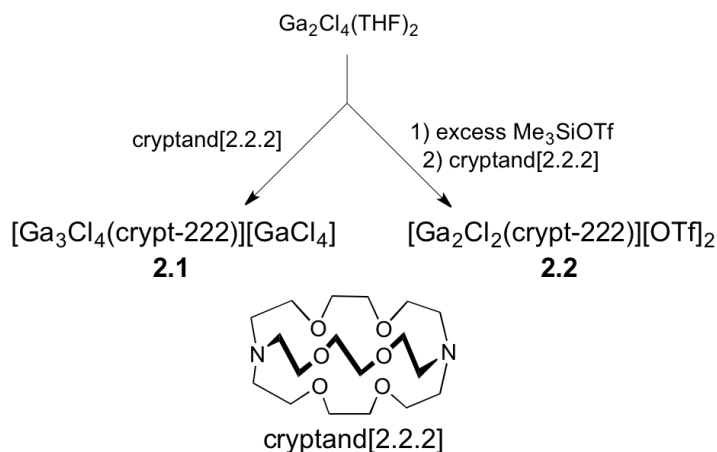
In this work, Ga K-edge XAS was performed to examine the chemical states of several Ga complexes, from relatively common compounds such as Ga[GaCl₄], and Ga₂Cl₄(1,4-dioxane)₂ (**3.5**), to novel macrocycle-stabilized Ga complexes such as [Ga(prismand)][GaCl₄], [Ga₂Cl₂(crypt-222)][OTf]₂ (**2.1**) and [Ga₃Cl₄(crypt-222)][GaCl₄] (**2.2**). All Ga complexes investigated here contain more than one Ga centre in their structures. In a K-edge XAS spectrum, the 1s electron of Ga is excited to a previously unoccupied electronic state of *p*-symmetry. Ab initio calculations utilizing FDMNES and SIESTA code were performed to rationalize the experimental results with a qualitative analysis of the charge density at each Ga site in the compounds.

3.2 Results and Discussion

3.2.1 X-ray Photoelectron Spectroscopy

As described in Chapter 2,¹⁷ several low valent gallium-cryptand[2.2.2] complexes were synthesized from the mixed valent halide salt Ga₂Cl₄ ([Ga][GaCl₄]).¹² The facile disproportionation of [Ga][GaCl₄] was utilized, giving Ga₂Cl₄(THF)₂,¹³ which was then added to cryptand[2.2.2], both without and in the presence of trimethylsilyl triflate (TMSOTf), leading to the generation of [Ga₃Cl₄(crypt-222)][GaCl₄], **2.1** and [Ga₂Cl₂(crypt-222)][OTf]₂, **2.2**, respectively (Scheme 3.2). The analogous derivative with iodide ligands, [Ga₂I₂(crypt-222)][GaI₄]_{1.75}[OTf]_{0.25}, (**3.1**), was synthesized from Ga₂I₄,

TMSOTf and cryptand[2.2.2]. Simple bonding descriptors of $[\text{Ga}_3\text{Cl}_4(\text{crypt-222})][\text{GaCl}_4]$ and $[\text{Ga}_2\text{Cl}_2(\text{crypt-222})][\text{OTf}]_2$ could not be unambiguously determined using conventional experimental techniques and computational methods, making it difficult to predict the reactivity of these novel complexes (Chapter 2).¹⁷

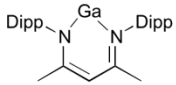
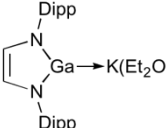
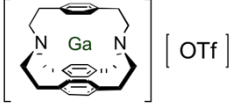
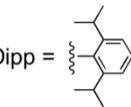
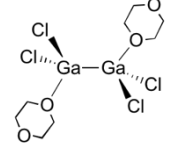
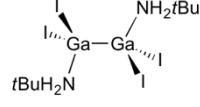
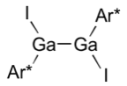
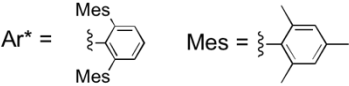


Scheme 3.2: Synthesis of gallium-cryptand[2.2.2] complexes, **2.1** and **2.2**.

To understand the chemical states of the gallium centres in complexes **2.1**, **2.2** and **3.1**, a series of gallium compounds with various oxidation numbers and structures were studied using XPS. The compounds are shown in Table 3.1. A wide range of ligands were chosen to gain as much information as possible on how the binding energies of gallium complexes vary as a function of the ligand, and their influence on the chemical state of the gallium centres. For $\text{Ga}_{(\text{m})}$,^{50,51,52} GaN ,³⁴ GaP ,³³ GaAs ,³² Ga_2O_3 ,^{32,50} and Ga_2Se_3 ,³⁵ XPS data were available from the literature, although experimental data were recollected for $\text{Ga}_{(\text{m})}$ and Ga_2O_3 .^{53,54}

Table 3.1: Gallium compounds studied by XPS. Valence numbers are given in parentheses following the compound names.

Assigned Oxidation number	Compounds
0	$\text{Ga}_{(\text{metal})}$

+1	 GaNacNac^{Dipp} (1) 3.2	 K[GaDAB^{Dipp}] 3.3 (3)	 [Ga(prismand)][OTf] 3.4 (1)
		 Dipp =	
+2	 Ga₂Cl₄(diox)₂ (3) 3.5	 Ga₂I₄(NH₂tBu)₂ (3) 3.6	 Ga₂I₂Ar*₂ (3) 3.7
		 Ar* =	
+3	GaCl₃ 3.8 (3)	GaBr₃ 3.9 (3)	GaI₃ 3.10 (3)
	GaCl₂Mes 3.11 (3)	Ga₂Cl₄ 3.12 (0, 3)	Ga₂I₄ 3.13 (0, 3)
Ga Materials	GaN 3.14 (3)	GaP 3.15 (3)	GaAs 3.16 (3)
	Ga₂O₃ 3.17 (3)		Ga₂Se₃ 3.18 (3)

Data collection began with survey scans of each sample. The purity of all synthesized compounds was initially evaluated by multinuclear NMR spectroscopy and ESI-MS before XPS data were collected, nonetheless, some contaminants were observed in the survey spectra. In each spectrum, adventitious carbon was present (C 1s), which was used as an internal charge correction standard set at 284.8 eV. Additionally, the adhesive tape used for sample preparation was carbon-based, leading to a large increase in the atomic percentage of carbon for all samples and skewing the percentages for the

other elements present. Other contaminants were oxygen, possibly arising from residual solvent molecules from synthesis of the samples, and fluorine, postulated to arise from leaching of the fluoropolymer from the vial caps used during synthesis and sample transport. The atomic percentages of each element based on the intensities of each signal in the survey spectra can be found in Appendix B (Table A.3).

High-resolution XPS spectra were then obtained of each compound. Although two gallium photoelectron signals were observed, namely the Ga 3d and the Ga 2p emissions, the discussion of the results will focus primarily on the Ga 3d photoelectron energies, as they are more intense, and closer in energy to the valence shell of gallium (4p), and thus, more sensitive to subtle changes in the chemical state of gallium. An example of a high-resolution Ga 3d spectrum is shown in Figure 3.6 and this spectrum will be used to explain the data analysis process. Initially, one signal is observed, which must be deconvoluted, as the Ga 3d peak is composed of two separate signals at slightly different energies: Ga 3d_{3/2} and Ga 3d_{5/2}. The energy separation is a consequence of spin-orbit splitting, which arises from the difference in the orientation of the emitted photoelectron with respect to the nuclear magnetic field ($m_s = +1/2$ or $-1/2$). These signals were fit with a spin orbit splitting of 0.449 eV, equivalent full-width at half-maxima (FWHM), and a 3d_{5/2}:3d_{3/2} area ratio of 3:2. The fit of these two signals to the experimentally observed spectrum is shown by the red curve. A standard Shirley background was used for all spectral fitting and is shown by the dashed line. The binding energy listed for all measurements is that of the Ga 3d_{5/2} signals, and not the observed signal maxima. A similar analysis was applied to the Ga 2p_{3/2} and Ga L₃M₄₅M₄₅ signals (Figure 3.7 and Figure 3.8, respectively), however, deconvolution was not necessary for the Ga 2p_{3/2} emission, as the Ga 2p_{1/2} and the Ga 2p_{3/2} signals are completely resolved (1143.2 eV versus 1116.4 eV, respectively).²⁴

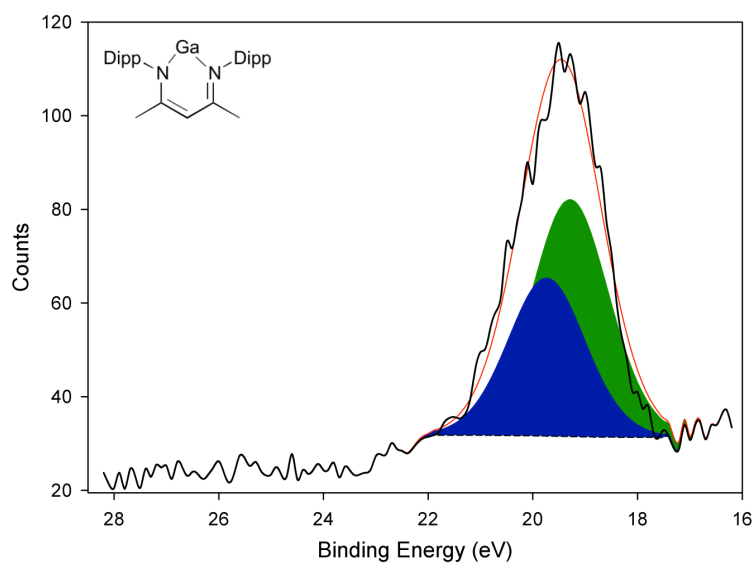


Figure 3.6: Ga 3d signal for GaNacNac^{Dipp}. The experimental (black), simulated (red), component Ga 3d_{3/2} (blue) and Ga 3d_{5/2} (green) and background spectra (dashes) are shown.

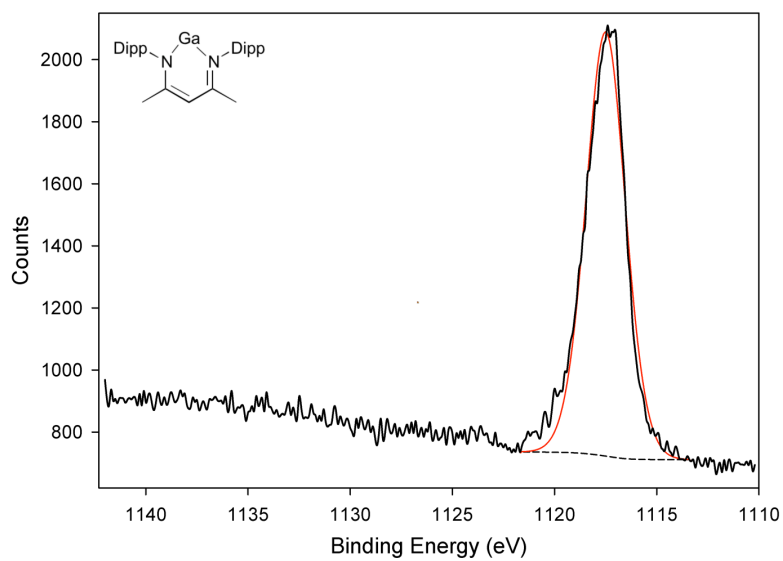


Figure 3.7: Ga 2p_{3/2} signal for GaNacNac^{Dipp}. The experimental (black), simulated Ga 2p_{3/2} (red) and background spectra (dashes) are shown.

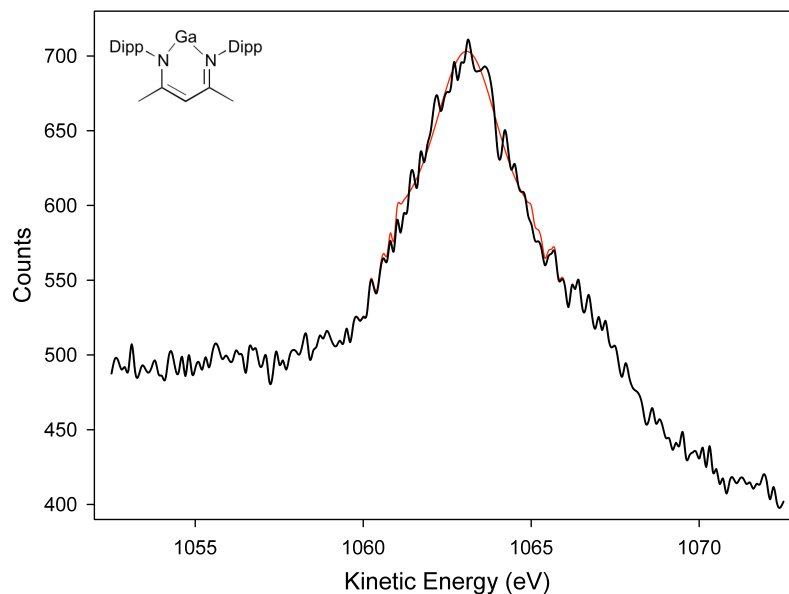


Figure 3.8: Ga L₃M₄₅M₄₅ signal for GaNacNac^{Dipp}. The experimental (black) and simulated Ga L₃M₄₅M₄₅ (red) spectra are shown.

Analysis of the data of the gallium trihalides, GaCl₃, GaBr₃, and GaI₃ (Figure 3.9) reveals that the photoelectron and Auger electron binding energies decrease upon substitution of the chloride for bromide and then iodide (for exact values, see Table 3.2). Thus, as the ligand is varied down Group 17, the Ga 3d_{5/2} binding energy decreases as the electronegativity of the halogen decreases and the gallium atom becomes more electron rich. A similar trend was observed in a study of nickel(II) halides by XPS.²⁷ Additionally, experimental and theoretical studies have demonstrated decreasing Lewis acidity for GaX₃ compounds while descending Group 17.⁵⁵ All of the gallium trihalides exhibit sharp signals, as evidenced by small FWHM values (Table 3.2), and satisfactory correlations between the fitted and the experimental spectra were obtained.

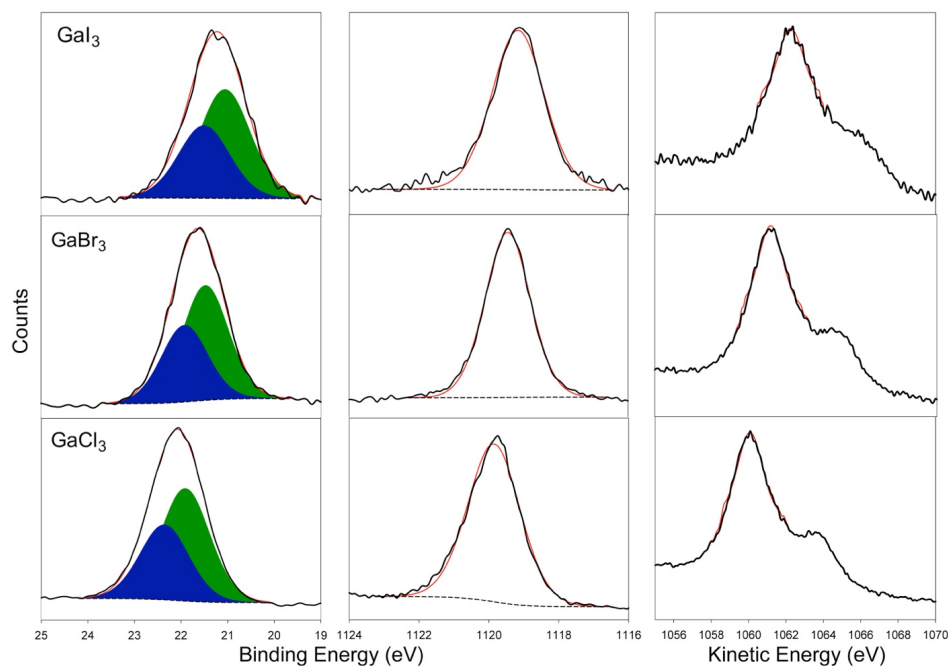


Figure 3.9: Ga 3d (left), Ga 2p_{3/2} (centre) and Ga L₃M₄₅M₄₅ (right) XPS spectra of GaCl₃ (bottom), GaBr₃ (middle) and GaI₃ (top).

Table 3.2: Photoelectron binding and Auger electron kinetic energies and full-width at half-maxima for high-resolution XPS spectra. Note: Ga L₃M₄₅M₄₅ signals are kinetic energy values, which have opposite trends to binding energies (Equation 3.1).

Compound	Peak	Binding or Kinetic Energy (eV)	FWHM (eV)
Ga _(m)	Ga 3d _{5/2}	18.39	0.57
	Ga 2p _{3/2}	1116.49	1.04
	Ga L ₃ M ₄₅ M ₄₅	1068.01	0.79
GaNacNac ^{Dipp} 3.2	Ga 3d _{5/2}	19.29	1.74
	Ga 2p _{3/2}	1117.50	2.27
	Ga L ₃ M ₄₅ M ₄₅	1063.09	2.05
K[GaDAB ^{Dipp}] 3.3	Ga 3d _{5/2}	20.17	1.77
	Ga 2p _{3/2}	1118.02	2.18
	Ga L ₃ M ₄₅ M ₄₅	1061.92	1.78

Compound	Peak	Binding or Kinetic Energy (eV)	FWHM (eV)
[Ga(prismand)][OTf] 3.4	Ga 3d _{5/2}	21.34	1.24
	Ga 2p _{3/2}	1119.31	1.87
	Ga L ₃ M ₄₅ M ₄₅	1060.65	1.41
Ga₂Cl₄(diox)₂ 3.5	Ga 3d _{5/2}	21.10	1.67
	Ga 2p _{3/2}	1118.86	2.13
	Ga L ₃ M ₄₅ M ₄₅	1061.39	2.16
Ga₂I₄(NH₂tBu)₂ 3.6	Ga 3d _{5/2}	20.53	1.64
	Ga 2p _{3/2}	1118.36	2.03
	Ga L ₃ M ₄₅ M ₄₅	1062.13	1.61
Ga₂I₂Ar[*]₂ 3.7	Ga 3d _{5/2}	20.48	1.34
	Ga 2p _{3/2}	1118.33	1.93
	Ga L ₃ M ₄₅ M ₄₅	1063.01	2.20
GaCl₃ 3.8	Ga 3d _{5/2}	21.91	1.23
	Ga 2p _{3/2}	1119.85	1.76
	Ga L ₃ M ₄₅ M ₄₅	1060.09	1.53
GaBr₃ 3.9	Ga 3d _{5/2}	21.48	1.16
	Ga 2p _{3/2}	1119.45	1.53
	Ga L ₃ M ₄₅ M ₄₅	1061.17	1.51
GaI₃ 3.10	Ga 3d _{5/2}	21.06	1.28
	Ga 2p _{3/2}	1119.17	1.76
	Ga L ₃ M ₄₅ M ₄₅	1062.26	1.57
GaCl₂Mes 3.11	Ga 3d _{5/2}	21.84	1.64
	Ga 2p _{3/2}	1120.10	1.94
	Ga L ₃ M ₄₅ M ₄₅	1060.16	1.92
Ga₂Cl₄ 3.12	Ga 3d _{5/2}	21.77	1.34
	Ga 2p _{3/2}	1119.54	1.85
	Ga L ₃ M ₄₅ M ₄₅	1060.43	1.61
Ga₂I₄ 3.13	Ga 3d _{5/2}	20.80	1.51
	Ga 2p _{3/2}	1118.72	2.08
	Ga L ₃ M ₄₅ M ₄₅	1061.98	2.06

Compound	Peak	Binding or Kinetic Energy (eV)	FWHM (eV)
Ga₂O₃ 3.17	Ga 3d _{5/2}	20.00	1.22
	Ga 2p _{3/2}	1117.80	1.55
	Ga L ₃ M ₄₅ M ₄₅	1062.60	1.49
[Ga₃Cl₄(crypt-222)] [GaCl₄] 2.1	Ga 3d _{5/2}	20.79	1.63
	Ga 2p _{3/2}	1118.51	2.10
	Ga L ₃ M ₄₅ M ₄₅	1061.64	1.82
[Ga₂Cl₂(crypt-222)] [OTf]₂ 2.2	Ga 3d _{5/2}	20.65	1.61
	Ga 2p _{3/2}	1118.57	2.47
	Ga L ₃ M ₄₅ M ₄₅	1061.62	1.84
[Ga₂I₂(crypt-222)] [GaI₄]_{1.75}[OTf]_{0.25} 3.1	Ga 3d _{5/2}	21.00	1.19
	Ga 2p _{3/2}	1118.90	1.57
	Ga L ₃ M ₄₅ M ₄₅	1061.91	1.85

The gallium XPS spectra for Ga_(m), GaNacNac^{Dipp}, Ga₂Cl₄(diox)₂ and GaCl₃, with oxidation numbers of 0, +1, +2 and +3, respectively, are shown in Figure 3.10. The spectra reveal a marked shift in the binding energies. For example, the binding energy of the Ga 3d_{5/2} signal increases by approximately 2 eV between GaNacNac^{Dipp} and Ga₂Cl₄(diox)₂, and by approximately 1 eV between Ga₂Cl₄(diox)₂ and GaCl₃ and between Ga_(m) and GaNacNac^{Dipp} (Table 3.2). It becomes increasingly more difficult to remove an electron as one progresses from Ga_(m) to GaCl₃, presumably because the gallium becomes more electron deficient from gallium metal (0) to GaCl₃ (+3), which is in agreement with the assigned oxidation numbers for these compounds. Despite the changes in chemical state, the line shapes of each compound are similar, with narrow FWHM, although the signals for Ga_(m) are markedly more intense and have a much narrower FWHM (≤ 1.0 eV). The FWHM of the Ga L₃M₄₅M₄₅ signal of GaCl₃ is narrower by more than 0.5 eV compared to the FWHM values of GaNacNac^{Dipp} and Ga₂Cl₄(diox)₂. The trend is likely a result of the highly symmetric bonding environment at the gallium centre (tetrahedral) in GaCl₃⁵⁶ in comparison to GaNacNac^{Dipp}⁵⁷ and Ga₂Cl₄(diox)₂, and therefore, is not related to the chemical state.⁵⁸

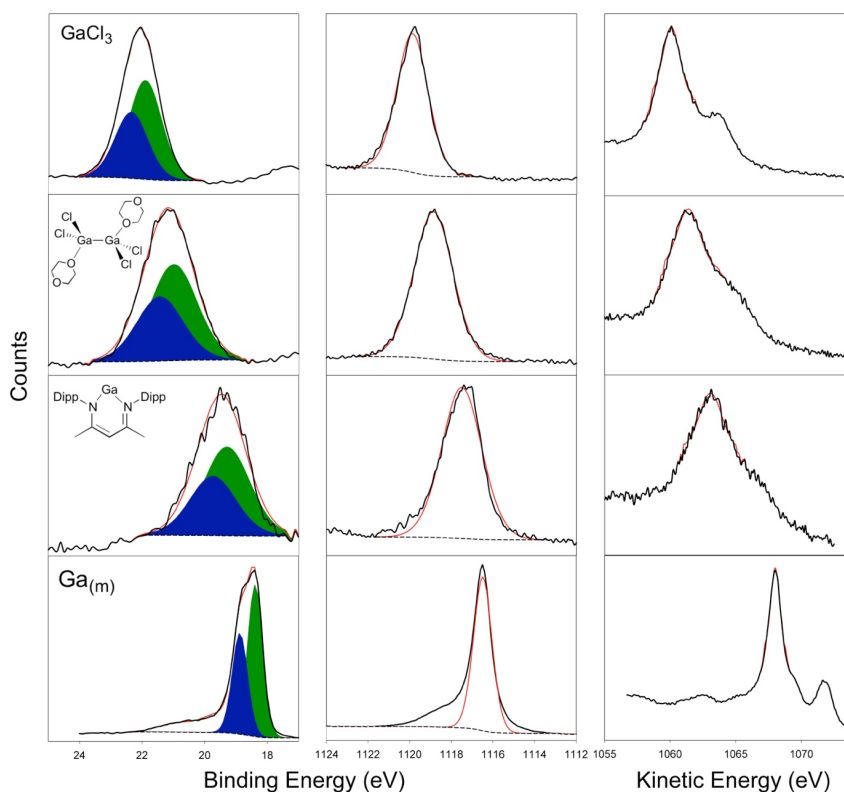


Figure 3.10: Ga 3d (left), Ga 2p_{3/2} (centre) and Ga L₃M₄₅M₄₅ (right) XPS spectra of Ga_(m) (bottom), GaNacNac^{Dipp} (lower middle), Ga₂Cl₄(diox)₂ (upper middle) and GaCl₃ (top).

Wagner plots were generated to reveal further trends in the chemical state of the gallium centres as a function of ligand type and assigned oxidation number. The Ga 3d_{5/2} binding energies, Ga L₃M₄₅M₄₅ kinetic energies and the Auger parameter values for the gallium halides and compounds with an assigned oxidation number of +3 are shown in Figure 3.11. As with nickel(II) halides,²⁷ increasing Auger electron kinetic energy, decreasing photoelectron binding energy, and increasing Auger parameter values were observed as the halide ligands were altered down Group 17. The nearly linear increase with a slope approaching 2 in the Auger parameter values from GaCl₃ to GaBr₃ to GaI₃ suggests that gallium trihalides are not dominated by initial or final state effects. This is corroborated by the calculated initial and final state shifts for each compound (Table 3.3),

where the initial state shifts for the gallium trihalides differ by 0.19 eV (from -1.32 eV for GaCl₃ to -1.13 eV for GaI₃), and the final state shifts differ by 0.66 eV (from -2.20 eV for GaCl₃ to -1.54 eV for GaI₃), which are small in comparison to nickel(II) halides, whose initial state shifts vary by 2.7 eV and final state shifts vary by 0.9 eV. The vast difference between the initial and final state shifts for nickel(II) halides lead to the conclusion that initial state effects dominate these compounds, but such a definitive trend was not apparent for the gallium trihalides.²⁷

The gallium chlorides GaCl₃, GaCl₂Mes and Ga₂Cl₄, possess similar Auger parameters. Specifically, GaCl₃ and GaCl₂Mes are nearly identical, possibly resulting from a similar solid-state structure, with four coordinate gallium atoms, and bridging chloride ligands.^{56,59} Electronically, both the chloride and mesityl ligands are electron withdrawing, and GaCl₃ and GaCl₂Mes demonstrate similar reactivity. Despite the solid-state structure of Ga₂Cl₄ having a gallium(I) cation and a tetrachlorogallate(III) anion ([Ga][GaCl₄]),¹² the signal was not broadened, as might be expected for a mixed valent salt. Given the known solid-state structure, three suggestions are put forward to rationalize the low FWHM: (1) Upon X-ray irradiation, the gallium cation in [Ga][GaCl₄] undergoes disproportionation and is oxidized; (2) the cation is volatilized under the conditions of the experiment and not detected, which is supported by the observation of gallium in the survey spectra of subsequently analyzed samples unrelated to this study; or (3) unlike the gallium(I) in GaNacNac^{Dipp}, the gallium(I) in [Ga][GaCl₄] is, essentially, a naked cation carrying a full positive charge and stabilized in the solid-state only by interactions with the chloride ligands of the tetrachlorogallate(III) anion.¹² Similar interactions are observed in the solid-state structure of GaCl₃.⁵⁶ Thus, the cationic gallium(I) has a chemical state similar to a gallium(III) with covalently bound ligands leading to a single signal and the observed location for [Ga][GaCl₄] on the Wagner plot. The data obtained for [Ga][GaCl₄] also reveal a higher Auger parameter (0.2 eV), with lower binding and higher kinetic energies, than GaCl₃ and GaCl₂Mes, suggesting that the presence of the additional chloride ligand on the tetrachlorogallate anion increases the electron density at the gallium centre.

As with Ga_2Cl_4 , the FWHM of the Ga $3d_{5/2}$ and $2p_{3/2}$ signals of Ga_2I_4 ($[\text{Ga}][\text{GaI}_4]$) were both less than 2.1 eV, indicating either a single species or multiple species with similar chemical states were present in the sample. As with the gallium trihalides, the gallium in the iodo derivative of Ga_2X_4 is more electron rich compared to the analogous chloro derivative. However, unlike $[\text{Ga}][\text{GaCl}_4]$ and GaCl_3 , the Auger parameter for $[\text{Ga}][\text{GaI}_4]$ was lower than that for GaI_3 . For both $[\text{Ga}][\text{GaCl}_4]$ and $[\text{Ga}][\text{GaI}_4]$, the photoelectron binding energies decrease compared to the corresponding GaX_3 ; however, the Auger electron kinetic energy increases going from $[\text{Ga}][\text{GaCl}_4]$ to GaCl_3 and decreases going from $[\text{Ga}][\text{GaI}_4]$ to GaI_3 , demonstrating the large, but subtle, effect the electronic properties of the ligands can have on the chemical state of the gallium centre.

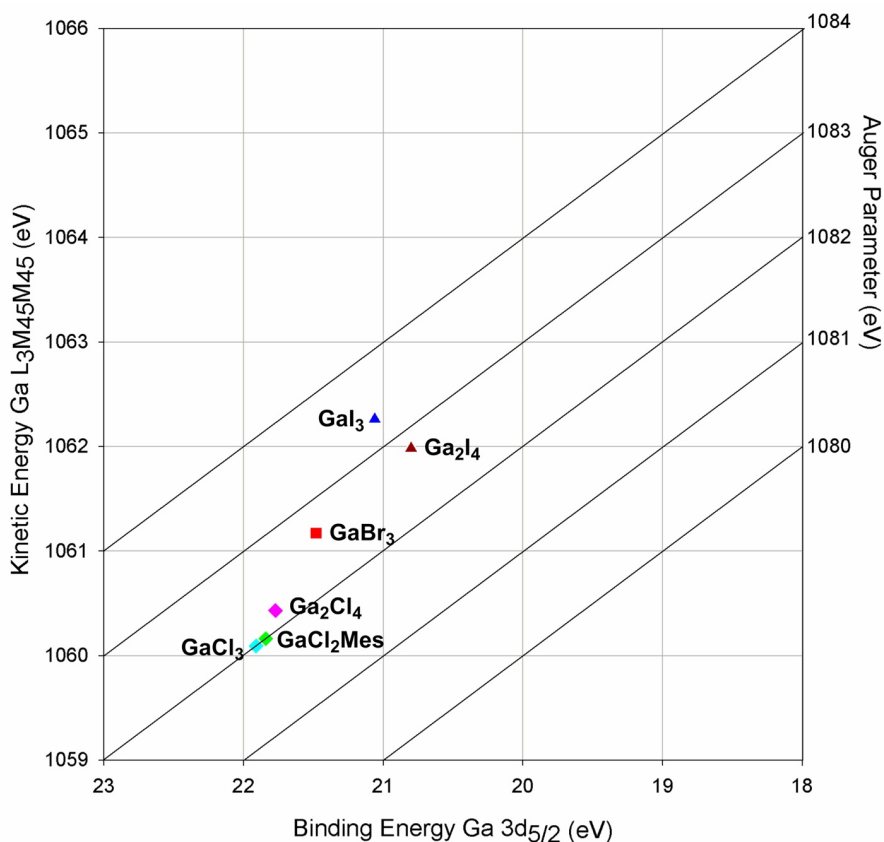


Figure 3.11: Wagner plot of gallium halides using Ga $3d_{5/2}$ binding energy. Symbol legend: diamond = chloride ligands; square = bromide ligands; triangle = iodide ligands.

Table 3.3: Auger parameters and relevant shifts for compounds analyzed using Ga 3d_{5/2} binding energy.*

Compound	Auger Parameter, α' (eV)	ΔE_B (eV)	ΔE_K (eV)	Relaxation Shift, $\Delta\alpha'$ (eV)	Final State Shift, ΔR (eV)	Initial State Shift, $\Delta\varepsilon$ (eV)
Ga_(m) (meas)	1086.40	-	-	-	-	-
Ga_(m) (lit)	1086.69	-	-	-	-	-
GaNacNac^{Dipp}	1082.38	0.90	-4.92	-4.02	-2.01	1.11
K[GaDAB^{Dipp}]	1081.84	1.84	-6.40	-4.56	-2.28	0.44
[Ga(prismand)] [OTf]	1081.99	2.95	-7.36	-4.41	-2.21	-0.75
Ga₂Cl₄(diox)₂	1082.39	2.61	-6.62	-4.01	-2.01	-0.61
Ga₂I₄(NH₂tBu)₂	1082.66	2.14	-5.88	-3.74	-1.87	-0.27
Ga₂I₂Ar*₂	1083.49	2.09	-5.00	-2.91	-1.46	-0.64
GaCl₃	1082.00	3.52	-7.92	-4.40	-2.20	-1.32
GaBr₃	1082.65	3.09	-6.84	-3.75	-1.88	-1.22
GaI₃	1083.32	2.67	-5.75	-3.08	-1.54	-1.13
GaCl₂Mes	1082.00	3.45	-7.85	-4.40	-2.20	-1.25
Ga₂Cl₄	1082.20	3.38	-7.58	-4.20	-2.10	-1.28
Ga₂I₄	1082.78	2.41	-6.03	-3.62	-1.81	-0.60
GaN	1084.05	1.21	-3.56	-2.35	-1.18	-0.35
GaP	1085.33	0.91	-1.98	-1.07	-0.54	-0.38
GaAs	1085.77	0.81	-1.44	-0.63	-0.32	-0.49
Ga₂O₃ (meas)	1082.60	1.61	-5.41	-3.80	-1.90	0.29
Ga₂O₃ (lit)	1082.85	2.01	-5.56	-3.55	-1.78	-0.24
Ga₂Se₃	1085.20	1.41	-2.61	-1.20	-0.60	-0.81
1	1082.43	2.40	-6.37	-3.97	-1.99	-0.42
2	1082.27	2.26	-6.39	-4.13	-2.07	-0.20
3	1082.91	2.61	-6.10	-3.49	-1.75	-0.87

*Note: Calculations were performed as follows using the measured data for Ga_(m): $\alpha' = E_B + E_K(\text{Auger})$; $\Delta E_B = E_B - E_B(\text{Ga}_{(m)})$; $\Delta E_K = E_K(\text{Auger}) - E_K(\text{Auger, Ga}_{(m)})$; $\Delta\alpha' = \alpha' - \alpha'(\text{Ga}_{(m)}) = 2\Delta R$; $\Delta\varepsilon = -\Delta E_B - \Delta R$.

A Wagner plot for the gallium compounds containing a Ga-Ga bond and an oxidation number of +2 is presented in Figure 3.12. $\text{Ga}_2\text{Cl}_4(\text{diox})_2$ is more electron deficient than $\text{Ga}_2\text{I}_4(\text{NH}_2t\text{Bu})_2$, with chloride being more electronegative than iodide and amines being better donors than ethers, decreasing the binding energy for the iodide derivative.⁶⁰ As with the gallium trihalides, a trendline with a slope approaching 2 is observed going from $\text{Ga}_2\text{Cl}_4(\text{diox})_2$ to $\text{Ga}_2\text{I}_4(\text{NH}_2t\text{Bu})_2$ and to $\text{Ga}_2\text{I}_2\text{Ar}^*_2$. The increase in the Auger parameter from $\text{Ga}_2\text{I}_4(\text{NH}_2t\text{Bu})_2$ to $\text{Ga}_2\text{I}_2\text{Ar}^*_2$ is mostly induced by an increase in the Auger electron kinetic energy. As the photoelectron binding energy does not undergo a significant shift, the gallium centres in both compounds must have a similar chemical state. The change in the Auger electron kinetic energy must result from an undetermined phenomenon after the initial ionization occurs in $\text{Ga}_2\text{I}_2\text{Ar}^*_2$. For compounds with a gallium oxidation number of +3 (Figure 3.11) and +2 (Figure 3.12), it appears that the expectation that final state effects are more influential than initial state effects is not observed within each oxidation number as the Auger parameters differ significantly as the ligands are varied for gallium compounds with higher assigned oxidation numbers unlike for the aforementioned copper compounds, where the higher oxidation number for copper, +2, resulted in domination of final state effects.²⁹

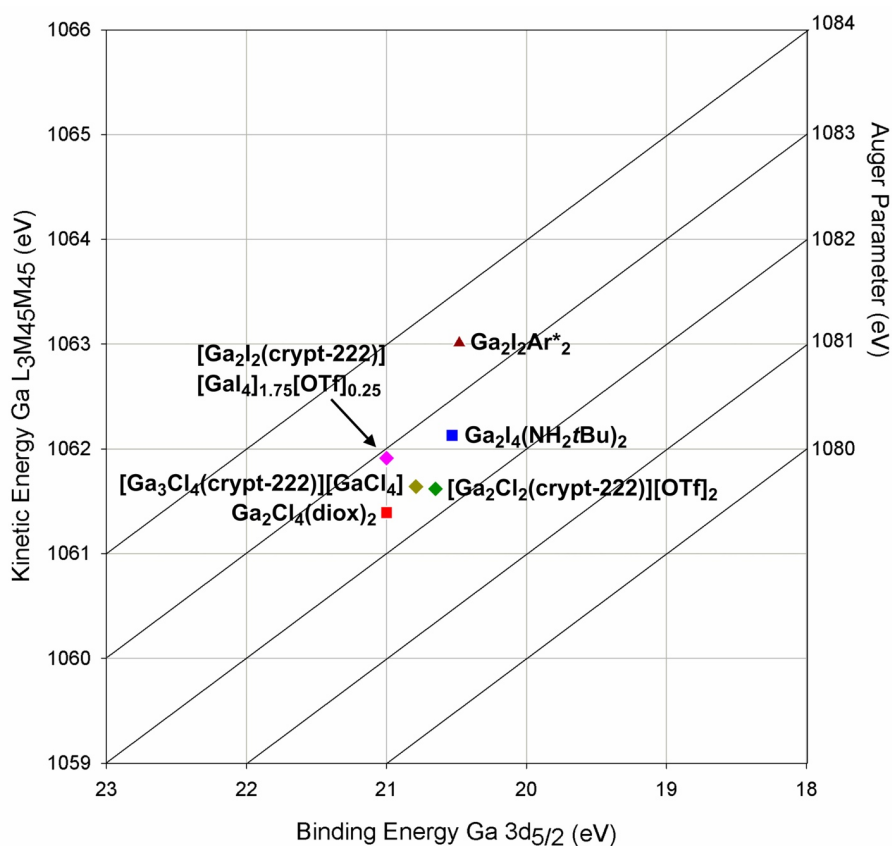


Figure 3.12: Wagner plot of Ga-Ga compounds using Ga 3d_{5/2} binding energy. Symbol legend: diamond = synthesized gallium-cryptand complexes; square = chloride and iodide ligands and O/N donors; triangle = iodide and terphenyl ligands.

Figure 3.13 shows the Wagner plot generated for gallium compounds with an oxidation number of +1. Although $\text{GaNaCNac}^{\text{Dipp}}$, $\text{K}[\text{GaDAB}^{\text{Dipp}}]$ and $[\text{Ga}(\text{prismand})][\text{OTf}]$ are classified as having the same oxidation number, they have significantly different Auger and photoelectron energies but similar Auger parameter values. The structures of $\text{GaNaCNac}^{\text{Dipp}}$ and $\text{K}[\text{GaDAB}^{\text{Dipp}}]$ are somewhat related, as they both possess anionic bidendate nitrogen ligands, however, the dianionic nature of the $[\text{DAB}^{\text{Dipp}}]^{2-}$ ligand leads to the coordination of a potassium counter-ion to the gallium centre in $\text{K}[\text{GaDAB}^{\text{Dipp}}]$, and thus, the gallium atom donates some of its electron density to the potassium cation, giving it a higher Ga 3d_{5/2} binding energy than $\text{GaNaCNac}^{\text{Dipp}}$. Similar to $[\text{Ga}][\text{GaCl}_4]$, the $[\text{Ga}(\text{prismand})]^+$ moiety in $[\text{Ga}(\text{prismand})][\text{OTf}]$ is cationic

with weak interactions between the neutral prismand macrocycle and the gallium, and thus, the gallium is more electron deficient in comparison to those complexes with covalent bidentate nitrogen ligands, leading to a lowering of the Ga $L_{3M_{45}M_{45}}$ kinetic energy, and an increase in the Ga $3d_{5/2}$ binding energy. The Auger parameter for [Ga(prismand)][OTf] is similar to that of [Ga][GaCl₄], where the gallium cation is also weakly stabilized and electron deficient. Despite the differences in the structures of the gallium compounds with an oxidation number of +1, they appear to have similar final state effects, as they all possess Auger parameter values of approximately 1082 eV, varying by only by 0.27 eV. Thus, the chemical states of these gallium compounds are more influenced by the nature of the attached ligands, and the polarization of the gallium centres upon ionization must be similar. The gallium in [Ga(prismand)][OTf] is similar in chemical state to the gallium trihalides (GaX₃) and would, therefore, be expected to act as a Lewis acid. Conversely, GaNacNac^{Dipp} and K[GaDAB^{Dipp}] are much more electron rich, and would be expected to act as Lewis bases, as well as being less reactive toward electron donors. Indeed, the Lewis basic nature of GaNacNac^{Dipp} and K[GaDAB^{Dipp}] is well-known.^{61,62} Finally, the difference in position on the Wagner plot between GaNacNac^{Dipp} and K[GaDAB^{Dipp}] can be attributed to the coordination of the potassium cation in the latter compound, decreasing the electron-richness of the gallium centre. The preceding analysis demonstrates how Wagner plots are effective at the prediction of reactivity pathways for novel main group compounds and can be a useful tool in the classification of the chemical states.

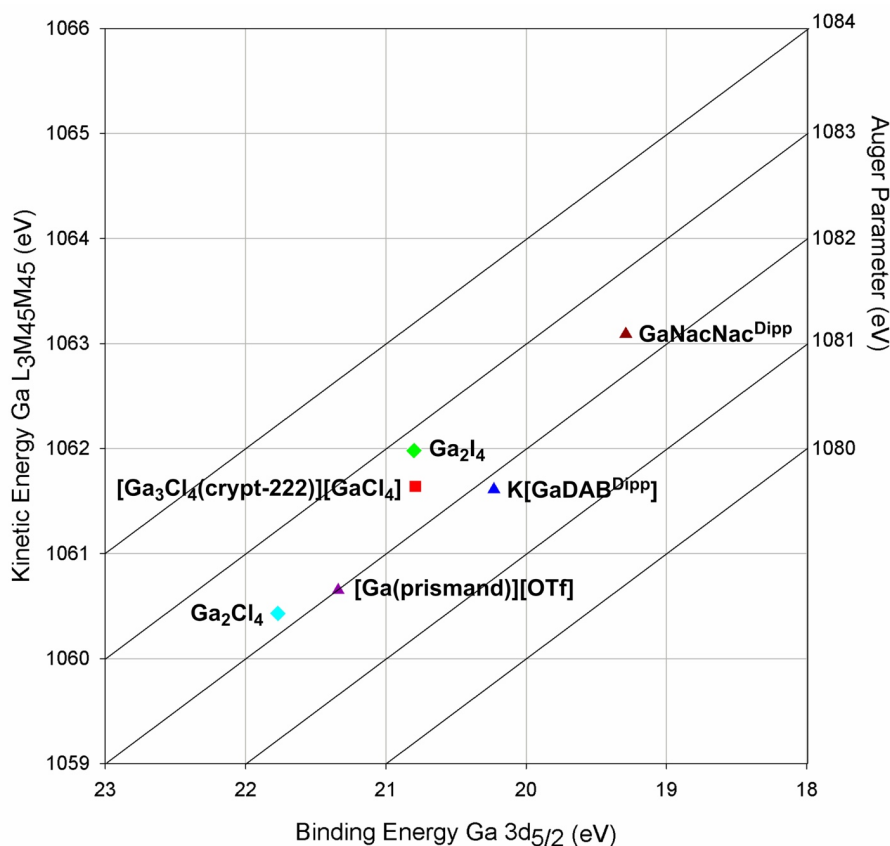


Figure 3.13: Wagner plot of Ga(I) compounds using Ga 3d_{5/2} binding energy. Symbol legend: diamond = halide ligands; square = chloride ligands and O/N donors; triangle = organic ligands.

Figure 3.14 gives the Wagner plot for selected gallium complexes stabilized by chlorine and/or nitrogen-based ligands of all oxidation numbers. It is evident that the Auger parameters are all very similar, leading to the generation of a trendline with a slope of approximately 1, indicating that, for this series of compounds, similar final state effects are observed whereas the initial state effects differ significantly ($\Delta(\Delta R) = 0.28$ eV; $\Delta(\Delta \epsilon) = 2.43$ eV). Again, the similarity of the final state effects can be understood on the basis of the nature of the ligands; chloride and nitrogen are both hard bases,³ with minimal polarizability and little effect on the polarizability of the gallium. However, their effect on the gallium centres can be observed in the significant initial state shifts. Three distinct regions of the Wagner plot can be identified in Figure 3.14. The bottom left area

of the plot with $\text{Ga } L_3M_{45}M_{45} \leq 1061 \text{ eV}$ and $\text{Ga } 3d_{5/2} \geq 21.5 \text{ eV}$, correlates to the most electron deficient gallium complexes often with an oxidation number of +3. An intermediate area is present in the centre of the plot ($1061 \leq \text{Ga } L_3M_{45}M_{45} \leq 1062 \text{ eV}$ and $21.5 \geq \text{Ga } 3d_{5/2} \geq 20.5 \text{ eV}$), where most compounds with an oxidation number of +2 and the gallium-cryptand complexes are located. Toward the upper right of the plot ($\text{Ga } L_3M_{45}M_{45} \geq 1062 \text{ eV}$; $\text{Ga } 3d_{5/2} \leq 20.5 \text{ eV}$), electron-rich gallium compounds that are in the +1 oxidation number can be found. Not only can the oxidation numbers be determined using this method, these data allow for a classification of the complexes on the basis of their chemical states. Furthermore, analogous reactivity might be expected from complexes with gallium in similar chemical states. The ability of XPS to differentiate clearly between multiple chemical states of molecular gallium compounds is a striking result, as this technique is widely accessible, although sparingly used, for this purpose. Furthermore, since XPS is widely accessible, our results suggest that this technique can be easily applied to the study of other main group molecular complexes to aid in the understanding of their electronic nature and reactivity.

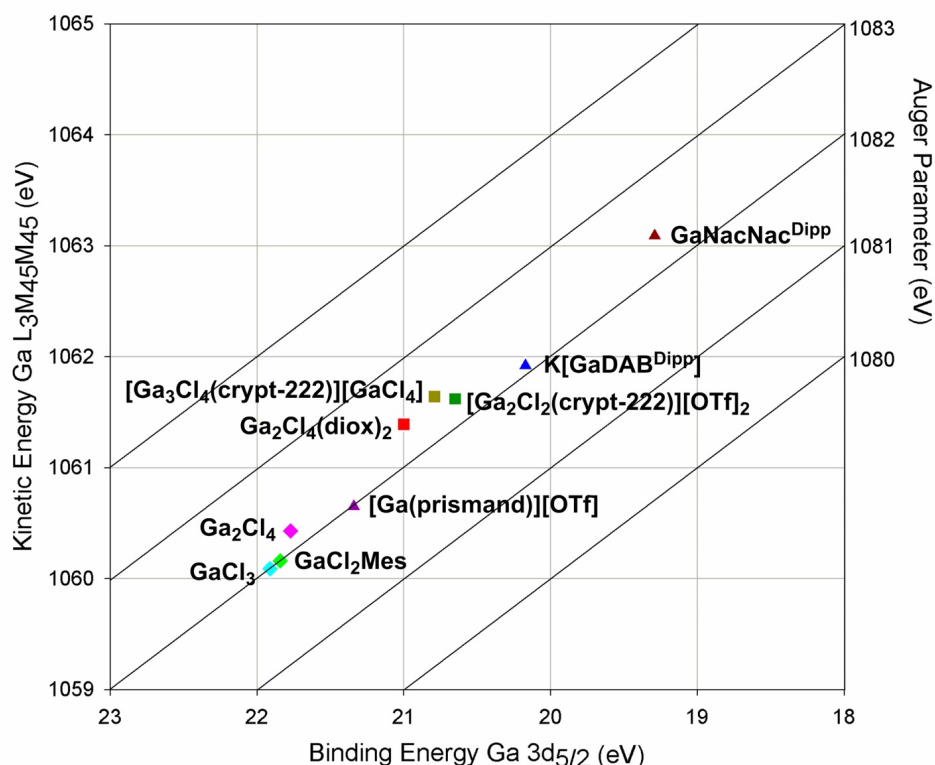


Figure 3.14: Wagner plot of gallium-chloride and gallium-nitrogen compounds using Ga $3d_{5/2}$ binding energy. Symbol legend: diamond = Ga(III); square = Ga(II); triangle = Ga(I).

The Wagner plot for gallium-iodide complexes, shown in Figure 3.15, does not appear to have distinct groupings as a function of ligand or oxidation number. Unlike the chloride-containing complexes, a trendline cannot be generated for the gallium-iodide compounds and it is unclear whether initial or final state effects dominate. This could be due to the increased number of electrons in iodide ligands in comparison to chloride, where it is able to donate more electron density to the gallium centre in gallium-iodide compounds, limiting the shifts in binding energy of the gallium centres. The polarizability of iodine, with its diffuse electron cloud could also contribute to the inconsistency of the Auger parameter for gallium-iodide complexes. Notably, compounds with different oxidation numbers ($\text{Ga}_2\text{I}_4(\text{NH}_2t\text{Bu})_2$, $[\text{Ga}_2\text{I}_2(\text{crypt-222})][\text{GaI}_4]_{1.75}[\text{OTf}]_{0.25}$

compared to $[\text{Ga}][\text{GaI}_4]$ and GaI_3) are in close proximity, which demonstrates that although the four compounds are classified differently based on their assigned oxidation numbers, the experimentally determined chemical states of the gallium centres indicate they are all very similar in nature and should exhibit similar reactivity. Once again, the formalism of oxidation or valence numbers fails to accurately describe the chemical state of a given element which may lead to misconceptions of the reactivity. Not surprisingly, experimental determinations of chemical states are more appropriate and should lead to more accurate predictions of reactivity.²

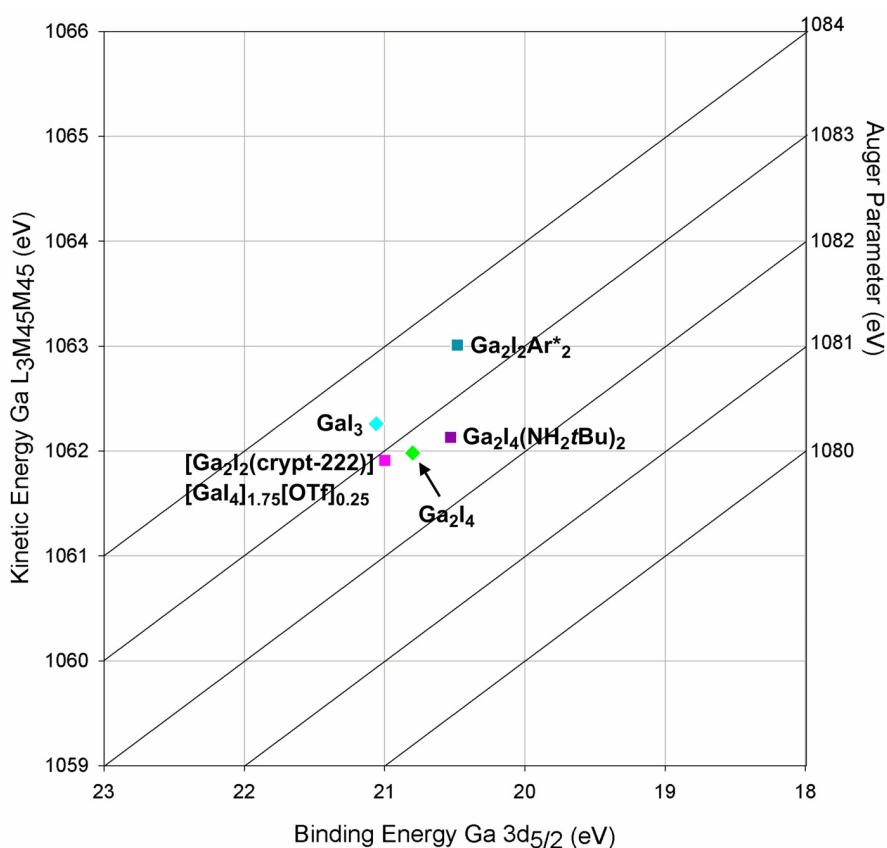


Figure 3.15: Wagner plot of gallium-iodide compounds using Ga 3d_{5/2} binding energy. Symbol legend: diamond = Ga(III); square = Ga(II).

As shown in Figure 3.14, the data points for $[\text{Ga}_3\text{Cl}_4(\text{crypt-222})][\text{GaCl}_4]$, $[\text{Ga}_2\text{Cl}_2(\text{crypt-222})][\text{OTf}]_2$ and $[\text{Ga}_2\text{I}_2(\text{crypt-222})][\text{GaI}_4]_{1.75}[\text{OTf}]_{0.25}$ fall within the

intermediate section of the Wagner plot. An oxidation number of +2 for $[\text{Ga}_2\text{Cl}_2(\text{crypt-222})][\text{OTf}]_2$ and its iodide-substituted analogue is consistent with the solution-state NMR spectroscopic data and computational data, where both gallium centres are equivalent and each have a charge of +1. Other compounds with similar connectivity are located in this area of the Wagner plot. The proximity of the data points for both $[\text{Ga}_2\text{Cl}_2(\text{crypt-222})][\text{OTf}]_2$ and $[\text{Ga}_2\text{I}_2(\text{crypt-222})][\text{GaI}_4]_{1.75}[\text{OTf}]_{0.25}$ on the Wagner plot indicates that the macrocyclic ether ligand has a stronger influence on the Auger parameter compared to the halide ligands attached to the gallium centre. Despite the presence of an additional gallium environment, namely the tetraiodogallate(III) anion, the location of $[\text{Ga}_2\text{I}_2(\text{crypt-222})][\text{GaI}_4]_{1.75}[\text{OTf}]_{0.25}$ on the Wagner plot it is not significantly different from the positions of the other two gallium-cryptand[2.2.2] complexes.

While the dicationic nature of the $[\text{Ga}_2\text{X}_2(\text{crypt-222})]^{2+}$ complexes might be expected to result in significant electron deficiency at the gallium centres, they are positioned within the intermediate region of the Wagner plot (Figure 3.14). Although XPS data of the precursor to $[\text{Ga}_2\text{X}_2(\text{crypt-222})]^{2+}$, $\text{Ga}_2\text{Cl}_4(\text{THF})_2$, was not obtained due to its poor stability,^{13,63} the THF complex is analogous to $\text{Ga}_2\text{Cl}_4(\text{diox})_2$, which also contains a $\text{Cl}_2\text{GaGaCl}_2$ core stabilized by ether donors. $\text{Ga}_2\text{Cl}_4(\text{diox})_2$ is located in close proximity to the two $[\text{Ga}_2\text{X}_2(\text{crypt-222})]^{2+}$ dications on the Wagner plot in Figure 3.14, suggesting that upon removal of halide ligands and coordination of cryptand[2.2.2], the chemical state of the gallium does not significantly differ from $\text{Ga}_2\text{Cl}_4(\text{diox})_2$, and therefore, from the $\text{Ga}_2\text{Cl}_4(\text{THF})_2$ precursor. The Auger parameters for both dications are slightly elevated from $\text{Ga}_2\text{Cl}_4(\text{diox})_2$ due to the effective coordination of the multidentate cryptand[2.2.2] donor; the gallium centres are more electron rich in these compounds, resulting in higher Auger electron kinetic energies, and lower photoelectron binding energies. This is quite striking, as upon initial scrutiny of the gallium-cryptand[2.2.2] complexes, it is not immediately obvious that the gallium centres in these cations would be more electron rich than the starting materials given the charge assigned to the gallium centres.

While several of the postulated bonding models for $[\text{Ga}_3\text{Cl}_4(\text{crypt-222})]^+$ suggested that it may have at least one gallium(I) centre, this is not reflected in the XPS

data on the basis of its Auger parameter, which was greater than those of $\text{GaNaCNac}^{\text{Dipp}}$ and $\text{K}[\text{GaDAB}^{\text{Dipp}}]$, and its position near the centre of the Wagner plot in Figure 3.14. While structural data for $[\text{Ga}_3\text{Cl}_4(\text{crypt-222})][\text{GaCl}_4]$ demonstrated four structurally unique gallium atoms, only one signal was observed in the XPS spectrum. The resolution of the experiment is limited by the natural line width of the gallium signals²⁴ and individual environments may not be resolved, however, if multiple gallium environments were present, the signal would be expected to be broad. The signals for $[\text{Ga}_3\text{Cl}_4(\text{crypt-222})][\text{GaCl}_4]$ are narrow with FWHM between 1.63 and 2.10 eV, consistent in magnitude with the FWHM of other compounds possessing only one unique gallium environment and suggesting that all gallium atoms in the complex have similar chemical states despite the variation in coordinating ligands.¹⁷ On the basis of the XPS data, the chemical state of $[\text{Ga}_3\text{Cl}_4(\text{crypt-222})]^+$ most closely resembles compounds with an oxidation number of +2, and would, therefore, be expected to react similarly to $\text{Ga}_2\text{Cl}_4(\text{diox})_2$ and $\text{Ga}_2\text{I}_4(\text{NH}_2t\text{Bu})_2$. The same trend was also observed for the $[\text{Ga}_2\text{X}_2(\text{crypt-222})]^{2+}$ complexes. Thus, in comparison to $\text{Ga}_2\text{Cl}_4(\text{diox})_2$, all three gallium-cryptand complexes are expected to act as electrophiles, and may react with a variety of Lewis bases and nucleophiles, however, such reactivity may be impeded by the bulkiness of the cryptand ligand. Once again, the ability of XPS to allow for more precise reactivity predictions compared to qualitative descriptors is evident.

As a significant amount of XPS data have been reported for a variety of solid-state gallium materials, a Wagner plot for the gallium materials is presented in Figure 3.16. The Auger parameter values were obtained by averaging all of the data available for each compound in the NIST XPS database.^{32,33,34,35,36,37,38,39,40,50,51,52,53,54,59} A sample of Ga_2O_3 was analyzed in this study to determine whether the analytical methods used in this study were within experimental error of the data reported. Although some variation was observed between the data obtained experimentally for Ga_2O_3 and that reported in the literature,^{32,35,50,51} the difference in the Ga $3d_{5/2}$ binding energy was approximately 0.4 eV, which falls within experimental error.²⁴ This could also be a result of the different possible polymorphs for Ga_2O_3 .³ In our study, $\beta\text{-Ga}_2\text{O}_3$ was used, which has both tetrahedral and octahedral sites for the gallium centres within the crystal structure.⁶⁴

Similar to the trends observed for the gallium trihalides, trendlines with large slopes were evident for Ga(Group 15) and Ga₂(Group 16)₃ materials. The slopes were larger than for the gallium trihalides, and demonstrate that for both Group 15 and 16 gallium materials, initial state shifts do not change nearly as much as the final state shifts upon descending the group, especially for Group 16 (Group 15: $\Delta(\Delta R) = 0.86$ eV; $\Delta(\Delta \epsilon) = 0.46$ eV; Group 16: $\Delta(\Delta R) = 3.34$ eV; $\Delta(\Delta \epsilon) = 1.1$ eV). Thus, final state effects dominate for these materials, which demonstrates that the nature of the Group 15 or 16 elements has a vast influence on the electronic properties of the material, specifically following ionization. Interestingly, the location of the gallium materials on the Wagner plot is close to gallium metal. All of the materials shown in Figure 3.16 except Ga₂O₃ have significantly elevated Auger parameters in comparison to the molecular gallium compounds (≥ 1084 eV for the gallium materials; ≤ 1083 eV for molecular compounds), despite the gallium in each of the compounds having an oxidation number of +3. The Ga 3d_{5/2} binding energies are lowered significantly, and suggest that these materials are alloy-like, with significant electron mobility. This is indeed the case for the Group 15 materials, as gallium nitride, phosphide and arsenide are all semiconductors used in the electronics industry.⁶⁵ Additionally, as the atomic number of the Group 15 element increases, the bonding becomes more metallic; the relative size of arsenic and gallium are more similar compared to nitrogen and gallium. Given the position of GaAs on the Wagner plot, clearly the individual atoms are more elemental in nature, and more closely related to gallium metal in terms of their electron richness, than to the electron deficient gallium trihalides. A similar trend is observed for the Group 16 gallium materials. Ga₂O₃ is a wide gap semiconductor and an important industrial material.⁶⁶ When oxygen is substituted for selenium, the material, Ga₂Se₃, has a smaller band gap, and therefore, there is a significant increase in electron motility.

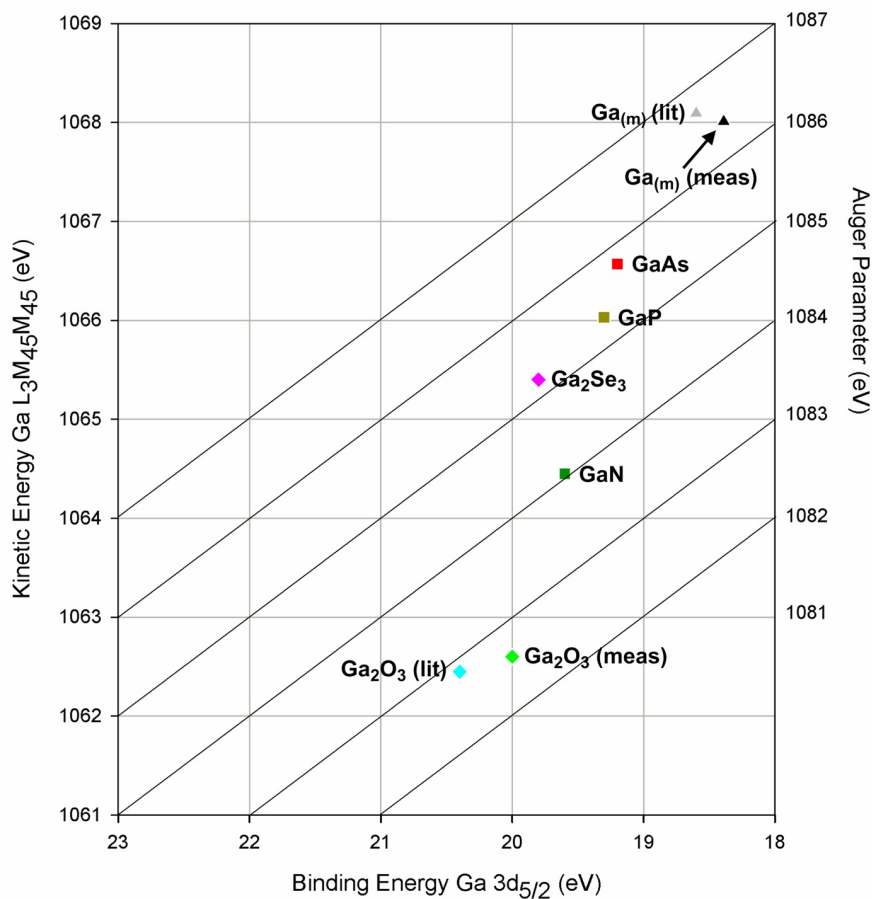


Figure 3.16: Wagner plot of gallium materials using Ga 3d_{5/2} binding energy. Symbol legend: square = Group 15 elements; diamond = Group 16 elements.

Similar Wagner plots were generated using the Ga 2p_{3/2} signal and compared to those generated using the Ga 3d_{5/2} signal. The Ga 2p_{3/2} Wagner plots are presented in the supplementary information (Figure A.8 to Figure A.12). The same trends were observed, including a slope approaching 3 for the gallium trihalides, indicating final state effects varied for GaX₃ compounds, and initial state effects did not, which is more pronounced than for the Ga 3d_{5/2} photoemission ($\Delta(\Delta R) = 0.73$ eV; $\Delta(\Delta \epsilon) = 0.11$ eV). As for the Ga 2p_{3/2} transition of the selected gallium-chloride and -nitrogen compounds, the trendline with a slope of approximately 1 and the initial and final state shifts ($\Delta(\Delta R) = 0.20$ eV; $\Delta(\Delta \epsilon) = 2.35$ eV) were similar to those observed with the Ga 3d_{5/2} data. While some of

the Auger parameter data points were more dispersed in the Ga $2p_{3/2}$ data, for example, in the gallium-chloride compounds, some overlap was observed (Figure A.12). Although the gap between the electron deficient and intermediate regions of the Wagner plot were more pronounced for the Ga $2p_{3/2}$ data, the intermediate and electron rich regions overlapped, suggesting that the Ga $3d_{5/2}$ data are more useful for chemical speciation as expected, due to the increased sensitivity of the Ga $3d_{5/2}$ signal to small changes experienced by the valence electrons.

3.2.2 X-ray Absorption Spectroscopy

Complexes possessing two Ga centres with different oxidation numbers (Ga(I)/(III)), namely [Ga(prismand)][GaCl₄] and Ga[GaCl₄] are examined first. The XAS spectrum of [Ga(prismand)][GaCl₄] contains two sharp peaks (labeled A and B, indicated with vertical dashed lines in Figure 3.17) at 10369 eV and 10372 eV, respectively, which can be attributed to different Ga centres exhibiting distinct chemical states. The energy position of peak B is the same as that of the ionic compound Na[GaCl₄] (Figure 3.17), which allows the assignment of peak B in the XAS of [Ga(prismand)][GaCl₄] to the tetrachlorogallate anion. Peak A, on the other hand, appears at lower energy, indicating the Ga centre at that site has higher electron density (i.e. a lower oxidation number),^{67,68} and thus, can be assigned to the prismand-complexed Ga⁺. Both peaks A and B are narrow and well-resolved, indicating the two Ga species are highly ionic. In other words, charge transfer between the Ga sites is minimal. Ga[GaCl₄] exhibits a different spectral profile. Unlike the two well-resolved peaks of [Ga(prismand)][GaCl₄], Ga[GaCl₄] contains a broad XAS spectral profile with the energy of the maximum absorption matching that of the tetrachlorogallate anion. A lower energy feature is present as a shoulder. The broad signal in the XAS of Ga[GaCl₄] suggests that even though there may be two distinct Ga chemical states in the complex, they are not isolated ions and cannot be well-resolved by XAS; the observed broadening of the spectrum is likely caused by charge transfer between the two Ga centres.

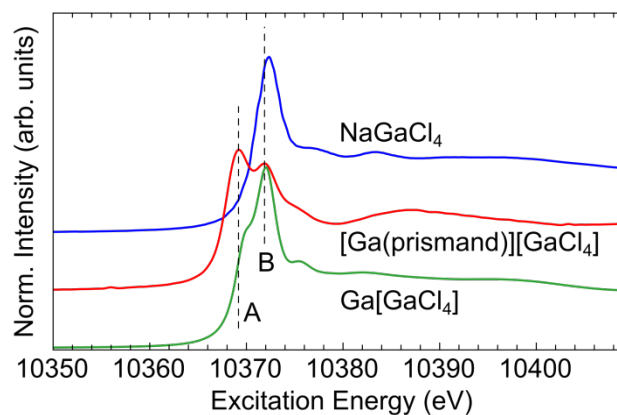


Figure 3.17: Ga K-edge XAS spectra of $[\text{Ga}(\text{prismand})][\text{GaCl}_4]$ and $\text{Ga}[\text{GaCl}_4]$ in comparison with $\text{Na}[\text{GaCl}_4]$.

FDMNES calculations reveal that the XAS spectrum of each salt can be deconvoluted into contributions from two gallium sites, as shown in Figure 3.18. The calculations of the tetrachlorogallate anion demonstrate that the XAS spectral features are dominated by the short-range chemical environment, since the tetrachlorogallate sites in $\text{Ga}[\text{GaCl}_4]$ and $[\text{Ga}(\text{prismand})][\text{GaCl}_4]$, as well as that of the simple salt, NaGaCl_4 , exhibit only minor differences due to the different cations (Ga^+ , Na^+ , or $[\text{Ga}(\text{prismand})]^+$), these minor differences mostly occur well above the absorption edge (i.e. above 10375 eV). More importantly, the calculated position of peak A in $[\text{Ga}(\text{prismand})][\text{GaCl}_4]$ appears at a slightly lower energy than the corresponding peak for $\text{Ga}[\text{GaCl}_4]$ and the intensity of peak A in $[\text{Ga}(\text{prismand})][\text{GaCl}_4]$ relative to the intensity of peak B is noticeably greater compared to the intensities of the analogous peaks in $\text{Ga}[\text{GaCl}_4]$.

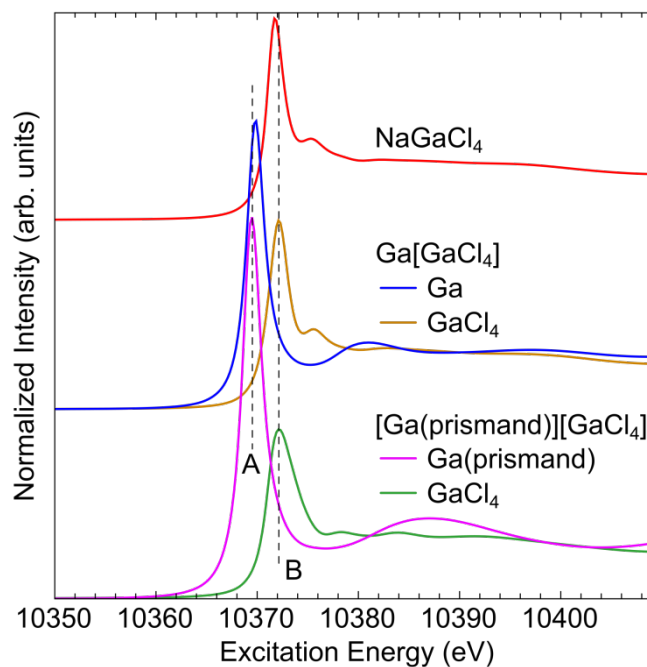


Figure 3.18: Calculated Ga K-edge XAS spectra of $[\text{Ga}(\text{prismand})][\text{GaCl}_4]$ and $\text{Ga}[\text{GaCl}_4]$, showing the influence of the chemical environment on the spectra.

X-ray absorption spectra, measured in fluorescence mode, often suffers from self-absorption, wherein X-rays emitted during the absorption process are re-absorbed by the sample and do not reach the fluorescence detector. A few strategies have been suggested to correct for self-absorption;^{69,70} however, removing the influence of self-absorption from a measured spectrum without introducing artefacts is very challenging. In our case, Ga is the only heavy element present, and the background absorption from the other light elements is approximately constant throughout the Ga K-edge measurement range employed. In this situation, the full expression for self-absorption,⁶⁹ which is complicated, can be reduced to that shown in Equation 4.

$$I(E) = \frac{A\mu_{\text{Ga}}(E)}{\mu_{\text{Ga}}(E)+B} \quad (4)$$

In Equation 4, $\mu_{\text{Ga}}(E)$ is the true absorption of Ga at excitation energy E , $I(E)$ is the measured absorption intensity at excitation energy E , A is the product of the fluorescence rate for Ga K-edge emission, as well as various experimental factors such as detector efficiency, and B is the sum the background absorption from the other elements and the

total absorption at the fluorescence energy, E_F . Despite the simple form of Equation 1, it is difficult to invert this equation to obtain $\mu_{Ga}(E)$ since some situations will result in division by values close to zero. Instead linear fitting with the measured spectrum was employed to find values of A and B that result in a “calculated with self-absorption” spectrum based on $\mu_{Ga}(E)$ obtained from FDMNES (the calculated spectrum). The resulting calculated spectra with and without self-absorption are shown along with the measured spectra in Figure 3.19. Self-absorption reduces the relative intensity of peak A relative to peak B in $[\text{Ga}(\text{prismand})][\text{GaCl}_4]$, resulting in a rather good agreement with the measured XAS spectrum. However self-absorption alone does not sufficiently reduce the intensity of peak A relative to peak B in $\text{Ga}[\text{GaCl}_4]$, unless the ratio of cationic to anionic Ga (nominally 1:1) is reduced to 1:3. Thus, for the self-absorption corrected spectrum, we only show the one using a 1:3 ratio of cationic to anionic Ga for $\text{Ga}[\text{GaCl}_4]$ in Figure 3.19.

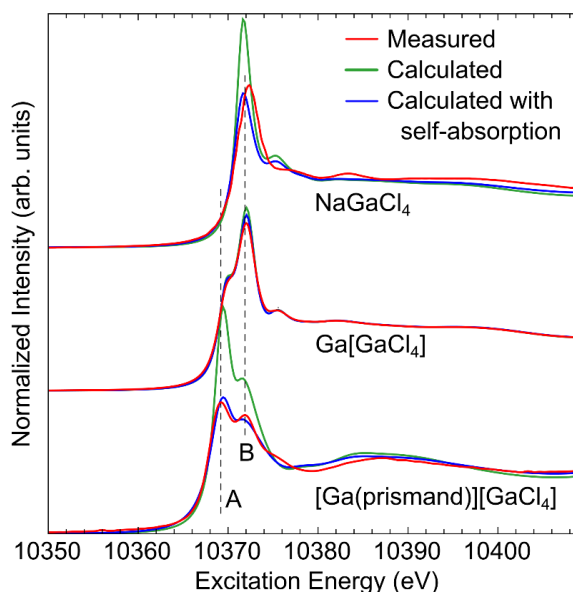


Figure 3.19: Measured and calculated (with and without self-absorption) Ga K-edge XAS of NaGaCl_4 , $\text{Ga}[\text{GaCl}_4]$, and $[\text{Ga}(\text{prismand})][\text{GaCl}_4]$.

Our interpretation of the XAS data of $[\text{Ga}(\text{prismand})][\text{GaCl}_4]$ and $\text{Ga}[\text{GaCl}_4]$ are consistent with the previous XPS results, as it was postulated that although both

[Ga(prismand)][GaCl₄] and Ga[GaCl₄] contain a gallium(I) centre, the gallium(I) cations are not as electron rich as one would expect on the basis of the assigned oxidation number and that the Ga(I) cation in Ga[GaCl₄] is more electron deficient than that in [Ga(prismand)][GaCl₄]. Therefore the reduction of the Ga(I):Ga(III) ratio necessary for the calculated spectrum of Ga[GaCl₄] to match the measured one, may in fact be a consequence of the *relative electron deficiency*, rather than *absence*, of Ga(I) sites in comparison to Ga(III) sites.

Gallium complexes which contain two Ga centres of purportedly the same oxidation number and similar coordination environments were then examined: [Ga₂Cl₂(crypt-222)][OTf]₂ and Ga₂Cl₄(1,4-dioxane)₂. Although the two gallium cores of [Ga₂Cl₂(crypt-222)][OTf]₂ are non-equivalent in the solid-state, the local structure of the Ga atoms are identical, with the same bonding arrangement: each Ga is bonded to a nitrogen, chlorine and a second Ga in a plane, with two oxygens in axial positions above and below the plane with only one being within bonding distance.¹⁷ Two crystal structures have been reported for Ga₂Cl₄(1,4-dioxane)₂;^{58,71} however, in our study a new polymorph was obtained using modified recrystallization conditions.⁷² In the new polymorph, each gallium is *pseudo*-five-coordinate, being linked to a strongly bound 1,4-dioxane molecule, in addition to two chlorines and a gallium, and a more weakly bound bridging dioxane fragment. Thus, the pseudo-five coordinate environment of the gallium centres in Ga₂Cl₄(1,4-dioxane)₂ is similar to the coordination environment of the Ga in [Ga₂Cl₂(crypt-222)][OTf]₂ (bond lengths to distal oxygen atoms: 2.631(1) vs 2.424(2) Å, respectively), as shown in Figure 3.20.

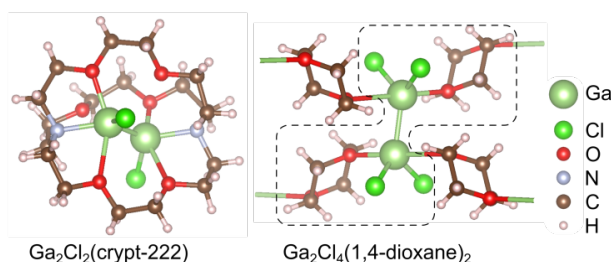


Figure 3.20: Local structures of *pseudo*-five coordinate Ga sites in [Ga₂Cl₂(crypt-222)][OTf]₂ (only the cation is shown, the OTf is omitted) and Ga₂Cl₄(1,4-dioxane)₂.

Figure 3.21 shows the Ga K-edge XAS spectra of $[\text{Ga}_2\text{Cl}_2(\text{crypt-222})][\text{OTf}]_2$ and $\text{Ga}_2\text{Cl}_4(1,4\text{-dioxane})_2$. Both complexes exhibit a broad peak in their XAS spectra: $\text{Ga}_2\text{Cl}_4(1,4\text{-dioxane})_2$ exhibits a low-energy shoulder, while $[\text{Ga}_2\text{Cl}_2(\text{crypt-222})][\text{OTf}]_2$ exhibits a high-energy shoulder. Compared to the XAS spectrum of $\text{Ga}[\text{GaCl}_4]$ (in which a shoulder was related to a different Ga site), one might be tempted to attribute these features to multiple Ga sites. However, the calculated (FDMNES) spectra reveal that this is not the case: calculated and experimental spectra all emphasize that a single Ga site, especially one in a covalent environment, can exhibit considerable fine structure in an XAS spectrum, rather than a single sharp spectral feature. The calculated XAS spectrum of $[\text{Ga}_2\text{Cl}_2(\text{crypt-222})][\text{OTf}]_2$ is in good agreement with the measured spectrum, especially after simulating the effect of self-absorption in the calculated spectrum. The agreement for $\text{Ga}_2\text{Cl}_4(1,4\text{-dioxane})_2$ is not as good, although the main features are present in both: a weak low-energy shoulder near 10370 eV, a main peak, and a weak high-energy shoulder above 10374 eV. The discrepancy observed between calculated and measured spectra occurs because $\text{Ga}_2\text{Cl}_4(1,4\text{-dioxane})_2$ measured in this work has high crystal symmetry (space group F_{ddd}), with only one crystallographically unique Ga site.⁷² This is in contrast to $[\text{Ga}_2\text{Cl}_2(\text{crypt-222})][\text{OTf}]_2$, in which the two Ga sites, while sharing the same local chemical environment, are crystallographically inequivalent due to a difference in long range order. In practice, including these two almost identical Ga sites in the calculated XAS spectrum of $[\text{Ga}_2\text{Cl}_2(\text{crypt-222})][\text{OTf}]_2$ produces a reasonable approximation of the *anharmonic* disorder, which is present in the measured spectrum. Since the approximation of anharmonic disorder is lacking in the calculated XAS spectrum for $\text{Ga}_2\text{Cl}_4(1,4\text{-dioxane})_2$, features in this spectrum are visibly more narrow than those in the measured spectrum. Nevertheless, as noted above, the three main spectral features (low energy shoulder, main peak, and high energy shoulder) are present in both measured and calculated spectra.

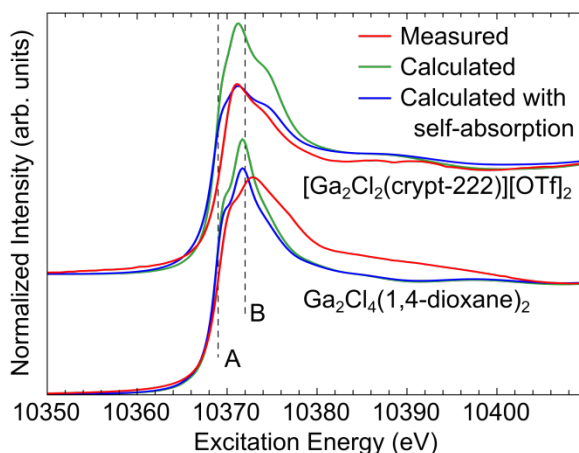


Figure 3.21: Experimental and calculated Ga K-edge XAS of $\text{Ga}_2\text{Cl}_4(1,4\text{-dioxane})_2$ and $[\text{Ga}_2\text{Cl}_2(\text{crypt-222})][\text{OTf}]_2$. The dashed lines A and B mark the energy position of the Ga(I) and Ga(III) features of $[\text{Ga}(\text{prismand})][\text{GaCl}_4]$ and $\text{Na}[\text{GaCl}_4]$ (see Figure 3.19).

It is apparent, however, that the main resonance of the cryptand-complex, $[\text{Ga}_2\text{Cl}_2(\text{crypt-222})][\text{OTf}]_2$, is located between the two peaks of either $\text{Ga}[\text{GaCl}_4]$ or $[\text{Ga}(\text{prismand})][\text{GaCl}_4]$ (the peak positions of $[\text{Ga}(\text{prismand})][\text{GaCl}_4]$ are marked by lines A and B in Figure 3.21). Compared to the single Ga isolated in a prismand cage, the chloride that is bonded to Ga in $[\text{Ga}_2\text{Cl}_2(\text{crypt-222})][\text{OTf}]_2$ withdraws electron density from the Ga, making it less electron rich than the Ga(I) core in $[\text{Ga}(\text{prismand})][\text{GaCl}_4]$ but not as electron deficient as the Ga core in $[\text{GaCl}_4]^-$, and thus, the main absorption appears at an energy between those which have been attributed to Ga(I) and Ga(III) and allows us to assign an oxidation number of Ga(II) to the gallium cores in the complex.

When the cryptand cage is replaced by the dioxane ligands, the main resonance further shifts to higher energy. The trend is similar to our previous XPS observation, that the chemical state of the Ga in $\text{Ga}_2\text{Cl}_4(1,4\text{-dioxane})_2$ is slightly more electron deficient than that of $[\text{Ga}_2\text{Cl}_2(\text{crypt-222})][\text{OTf}]_2$. As is evident in the Ga K-edge XAS, the absorption for $\text{Ga}_2\text{Cl}_4(1,4\text{-dioxane})_2$ shares the same energy onset as that of $[\text{Ga}_2\text{Cl}_2(\text{crypt-222})][\text{OTf}]_2$ indicating the gallium in the dioxane complex has the same chemical state as in the cryptand complex, and thus, is a Ga(II) compound; differences at higher energies, including the energy of the maximum absorption feature, are due to a

different distribution of unoccupied Ga states in the two compounds. With an additional electronegative chloride ligand on the Ga core, the main absorption peak shifts to higher energy. Furthermore, as is evident from the broadness of the signal, the interaction between the Ga core and the dioxane ligand is stronger than the interaction of Ga with the cryptand ligand. A recent study on the Ga-modified zeolites using Ga K-edge XAS revealed that the changes in the identity and number of Ga nearest neighbors can give rise to changes in XAS that exhibit a similar trend caused by oxidation number variation, so that the commonly interpreted spectral evidence for Ga(III) to Ga(I) reduction during catalysis is not always accurate.⁷³ This again supports our hypothesis that to predict the chemical nature of the core element in a coordination complex using oxidation number formalism is not always reliable.

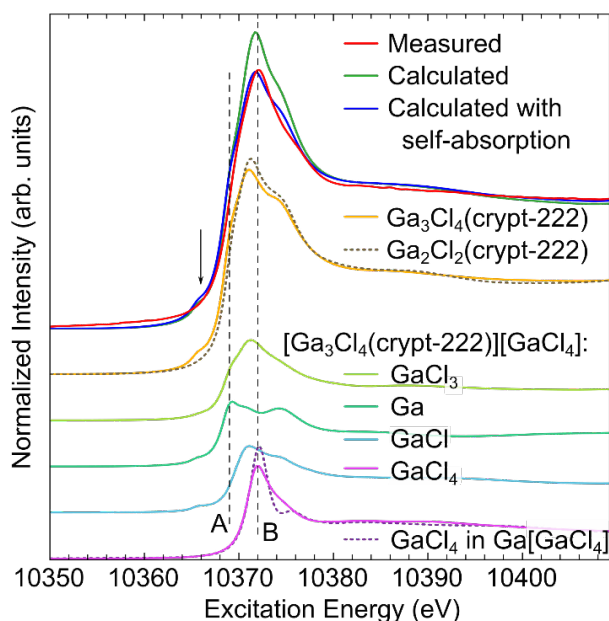


Figure 3.22: Experimental and calculated Ga K-edge XAS of $[\text{Ga}_3\text{Cl}_4(\text{crypt-222})][\text{GaCl}_4]$ shown at the top. Below that, the calculated contribution from the sum of the Ga sites within the cryptand (labeled $\text{Ga}_3\text{Cl}_4(\text{crypt-222})$, solid orange line) is directly compared to the calculated spectrum of $[\text{Ga}_2\text{Cl}_2(\text{crypt-222})][\text{OTf}]_2$ (dotted brown line).

Finally, the calculated spectrum from each Ga site in $[\text{Ga}_3\text{Cl}_4(\text{crypt-222})][\text{GaCl}_4]$ is shown independently. The calculated spectrum from the $[\text{GaCl}_4]^-$ in $\text{Ga}[\text{GaCl}_4]$ is shown at the bottom (dotted purple line) in direct comparison with the $[\text{GaCl}_4]^-$ site in the cryptand. The dashed lines A and B mark the energy position of the Ga(I) and Ga(III) features of $[\text{Ga}(\text{prismand})][\text{GaCl}_4]$ and $\text{Na}[\text{GaCl}_4]$ (see Figure 3.19).

Lastly, an interesting complex containing four unique gallium centres, $[\text{Ga}_3\text{Cl}_4(\text{crypt-222})][\text{GaCl}_4]$ was examined. Multiple bonding descriptions were proposed on the basis of calculations, some of which suggested the presence of a Ga(0) core within in the cryptand.¹⁷ Figure 3.22 shows the XAS spectrum of this compound. Again, the calculated XAS spectrum is in good agreement with our measurements, albeit the calculations do predict a weak shoulder in the pre-edge (indicated by the arrow in Figure 3.22) that is not observed in our measurements. Since the predicted feature is at lower energies compared to the remaining features of the spectrum, it is tempting to ascribe this feature to a Ga(0) site. However, examination of the spectra from each of the Ga sites (Figure 3.22) shows that *all* of the cryptand-coordinated Ga sites ($[\text{GaCl}_3]$, $[\text{Ga}]$, and $[\text{GaCl}]$) provide some contribution to the low-energy feature; it is not due to one single site. Thus, our calculation does not predict the presence of Ga(0); the lowest unoccupied molecular orbital (LUMO) is delocalized over all three cryptand-coordinated Ga sites. The lack of this feature in our measured spectrum suggests that the LUMO is at higher energies than predicted by FDMNES. However, apart from this pre-edge feature, the remaining features in the calculated spectra can be correlated to the measured spectrum.

While the cryptand-coordinated Ga sites exhibit a unique fine structure in their respective calculated Ga K-edge XAS, the sum of these sites is in excellent agreement with the calculated XAS of $[\text{Ga}_3\text{Cl}_4(\text{crypt-222})][\text{GaCl}_4]$, as shown in Figure 3.22. Even though the cation has a $[\text{GaCl}]$, a $[\text{Ga}]$, and even a $[\text{GaCl}_4]$ unit that is located outside the cryptand cavity, all Ga centres within the cationic fragment of the complex have an electronic structure similar to $[\text{Ga}_2\text{Cl}_2(\text{crypt-222})][\text{OTf}]_2$. On the basis of the energy of the maximum absorption features in the calculated XAS, we could classify the central $[\text{Ga}]$ as Ga(I), the $[\text{GaCl}]$ as Ga(II), and the $[\text{GaCl}_3]$ as Ga(III), although based on the

rather broad width of these features and the additional significant fine structure, assigning a strict oxidation number is misleading. The conclusions from the XPS data is similar; $[\text{Ga}_3\text{Cl}_4(\text{crypt-222})]^+$ is best described as having an overall electronic environment most similar to an oxidation number of +2.

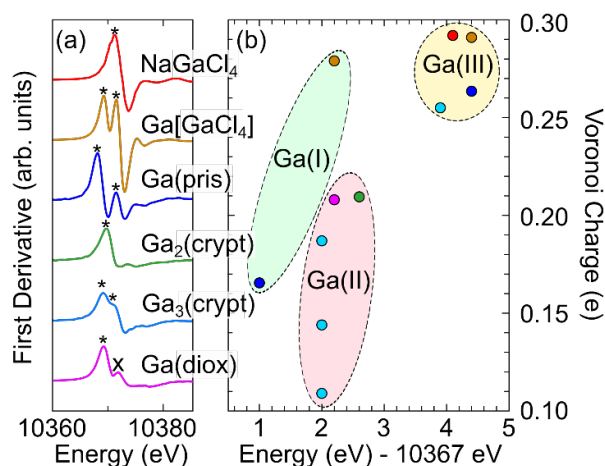


Figure 3.23: The first derivatives of the measured Ga K-edge XAS are shown in (a). The features that correlate with oxidation numbers are marked with *. A plot of the energies of these features (relative to the metallic Ga onset of 10367 eV) in comparison with the calculated atomic charge is shown in (b). The colour of the data markers in (b) matches the colour of the spectra in (a).

It is worth comparing the results of the assessment of the chemical states in these compounds using a joint experimental and theoretical approach to those that would be obtained by only inspecting the measured spectra, or only relying on electronic structure calculations. Since the onset of the XAS is often a clue to the oxidation number of the site under investigation, it is common to use the maxima in the first derivative of the spectrum to identify chemical states.⁷³ Figure 3.23(a) shows the first derivative of the measured XAS for all compounds under investigation near the absorption edge and the maxima associated with distinct chemical states are indicated by an asterisk in the figure. For most of these compounds the number of significant maxima in the first derivative of the XAS is in agreement with the expected number of distinct Ga oxidation numbers.

However, for $[\text{Ga}_3\text{Cl}_4(\text{crypt})\text{-222}][\text{GaCl}_4]$, there is only one significant maximum and a high energy shoulder; the former can be associated with all three of the cryptand-coordinated Ga sites, while the shoulder can be associated with the tetrachlorogallate anion. On the other hand, there is a small but clear secondary maxima observed in the XAS of $\text{Ga}_2\text{Cl}_4(1,4\text{-dioxane})_2$, which is evident in the first derivative of the spectrum that should *not* be considered a distinct chemical state, as it is part of the fine structure of the single Ga site and is predicted by the calculations. Our results show that for systems with significant core-ligand interaction, interpreting the XAS without the aid of calculated spectra may lead to erroneous conclusions.

The energy of the first derivative maxima that are associated with $[\text{GaCl}_4]^-$ are in good agreement with the calculated oxidation numbers based on Voronoi net charges using density functional theory. Although the Voronoi net charges are considerably less than the oxidation number, the Voronoi charges of Ga(III) sites correlate well with the higher energy in the first derivative maxima, as shown in Figure 3.23(b). The Ga(I) site of $[\text{Ga}(\text{prismand})][\text{GaCl}_4]$ also follows this pattern, with a small Voronoi charge and a lower energy in the first derivative maximum. However, the situation for the other Ga sites is less clear: The sites identified as Ga(II) all share very similar energies of the first derivative maxima, however, have a wide spread of calculated Voronoi charges, while the site nominally identified as Ga(I) in $\text{Ga}[\text{GaCl}_4]$ has a relatively high Voronoi charge (similar to Ga(III)) and a high energy of the first derivative maximum (similar to Ga(II)). This further reinforces that experimental and theoretical approaches should be combined when attempting to classify systems with significant core-ligand interaction.

3.3 Conclusions

In conclusion, we have performed XPS studies on a series of molecular gallium compounds with varying ligands and chemical environments. The photoelectron emissions of the Ga $3d_{5/2}$ and Ga $2p_{3/2}$ core electrons were measured, as well the Auger electron Ga $L_3M_{45}M_{45}$ emissions. Auger parameters were calculated and Wagner plots were generated which allowed for the chemical state determination of $[\text{Ga}_3\text{Cl}_4(\text{crypt-222})][\text{GaCl}_4]$ (2.1), $[\text{Ga}_2\text{Cl}_2(\text{crypt-222})][\text{OTf}]_2$ (2.2) and $[\text{Ga}_2\text{I}_2(\text{crypt-}$

222)][GaI₄]_{1.75}[OTf]_{0.25} (**3.1**). The XPS data demonstrate that the cations of **2.1**, **2.2**, and **3.1** are in an intermediate chemical state. The data also reveal that for **2.1**, although a single bonding model could not describe the bonding of the gallium centres of [Ga₃Cl₄(crypt-222)]⁺, which was demonstrated in the previously obtained data, it exists in an intermediate chemical state that is very similar to the other gallium-cryptand cations. The gallium trihalides have similar initial state effects, whereas gallium-chloride and -nitrogen complexes have similar final state effects. For molecular gallium complexes of different chemical states, namely electron rich and electron deficient, each were sufficiently separated to allow for the chemical state determination of these compounds. We have demonstrated the applicability of XPS to assess the chemical states of a variety of novel main group complexes giving valuable insights into the reactivity.

XAS is a facile, non-destructive spectroscopic technique that can be employed to investigate coordination complexes with multiple cores of the same element. When XAS measurements are supported by the appropriate calculations, or suitable reference spectra, in-depth analysis of the chemical environment of the cores can be performed. Macrocyclic ligands enable effective isolation of cationic Ga, as demonstrated by [Ga(prismand)][GaCl₄] and [Ga₂Cl₂(crypt-222)][OTf]₂. The former complex clearly contains features of a mixed valent complex (Ga(I)/(III)), and the latter is assigned as a Ga(II) species. The combined theoretical and experimental approach allows us to unambiguously determine the number of components present in XAS and to provide a qualitative assessment of the chemical state (oxidation number) of each Ga core, even for compounds that exhibit significant core-ligand interactions, such as in Ga[GaCl₄] and Ga₂Cl₄(1,4-dioxane)₂, that frustrates their analysis by XPS. We have also found that cryptand-coordinated Ga sites in [Ga₃Cl₄(crypt-222)][GaCl₄] exhibit Ga(II)-like features. A comprehensive approach using XAS to investigate the chemical states of coordination complexes can also be easily extended to the study of a variety of inorganic coordination complexes and organometallic compounds to gain valuable insights into their reactivities.

3.4 Experimental

3.4.1 General Considerations

All manipulations were performed under an inert atmosphere of argon using general Schlenk techniques or under an atmosphere of nitrogen in an MBraun glovebox unless otherwise stated. All solvents were purified using an Innovative Technologies 400-5 Solvent Purification System and were stored over activated 3 or 4 Å molecular sieves, unless otherwise stated. All reagents were used as received from Sigma-Aldrich, Alfa Aesar, Strem Chemicals or Gelest. Commercially available compounds (GaCl_3 , Strem; GaBr_3 , Alfa Aesar; GaI_3 , Gelest; Ga_2O_3 , Alfa) were used as received. ‘GaI’,⁷⁴ $[\text{Ga}_3\text{Cl}_4(\text{crypt-222})][\text{GaCl}_4]$ (**2.1**), $[\text{Ga}_2\text{Cl}_2(\text{crypt-222})][\text{OTf}]_2$ (**2.2**),¹⁷ $\text{GaNacNac}^{\text{Dipp}}$ (**3.2**),⁵⁷ $\text{K}[\text{GaDAB}^{\text{Dipp}}]$ (**3.3**),⁷⁵ $\text{Ga}_2\text{Cl}_4(1,4\text{-dioxane})_2$ (**3.5**),⁵⁸ $\text{Ga}_2\text{I}_4(\text{NH}_2^t\text{Bu})_2$ (**3.6**),⁷⁶ $\text{Ga}_2\text{I}_2(2,6\text{-dimesitylphenyl})_2$ (**3.7**),⁷⁷ GaCl_2Mes (**3.11**),⁷⁸ Ga_2Cl_4 (**3.12**),^{79,80} and Ga_2I_4 (**3.13**)⁷⁹ were synthesized according to literature procedures. The purity of the synthesized compounds was determined using ^1H , ^{19}F , and ^{71}Ga NMR spectroscopy. To avoid any potential contamination or oxidation of the air sensitive compounds, the samples were stored in air-tight, capped vials with fluoropolymer linings. The vials were further sealed using parafilm and tape. The vials were then transported to the XPS instrument and were opened and prepared in a purged argon-filled glove box, which was directly attached to the introduction chamber of the XPS instrument. NMR spectra were recorded on a Varian INOVA I400 (^1H 400 MHz; ^{13}C 101 MHz; ^{19}F 376 MHz) or a Varian INOVA I600 (^1H 600 MHz; ^{13}C 151 MHz; ^{19}F 564 MHz; ^{71}Ga 183 MHz) FT-NMR spectrometer. Chemical shifts (δ) are reported in ppm and were internally referenced to the residual protonated solvent peaks for ^1H spectra, and the deuterated solvent for ^{13}C spectra. ^{19}F NMR spectra were referenced to CFCl_3 (0.0 ppm) using the internal lock signal from the deuterated solvent and to $\text{Ga}(\text{NO}_3)_3$ (0.0 ppm) in D_2O for ^{71}Ga spectra. Coupling constants (J) are reported in Hz and multiplicities are reported as singlet (s), doublet (d), triplet (t), quartet (q), multiplet (m), broad (br) and overlapping (ov). Electrospray ionization mass spectra were collected using a Bruker micrOTOF II spectrometer. Mass spectral data are reported in mass-to-charge units (m/z).

3.4.2 Syntheses

3.4.2.1 Synthesis of $[\text{Ga}_2\text{I}_2(\text{crypt-222})][\text{GaI}_4]_{1.75}[\text{OTf}]_{0.25}$

Solid Ga_2I_4 (0.172 g, 0.266 mmol) was dissolved in THF (4 mL). The solution turned yellow, and was allowed to stir for several hours, at which point the solvent was removed under reduced pressure. Toluene (4 mL) was added to the reaction flask, along with THF (1 drop), followed by a solution of Me_3SiOTf (0.472 g, 2.12 mmol) dissolved in toluene (2 mL). The mixture was allowed to stir for 1 hour, at which point a solution of cryptand[2.2.2] (0.100 g, 0.266 mmol) dissolved in toluene (2 mL) was added, leading to the immediate formation of a white precipitate. The mixture was allowed to stir for 36 hours, after which a green-grey oil had separated in the vessel. The supernatant was decanted, and the oil was triturated in CH_3CN (3 mL). A grey solid was removed by filtration, and the filtrate was dried under reduced pressure. The resultant solid was dissolved in CH_3CN (3 mL), and ether (2 mL) was added. The solution was concentrated under reduced pressure, resulting in the formation of a white precipitate. The mixture was cooled to $-20\text{ }^\circ\text{C}$ for several hours, the supernatant was decanted and the precipitate was washed with ether (3 x 2 mL) and dried under reduced pressure.

Yield: 0.094 g (33 %); mp: $265 - 268\text{ }^\circ\text{C}$ (decomposition); ^1H NMR (600 MHz, CD_3CN , 298 K)⁸¹ δ : 4.41 – 4.38 (m, 2H, $[\text{O}-\text{CHH}-\text{CH}_2-\text{O}]_{\text{coord}}$), 4.20 – 4.12 (m, 8H, $[\text{O}-\text{CHH}-\text{CH}_2-\text{N}]_{\text{coord}}$, $[\text{O}-\text{CH}_2-\text{CHH}-\text{O}]_{\text{coord}}$, $[\text{O}-\text{CH}_2-\text{CH}_2-\text{O}]_{\text{free}}$), 4.05 – 3.97 (m, 6H, $[\text{O}-\text{CHH}-\text{CH}_2-\text{N}]_{\text{coord}}$, $[\text{O}-\text{CHH}-\text{CH}_2-\text{N}]_{\text{free}}$), 3.92 (dddd, $J = 2\text{ Hz}, 5\text{ Hz}, 13\text{ Hz}, 19\text{ Hz}$, 2H, $[\text{O}-\text{CH}_2-\text{CHH}-\text{N}]_{\text{coord}}$), 3.86 – 3.76 (m, 8H, $[\text{O}-\text{CH}_2-\text{CHH}-\text{N}]_{\text{coord}}$, $[\text{O}-\text{CHH}-\text{CH}_2-\text{N}]_{\text{coord}}$, $[\text{O}-\text{CH}_2-\text{CHH}-\text{O}]_{\text{coord}}$, $[\text{O}-\text{CHH}-\text{CH}_2-\text{O}]_{\text{coord}}$), 3.73 (ddd, $J = 1\text{ Hz}, 5\text{ Hz}, 12\text{ Hz}$, 2H, $[\text{O}-\text{CHH}-\text{CH}_2-\text{N}]_{\text{coord}}$), 3.45 (ddd, $J = 1\text{ Hz}, 4\text{ Hz}, 14\text{ Hz}$, 2H, $[\text{O}-\text{CH}_2-\text{CHH}-\text{N}]_{\text{free}}$), 3.35 (dddd, $J = 1\text{ Hz}, 2\text{ Hz}, 12\text{ Hz}, 14\text{ Hz}$, 2H, $[\text{O}-\text{CH}_2-\text{CHH}-\text{N}]_{\text{free}}$), 3.19 – 3.16 (m, 2H, $[\text{O}-\text{CH}_2-\text{CHH}-\text{N}]_{\text{coord}}$), 3.06 (ddd, $J = 1\text{ Hz}, 2\text{ Hz}, 14\text{ Hz}$, 2H, $[\text{O}-\text{CH}_2-\text{CHH}-\text{N}]_{\text{coord}}$); $^{13}\text{C}\{^1\text{H}\}$ NMR (151 MHz, CD_3CN , 298 K) δ : 121.1 (q, $J = 321\text{ Hz}$, $[\text{O}_3\text{SCF}_3]$),⁸² 74.47 ($[\text{O}-\text{CH}_2-\text{CH}_2-\text{O}]_{\text{free}}$), 72.26 ($[\text{O}-\text{CH}_2-\text{CH}_2-\text{O}]_{\text{coord}}$), 70.91 ($[\text{O}-\text{CH}_2-\text{CH}_2-\text{N}]_{\text{free}}$), 68.06 ($[\text{O}-\text{CH}_2-\text{CH}_2-\text{O}]_{\text{coord}}$), 66.50 ($[\text{O}-\text{CH}_2-\text{CH}_2-\text{N}]_{\text{coord}}$), 66.43 ($[\text{O}-\text{CH}_2-\text{CH}_2-\text{N}]_{\text{coord}}$), 61.14 ($[\text{O}-\text{CH}_2-\text{CH}_2-\text{N}]_{\text{coord}}$), 56.34 ($[\text{O}-\text{CH}_2-\text{CH}_2-\text{N}]_{\text{coord}}$), 55.32 ($[\text{O}-\text{CH}_2-\text{CH}_2-\text{N}]_{\text{free}}$); ^{19}F NMR (564

MHz, CD₃CN, 298 K) δ : -79.3 ([O₃SCF₃]⁻); ⁷¹Ga{¹H} NMR (183 MHz, CD₃CN, 298 K) δ : -455.4 ([GaI₄]⁻); LR ESI-TOF MS (*m/z*; positive ion): 895 [(⁶⁹Ga₂I₂(crypt-222))[I]⁺]; 917 [(⁶⁹Ga₂I₂(crypt-222))[OTf]⁺]; LR ESI-TOF MS (*m/z*; negative ion): 149 ([OTf]⁻); 577 ([⁶⁹GaI₄]⁻); HR ESI-TOF MS (*m/z*; positive ion): Calcd. for C₁₉H₃₆F₃I₂N₂O₉S⁶⁹Ga₂ [(⁶⁹Ga₂I₂(crypt-222))[OTf]⁺]: 916.8695, Found: 916.8707; Elemental analysis (%) calcd. for [Ga₂I₂(crypt-222)][GaI₄]_{1.75}[OTf]_{0.25} (C_{18.25}H₃₆F_{0.75}Ga_{3.75}I₉N₂O_{6.75}S_{0.25}): C, 12.06; H, 2.00; N, 1.54; S, 0.44; found C, 12.08; H, 2.04; N, 1.51; S, 0.39.

3.4.2.2 Synthesis of [Ga(prismand)][OTf]

[Ga(prismand)][GaCl₄] was synthesized according to literature procedures.⁸³ [Ga(prismand)][GaCl₄] (0.100 g, 0.142 mmol) was suspended in acetonitrile (3 mL), to which a solution of trimethylsilyl triflate (TMSOTf; 0.063 g, 0.284 mmol) in acetonitrile (2 mL) was added. After several hours the suspension had changed color from off-white to grey. After stirring for 36 hours, the suspension was filtered, removing a grey metallic-like precipitate. The resultant solution was dried under reduced pressure, yielding an off-white residue. ⁷¹Ga{¹H} NMR spectroscopy revealed that the characteristic signal for [GaCl₄]⁻ ($\delta \sim 251$ ppm) was not present, indicating that the anion had been removed. ¹⁹F NMR spectroscopy revealed the presence of the [OTf]⁻ anion.

3.4.3 XPS Analysis

XPS analyses were carried out with a Kratos AXIS Ultra spectrometer using a monochromatic Al K α (15 mA, 14 kV) X-ray source. The instrument work function was calibrated to give an Au 4f_{7/2} metallic gold binding energy of 83.95 eV. The spectrometer dispersion was adjusted to give a binding energy of 932.63 eV for metallic Cu 2p_{3/2}. The Kratos charge neutralizer system was used for analyses of non-conductive samples. Charge neutralization was deemed to have been fully achieved by monitoring the C 1s signal for adventitious carbon. A sharp main peak with no lower binding energy structure is generally expected. Instrument base pressure was 9 x 10⁻¹⁰ Torr. Survey scans were obtained using an analysis area of $\sim 300 \times 700$ μm and a 160 eV pass energy. High

resolution spectra were obtained using an analysis area of $\sim 300 \times 700 \mu\text{m}$ and a 20 eV pass energy. A 20 eV pass energy corresponded to Ag $3d_{5/2}$ FWHM of 0.55 eV.

A single peak (Gaussian 70%—Lorentzian 30%), ascribed to alkyl type carbon (C–C, C–H), was fitted to the main peak of the C 1s spectrum for adventitious carbon. A second peak is usually added that is constrained to be 1.5 eV above the main peak, and of equal full width half maximum (FWHM) to the main peak. This higher binding energy peak is ascribed to an alcohol (C–OH) and/or ester (C–O–C) functionality. Further high binding energy components (e.g. C=O, 2.8–3.0 eV above the main peak; O–C=O, 3.6–4.3 eV above the main peak; CO_3^{2-} , 3.8–4.8 eV above the main peak) can also be added if required. Spectra from insulating samples have been charge corrected to give the adventitious C 1s spectral component (C–C, C–H) a binding energy of 284.8 eV. This process has an associated error of ± 0.1 – 0.2 eV.⁸⁴

Survey scan analyses for selected samples are presented in Appendix B.

Spectra were analyzed using CasaXPS software (version 2.3.14).⁸⁵ Gaussian (100–X%)—Lorentzian (X%), defined in CasaXPS as GL(X), profiles were used for each component. All C 1s component species spectra have been fit with line-shapes of GL(30). A Ga $3d_{5/2}$ – Ga $3d_{3/2}$ splitting of 0.449 eV was used for all samples. A standard Shirley background is used for all spectra.

All samples were mounted on non-conductive double sided 3M Scotch® adhesive tape. The powder samples were not sputter cleaned prior to analysis, as it is well known that this can cause reduction of oxidized species. The main stage was precooled to -130°C prior to introducing the sample. After addition of the sample holder to the stage it was allowed to cool fully before analysis began. Cooling of the sample has been shown to reduce X-ray and thermal degradation effects in metal compounds such as copper and vanadium.⁸⁶

3.4.4 XAS Analysis

XAS experiments were performed at beamline BL01C1 at the National Synchrotron Radiation Research Centre (NSRRC), Taiwan and at the hard X-ray microanalysis beamline (HXMA, BL01ID-1), Canadian Light Source. The samples were

pressed into thin pellets and sealed with Kapton tape. To minimize degradation, the samples were prepared inside a N₂-filled glovebox and transferred under N₂ to the synchrotron facility. XAS spectra were obtained by positioning the sample under the incident X-ray beam. As the X-ray energy was gradually tuned across the Ga K-edge, the incident photon intensity (I_0) was recorded using an ion chamber which is placed in front of the sample, and the emitted X-ray fluorescence from the sample was collected using a multi-element Ge detector. For each sample, multiple scans were conducted on multiple spots to check for beam damage. No obvious spectral profile change was observed during the measurements. All spectra are normalized to the incident photon intensity I_0 .

The experimental XAS spectra were compared with those calculated using the FDMNES code.⁴⁹ The experimental single crystal XRD data of the compounds,^{12,17,58,83} and the highly accurate finite difference method (FDM) were used to calculate the XAS spectra near the absorption edge. Calculations of the spectra far above the edge were carried out using the computationally-inexpensive Green's function method. The switch between the two computational methods occurred somewhere between 25 and 35 eV above the absorption edge, at a point where both methods produced the same result, within the expected error.

The net electric charge of the Ga sites was calculated using density functional theory (DFT) with the SIESTA code,^{87,88} based on the empirical crystal structures. Ultrasoft norm-conserving pseudopotentials, double-zeta basis sets with polarization orbitals, the Perdew-Burke-Ernzerhof exchange-correlation functional,⁸⁹ and the basis-set independent Voronoi method^{90,91} were utilized for the determination of atomic charges.

3.5 References

[1] In this manuscript, we distinguish between oxidation numbers, assigned using the standard formalism, and chemical states, the experimentally determined physical state of an atom in a complex or partial charge located on an atom of interest within a complex. We do not use the term oxidation state to avoid ambiguity.

- [2] Parkin, G. *J. Chem. Educ.* **2006**, *83*, 791-799
- [3] Atkins, P. *Shriver and Atkins' Inorganic Chemistry*, 4th ed.; Oxford University Press: Oxford, England, 2010.
- [4] Pubill-Ulldemolins, C.; Fernandez, E.; Bo, C.; Brown, J.M. *Org. Biomol. Chem.* **2015**, *13*, 9619-9628.
- [5] Santelli, M.; Pons, J.M. *Lewis Acids and Selectivity in Organic Synthesis*; Taylor & Francis: Boca Raton, Florida, 1995.
- [6] Bonet, A.; Gulyas, H.; Fernandez, E. *Angew. Chem., Int. Ed.* **2010**, *49*, 5130-5134.
- [7] Hardman, N.J.; Wright, R.J.; Phillips, A.D.; Power, P.P. *J. Am. Chem. Soc.* **2003**, *125*, 2667-2679.
- [8] Fink, M.J.; Michalczyk, M.J.; Haller, K.J.; West, R.; Michl, J. *J. Chem. Soc., Chem. Commun.* **1983**, 1010-1011.
- [9] Zhu, Z.; Wang, X.; Olmstead, M.M.; Power, P.P. *Angew. Chem., Int. Ed.* **2009**, *48*, 2027-2030.
- [10] Zhu, Z.; Wang, X.; Peng, Y.; Lei, H.; Fettinger, J.C.; Rivard, E.; Power, P.P. *Angew. Chem., Int. Ed.* **2009**, *48*, 2031-2034.
- [11] Malbrecht, B.J.; Dube, J.W.; Willans, M.J.; Ragogna, P.J. *Inorg. Chem.* **2014**, *53*, 9644-9656.
- [12] Garton, G.; Powell, H.M. *J. Inorg. Nucl. Chem.* **1957**, *4*, 84-89.
- [13] Schmidt, E.S.; Schier, A.; Mitzel, N.W.; Schmidbaur, H. *Z. Naturforsch., B: Chem. Sci.* **2001**, *56b*, 337-341.
- [14] Chapman, R.P.; Bryce, D.L. *Phys. Chem. Chem. Phys.* **2009**, *11*, 6987-6998.
- [15] Schmidbaur, H. *Angew. Chem., Int. Ed. Engl.* **1985**, *24*, 893-904.
- [16] Dange, D.; Choong, S.L.; Schenk, C.; Stasch, A.; Jones, C. *Dalton Trans.* **2012**, *41*, 9304-9315.
- [17] Bourque, J.L.; Boyle, P.D.; Baines, K.M. *Chem. Eur. J.* **2015**, *21*, 9790-9796.

- [18] Gibb, T.C. *Principles of Mössbauer Spectroscopy*; Chapman and Hall: Norwich, England, 1976.
- [19] Dickson, D.P.E.; Berry, F.J. *Mössbauer Spectroscopy*; Cambridge University Press: Cambridge, England, 1986.
- [20] Al-Rafia, S.M.; Shynkaruk, O.; McDonald, S.M.; Liew, S.K.; Ferguson, M.J.; McDonald, R.; Herber, R.H.; Rivard, E. *Inorg. Chem.* **2013**, *52*, 5581-5589.
- [21] Henning, J.; Schubert, H.; Eichele, K.; Winter, F.; Pottgen, R.; Mayer, H.A.; Wesemann, L. *Inorg. Chem.* **2012**, *51*, 5787-5794.
- [22] Tondreau, A.M.; Atienza, C.C.H.; Darmon, J.M.; Milsmann, C.; Hoyt, H.M.; Weller, K.J.; Nye, S.A.; Lewis, K.M.; Boyer, J.; Delis, J.G.P.; Lobkovsky, E.; Chirik, P.J. *Organometallics* **2012**, *31*, 4886-4893.
- [23] Hanson, M.A.; Terskikh, V.V.; Baines, K.M.; Huang, Y. *Inorg. Chem.* **2014**, *53*, 7377-7388.
- [24] van der Heide, P. *X-ray Photoelectron Spectroscopy: An Introduction to Principles and Practices*; John Wiley & Sons, Inc.: Hoboken, New Jersey, 2012.
- [25] Wagner, C.D. *Anal. Chem.* **1972**, *44*, 967-973.
- [26] Moretti, G. *J. Electron Spectrosc. Relat. Phenom.* **1998**, *95*, 95-144.
- [27] Biesinger, M.C.; Lau, L.W.; Gerson, A.R.; Smart, R.S. *Phys. Chem. Chem. Phys.* **2012**, *14*, 2434-2442.
- [28] Wagner, C.D.; Joshi, A. *J. Electron Spectrosc. Relat. Phenom.* **1988**, *47*, 283-313.
- [29] Moretti, G. *Surf. Sci.* **2013**, *618*, 3-11.
- [30] Watts, J.F.; Wolstenholme, J. *An Introduction to Surface Analysis by XPS and AES*; Wiley: Chichester, England, 2003.
- [31] McGuire, G.E.; Schweitzer, G.K.; Carlson, T.A. *Inorg. Chem.* **1973**, *12*, 2450-2453.
- [32] Mizokawa, Y.; Iwasaki, H.; Nishitani, R.; Nakamura, S. *J. Electron Spectrosc. Relat. Phenom.* **1978**, *14*, 129-141.

- [33] Nishitani, R.; Iwasaki, H.; Mizokawa, Y.; Nakamura, S. *Jpn. J. Appl. Phys.* **1978**, *17*, 321-327.
- [34] Hedman, J.; Mårtensson, N. *Phys. Scr.* **1980**, *22*, 176-178.
- [35] Iwakuro, H.; Tatsuyama, C.; Ichimura, S. *Jpn. J. Appl. Phys.* **1982**, *21*, 94-99.
- [36] Stepniak, F.; Rioux, D.; Weaver, J. *Phys. Rev. B: Condens. Matter* **1994**, *50*, 1929-1933.
- [37] Simpson, W.C.; Shuh, D.K.; Hung, W.H.; Hakansson, M.C.; Kanski, J.; Karlsson, U.O.; Yarmoff, J.A. *J. Vac. Sci. Technol., A* **1996**, *14*, 1815-1821.
- [38] Hung, W.-H.; Wu, S.-L.; Chang, C.-C. *J. Phys. Chem. B* **1998**, *102*, 1141-1148.
- [39] Shaporenko, A.; Adlkofer, K.; Johansson, L.S.O.; Ulman, A.; Grunze, M.; Tanaka, M.; Zharnikov, M. *J. Phys. Chem. B* **2004**, *108*, 17964-17972.
- [40] Mayer, T.; Lebedev, M.V.; Hunger, R.; Jaegermann, W. *J. Phys. Chem. B* **2006**, *110*, 2293-2301.
- [41] Wagner, C.D.; Passoja, D.E.; Hillery, H.F.; Kinisky, T.G.; Six, H.A.; Jansen, W.T.; Taylor, J.A. *J. Vac. Sci. Technol.* **1982**, *21*, 933-944.
- [42] Reiche, R.; Dobler, D.; Holgado, J.P.; Barranco, A.; Martín-Concepción, A.I.; Yubero, F.; Espinós, J.P.; González-Elipe, A.R. *Surf. Sci.* **2003**, *537*, 228-240.
- [43] Engemann, C.; Franke, R.; Hormes, J.; Lauterbach, C.; Hartmann, E.; Clade, J.; Jansen, M. *Chem. Phys.* **1999**, *243*, 61-75.
- [44] Mansour, A.N.; Melendres, C.A.; Pankuch, M.; Brizzolara, R.A. *J. Electrochem. Soc.* **1994**, *141*, L69-L71.
- [45] Vodyanitskii, Yu.N. *Eurasian Soil Sci.* **2013**, *46*, 1139-1149.
- [46] Ward, M.J.; Rupar, P.A.; Murphy, M.W.; Yiu, Y.M.; Baines, K.M.; Sham, T.K. *Chem. Commun.* **2010**, *46*, 7016-7018.
- [47] Ankudinov, A.L.; Ravel, B.; Rehr, J.J.; Conradson, S.D. *Phys. Rev. B* **1998**, *58*, 7565-7576.

- [48] Hermann, K.; Pettersson, L.G.M.; Casida, M.E.; Daul, C.; Goursot, A.; Koester, A.; Proynov, E.; St-Amant, A.; Salahub, D.R. StoBe-deMon version 3.3, 2014, www.fhi-berlin.mpg.de/KHsoftware/StoBe/
- [49] Bunau, O.; Joly, Y. *J. Phys. Condens. Matter* **2009**, *21*, 345501-345511.
- [50] Schön, G. *J. Electron Spectrosc. Relat. Phenom.* **1973**, *2*, 75-86.
- [51] Wagner, C.D. *Faraday Discuss. Chem. Soc.* **1975**, *60*, 291-300.
- [52] Evans, S. *Surf. Interface Anal.* **1985**, *7*, 299-302.
- [53] Wagner, C.D.; Muilenberg, G.E. *Handbook of X-ray photoelectron spectroscopy: a reference book of standard data for use in X-ray photoelectron spectroscopy*; Physical Electronics Division, Perkin-Elmer Corp., 1979.
- [54] Mizokawa, Y.; Iwasaki, H.; Nakamura, S. *Jpn. J. Appl. Phys.* **1981**, *20*, L491-L494.
- [55] Timoshkin, A.Y.; Bodensteiner, M.; Sevastianova, T.N.; Lisovenko, A.S.; Davydova, E.I.; Scheer, M.; Grassl, C.; Butlak, A.V. *Inorg. Chem.* **2012**, *51*, 11602-11611.
- [56] Wallwork, S.C.; Worrall, I.J. *J. Chem. Soc.* **1965**, 1816-1820.
- [57] Hardman, N.J.; Eichler, B.E.; Power, P.P. *Chem. Commun.* **2000**, 1991-1992.
- [58] Beamish, J.C.; Small, R.W.H.; Worrall, I.J. *Inorg. Chem.* **1979**, *18*, 220-223.
- [59] Beachley, O.T.; Churchill, M.R.; Pazik, J.C.; Ziller, J.W. *Organometallics* **1987**, *6*, 2088-2093.
- [60] Smith, M.B. *Organic Chemistry: An Acid—Base Approach*; CRC Press: Boca Raton, Florida, 2010.
- [61] Hardman, N.J.; Power, P.P.; Gorden, J.D.; Macdonald, C.L.B.; Cowley, A.H. *Chem. Commun.* **2001**, 1866-1867.
- [62] Green, S.P.; Jones, C.; Lippert, K.A.; Mills, D.P.; Stasch, A. *Inorg. Chem.* **2006**, *45*, 7242-7251.
- [63] Beachley, Jr., O.T.; Gardinier, J.R.; Churchill, M.R. *Organometallics* **2000**, *19*, 4544-4549.

- [64] Geller, S. *J. Chem. Phys.* **1960**, *33*, 676-684.
- [65] Housecroft, C.E.; Sharpe, A.G. *Inorganic Chemistry*, 3rd ed.; Pearson Prentice Hall: Harlow, England, 2008.
- [66] Kumar, S.S.; Rubio, E.J.; Noor-A-Alam, M.; Martinez, G.; Manandhar, S.; Shutthanandan, V.; Thevuthasan, S.; Ramana, C.V. *J. Phys. Chem. C* **2013**, *117*, 4194-4200.
- [67] Wilke, M.; Farges, F.; Petit, P.E.; Brown, G.E.; Martin, F. *Am. Mineral.* **2001**, *86*, 714-730.
- [68] Hensen, E.J.M.; Garcia-Sanchez, M.; Rane, N.; Magusin, P.C.M.M.; Liu, P.H.; Chao, K.J.; van Santen, R.A. *Catal. Lett.* **2005**, *101*, 79-85.
- [69] Achkar, A.; Regier, T.; Wadati, H.; Kim, Y.; Zhang, H.; Hawthorn, D. *Phys. Rev. B* **2011**, *83*, 081106R.
- [70] Tröger, L.; Arvanitis, D.; Baberschke, K.; Michaelis, H.; Grimm, U.; Zschech, E. *Phys. Rev. B* **1992**, *46*, 3283-3289.
- [71] Wei, P.; Li, X.-W.; Robinson, G.H. *Chem. Commun.* **1999**, 1287-1288.
- [72] Ga₂Cl₄(1,4-dioxane)₂ was synthesized according to reference 20 and was recrystallized from a solution of toluene and 1,4-dioxane in a 3:1 ratio at -20 °C. Crystallographic details can be found in Appendix B.
- [73] Getsoian, A.B.; Das, U.; Camacho-Bunquin, J.; Zhang, G.; Gallagher, J.R.; Hu, B.; Cheah, S.; Schaidle, J.A.; Ruddy, D.A.; Hensley, J.E.; Krause, T.R.; Curtiss, L.A.; Miller, J.T.; Hock, A.S. *Catal. Sci. Technol.* **2016**, *6*, 6339-6353.
- [74] Green, M.L.H.; Mountford, P.; Smout, G.J.; Speel, S.R. *Polyhedron* **1990**, *9*, 2763-2765.
- [75] Baker, R.J.; Farley, R.D.; Jones, C.; Kloth, M.; Murphy, D.M. *J. Chem. Soc., Dalton Trans.* **2002**, 3844-3850.
- [76] Baker, R.J.; Bettentrup, H.; Jones, C. *Eur. J. Inorg. Chem.* **2003**, *2003*, 2446-2451.

- [77] Serrano, O.; Fettinger, J.C.; Power, P.P. *Polyhedron* **2013**, *58*, 144-150.
- [78] Yamaguchi, T.; Ueno, K.; Ogino, H. *Organometallics* **2001**, *20*, 501-507.
- [79] Beamish, J.C.; Wilkinson, M.; Worrall, I.J. *Inorg. Chem.* **1978**, *17*, 2026-2027.
- [80] Schmidt, E.S.; Schier, A.; Schmidbaur, H. *J. Chem. Soc., Dalton Trans.* **2001**, 505-507.
- [81] The subscript "coord" refers to the two arms of cryptand[2.2.2] coordinated to the gallium centres; the subscript "free" refers to the arm of cryptand[2.2.2] that is not coordinated to a gallium centre.
- [82] The chemical shift of the carbon atom in the triflate anion was obtained using a $^{13}\text{C}\{^1\text{H}\}\text{-}^{19}\text{F}$ HSQC experiment.
- [83] Kunze, A.; Gleiter, R.; Bethke, S.; Rominger, F. *Organometallics* **2006**, *25*, 4787-4791.
- [84] Miller, D.J.; Biesinger, M.C.; McIntyre, N.S. *Surf. Interface Anal.* **2002**, *33*, 299-305.
- [85] Fairley, N. *Casa XPS*, **2005**, Casa Software Ltd.
- [86] Biesinger, M.C.; Lau, L.W.M.; Gerson, A.R.; Smart, R.S.C. *Appl. Surf. Sci.* **2010**, *257*, 887-898.
- [87] Ordejon, P.; Artacho, E.; Soler, J.M. *Phys. Rev. B* **1996**, *53*, R10041.
- [88] Soler, J.M.; Artacho, E.; Gale, J.D.; Garcia, A.; Junquera, J.; Ordejon, P.; Daniel, S.P. *J. Phys. Condens. Matter.* **2002**, *14*, 2745-2780.
- [89] Perdew, J.; Burke, K.; Ernzerhof, M. *Phys. Rev. Lett.* **1996**, *77*, 3865-3868.
- [90] Bickelhaupt, F.M.; van Eikema Hommes, N.J.R.; Guerra, C.F.; Baerends, E.J. *Organometallics* **1996**, *15*, 2923-2931.
- [91] Guerra, C.F.; Handgraaf, J.W.; Baerends, E.J.; Bickelhaupt, F.M. *J. Comput. Chem.* **2004**, *25*, 189-210.

Chapter 4

4 Synthesis and Reactivity of Cationic Gallium(I) Crown Ether Complexes

4.1 Introduction

The chemistry of low valent gallium compounds (Chart 4.1)¹ is of much interest because of the potential of the compounds to be utilized as alternatives to transition metal catalysts. Some transition metals are expensive, have poor natural abundances, and are toxic, which impacts their use in industrial processes.² The study of low valent gallium compounds offers the potential for efficient synthetic routes and alternative or complementary reaction mechanisms that could drive development in this field. In addition, the reactivity of novel gallium compounds could guide the use of more abundant main group metals such as aluminum as catalysts. Like transition metals, gallium(I) compounds can undergo oxidative addition reactions with H-E bonds (where E = SnPh₃, NEt₂, PPh₂, OH, OEt), and reagents such as H₂ and NH₃, as well as cycloaddition reactions with alkenes.³ This varied reactivity is a consequence of the ambiphilic nature of gallium(I), with its empty *p*-orbital and lone pair of electrons, which enables the Group 13 element to act as both a Lewis acid and a Lewis base.⁴ For example, [Ga(C₆H₅F)₂][Al(OC(CF₃)₃)₄]⁵ has been shown to be an effective catalyst for the polymerization of isobutylene where the ambiphilicity of the gallium(I) centre is critical for the reactivity.⁶ Gallium(I) cations have also been used as catalysts when generated *in situ*. Ultrasonic activation of gallium metal, silver triflate, 18-crown-6, and 1,4-dioxane gave a gallium(I) species, the presence of which was confirmed by ⁷¹Ga NMR spectroscopy. While the complex was not isolated, it was proposed to be the active catalyst for carbon-carbon bond forming reactions between allyl or allenyl boronic esters and acetals, ketals or amins.⁷

Despite the promise of gallium(I) reagents as catalysts, gallium(I) complexes are often unstable towards donor solvents, limiting the scope of the chemistry. The development of novel gallium(I) reagents and starting materials that are easily

synthesized using commercially available ligands and stable toward a wide range of solvents is desirable and may facilitate progress in the field of main group catalysis. To this end, the synthesis and stability of crown ether derivatives of gallium(I) cations was explored.

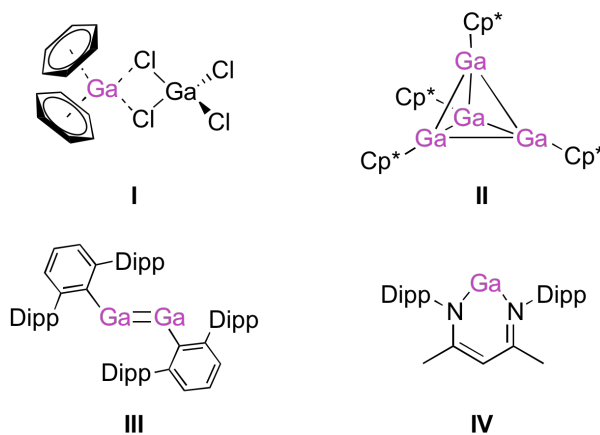


Chart 4.1: Examples of gallium(I) compounds¹ (Cp* = pentamethylcyclopentadienyl, Dipp = 2,6-diisopropylphenyl).

The use of macrocyclic compounds as stabilizing ligands for low valent main group cations has been known for many years. The first report described the complexation of tin(II) with 18-crown-6 and its dibenzo- derivative; the resulting tin(II) cations retained a strongly coordinated chloride ligand.⁸ These early reports were followed by the use of [2.2.2]paracyclophane to stabilize germanium(II) and tin(II) cations possessing coordinating chloride ligands or $[\text{AlCl}_4]^-$ counteranions, respectively.⁹ Germanium(II) dications with triflate counteranions have also been complexed by two 12-crown-4 molecules (V, Chart 4.2) and symmetrically coordinated in 15-crown-5 and 18-crown-6 (VI, Chart 4.2). When the anion of the latter examples is a trichlorogermanate instead of triflate, the 15-crown-5 and 18-crown-6 stabilized Ge(II) dications displayed asymmetrical coordination within the crown ether ligands (VII, Chart 4.2).¹⁰ Analogous germanium(II) dications complexed by azamacrocycles have also been isolated.^{10a,11} Complexation of tin(II) cations has been reported using crown ethers and non-coordinating anions, where the tin(II) dication is sandwiched between two 12-crown-4

molecules, two 15-crown-5 molecules, or sequestered in 18-crown-6.¹² A naked germanium(II) dication has been encapsulated in cryptand[2.2.2], surrounding the dication in three dimensions.¹³ Tin(II) mono- and dications were also isolated using cryptand[2.2.2] as a donor ligand; a naked tin(II) dication was isolated when triflate counteranions were used, whereas umbrella-like structures with the coordination of a halide ligand were obtained when tin(II) halides were used as starting materials.¹⁴ Indium(I)-crown ether complexes have also been reported. Reactions of InOTf with 18-crown-6 gave [In(18-crown-6)][OTf], whereas reactions between InOTf and 15-crown-5 resulted in sandwich complexes without coordination to the triflate counteranion.¹⁵ Recent work with weakly coordinating perfluorinated aluminate counteranions has led to the isolation of [In(18-crown-6)(C₆H₅F)₂][Al(OC(CF₃)₃)₄], with coordinating fluorobenzene solvent molecules.¹⁶

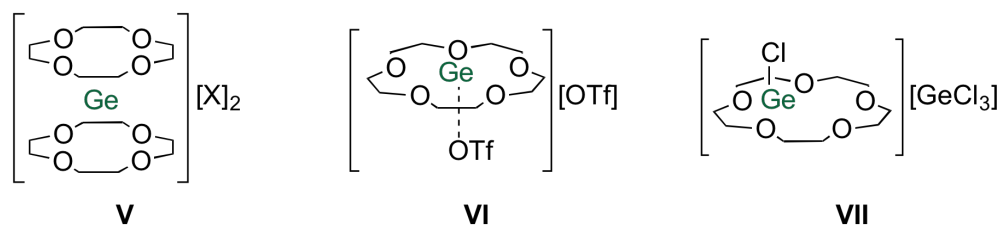


Chart 4.2: Germanium(II) complexes of 12-crown-4 and 15-crown-5^{10b} (X = [OTf]⁻ or [GeCl₃]).

Despite the many reports of low valent macrocycle-stabilized main group cations, few examples with gallium exist. Gallium(III)-crown ether complexes have been reported as dihalogenated gallium(III) cations, [GaX₂L][GaX₄] (where X = Cl, Br; L = 12-crown-4, 15-crown-5, or 18-crown-6). Although characterized by IR and Raman spectroscopy, no other spectroscopic data were presented to unambiguously determine the structure of the reported compounds.¹⁷ IR and Raman spectroscopic methods were used to characterize [GaI₂(18-crown-6)][GaI₄], synthesized from GaI₃; however, no NMR or mass spectrometric data were reported. A solid state structure was determined by X-ray diffraction methods, however, it was of poor quality and structural metrics of the

$[\text{GaI}_2(18\text{-crown-6})]^+$ cation could not be extracted.¹⁸

Gallium(I) cations have also been complexed in non-ethereal macrocycles, for example, ([2.2.2]paracyclophane)gallium(I) tetrabromogallate (**VIII**, Chart 4.3). The gallium(I) cation is in the centre of the paracyclophane cavity, with additional coordination of the tetrabromogallate anion.¹⁹ Three-dimensional complexation of a gallium(I) cation was accomplished using a π -prismand, where the cation was without contact to the $[\text{GaCl}_4]^-$ anion (**IX**, Chart 4.3), highlighting the appropriate shape, size, and donor strength of the π -prismand for the coordination of a gallium(I) cation.²⁰

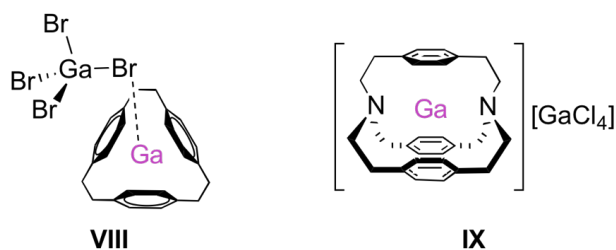


Chart 4.3: Gallium(I) cations complexed by macrocyclic ligands.^{19,20}

The sole report of a gallium(I)-crown ether complex described the synthesis and characterization of $[\text{Ga}(18\text{-crown-6})(\text{C}_6\text{H}_5\text{F})_2][\text{Al}(\text{OC}(\text{CF}_3)_3)_4]$.¹⁶ The crystal structure, while of poor quality, reveals the complexation of a gallium(I) cation within 18-crown-6, along with coordination of the gallium(I) cation by fluorobenzene molecules both above and below the plane of the crown ether. The synthesis of $[\text{Ga}(18\text{-crown-6})(\text{C}_6\text{H}_5\text{F})_2]^+$ highlights the potential for the isolation of a gallium(I) cation complexed by a crown ether and, perhaps, solvent molecules or counteranions. $[\text{Ga}(12\text{-crown-4})][\text{GaCl}_4]$ has been synthesized, but not reported in a peer-reviewed journal. A crystal structure of the complex was presented without any additional spectroscopic characterization data.²¹ Recent work in our group described the synthesis of a binuclear gallium(II) complex stabilized by cryptand[2.2.2], as well as a trinuclear complex,²² where the overall chemical state of the gallium centres in the cationic unit of the latter was found to correspond most closely to an oxidation number of +2.²³

The two well-known gallium(I) starting materials, ‘GaI’²⁴ and Ga₂Cl₄,²⁵ although commonly used to synthesize gallium(I) complexes, are associated with many challenges. ‘GaI’ has a variable composition which depends on the reaction time used in its preparation. In its most common and widely used form, the green amorphous solid has been shown to have the formula [Ga⁰]₂[Ga^I]₂[Ga₂I₆], as determined by powder X-ray diffraction, Raman and NQR spectroscopies.²⁶ Although gallium(I) cations are present in ‘GaI’, gallium(II) or gallium(III) compounds are often isolated from reactions using this starting material.^{26,27} The synthesis of gallium(I) compounds such as GaNacNac^{Dipp} (**IV**, Chart 4.1) using ‘GaI’ requires the addition of potassium metal to the reaction mixture to give the gallium(I) species in moderate yield.^{1b} Furthermore, ‘GaI’ decomposes or comproportionates upon exposure to donor solvents such as ether and THF.²⁴ When Ga₂Cl₄, which contains a gallium(I) cation and a tetrachlorogallate(III) anion ([Ga][GaCl₄]),^{25a} is used as a starting material for the synthesis of gallium(I) complexes, comproportionation reactions are common; upon exposure of [Ga][GaCl₄] to donor molecules, products of the form LCl₂GaGaCl₂L, are isolated.^{22,28,29} Despite the inherent issues with [Ga][GaCl₄], it has been successfully used as a source of gallium(I); [Ga(prismand)][GaCl₄] (**IX**, Chart 4.3) was synthesized from this starting material.²⁰ Although Krossing’s reagent, [Ga(C₆H₅F)₂][Al(OC(CF₃)₃)₄], and derivatives with different arene ligands on the gallium(I) centre⁵ can be used as sources of gallium(I) for synthesis and catalysis, the stability of [Ga(C₆H₅F)₂][Al(OC(CF₃)₃)₄] in donor solvents has not been described. Additionally, the large perfluorinated anion requires fluorinated alcohols for its synthesis as well as AgF, which are moderately expensive.³⁰ Significant problems are often encountered in the characterization of new gallium(I) cations derived from this starting material; disorder of the anion is common in the X-ray crystallographic structures of the products.¹⁶

The synthesis of gallium(I) cations that are stable under a variety of conditions but remain reactive may enable a wide range of chemistry. As of present, the chemistry of gallium(I) cations has yet to be thoroughly explored, due to the poor stability of gallium(I) species to donor solvents. Herein, we describe the facile synthesis of two

gallium(I) complexes of 12-crown-4, and the reactivity of the $[\text{Ga}(\text{12-crown-4})]^+$ cation towards other donor ligands, demonstrating its versatility as a source of gallium(I).

4.2 Results and Discussion

4.2.1 Synthesis and Characterization

Reactions between $[\text{Ga}][\text{GaCl}_4]$ and 12-crown-4 in a 1:1 ratio in toluene resulted in the rapid formation of a precipitate and conversion to a single product, as determined by a singlet observed in the ^1H NMR spectrum of the precipitate dissolved in CD_3CN . ESI-MS data of the solid indicated the presence of $[\text{Ga}(\text{12-crown-4})]^+$ ($m/z = 245$). ^{71}Ga NMR spectra of the reaction mixture revealed two signals; one at +251 ppm, which was assigned to the tetrachlorogallate(III) anion ($[\text{GaCl}_4]^-$),³¹ and one at -471 ppm. The ^{71}Ga chemical shift of gallium(I) cations is typically observed in the range of -600 to -800 ppm;^{5,31} however, a gallium(I) complex with three PPh_3 ligands, $[\text{Ga}(\text{PPh}_3)_3]^+$, has a ^{71}Ga NMR chemical shift of -144 ppm.⁵ If one compares the ^{71}Ga chemical shift of the starting material, $[\text{Ga}(\text{C}_6\text{H}_5\text{F})_2][\text{Al}(\text{OC}(\text{CF}_3)_3)_4]$ ($\delta = -756$ ppm), to that of the $[\text{Ga}(\text{PPh}_3)_3]^+$ complex ($\delta = -144$ ppm),⁵ a chemical shift of -471 ppm is not unreasonable for $[\text{Ga}(\text{12-crown-4})]^+$, as the ^{71}Ga chemical shift for the gallium(I) cation of our Ga_2Cl_4 starting material is approximately -650 ppm.³¹ Single crystals suitable for X-ray crystallography were obtained; the molecular structure of $[\text{Ga}(\text{12-crown-4})][\text{GaCl}_4]$, **4.1** (Figure 4.1, Table 4.1) was confirmed by X-ray diffraction.

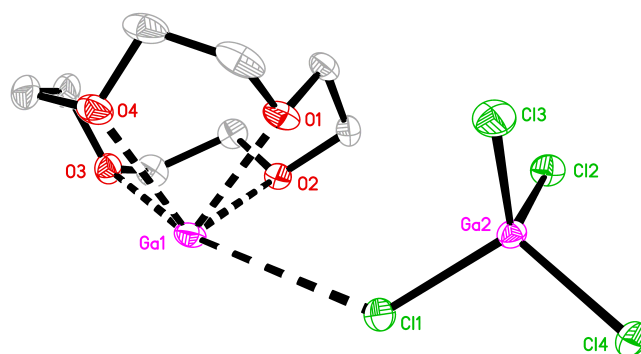


Figure 4.1: Displacement ellipsoid plot of **4.1**. Ellipsoids are drawn at the 50% probability level and hydrogen atoms are omitted for clarity. Selected bond lengths and angles (\AA , $^\circ$): Ga1-O1 2.3599(11), Ga1-O2 2.5041(13), Ga1-O3 2.3789(11), Ga1-O4 2.5008(13), Ga1 \cdots Cl1 3.5937(9); O1-Ga1-O2 68.12(3), O1-Ga1-O3 102.21(3).

The solid state structure of **4.1** is remarkable for several reasons. Due to the increased ionic radius of Ga^+ versus Li^+ (1.13 \AA ³² and 0.59 \AA ,³³ respectively), the cation is not centred within the 12-crown-4 cavity; it is displaced from the plane of the four oxygen atoms by 1.4734(7) \AA . The bond lengths between the gallium centre and the oxygen atoms vary quite substantially, from 2.3599(11) \AA (Ga1-O1) to 2.5041(13) \AA (Ga1-O2), a difference of greater than 0.14 \AA . The shortening of Ga1-O1 and Ga1-O3 bonds could be due to the repulsion caused by the chloride ligands of the $[\text{GaCl}_4]^-$ anion that is coordinating to the gallium(I) cation, which results in the puckered-type arrangement of the crown ether, where O1 and O3 are pushed toward one another, and O2 and O4 are pushed away from each other.

Preliminary reactivity studies of **4.1** revealed that the chemistry of the $[\text{GaCl}_4]^-$ anion obscured that of the $[\text{Ga}(12\text{-crown-4})]^+$ cation. For example, the reaction of **4.1** with tris(pentafluorophenyl)borane ($\text{B}(\text{C}_6\text{F}_5)_3$, BCF) appeared to give $[\text{Ga}(12\text{-crown-4})][\text{ClB}(\text{C}_6\text{F}_5)_3]$, where the strongly Lewis acidic borane abstracted a chloride anion from the tetrachlorogallate anion. The formation of $[\text{ClB}(\text{C}_6\text{F}_5)_3]^-$ is supported by the absence of a signal corresponding to $[\text{GaCl}_4]^-$ in the ^{71}Ga NMR spectrum of the reaction mixture, and a signal at -1.4 ppm in the ^{11}B NMR spectrum of the product that is comparable to

that of $[\text{FB}(\text{C}_6\text{F}_5)_3]^-$ which has a chemical shift of -2.1 ppm.³⁴ An attempt to oxidize the gallium(I) centre of **4.1** using MeI did not proceed as expected; halide scrambling in the $[\text{GaCl}_4]^-$ anion was detected by ESI-MS and ^{71}Ga NMR spectroscopy, giving a mixture of $[\text{GaCl}_4]^-$, $[\text{GaCl}_3\text{I}]^-$, $[\text{GaCl}_2\text{I}_2]^-$, $[\text{GaClI}_3]^-$ and $[\text{GaI}_4]^-$. As the anion was observed to mask the reactivity of the $[\text{Ga}(\text{12-crown-4})]^+$ cation, anion exchange reactions were explored to replace the reactive tetrachlorogallate with a less reactive anion.

Exchange of the $[\text{GaCl}_4]^-$ anion in $[\text{Ga}(\text{prismand})][\text{GaCl}_4]$ (**IX**, Chart 4.3) was accomplished using trimethylsilyl triflate (TMSOTf) as a halide abstraction agent, giving $[\text{Ga}(\text{prismand})][\text{OTf}]$ (**3.4**), and TMSCl and GaCl_3 as by-products, both of which were easily separated from **3.4** (Chapter 3).^{23a} The reaction of TMSOTf and **4.1** was performed; however, no reaction was observed at room temperature, as shown by ^{71}Ga NMR spectroscopy. When a mixture of excess TMSOTf and **1** was heated at 60 °C, the signal assigned to the $[\text{Ga}(\text{12-crown-4})]^+$ cation disappeared from the ^{71}Ga NMR spectrum; however, the signal for the $[\text{GaCl}_4]^-$ anion remained. Anion exchange reactions using simple ionic reagents such as NaBPh_4 and NMe_4BPh_4 were attempted, but mixtures of the $[\text{GaCl}_4]^-$ and $[\text{BPh}_4]^-$ anions were obtained in all reactions. Given the lack of success in exchanging the anion of **4.1**, anion exchange reactions of the $[\text{Ga}][\text{GaCl}_4]$ starting material were explored. The reaction of NaBPh_4 with $[\text{Ga}][\text{GaCl}_4]$ resulted in the formation of crystals of $\text{Na}[\text{GaCl}_3\text{Ph}]$ (**4.2**) (Appendix C, Figure A.15). BPh_3 was detected as a by-product in the ^{11}B NMR spectrum of the crude reaction mixture. The mechanism for the formation of $\text{Na}[\text{GaCl}_3\text{Ph}]$ is unknown, but a modified Wheland intermediate is postulated to form, giving the free borane and **4.2**.

Silylium cations ($[\text{R}_3\text{Si}]^+$) have been known for several decades³⁵ and have been used as halide abstraction agents for main group halides.³⁶ Thus, the reaction of **4.1** with $[(\text{Et}_3\text{Si})_2(\mu\text{-H})][\text{B}(\text{C}_6\text{F}_5)_4]^{37}$ was performed in fluorobenzene. A white precipitate was observed within minutes, and was examined using multinuclear NMR spectroscopy, ESI-MS and X-ray crystallography following isolation. The ^1H NMR spectrum of the solid in CD_3CN revealed a singlet with a chemical shift at 3.85 ppm similar to that of **4.1** (3.82

ppm). A signal assigned to the $[\text{GaCl}_4]^-$ anion was not observed in the ^{71}Ga NMR spectrum of the product. A signal which could be assigned to the gallium(I) cation was also not observed in the ^{71}Ga NMR spectrum of the product; however, the relaxation rates of ^{71}Ga nuclei are often fast which leads to significant broadening of the signals. The ESI mass spectrum of the solid indicated that the $[\text{Ga}(\text{12-crown-4})]^+$ cation was present, as a signal with a mass to charge ratio of 245 was observed. Furthermore, a signal in the negative ion ESI mass spectrum corresponding to $[\text{B}(\text{C}_6\text{F}_5)_4]^-$ (m/z 678) was observed. This allowed for the assignment of the product as $[\text{Ga}(\text{12-crown-4})][\text{B}(\text{C}_6\text{F}_5)_4]$ (**4.3**); the formulation of the salt was confirmed using X-ray crystallography (Figure 4.2, Table 4.1). We propose that the mechanism of the transformation of **4.1** to **4.3** involves the abstraction of a chloride ligand by the $[\text{Et}_3\text{Si}]^+$ cation from the tetrachlorogallate anion, giving one equivalent of Et_3SiH , Et_3SiCl , and GaCl_3 , all of which are volatile or soluble in non-polar organic solvents. This allows for the simple isolation and purification of the new salt, $[\text{Ga}(\text{12-crown-4})][\text{B}(\text{C}_6\text{F}_5)_4]$, **4.3**, by removal of the volatiles under vacuum and trituration with non-polar solvents.

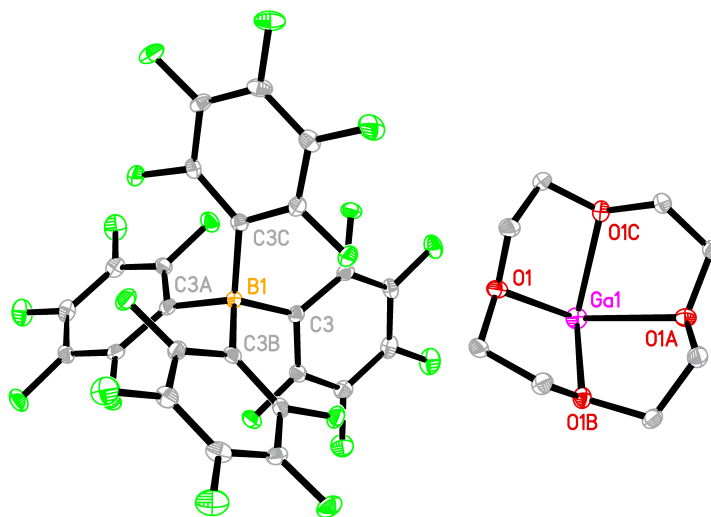


Figure 4.2: Displacement ellipsoid plot of **4.3**. Ellipsoids are drawn at the 50% probability level and hydrogen atoms are omitted for clarity. Selected bond lengths and angles (\AA , $^\circ$): Ga1-O1 2.4122(9), B1-C3 1.6617(11), Ga1 \cdots F2 3.4923(8), Ga1 \cdots F3

3.8518(10), Ga1•••C5 3.9747(11), Ga1•••C6 4.1431(12); O1-Ga1-O1A 106.50(4), O1-Ga1-O1B 69.02(2).

When comparing the structural metrics of **4.1** to those of **4.3**, several key differences are noted. First, the gallium-oxygen bond lengths of **4.3** are comparable to the shortest Ga-O distances observed in **4.1** (**4.1**: 2.3599(11) Å – 2.5041(13) Å; **4.3**: 2.4122(9) Å), suggesting that the gallium cation is closer to the centre of the 12-crown-4 molecule in **4.3**. This is corroborated by the distance of the gallium centre above the plane of the oxygen atoms, which is 1.4734(7) Å for **4.1** compared to 1.4433(10) Å for **4.3**. Despite the weakly coordinating nature of the [B(C₆F₅)₄]⁻ anion in **4.3**, short contacts between the gallium cation and F2, F3, C5, and C6 of the anion are observed in the solid state (Ga1-F2, 3.492 Å; Ga1-F3, 3.852 Å), however, the contacts are longer than the sum of the ionic radii.

4.2.2 XPS Analysis of [Ga(12-crown-4)][B(C₆F₅)₄], **4.3**

Complex **4.3** was characterized using X-ray photoelectron spectroscopy (XPS) and the data were compared to the data of related gallium complexes using a Wagner plot.^{23a} The portion of the plot containing electron rich gallium complexes is in the upper right (gallium(I) compounds), whereas the bottom left portion is where electron deficient compounds are found (gallium(III) complexes). The central area contains data of compounds of intermediate electron density (gallium(II) compounds). In the Wagner plot, the data for **4.3** are plotted along with compounds with an unambiguously assigned oxidation number representing the three possible oxidation numbers for gallium (Figure 4.3).

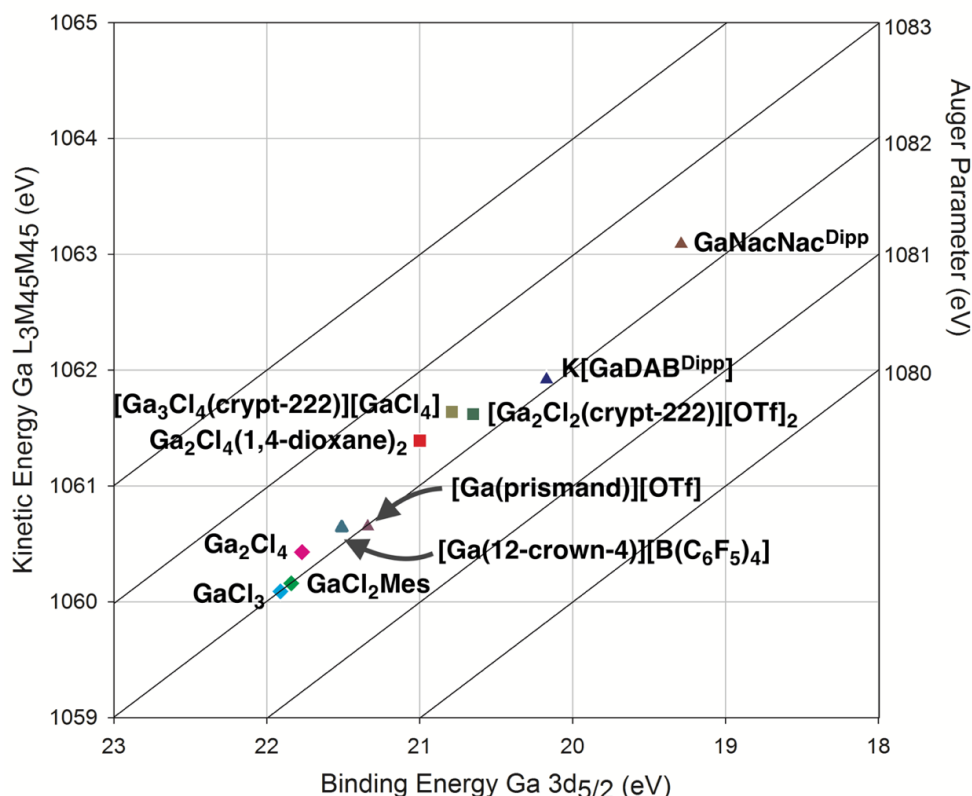


Figure 4.3: Wagner plot of representative Ga(I), Ga(II) and Ga(III) compounds and $[\text{Ga}(12\text{-crown-4})][\text{B}(\text{C}_6\text{F}_5)_4]$, **4.3**.

As shown in Figure 4.3, **4.3** is found in the region of the Wagner plot typical of gallium(III) compounds. Notably, $[\text{Ga}(\text{prismand})][\text{OTf}]$ (**3.4**) is found in the same region. The donor strength of the neutral crown ether in **4.3** can be considered to be quite weak in comparison to covalently bound ligands in gallium(I) species such as in $\text{GaNacNac}^{\text{Dipp}}$ (**3.2**). In addition, **4.3** has a cationic gallium(I) centre, further decreasing the electron density at gallium. While $\text{GaNacNac}^{\text{Dipp}}$ is found in the electron rich portion of the Wagner plot and has been used as a Lewis base, the gallium(I) cation of **4.3** may not react in a similar fashion, as its position on the Wagner plot indicates that its chemistry will be more similar to that of Lewis acidic gallium(III) compounds. Without these experimental data, it would be unclear as to the electronic nature of **4.3**; the use of XPS enables an understanding of the potential reactivity of **4.3**. Given the electron deficient nature of **4.3**,

its reactivity with donor molecules was explored

4.2.3 Computational Analysis of $[\text{Ga}(12\text{-crown-4})]^+$

Computational analyses were performed to further assist in the understanding of the electronic structure of the $[\text{Ga}(12\text{-crown-4})]^+$ cation in **4.3**. The frontier molecular orbitals were calculated and visualized from a geometry-optimized structure of the cation. As shown in Figure 4.4, the HOMO of the cation was found to correlate to the lone pair on gallium, and the LUMO+1 and LUMO+2 to the empty p orbitals on gallium. The bonding interactions between the oxygen atoms of the 12-crown-4 ligand and the gallium(I) cation were found to correspond to the HOMO-10 and HOMO-4, whereas the antibonding interaction was found to be the LUMO+6.

Natural bond orbital (NBO) calculations were performed to explore the Lewis structure of $[\text{Ga}(12\text{-crown-4})]^+$. The natural charge on the gallium(I) centre was found to be 0.841, indicating that the +1 overall charge of the cation is primarily located at the gallium centre with a small fraction of the charge located on the 12-crown-4 ligand (0.159). The Wiberg bond indices (WBI) between the gallium and oxygen atoms were calculated and found to be small; each gallium-oxygen interaction had a WBI of 0.071, totalling to 0.284 for all four Ga-O bonds. The low bond order for the gallium-crown ether interaction reaffirms that the 12-crown-4 ligand offers weak stabilization to the gallium(I) cation. In fact, examination of the orbitals in the NBO calculation reveals that the gallium-oxygen interactions are not classified as bonding; the lone pair on gallium has 97.6 % s character. The weak interaction between the gallium and the crown ether involves a p type orbital at gallium. The lone pairs on the oxygen atoms are not located in sp^3 hybrid orbitals, but rather one sp^2 hybrid orbital and one p type orbital with 95.9 % p character.

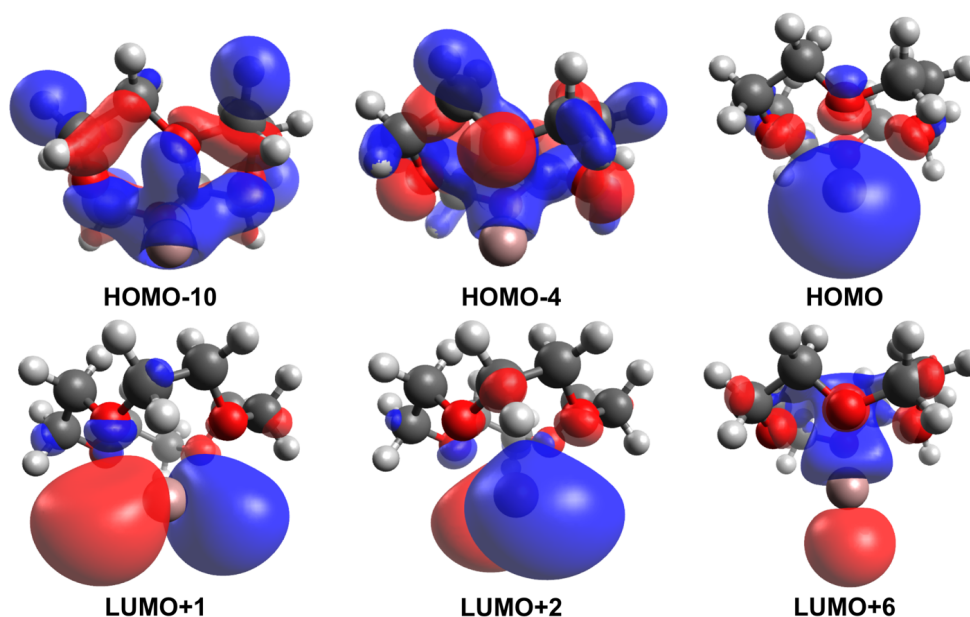


Figure 4.4: Calculated frontier molecular orbitals for $[\text{Ga}(12\text{-crown-4})]^+$ at the UM062X/6-311+G(2d,p) level of theory (isovalue = 0.03).

To complement the above analysis, time-dependent DFT (TD-DFT) calculations were conducted. The lowest energy excitations were found to exclusively arise from the lone pair of electrons on the gallium(I) cation and the lowest allowed transition had an excitation energy of 6.10 eV. The destination orbitals for the exciton were found to be one of the two empty p type orbitals on gallium with a probability of 95.2 % for either the LUMO+1 or LUMO+2. Although lower energy electron excitations exist, they were found to be forbidden transitions. The lowest energy allowed transition was significantly greater in energy than the excitation energies reported for gallium(I) complexes that undergo small molecule activation.³⁸ Thus, with both the computational and XPS data suggesting that the lone pair on the gallium centre in $[\text{Ga}(12\text{-crown-4})]^+$ may not be able to undergo oxidative addition due to the contraction of the lone pair into an s type orbital and the large HOMO-LUMO+1 gap; the reactivity of **4.3** with Lewis bases and its potential use as a donor-solvent stable gallium(I) starting material was investigated.

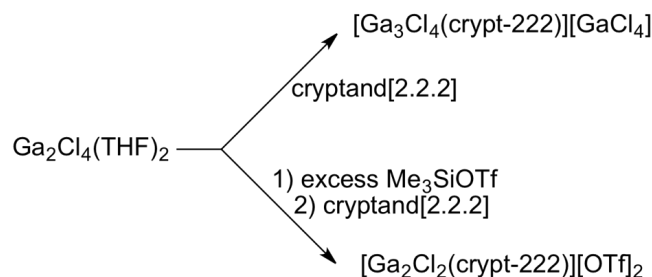
4.2.4 Reactivity of [Ga(12-crown-4)][B(C₆F₅)₄], **4.3**

Unlike 'GaI' and [Ga][GaCl₄], **4.1** and **4.3** are stable in Et₂O, THF and acetonitrile. In fact, **4.3** was found to have appreciable solubility only in acetonitrile. As such, it was envisioned that **4.3** could act as a donor-solvent stable source of gallium(I). Thus, we investigated the use of **4.3** to improve the synthesis of useful gallium(I) compounds, and to generate gallium(I) complexes that could not be synthesized from 'GaI' or [Ga][GaCl₄]. We also explored the chemistry of the [Ga(12-crown-4)]⁺ cation with other donor molecules.

Cp*Ga is a useful two electron σ donating ligand in transition metal chemistry and has been synthesized previously using three different methods: the metastable GaCl was reacted with Cp*Li at low temperature,³⁹ 'GaI' was reacted with Cp*K⁴⁰ or a gallium(III)-Cp* complex with halide ligands was synthesized and subsequently reduced to the gallium(I) species using potassium metal.⁴¹ When **4.3** and Cp*K were combined in fluorobenzene at room temperature, the major product was identified as Cp*Ga in approximately a 6:1 ratio as determined by ¹H NMR spectroscopy (assuming that all signals corresponded to species with only one Cp* ligand). When the mixture was analyzed using ⁷¹Ga NMR spectroscopy, a signal was observed at -648 ppm, which is consistent with the ⁷¹Ga chemical shift reported for Cp*Ga (-653 ppm).³⁹ Mass spectral data were also consistent with the formation of Cp*Ga; a signal at *m/z* 204 was observed in the mass spectrum, consistent with previous results.³⁹ **4.3** is an effective starting material for the generation of Cp*Ga. As the use of pyrophoric alkali metals and a metastable gallium(I) reagents that must be used in a cooling bath are avoided using this method, the synthesis of known gallium(I) complexes including Cp*Ga using **4.3** demonstrates the potential for **4.3** to be used as a well defined gallium(I) source.

Previous attempts to synthesize a gallium(I) cation encapsulated within cryptand[2.2.2], analogous to the germanium(II) dication derivative, failed. The reaction between Ga₂Cl₄ and cryptand[2.2.2] in non-donor solvents led to the formation of insoluble solids of variable composition despite changes in reaction conditions. When

‘GaI’ was used as a starting material, insoluble products were also formed. Products could only be isolated when $\text{Ga}_2\text{Cl}_4(\text{THF})_2$ ²⁸ was used as a starting material. In this case, mixed valent and gallium(II) species were obtained (Scheme 4.1).²²



Scheme 4.1: Synthesis of previously reported multinuclear gallium cations stabilized by cryptand[2.2.2].²²

When cryptand[2.2.2] was added to **4.1**, the results of the experiments were not reproducible. In some experiments, complexes containing gallium-chlorine fragments were formed as assessed by ESI-MS and ^1H NMR spectroscopy, where signals similar to what was observed for reactions between Ga_2Cl_4 and cryptand[2.2.2] were observed. Other reactions gave what appeared to be a gallium(I)-cryptand complex on the basis of the signal with a chemical shift at -600 ppm detected in the ^{71}Ga NMR spectrum of the product; however, the compound was unstable in solution. The inconsistency of the results was postulated to be due to the presence of the reactive $[\text{GaCl}_4]^-$ anion in **4.1**.²² Therefore, reactions between **4.3** and cryptand[2.2.2] in acetonitrile were attempted. Notably, the traditional gallium(I) starting materials, ‘GaI’ and $[\text{Ga}][\text{GaCl}_4]$, are not stable in acetonitrile. After removing the solvent from the reaction mixture and triturating the resultant solid, the product was identified as $[\text{Ga}(\text{crypt-222})][\text{B}(\text{C}_6\text{F}_5)_4]$, **4.4**, by NMR spectroscopy, ESI-MS and X-ray crystallography. The compound exhibited a signal in the ^{71}Ga NMR spectrum at -600 ppm, consistent with the formation of a gallium(I) cation. The ^{71}Ga chemical shift of **4.4** is similar to what was reported by Krossing for $[\text{Ga}(\text{arene})_x]^+$ cations,⁵ although shifted downfield by approximately 100 ppm. The crystal structure of **4.4** (Figure 4.5, Table 4.1) was obtained, confirming the formula of

the salt and the presence of a gallium(I) cation encapsulated within a molecule of cryptand[2.2.2].

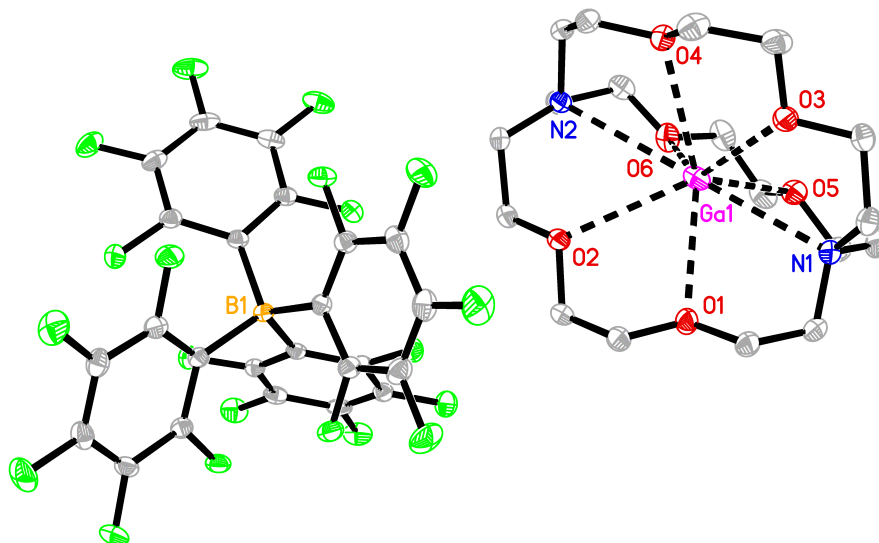


Figure 4.5: Displacement ellipsoid plot of **4.4**. Ellipsoids are drawn at the 50% probability level, hydrogen atoms and the second formula unit are omitted for clarity. Selected bond lengths and angles (\AA , $^\circ$): Ga1-N1 2.9218(14), Ga1-N2 3.1242(14), Ga1-O1 2.8418(15), Ga1-O2 2.9081(12), Ga1-O3 2.7709(14), Ga1-O4 2.9177(14), Ga1-O5 2.8037(14), Ga1-O6 2.8510(13); N1-Ga1-N2 179.53(3).

Although the cation of **4.4** exhibited 3-fold rotational symmetry in solution, this was not observed in the solid state, as **4.4** crystallized in the P-1 space group with two formula units in the asymmetric unit. As a result, there is a significant range observed for the Ga-N bond lengths (2.9218(14) to 3.1242(14) \AA) and the Ga-O bond lengths (2.7709(14) to 2.9177(14) \AA) in both $[\text{Ga}(\text{crypt-222})]^+$ cations in the asymmetric unit. These differences are postulated to be due to packing effects. The N-Ga-N bond angles were found to be approximately 180° ($179.53(3)^\circ$ and $178.70(3)^\circ$) and the gallium(I) cation is located approximately in the centre of the macrocycle in both formula units. The coordination environment at gallium is an end-bicapped trigonal prism, with a coordination number of 8 and eclipsed Ga-O bonds.⁴²

Table 4.1: Crystallographic data for **4.1**, **4.3**, and **4.4**.

	4.1	4.3	4.4
Formula	C ₈ H ₁₆ Cl ₄ Ga ₂ O ₄	C ₃₂ H ₁₆ BF ₂₀ GaO ₄	C ₄₂ H ₃₆ BF ₂₀ GaN ₂ O ₆
M _r (g mol ⁻¹)	457.45	924.98	1125.26
Crystal Colour and Habit	colourless plate	colourless prism	colourless prism
Crystal System	orthorhombic	tetragonal	triclinic
Space Group	P b c a	P 4/n	P -1
Temperature, K	110	110	110
<i>a</i> , Å	14.936(6)	14.295(4)	12.611(4)
<i>b</i> , Å	13.913(5)	14.295(4)	16.128(7)
<i>c</i> , Å	15.520(5)	7.8501(19)	24.654(10)
α, °	90	90	98.292(16)
β, °	90	90	99.222(11)
γ, °	90	90	111.011(16)
V, Å ³	3225.1(19)	1604.2(10)	4509(3)
Z	8	2	4
F(000)	1808	912	2264
ρ (g/cm ³)	1.884	1.915	1.658
λ, Å, (MoKα)	0.71073	0.71073	0.71073
μ, (cm ⁻¹)	4.005	1.015	0.743
No. of refl. meas.	117143	47177	163777
Unique refl. meas.	7103	3470	36259
R _{merge}	0.0566	0.0504	0.0426
No. of refl. incld in refinm.	7103	3470	36259
No. of params. in least-squares	227	132	1297
R ₁	0.0221	0.0324	0.0396
wR ₂	0.0415	0.0798	0.0860
R ₁ (all data)	0.0362	0.0508	0.0739
wR ₂ (all data)	0.0453	0.0867	0.0961
GOF	1.018	1.040	1.020

Where: $R_1 = \Sigma(|F_o| - |F_c|) / \Sigma F_o$; $wR_2 = [\Sigma(w(F_o^2 - F_c^2)^2) / \Sigma(wF_o^4)]^{1/2}$; $GOF = [\Sigma(w(F_o^2 - F_c^2)^2) / (\text{No. of reflns.} - \text{No. of params.})]^{1/2}$

As with **4.3**, the cation of **4.4** was analyzed computationally using a geometry-optimized structure of D₃ symmetry. The frontier molecular orbitals of the [Ga(crypt-222)]⁺ cation demonstrated that, analogous to [Ga(12-crown-4)]⁺, the HOMO is the

gallium-centred lone pair. The HOMO-2 corresponds to a bonding interaction between the nitrogen atoms and the gallium centre and the HOMO-16 corresponds to a bonding interaction between the oxygen atoms and the gallium cation. The LUMO and LUMO+1 correspond to the empty p-type orbitals on gallium, although due to the three-dimensional stabilization imparted by the cryptand, they are distorted from idealized p orbitals (Figure 4.6). Similar p type orbitals are also observed for the LUMO+4 and LUMO+5 orbitals. NBO calculations were performed on the $[\text{Ga}(\text{crypt-222})]^+$ cation and the lone pair on the gallium centre was located in an s orbital, with 100 % s character. The lone pairs on the nitrogen atoms were primarily of p character, with 84.2 % p and 15.7 % s character. The oxygen atom lone pairs were similar in electronic structure to those in the cation of **4.3**, where one lone pair is located in an sp^2 -like orbital and another in a p orbital, with 57.8 % and 99.8 % p character for the two orbitals, respectively. The natural charge on the gallium(I) cation was found to be 0.666, which is slightly lower than the charge on the gallium(I) cation in $[\text{Ga}(\text{12-crown-4})]^+$ (0.841). This is expected with the greater number of donor atoms provided by the cryptand in comparison to 12-crown-4, lowering the charge localized on the gallium centre. TD-DFT calculations demonstrated that, similar to $[\text{Ga}(\text{12-crown-4})]^+$, the lowest allowed electronic transition of the $[\text{Ga}(\text{crypt-222})]^+$ cation is from the HOMO to the LUMO or the LUMO+4, with the energy required for the transition being 5.41 eV. The calculated lowest energy transition of $[\text{Ga}(\text{crypt-222})]^+$ is approximately 0.7 eV lower in energy compared to that of $[\text{Ga}(\text{12-crown-4})]^+$ (6.10 eV), demonstrating that stronger electron donation from the ligand to the gallium(I) cation increases the potential for reactivity.

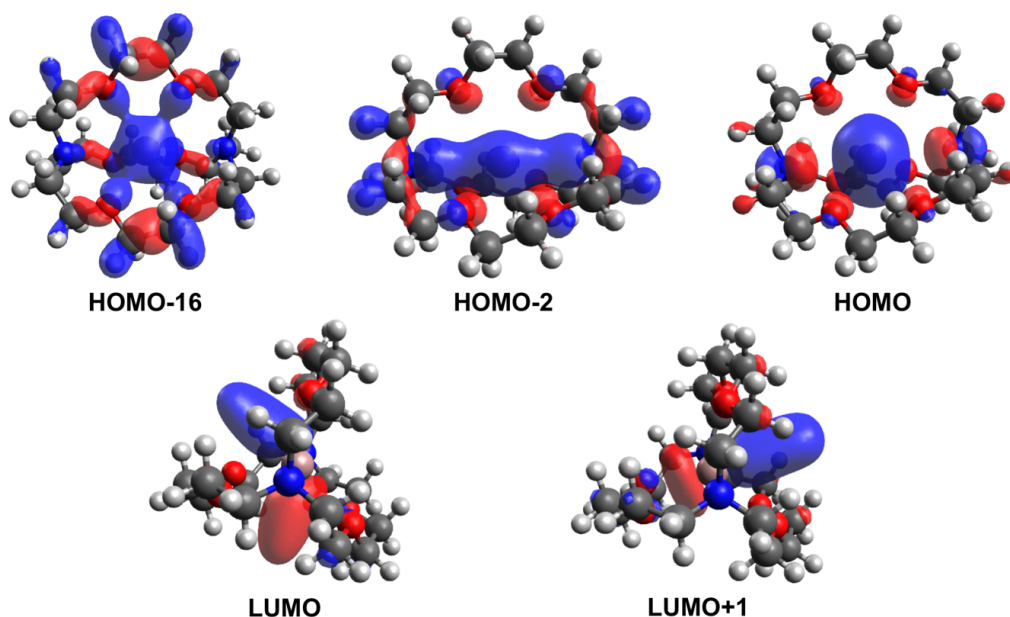
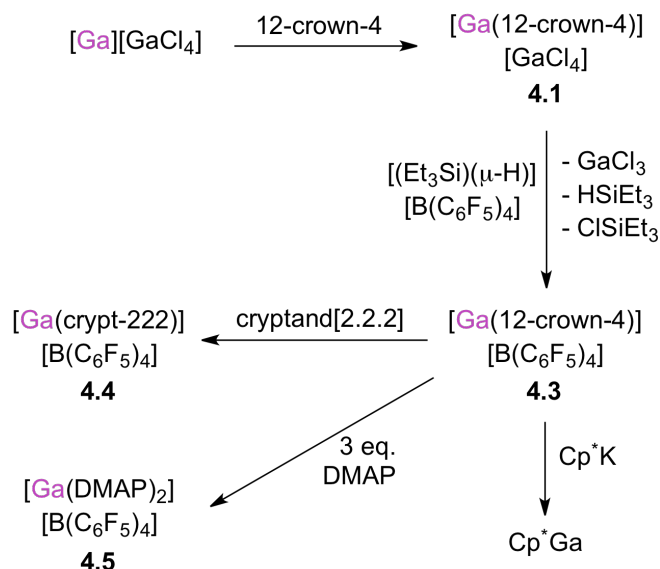


Figure 4.6: Calculated frontier molecular orbitals for $[\text{Ga}(\text{crypt-222})]^+$ at the UM062X/6-311+G(2d,p) level of theory (isovalue = 0.03).

Reactions of **4.3** with Lewis bases were also explored (Scheme 4.2); the reaction between **4.3** and 4-dimethylaminopyridine (DMAP) was examined. The addition of phosphorus and nitrogen donors to Krossing's $[\text{Ga}(\text{arene})_x]^+$ cations resulted in the formation of $[\text{Ga}(\text{donor})_3]^+$ complexes when the Lewis bases were not bulky.^{5,43} Thus, three equivalents of DMAP were used in the reaction with **4.3**. A single product appeared to be formed in the ^1H NMR spectrum of the reaction mixture of **4.3** and three equivalents of DMAP, although the chemical shifts of the DMAP ligand did not change significantly. However, the ^1H chemical shift of the 12-crown-4 ligand did change significantly and was consistent with that of the free crown ether. No signal was observed in the ^{71}Ga NMR spectrum of the product, similar to what was reported for the $[\text{Ga}(\text{pyrazine})_3]^+$ cation.⁴³ The ESI-MS data did not reveal any signals that could be assigned to any gallium-DMAP cationic complex. Single crystals suitable for X-ray diffraction experiments were obtained, however, the cation was severely disordered; the exact structure of the gallium(I) complex could not be determined, however, a model for the disorder could be obtained, suggesting that the cation was $[\text{Ga}(\text{DMAP})_2]^+$. Based on

the obtained data, a 2:1 complex, $[\text{Ga}(\text{DMAP})_2][\text{B}(\text{C}_6\text{F}_5)_4]$ (**4.5**), is proposed to be the empirical formula for the product.



Scheme 4.2: Summary of the reactivity of **4.1** and **4.3**.

XPS data were obtained on compounds **4.4** and **4.5** in order to compare the data to those of the starting material, **4.3**, as well as other gallium-cryptand complexes (Table 4.2). In comparing to the Ga $3d_{5/2}$ binding energy of the cryptand complex **4.4** with that of the crown ether complex **4.3**, the cryptand[2.2.2] complex possesses a gallium centre with more electron density, as revealed by the decrease of approximately 1 eV in the Ga $3d_{5/2}$ binding energy, and a similar increase in the Ga $L_3M_{45}M_{45}$ Auger kinetic energy. The Ga $3d_{5/2}$ binding energy of **4.4** is also very close to what was observed previously for our gallium(II)-cryptand complexes, again supporting the conclusion that cryptand[2.2.2] is a stronger donor toward the gallium(I) cation and the electronic nature of the gallium(I) cation in **4.4** is more electron rich than in **4.3**. The XPS data for **4.5** demonstrate stronger donor ligands such as DMAP increase the electron density at the gallium(I) centre; the Ga $3d_{5/2}$ binding energy is decreased from the starting material **4.3** by approximately 1.25 eV, and the Ga $L_3M_{45}M_{45}$ kinetic energy is increased by almost 2 eV. The electron energies for **4.5** indicate that the gallium(I) cation is more electron rich when bound by

DMAP ligands versus a cryptand macrocycle, as observed in **4.4** (**4.4**: 20.63 eV [Ga 3d_{5/2}] and 1061.26 eV [Ga 2p_{3/2}]; **4.5**: 20.26 eV and 1062.58 eV). These XPS data place **4.5** in between K[DAB^{Dipp}] (**3.3**) and GaNacNac^{Dipp} (**3.2**) on the Wagner plot shown in Figure 4.3, in terms of the electronic environment of the gallium(I) centre.

Table 4.2: Summary of XPS data for standard compounds and **4.3**, **4.4**, and **4.5**.*

Compound	Ga 3d _{5/2} (eV)	Ga 2p _{3/2} (eV)	Ga L ₃ M ₄₅ M ₄₅ (eV)	Auger Parameter (eV)
GaNacNac ^{Dipp} , 3.2	19.29	1117.50	1063.09	1082.38
K[GaDAB ^{Dipp}], 3.3	20.17	1118.02	1061.92	1081.84
[Ga(prismand)] [OTf], 3.4	21.34	1119.31	1060.65	1081.99
Ga ₂ Cl ₄ (1,4-dioxane) ₂ , 3.5	21.10	1118.86	1061.39	1082.39
[Ga ₃ Cl ₄ (crypt-222)] [GaCl ₄], 2.1	20.79	1118.51	1061.64	1082.43
[Ga ₂ Cl ₂ (crypt-222)] [OTf] ₂ , 2.2	20.65	1118.57	1061.62	1082.27
GaCl ₃ , 3.8	21.91	1119.85	1060.09	1082.00
GaCl ₂ Mes, 3.11	21.84	1120.10	1060.16	1082.00
Ga ₂ Cl ₄ , 3.12	21.77	1119.54	1060.43	1082.00
[Ga(12-crown-4)] [B(C ₆ F ₅) ₄], 4.3	21.51	1119.23	1060.64	1082.15
[Ga(crypt-222)] [B(C ₆ F ₅) ₄], 4.4	20.63	1118.49	1061.26	1081.89
[Ga(DMAP) ₃] [B(C ₆ F ₅) ₄], 4.5	20.26	1118.21	1062.58	1082.84

*Note: The Ga 3d_{5/2} and Ga 2p_{3/2} are photoelectron emissions and are expressed as binding energy; the Ga L₃M₄₅M₄₅ is an Auger emission and is expressed as kinetic energy. The Auger parameter is the sum of the Ga 3d_{5/2} and Ga L₃M₄₅M₄₅ energies.

Although **4.3** was shown by XPS and experimental results to be electron deficient, the potential for this compound and others that have or may be synthesized using **4.3** as a synthon to act as catalytic species or be used in small molecule activation can be envisioned. There are many examples of Lewis acid catalysts, including complex

reactions such as the polymerization of isobutylene,⁶ that the reported complexes may be well suited for. We have demonstrated the ability to track the electron density at the gallium(I) centre as the ligands are varied using XPS, and the synthesis of new complexes and cations with moderate to high electron density may give rise to new gallium(I) compounds capable of oxidative addition with important small molecules such as H₂, and other substrates. Experimental work toward the evaluation of the reactivity of **4.3**, **4.4** and **4.5** for catalytic applications and the use of **4.3** as a synthon for additional gallium(I) complexes will be performed in due course.

4.3 Conclusions

Herein, we report the use of a commercially available ligand, 12-crown-4, for the facile complexation of gallium(I) cations from Ga₂Cl₄. Comproportionation, a common reaction for Ga₂Cl₄, did not occur, allowing for the isolation of [Ga(12-crown-4)][GaCl₄], **4.1**. **4.1** is a gallium(I) cation which is stable toward donor solvents. The subsequent anion exchange reaction of **4.1** with [(Et₃Si)₂(μ-H)][B(C₆F₅)₄] allowed for the removal of the reactive [GaCl₄]⁻ anion, to give **4.3**. The chemical state of **4.3**, as revealed by XPS, indicated the Lewis acidic nature of the cation, which was corroborated by computational analysis. The synthesis of **4.4** and **4.5** from **4.3** demonstrates how **4.3** may be utilized as a gallium(I) starting material that does not decompose or undergo comproportionation upon exposure to donor solvents and the ability of **4.3** to act as a versatile gallium(I) source that can complement the existing starting materials for gallium(I) chemistry.

4.4 Experimental

4.4.1 General Considerations

All manipulations were performed under an inert atmosphere of argon using Schlenk techniques or under an atmosphere of nitrogen in an MBraun glovebox unless otherwise stated. All solvents were purified using an Innovative Technologies 400-5 Solvent Purification System and were stored over activated 3 or 4 Å molecular sieves, unless otherwise stated. C₆D₆ was dried over activated 4 Å molecular sieves. CH₃CN was

purified by distillation over CaH_2 and stored over 3 Å molecular sieves. All reagents were used as received from Sigma-Aldrich, Alfa Aesar, Strem Chemicals or Gelest. Ga_2Cl_4 ^{25b} and $[(\text{Et}_3\text{Si})_2(\mu\text{-H})][\text{B}(\text{C}_6\text{F}_5)_4]$ ³⁷ were synthesized according to literature procedures. NMR spectra were recorded on a Varian INOVA I600 (^1H 600 MHz; ^{11}B 192 MHz, ^{13}C 151 MHz; ^{19}F 564 MHz; ^{71}Ga 183 MHz) spectrometer. Chemical shifts (δ) are reported in ppm and were internally referenced to the residual protonated solvent peaks for ^1H spectra (1.94 ppm for the central signal of CD_2HCN , 7.15 ppm for $\text{C}_6\text{D}_5\text{H}$), and the deuterated solvent for ^{13}C (118.69 ppm for CD_3CN). ^{11}B NMR spectra were referenced to 15 % $\text{BF}_3\cdot\text{OEt}_2$ in CDCl_3 (0.0 ppm) using the internal lock signal from the deuterated solvent, to CFCl_3 (0.0 ppm) for ^{19}F NMR spectra, and to 1.1 M $\text{Ga}(\text{NO}_3)_3$ (0.0 ppm) in D_2O for ^{71}Ga spectra. Coupling constants (J) are reported in Hz and multiplicities are reported as singlet (s), doublet (d), triplet (t), quartet (q), multiplet (m), broad (br) and overlapping (ov). All NMR assignments were confirmed using two-dimensional techniques (gCOSY, gHSQC, gHMBC) where appropriate. Electrospray ionization mass spectra were collected using a Bruker micrOTOF II spectrometer. Electron impact mass spectra were collected using a Thermo Scientific DFS spectrometer. Mass spectral data are reported in mass-to-charge units (m/z). Elemental analyses were performed by Laboratoire d'Analyse Élémentaire de l'Université de Montréal (Montréal, QC).

4.4.2 Synthesis of $[\text{Ga}(12\text{-crown-4})][\text{GaCl}_4]$, **4.1**

Solid Ga_2Cl_4 (0.92 g, 3.28 mmol) was added to toluene (8 mL), producing a yellow solution which was added to a stirring solution of 12-crown-4 (0.58 g, 3.28 mmol) dissolved in toluene (4 mL). The orange solution was allowed to stir for 24 hours. After the first five minutes of reaction, the colour of the mixture faded to yellow and a precipitate formed; after an hour of reaction, the colour of the mixture had faded to off-white. The solvent was removed under reduced pressure, giving an off-white solid. The solid was suspended in acetonitrile (10 mL) and then removed by filtration to give a pale yellow solution. The solvent was removed from the yellow filtrate under reduced

pressure to give an off-white solid which was washed with Et₂O (3 x 3 mL). The solid was dried under reduced pressure giving **4.1**, which was dissolved in CH₃CN (4 mL). Et₂O (5 mL) was added to the CH₃CN solution, and the resulting mixture was cooled to -20 °C for 24 hours, from which X-ray diffraction quality crystals were obtained.

Yield: 1.11 g (74 %) of a white solid; mp: 124 – 129 °C (decomposition); ¹H NMR (CD₃CN, 600 MHz, 298 K) δ: 3.82 (s, [-O-CH₂-CH₂-]); ¹³C{¹H} NMR (CD₃CN, 151 MHz, 298 K) δ: 70.98 ([-O-CH₂-CH₂-]); ⁷¹Ga NMR (CD₃CN, 183 MHz, 298 K) δ: 251.2 ([GaCl₄]⁻), -470.7 ([Ga(12-crown-4)]⁺); LR ESI-TOF (*m/z*; positive ion): [⁶⁹Ga(12-crown-4)]⁺: 245, LR ESI-TOF (*m/z*; negative ion): [⁶⁹GaCl₄]⁻: 211; HR ESI-TOF (*m/z*; positive ion): Calcd. for [C₈H₁₆⁶⁹GaO₄]⁺: 245.0304, Found: 245.0308; Elemental analysis (%) for [Ga(12-crown-4)][GaCl₄] (C₈H₁₆Cl₄Ga₂O₄): Calcd. C 21.00, H 3.53; Found C 21.99, H 3.38.

4.4.3 Synthesis of [Ga(12-crown-4)][B(C₆F₅)₄], **4.3**

An orange solution of [(Et₃Si)₂(μ-H)][B(C₆F₅)₄] (2.14 g, 2.35 mmol) dissolved in fluorobenzene (5 mL) was added dropwise to a stirring suspension of **4.1** (1.07 g, 2.35 mmol) in fluorobenzene (5 mL). The orange colour quickly dissipated. The mixture was allowed to stir for 18 hours, at which point the solvent was removed under reduced pressure, yielding a grey solid. The solid was suspended in acetonitrile (8 mL), the suspension was filtered, and the solvent was removed from the filtrate under reduced pressure, yielding a white solid, **4.3**. The white solid was washed with Et₂O (3 x 3 mL) and dried under reduced pressure. X-ray quality crystals of **4.3** were obtained by a vapour diffusion of Et₂O into a solution of **4.3** in acetonitrile at -20 °C.

Yield: 1.57 g (72 %) of a white solid; mp: 261 – 263 °C (decomposition); ¹H NMR (CD₃CN, 600 MHz, 298 K) δ: 3.84 (s, [-O-CH₂-CH₂-]); ¹¹B{¹H} NMR (192 MHz, CD₃CN, 298 K) δ: -16.7 (s, [B(C₆F₅)₄]⁻); ¹³C{¹H} NMR (CD₃CN, 151 MHz, 298 K) δ: 149.48 (d, ¹J_{C-F} = 236 Hz, *o*-C-F), 139.68 (d, ¹J_{C-F} = 243 Hz, *p*-C-F), 137.73 (d, ¹J_{C-F} = 248 Hz, *m*-C-F), 125.22 (br m, *ipso*-C-B), 68.33 ([-O-CH₂-CH₂-]); ¹⁹F NMR (564 MHz,

CD₃CN, 298 K) δ : -133.8 (br m, *o*-C-F), -164.0 (t, $^3J_{F-F} = 20$ Hz, *p*-C-F), -168.4 (t, $^3J_{F-F} = 17$ Hz, *m*-C-F); ^{71}Ga NMR (CD₃CN, 183 MHz, 298 K) δ : no signal; LR ESI-TOF (*m/z*; positive ion): [$^{69}\text{Ga}(12\text{-crown-4})$]⁺: 245; LR ESI-TOF (*m/z*; negative ion): [$^{10}\text{B}(\text{C}_6\text{F}_5)_4$]⁻: 678; HR ESI-TOF (*m/z*; positive ion): Calcd. for [$\text{C}_8\text{H}_{16}^{69}\text{GaO}_4$]⁺: 245.0304, Found: 245.0304; Elemental analysis (%) for [$\text{Ga}(12\text{-crown-4})$][$\text{B}(\text{C}_6\text{F}_5)_4$] ($\text{C}_{32}\text{H}_{16}\text{BF}_{20}\text{GaO}_4$): Calcd. C 41.55, H 1.74, N 0.00; Found C 41.42, H 1.84, N 0.20.

4.4.4 [Ga(crypt-222)][B(C₆F₅)₄], **4.4**

Cryptand[2.2.2] (0.14 g, 0.15 mmol) was dissolved in acetonitrile (2 mL) and added dropwise to a stirring suspension of **4.3** (0.057 g, 0.15 mmol) in acetonitrile (3 mL). The suspended solid dissolved over 30 minutes to give a pale yellow solution. The solution was allowed to stir at room temperature for 4 hours, at which point the solvent was removed under reduced pressure yielding a pale yellow solid. The solid was washed with Et₂O (3 x 2 mL), and was dried under reduced pressure yielding a pale yellow solid, **4.4**. X-ray quality crystals were obtained by concentrating a solution of **4.4** in acetonitrile and Et₂O (1:3).

Yield: 0.12 g (73 %) of a pale yellow solid; mp: 198 – 202 °C (decomposition); ^1H NMR (CD₃CN, 600 MHz, 298 K) δ : 3.58 (s, 12H, O-CH₂-CH₂-O), 3.58 – 3.57 (m, 12H, N-CH₂-CH₂-O), 2.59 – 2.57 (m, 12H, N-CH₂-CH₂-O); $^{11}\text{B}\{^1\text{H}\}$ NMR (192 MHz, CD₃CN, 298 K) δ : -16.7 (s, [$\text{B}(\text{C}_6\text{F}_5)_4$]⁻); $^{13}\text{C}\{^1\text{H}\}$ NMR (CD₃CN, 151 MHz, 298 K) δ : 149.46 (d, $^1J_{C-F} = 239$ Hz, *o*-C-F), 139.65 (d, $^1J_{C-F} = 244$ Hz, *p*-C-F), 137.70 (d, $^1J_{C-F} = 246$ Hz, *m*-C-F), 125.28 (br m, *ipso*-C-B), 70.78 (O-CH₂-CH₂-O), 69.19 (N-CH₂-CH₂-O), 55.30 (N-CH₂-CH₂-O); ^{19}F NMR (564 MHz, CD₃CN, 298 K) δ : -133.8 (br s, *o*-C-F), -164.0 (t, $^3J_{F-F} = 20$ Hz, *p*-C-F), -168.4 (t, $^3J_{F-F} = 18$ Hz, *m*-C-F); $^{71}\text{Ga}\{^1\text{H}\}$ NMR (CD₃CN, 183 MHz, 298 K) δ : -600 ([$\text{Ga}(\text{crypt-222})$]⁺); LR ESI-TOF (*m/z*; positive ion): [$^{69}\text{Ga}(\text{crypt-222})$]⁺: 445; LR ESI-TOF (*m/z*; negative ion): [$^{10}\text{B}(\text{C}_6\text{F}_5)_4$]⁻: 678; HR ESI-TOF (*m/z*; positive ion): Calcd. for [$\text{C}_{18}\text{H}_{36}^{69}\text{GaN}_2\text{O}_6$]⁺ ([$\text{Ga}(\text{crypt-222})$]⁺): 445.1829, Found: 445.1814; Elemental analysis (%) for [$\text{Ga}(\text{crypt-222})$][$\text{B}(\text{C}_6\text{F}_5)_4$] ($\text{C}_{42}\text{H}_{36}\text{BF}_{20}\text{GaN}_2\text{O}_6$): Calcd. C 44.83, H 3.22, N 2.49; Found C 44.60, H 3.18, N 2.44.

4.4.5 Synthesis of $[\text{Ga}(\text{DMAP})_2][\text{B}(\text{C}_6\text{F}_5)_4]$, **4.5**

A solution of DMAP (0.099 g, 0.81 mmol) dissolved in acetonitrile (3 mL) was added to a stirring solution of **4.3** (0.25 g, 0.27 mmol) dissolved in acetonitrile (3 mL). The solution was stirred for 2 hours, at which point the solvent was removed under reduced pressure. The resulting solid was suspended in Et_2O (4 mL) and the mixture was centrifuged. The supernatant was decanted, and the solid was washed twice more with Et_2O (3 mL). The solid was then dried under reduced pressure, yielding an off-white solid, **4.5**.

Yield: 0.23 g (76 %) of an off-white solid; mp: 221 – 226 °C (decomposition); ^1H NMR (CD_3CN , 600 MHz, 298 K) δ : 8.07 (d, $J = 7$ Hz, 6H, N-CH-CH-), 6.56 (d, $J = 7$ Hz, 6H, N-CH-CH-), 3.04 (s, 18H, N-(CH_3)₂); $^{11}\text{B}\{^1\text{H}\}$ NMR (192 MHz, CD_3CN , 298 K) δ : -16.7 (s, $[\text{B}(\text{C}_6\text{F}_5)_4]^-$); $^{13}\text{C}\{^1\text{H}\}$ NMR (CD_3CN , 151 MHz, 298 K) δ : 157.00 (s, C-N-(CH_3)₂), 149.43 (d, $^1J_{\text{C-F}} = 254$ Hz, *o*-C-F), 148.59 (s, N-CH-CH-), 139.66 (d, $^1J_{\text{C-F}} = 245$ Hz, *p*-C-F), 137.71 (d, $^1J_{\text{C-F}} = 245$ Hz, *m*-C-F), 125.28 (br m, *ipso*-C-B), 107.16 (s, N-CH-CH-), 40.06 (s, N-(CH_3)₂); ^{19}F NMR (564 MHz, CD_3CN , 298 K) δ : -133.8 (br s, *o*-C-F), -164.0 (t, $^3J_{\text{F-F}} = 20$ Hz, *p*-C-F), -168.4 (t, $^3J_{\text{F-F}} = 16$ Hz, *m*-C-F); $^{71}\text{Ga}\{^1\text{H}\}$ NMR (CD_3CN , 183 MHz, 298 K) δ : no signal; LR ESI-MS: no signal corresponding to $[\text{Ga}(\text{DMAP})_2]^+$ or $[\text{Ga}(\text{DMAP})]^+$ was observed; Satisfactory elemental analysis data could not be obtained presumably due to the decomposition of **4.5** upon exposure to air or the experimental conditions.

4.4.6 Synthesis of Cp^*Ga

A suspension of **4.3** (0.010 g, 0.011 mmol) in fluorobenzene (2 mL) was added to a stirring suspension of Cp^*K (0.002 g, 0.011 mmol) in fluorobenzene (2 mL). Within 30 minutes, the solids had dissolved, leaving a clear, colourless solution. After stirring for 8 hours, the solvent was removed under reduced pressure. The resulting residue was analyzed using ^1H and ^{71}Ga NMR spectroscopy, and mass spectrometry, demonstrating the formation of Cp^*Ga .

^1H NMR (C_6D_6 , 600 MHz, 298 K) δ : 1.91 (s, $(\text{CH}_3\text{-C})_5$); $^{71}\text{Ga}\{\text{H}\}$ NMR (CD_3CN , 183 MHz, 298 K) δ : -648 (s); HR EI-MS (source temperature = 80 °C): Calcd. for $[\text{C}_{10}\text{H}_{15}^{69}\text{Ga}]^+$ (Cp^*Ga^+): 204.0430, Found: 204.0429.

4.4.7 X-ray Crystallographic Details

Data Collection and Processing: The sample was mounted on a MiTeGen polyimide micromount with a small amount of Paratone N oil. All X-ray measurements were made on a Bruker Kappa Axis Apex2 diffractometer at a temperature of 110 K. The frame integration was performed using SAINT.⁴⁴ The resulting raw data were scaled and absorption corrected using a multi-scan averaging of symmetry equivalent data using SADABS.⁴⁵

Structure Solution and Refinement: The structure was solved by using a dual space methodology using the SHELXT program.⁴⁶ All non-hydrogen atoms were obtained from the initial solution. The hydrogen atoms were introduced at idealized positions and were treated in a mixed fashion. For **4.1**, the C8-H8A bond distance was found to refine to a value that unacceptable short after allowing the hydrogen atoms to refine isotropically. This bond length was then constrained to an idealized distance, and allowed to refine isotropically, along with the remaining hydrogen atoms. The remaining compounds were refined with a riding model for the hydrogen atoms. The structural model was fit to the data using full matrix least-squares based on F^2 . The calculated structure factors included corrections for anomalous dispersion from the usual tabulation. The structure was refined using the SHELXL-2014 program from the SHELXTL suite of crystallographic software.⁴⁷ Graphic plots were produced using the XP program suite.⁴⁸

4.4.8 Computational Details

All calculations were performed using Gaussian 09⁴⁹ on the Shared Hierarchical Academic Research Computing Network (SHARCNET, <http://www.sharcnet.ca>). Computations were run in parallel using two AMD Opteron 2.2 GHz 24 core CPUs with 32 GB of memory. All initial data were obtained using crystallographically determined

atomic coordinates, which were then optimized using the standard optimization procedure implemented in Gaussian 09. The optimized structure of [Ga(crypt-222)]⁺ (**4.4**) was constrained to have D₃ symmetry during optimization to obtain a stationary point as the optimized geometry. All optimized structures were determined to be stationary points by examining the number of imaginary frequencies obtained from a default frequency calculation (NIMAG = 0). All calculations were performed using the M06-2X functional⁵⁰ and the 6-311+G(2d,p) basis set. Natural bond orbital calculations were performed using NBO, version 6,⁵¹ as implemented in Gaussian 09. Visualizations of the molecular orbitals were performed using Avogadro, version 1.0.3.⁵² The lowest energy electron excitations were calculated using the time-dependent DFT method,⁵³ using the same functional and basis set.

4.5 References

- [1] Several reports of seminal gallium(I) compounds: a) Schmidbaur, H.; Thewalt, U.; Zafiroopoulos, T. *Organometallics* **1983**, *2*, 1550-1554; b) Loos, D.; Schnöckel, H.; Gauss, J.; Schneider, U. *Angew. Chem., Int. Ed. Engl.* **1992**, *31*, 1362-1364; c) Hardman, N.J.; Wright, R.J.; Phillips, A.D.; Power, P.P. *Angew. Chem., Int. Ed.* **2002**, *41*, 2842-2844; d) Hardman, N.J.; Eichler, B.E.; Power, P.P. *Chem. Commun.* **2000**, 1991-1992; e) Schmidt, E.S.; Jockisch, A.; Schmidbaur, H. *J. Am. Chem. Soc.* **1999**, *121*, 9758-9759.
- [2] Power, P. P. *Nature* **2010**, *463*, 171–177.
- [3] Oxidative Addition: a) Seifert, A.; Scheid, D.; Linti, G.; Zessin, T. *Chem. Eur. J.* **2009**, *15*, 12114–12120; b) Zhu, Z.; Wang, X.; Olmstead, M.M.; Power, P.P. *Angew. Chem., Int. Ed.* **2009**, *48*, 2027-2030; Cycloadditions: c) Zhu, Z.; Wang, X.; Peng, Y.; Lei, H.; Fettinger, J.C.; Rivard, E.; Power, P.P. *Angew. Chem., Int. Ed.* **2009**, *48*, 2031-2034; d) Caputo, C.A.; Zhu, Z.; Brown, Z.D.; Fettinger, J.C.; Power, P.P. *Chem. Commun.* **2011**, *47*, 7506-7508; e) Caputo, C.A.; Guo, J.-D.; Nagase, S.; Fettinger, J.C.; Power, P.P. *J. Am. Chem. Soc.* **2012**, *134*, 7155-7164.

- [4] For an example of the ambiphilicity of gallium(I): Dange, D.; Li, J.; Schenk, C.; Schnöckel, H.; Jones, C. *Inorg. Chem.* **2012**, *51*, 13050-13059.
- [5] Slattery, J.M.; Higelin, A.; Bayer, T.; Krossing, I. *Angew. Chem., Int. Ed.* **2010**, *49*, 3228-3231.
- [6] Lichtenthaler, M.R.; Higelin, A.; Kraft, A.; Hughes, S.; Steffani, A.; Plattner, D.A.; Slattery, J.M.; Krossing, I. *Organometallics* **2013**, *32*, 6725 – 6735.
- [7] Qin, B.; Schneider, U. *J. Am. Chem. Soc.* **2016**, *138*, 13119-13122.
- [8] a) Herber, R.H.; Smelkinson, A.E. *Inorg. Chem.* **1978**, *17*, 1023-1029; b) Drew, M.G.B.; Nicholson, D.G. *J. Chem. Soc., Dalton Trans.* **1986**, 1543-1549.
- [9] Probst, T.; Steigelmann, O.; Riede, J.; Schmidbaur, H. *Angew. Chem., Int. Ed. Engl.* **1990**, *29*, 1397-1398.
- [10] a) Cheng, F.; Hector, A.L.; Levason, W.; Reid, G.; Webster, M.; Zhang, W. *Angew. Chem., Int. Ed.* **2009**, *48*, 5152-5154; b) Rupar, P. A.; Bandyopadhyay, R.; Cooper, B. F. T.; Stinchcombe, M. R.; Ragogna, P. J.; Macdonald, C. L. B.; Baines, K. M. *Angew. Chem., Int. Ed.* **2009**, *48*, 5155-5158; c) Bandyopadhyay, R.; Nguyen, J.H.; Swidan, A.; Macdonald, C.L.B. *Angew. Chem., Int. Ed.* **2013**, *52*, 3469-3472.
- [11] Everett, M.; Jolleys, A.; Levason, W.; Light, M.E.; Pugh, D.; Reid, G. *Dalton Trans.* **2015**, *44*, 20898-20905.
- [12] a) Bandyopadhyay, R.; Cooper, B.F.T.; Rossini, A.J.; Schurko, R.W.; Macdonald, C.L.B. *J. Organomet. Chem.* **2010**, *695*, 1012-1018; b) Macdonald, C.L.B.; Bandyopadhyay, R.; Cooper, B.F.T.; Friedl, W.W.; Rossini, A.J.; Schurko, R.W.; Eichhorn, S.H.; Herber, R.H. *J. Am. Chem. Soc.* **2012**, *134*, 4332–4345.
- [13] Rupar, P.A.; Staroverov, V.N.; Baines, K.M. *Science* **2008**, *322*, 1360-1363.
- [14] Avery, J.C.; Hanson, M.A.; Herber, R.H.; Bladec, K.J.; Rupar, P.A.; Nowik, I.; Huang, Y.; Baines, K.M. *Inorg. Chem.* **2012**, *51*, 7306-7316.
- [15] a) Andrews, C.G.; Macdonald, C.L.B. *Angew. Chem., Int. Ed.* **2005**, *44*, 7453-7456; b) Cooper, B.F.T.; Macdonald, C.L.B. *J. Organomet. Chem.* **2008**, *693*, 1707-1711.

- [16] Higelin, A.; Haber, C.; Meier, S.; Krossing, I. *Dalton Trans.* **2012**, *41*, 12011-12015.
- [17] a) Ivanov, M.G.; Vashchenko, S.D.; Kalinichenko, I.I.; Vokhmyakov, A.N.; Barybin, A.S. *Dokl. Akad. Nauk. SSSR* **1987**, *293*, 617-619; b) Ivanov, M.G.; Vashchenko, S.D.; Baklykov, V.G.; Kalinichenko, I.I.; Reznikova, L.A. *Russ. J. Coord. Chem.* **1989**, *3*, 329-332.
- [18] Kloo, L.A.; Taylor, M.J. *J. Chem. Soc., Dalton Trans.* **1997**, *15*, 2693-2696.
- [19] Schmidbaur, H.; Hager, R.; Huber, B.; Müller, G. *Angew. Chem., Int. Ed. Engl.* **1987**, *26*, 338-340.
- [20] Kunze, A.; Gleiter, R.; Bethke, S.; Rominger, F. *Organometallics* **2006**, *25*, 4787-4791.
- [21] Fiolka, C. Polyiodide komplexer Übergangsmetalle. Ph.D. Thesis, Universität zu Köln, Köln, Germany, 2010.
- [22] Bourque, J.L.; Boyle, P.D.; Baines, K.M. *Chem. Eur. J.* **2015**, *21*, 9790-9796.
- [23] a) Bourque, J.L.; Biesinger, M.C.; Baines, K.M. *Dalton Trans.* **2016**, *45*, 7678-7696; b) Yang, L.; Bourque, J.L.; McLeod, J.A.; Shen, P.; Baines, K.M.; Liu, L. *Inorg. Chem.* **2017**, *56*, 2985-2991.
- [24] Green, M.L.H.; Mountford, P.; Smout, G.J.; Speel, R. *Polyhedron* **1990**, *9*, 2763-2765.
- [25] a) Crystal structure: Garton, G.; Powell, H.M. *J. Inorg. Nucl. Chem.* **1957**, *4*, 84-89; b) Convenient synthesis: Beamish, J.C.; Wilkinson, M.; Worrall, I.J. *Inorg. Chem.* **1978**, *17*, 2026-2027.
- [26] Malbrecht, B.J.; Dube, J.W.; Willans, M.J.; Ragona, P.J. *Inorg. Chem.* **2014**, *53*, 9644-9656.
- [27] Baker, R.J.; Jones, C. *Dalton Trans.* **2005**, 1341-1348.
- [28] Schmidt, E.S.; Schier, A.; Mitzel, N.W.; Schmidbaur, H. *Z. Naturforsch.* **2001**, *56b*, 337-341.
- [29] Ball, G.E.; Cole, M.L.; McKay, A.I. *Dalton Trans.* **2012**, *41*, 946-952.

- [30] Krossing, I. *Chem. Eur. J.* **2001**, *7*, 490-502.
- [31] Schmidbaur, H. *Angew. Chem., Int. Ed. Engl.* **1985**, *24*, 893-904.
- [32] Downs, A.J.; Himmel, H.-J. In *The Group 13 Metals Aluminium, Gallium, Indium and Thallium: Chemical Patterns and Peculiarities*, eds. Aldridge, S.; Downs, A.J. 2011, John Wiley & Sons Ltd.; Chichester, West Sussex, United Kingdom.
- [33] Schriver, D.F.; Atkins, P.W.; Overton, T.L.; Rourke, J.P.; Weller, M.T.; Armstrong, F.A. *Schriver & Atkins Inorganic Chemistry, Fourth Edition*; Oxford University Press: Oxford, 2006.
- [34] Kronig, S.; Theuergarten, E.; Holschumacher, D.; Bannenberg, T.; Daniliuc, C.G.; Jones, P.G.; Tamm, M. *Inorg. Chem.* **2011**, *50*, 7344-7359.
- [35] Müller, T. Silylium Ions. In *Functional Molecular Silicon Compounds I: Structure and Bonding*, Volume 155; Springer International Publishing: Switzerland, 2014; pp 107-162.
- [36] For recent examples: a) Holthausen, M.H.; Hiranandani, R.R.; Stephan, D.W. *Chem. Sci.* **2015**, *6*, 2016-2021; b) Caputo, C.B.; Winkelhaus, D.; Dobrovetsky, R.; Hounjet, L.J.; Stephan, D.W. *Dalton Trans.* **2015**, *44*, 12256-12264.
- [37] Connelly, S.J.; Kaminsky, W.; Heinekey, D.M. *Organometallics* **2013**, *32*, 7478-7481.
- [38] Zhu, Z.; Fisher, R.C.; Ellis, B.D.; Rivard, E.; Merrill, W.A.; Olmstead, M.M.; Power, P.P.; Guo, J.D.; Nagase, S.; Pu, L. *Chem. Eur. J.* **2009**, *15*, 5263-5272.
- [39] Loos, D.; Schnöckel, H. *J. Organomet. Chem.* **1993**, *463*, 37-40.
- [40] Jutzi, P.; Schebaum, L.O. *J. Organomet. Chem.* **2002**, *654*, 176-179.
- [41] Jutzi, P.; Neumann, B.; Reumann, G.; Stämmler, H.-G. *Organometallics* **1998**, *17*, 1305-1314.
- [42] Burdett, J.K.; Hoffmann, R.; Fay, R.C. *Inorg. Chem.* **1978**, *17*, 2553-2568.
- [43] Lichtenthaler, M.R.; Stahl, F.; Kratzert, D.; Benkmil, B.; Wegner, H.A.; Krossing, I. *Eur. J. Inorg. Chem.* **2014**, 4335-4341.

- [44] Bruker-AXS, SAINT version 2013.8, **2013**, Bruker-AXS, Madison, WI 53711, USA.
- [45] Bruker-AXS, SADABS version 2012.1, **2012**, Bruker-AXS, Madison, WI 53711, USA.
- [46] Sheldrick, G.M. *Acta Cryst.* **2015**, *A71*, 3-8.
- [47] Sheldrick, G.M. *Acta Cryst.* **2015**, *C71*, 3-8.
- [48] Bruker-AXS, XP version 2013.1, **2013**, Bruker-AXS, Madison, WI 53711, USA.
- [49] Gaussian 09, Revision E.01, Frisch, M.J.; Trucks, G.W.; Schlegel, H.B.; Scuseria, G.; Robb, M.A.; Cheeseman, J.R.; Scalmani, G.; Barone, V.; Mennucci, B.; Petersson, G.A.; Nakatsuji, H.; Caricato, M.; Li, X.; Hratchian, H.P.; Izmaylov, A.F.; Bloino, J.; Zheng, G.; Sonnenberg, J.L.; Hada, M.; Ehara, M.; Toyota, K.; Fukuda, R.; Hasegawa, J.; Ishida, M.; Nakajima, T.; Honda, Y.; Kitao, O.; Nakai, H.; Vreven, T.; Montgomery, Jr., J.A.; Peralta, J.E.; Ogliaro, F.; Bearpark, M.; Heyd, J.J.; Brothers, E.; Kudin, K.N.; Staroverov, V.N.; Kobayashi, R.; Normand, J.; Raghavachari, K.; Rendell, A.; Burant, J.C.; Iyengar, S.S.; Tomasi, J.; Cossi, M.; Rega, N.; Millam, M.J.; Klene, M.; Knox, J.E.; Cross, J.B.; Bakken, V.; Adamo, C.; Jaramillo, J.; Comperts, R.; Stratmann, R.E.; Yazyev, O.; Austin, A.J.; Cammi, R.; Pomelli, C.; Ochterski, J.W.; Martin, R.L.; Morokuma, K.; Zakrzewski, V.G.; Voth, G.A.; Salvador, P.; Dannenberg, J.J.; Dapprich, S.; Daniels, A.D.; Farkas, Ö.; Foresman, J.B.; Ortiz, J.V.; Cioslowski, J.; Fox, D.J. **2013**, Gaussian, Inc., Wallingford, CT, USA.
- [50] Yhao, Y.; Truhlar, D.G. *Theor. Chem. Acc.* **2008**, *120*, 215-241.
- [51] NBO, version 6.0, Glendenning, E.D.; Badenhoop, J.K.; Reed, A.E.; Carpenter, J.E.; Bohmann, J.A.; Morales, C.M.; Landis, C.R.; Weinhold, F. **2013**, Theoretical Chemistry Institute, University of Wisconsin, Madison, WI, USA
- [52] Avogadro: an open-source molecular builder and visualization tool. Version 1.0.3. <http://avogadro.cc/>
- [53] Bauernschmitt, R.; Ahlrichs, R. *Chem. Phys. Lett.* **1996**, *256*, 454-464.

Chapter 5

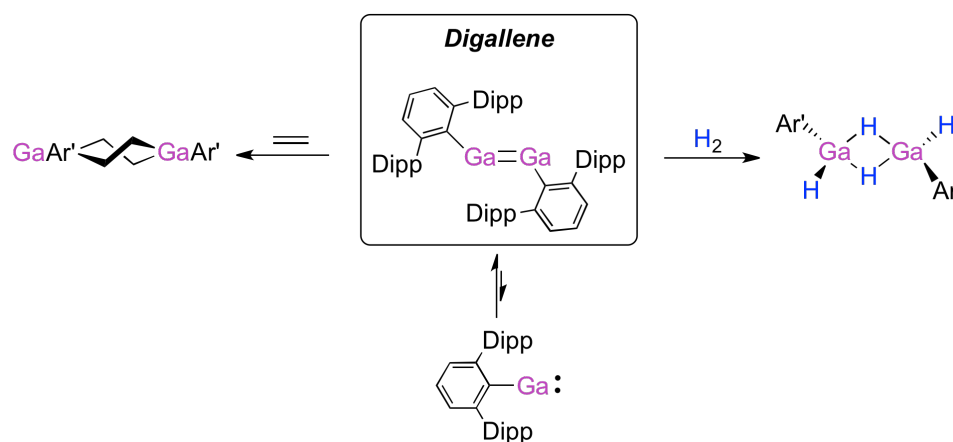
5 Synthesis of Donor-Stabilized Organogallium Complexes and a Compound with a Gallium-Carbon Double Bond

5.1 Introduction

Low valent chemistry of the Group 13 elements, where the elements have an assigned oxidation number lower than +3, has often been driven by the desire to isolate synthetically challenging and theoretically interesting compounds from a structure and bonding perspective. Recently, a shift in focus toward the reactivity of new low valent Group 13 complexes has occurred due to the recent realization that low valent main group compounds can undergo transformations previously thought to only be possible for transition metals, such as small molecule activation and catalysis.¹ Of the Group 13 elements, the chemistry of gallium is uniquely able to balance the ability to synthesize new compounds with the needed reactivity to activate small molecules or be used as catalysts.

Gallium compounds that activate small molecules are generally low valent.² Gallium(II) complexes are normally unreactive toward industrially important molecules such as alkenes and alkynes, but unlike gallium(I) species, they do not require strongly donating or sterically encumbered ligands for their stabilization. As a result, recent work studying low valent gallium complexes has focussed on gallium(I) compounds. In most instances, gallium(I) compounds require strongly donating³ or large, bulky ligands to facilitate isolation. An important class of gallium(I) complexes exhibit homoatomic gallium-gallium multiple bonds.^{4,5} Digallenes,⁶ with a double bond between two gallium centres ($\text{RGa}=\text{GaR}$) and digallynes,^{6a,7} with a triple bond ($[\text{RGa}\equiv\text{GaR}]$), can be synthesized through the use of sterically encumbered *m*-terphenyl ligands. Despite the bulky ligands, digallenes react with small molecules such as H_2 and NH_3 ,⁸ undergo cycloaddition chemistry (Scheme 5.1),⁹ and react with Lewis acids.¹⁰ In addition to the

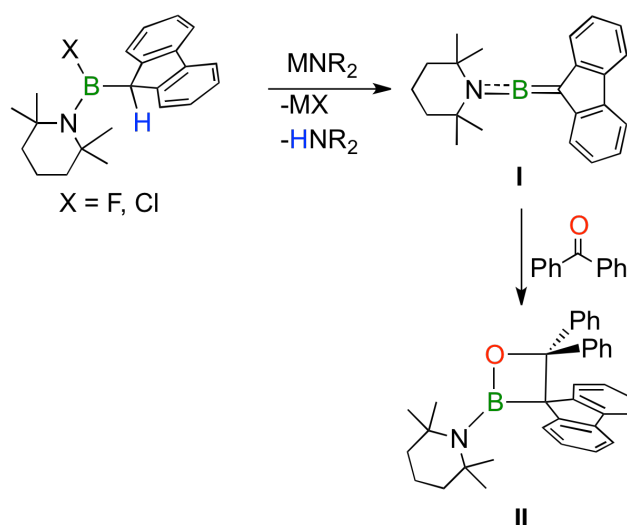
gallium(I) multiply bonded species, other main group elements have been isolated with homoatomic double and triple bonds using bulky aryl ligands.¹¹ Dimetallynes from Group 14 and 15, which possess a homoatomic triple bond, have shown similar reactivity to the gallium derivatives, namely the activation of H_2 ¹² and extensive cycloaddition chemistry.¹³ For the Group 14 and Group 15 elements, multiple bonds to carbon have also been well studied and found to have rich chemistry.



Scheme 5.1: Structure of a digallene, its reactivity with H_2 and ethylene, and its dimer-monomer equilibrium.^{6,8,9}

Compounds of main group elements with double bonds to carbon have been known for over 30 years: silenes,¹⁴ germenes¹⁵ and stannenes^{15b,16} from Group 14¹⁷ and phosphalkenes¹⁸ and arsaalkenes¹⁹ from Group 15. Doubly-bonded main group element-carbon systems, unlike their carbon-carbon analogues, have poor p orbital overlap between the main group centre and the carbon atom due to the increased size of the valence orbital on the main group element, which results in a weak π bond.¹⁷ Furthermore, the heavy element-carbon double bonds are naturally polarized. As a consequence, unsaturated complexes exhibit a diverse range of reactivity under mild conditions and have been used in numerous applications including the synthesis of inorganic polymers²⁰ and the activation of small molecules.²¹

While there are numerous reports of Group 14/15 element-carbon doubly bonded compounds, very few compounds containing a Group 13 element-carbon double bond have been synthesized. Indeed, only boron is represented.²² Borenes, compounds with a boron-carbon double bond (**I**, Scheme 5.2), show similar reactivity to their Group 14 analogues, as they undergo cycloaddition chemistry with carbonyl compounds, giving four-membered ring products (**II**, Scheme 5.2). As there are no examples of element-carbon double bonds with Group 13 elements other than boron, we aimed to synthesize a compound with a gallium-carbon double bond, a gallene, and explore its reactivity.

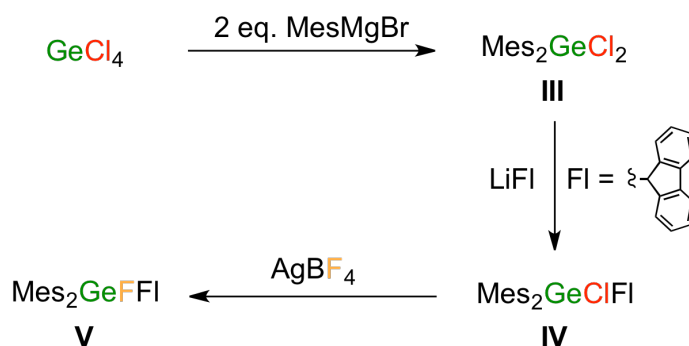


Scheme 5.2: Synthesis and reactivity of a boron-carbon doubly bonded compound, a borene (**I**).^{22c}

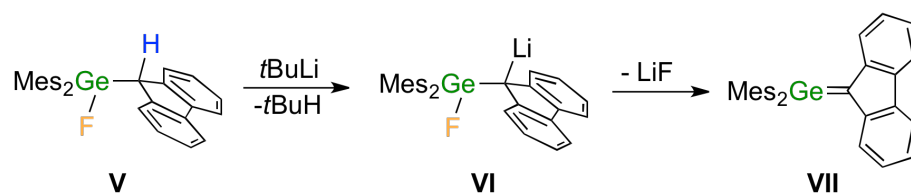
Borene **I** (Scheme 5.2) is unique, in that the nitrogen-centred lone pair of the 2,2,6,6-tetramethylpiperidinylligand aids in the stabilization of the compound as electron density is donated into the empty p type orbital on boron. An alternative strategy for the synthesis of stable compounds containing a Group 13 element-carbon double bond involves the use of separate neutral donor ligands. *N*-heterocyclic carbenes (NHCs) have been used to stabilize monomeric gallium(III) alkyl and halide complexes. The NHC-substituted gallium(III) halides can easily be converted to hydrides and other functional gallium compounds.²³ To a lesser extent, nitrogen and phosphorus donors, such as 4-

dimethylaminopyridine (DMAP), triethylamine, or triphenylphosphine, have been used to complex various Group 13 halides and hydrides; however, the reactivity of the complexes has not been extensively explored.²⁴

As gallium and germanium are in the same row of the periodic table, the syntheses of germene precursors were examined for the development of a strategy to generate a gallene. The first germene, $\text{Mes}_2\text{Ge}=\text{Fl}$ (Fl = fluorenyl), was synthesized by the dehydrohalogenation of Mes_2GeFFl .^{15c} Our group has reported an improved synthesis of $\text{Mes}_2\text{Ge}=\text{Fl}$ (Scheme 5.3).²⁵ Two equivalents of MesMgBr are added to GeCl_4 , giving $\text{Mes}_2\text{GeCl}_2$ (**III**) as the major product. $\text{Mes}_2\text{GeCl}_2$ is then reacted with fluorenyllithium, yielding $\text{Mes}_2\text{GeClFl}$ (**IV**), which is fluorinated using AgBF_4 , giving Mes_2GeFFl (**V**).²⁶ Dehydrohalogenation at low temperature using $t\text{BuLi}$ gives the lithiated intermediate **VI** (Scheme 5.4), which eliminates LiF upon warming to yield the germene, $\text{Mes}_2\text{Ge}=\text{Fl}$ (**VII**, Scheme 5.4).^{15c} $\text{Mes}_2\text{Ge}=\text{Fl}$ is stable under inert conditions and its solid state structure has been determined using X-ray diffraction, confirming the presence of a germanium-carbon double bond.^{15d} The fluoride derivative **V** must be used, as a non-polarizable leaving group is required to avoid lithium-halogen exchange upon reaction with $t\text{BuLi}$. Additionally, the use of a bulky base is critical; the steric bulk favours deprotonation of the fluorenyl group over nucleophilic substitution of the fluoride.



Scheme 5.3: Modified synthesis of the germene precursor Mes_2GeFFl (**V**).²⁶



Scheme 5.4: Dehydrohalogenation of Mes₂GeFFl (**V**) to give Mes₂Ge=Fl, a germene (**VII**).^{15c}

As shown in Figure 5.1, three different strategies for the synthesis of a gallene were envisioned. Route **A** employs a four-coordinate anionic gallene precursor with two mesityl ligands, a fluorenyl group and a fluoride ligand on gallium, the direct analogue of germene precursor **V** (Scheme 5.3). The resultant gallene from strategy **A** would therefore be anionic. For route **B**, a neutral, three-coordinate gallium(III) target with a fluoride ligand could undergo dehydrohalogenation, resulting in the formation of a neutral gallene. However, the gallene generated using strategy **B** would be expected to be quite reactive, as the gallium centre would be coordinatively unsaturated and electron deficient. Route **C** employs a donor ligand to stabilize both the gallene precursor and the gallene. The neutral donor is expected to stabilize the gallium centre by satisfying the valence at gallium in both the precursor and the gallene (Figure 5.1).

Herein, we describe the synthesis of a series of donor-stabilized organogallium complexes using an *N*-heterocyclic carbene (NHC) and 4-dimethylaminopyridine (DMAP), with the goal of generating a gallene. The gallene will be synthesized using a dehydrohalogenation strategy, similar to the previously successful methods for the synthesis of a borene and germene (**I** in Scheme 5.2 and **VII** in Scheme 5.4, respectively).

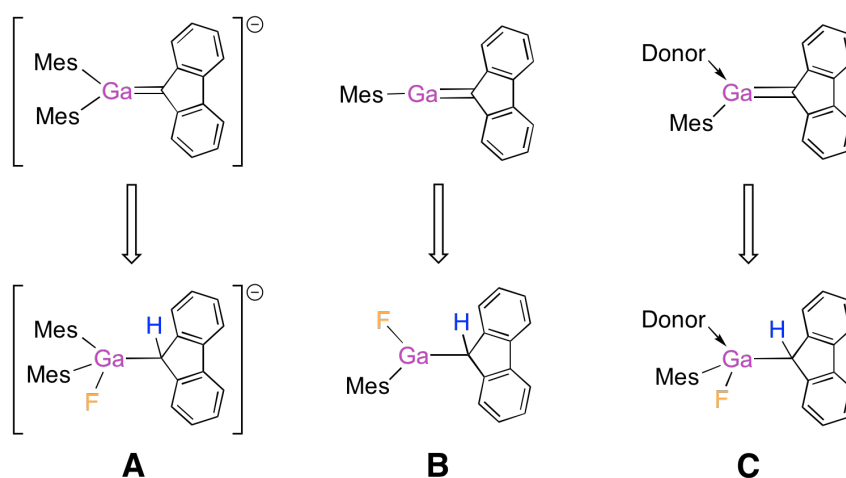
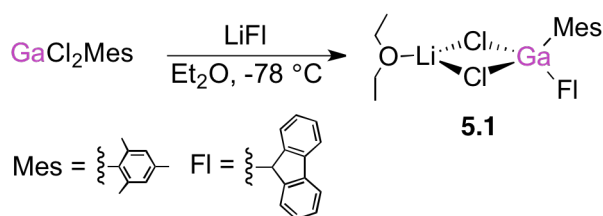


Figure 5.1: Three strategies for the synthesis of gallenes and gallene precursors.

5.2 Results and Discussion

5.2.1 Synthesis of Gallene Precursors

The attempted syntheses of gallene precursors for strategy **B** and **C** (Figure 5.1) began with GaCl₂Me, dichloromesitylgallane,²⁷ which was readily synthesized in high yield using a redistribution reaction between GaMe₃^{27a} and GaCl₃. GaCl₂Me was reacted with LiF, generated from the reaction of fluorene and *t*BuLi or BuLi, to give an off-white solid (Scheme 5.5). The solid was determined to be [Li(Et₂O)][GaCl₂FIMes], **5.1**, as elucidated by multinuclear NMR spectroscopy, ESI-MS and X-ray crystallography (Figure 5.2, Table 5.1). In the solution state, **5.1** possesses 2-fold symmetry, and the organic fragments are detected as single sets of signals in the ¹H and ¹³C{¹H} NMR spectra. The anion, [GaCl₂FIMes], was directly detected using ESI-MS. **5.1** was determined to have an equivalent of Et₂O in its formula by integration of the ¹H NMR spectrum, however, the crystal structure of **5.1** contained one additional equivalent of Et₂O coordinated to the lithium cation, giving **5.1**•Et₂O. The geometry around the gallium centre in the solid state is tetrahedral, although the bond angles range from 92.12(5)° for C11-Ga1-Cl2 to 124.51(17)° for C1-Ga1-C14. As would be expected, the bond angle between the two chloride ligands is small due to the steric bulk of the organic fragments.



Scheme 5.5: Synthesis of **5.1** from GaCl₂Mes.

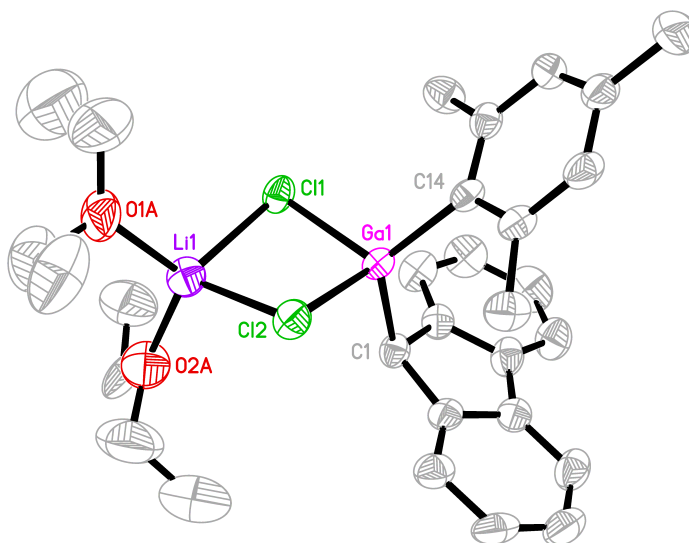


Figure 5.2: Displacement ellipsoid plot of **5.1**·Et₂O. Ellipsoids are drawn at the 50% probability level. Hydrogen atoms and disorder about the ether molecules are omitted for clarity. Selected parameters (bond lengths in Å; bond angles in °): Ga1-C1 2.003(4), Ga1-C14 1.986(4), Ga1-Cl1 2.3080(13), Ga1-Cl2 2.3052(13), Li1-Cl1 2.369(9), Li1-Cl2 2.402(8); C1-Ga1-C14 124.51(17), C1-Ga1-Cl1 103.32(13), C1-Ga1-Cl2 104.17(14), C14-Ga1-Cl1 114.59(12), C14-Ga1-Cl2 112.20(14), Cl1-Ga1-Cl2 92.12(5).

Following the successful synthesis of **5.1**, the generation [Li][Mes₂GaClFl] was attempted by reacting LiFl with GaClMes₂ with the goal of generating the gallium analogue of Mes₂GeClFl (**IV**, Scheme 5.3) for strategy **A** (Figure 5.1). The reaction mixture of LiFl and GaClMes₂ did not result in the formation of GaFlMes₂ suggesting that GaClMes₂ contains too much steric bulk about the gallium centre to allow for

addition or substitution of a fluorenyl group. $\text{GaFMes}_2^{27\text{d,e}}$ was also employed as a starting material, again without success.

Abstraction of one of the chloride ligands to generate the neutral GaClFIMes was then attempted. When GaCl_3 was added to **5.1** in toluene, a new product was formed as shown by ^1H NMR spectroscopy; however, the expected $[\text{GaCl}_4]^-$ anion was not detected in the ^{71}Ga NMR spectrum of the product. Several attempts at obtaining X-ray quality crystals from non-polar solvents were unsuccessful, however, when THF was added to the mixture, an oil was obtained and, after allowing the oil to stand at room temperature, X-ray quality crystals formed. The product was identified as $\text{THF} \rightarrow \text{GaCl}_2\text{Fl}$, **5.2** (Figure 5.3, Table 5.2). The generation of **5.2** as a product of the reaction of **5.1** and GaCl_3 was surprising. Evidently, the Ga-Cl bonds in **5.1** are less reactive toward GaCl_3 than the Ga- C_{Mes} bond, resulting in electrophilic cleavage of the mesityl group rather than chloride abstraction.

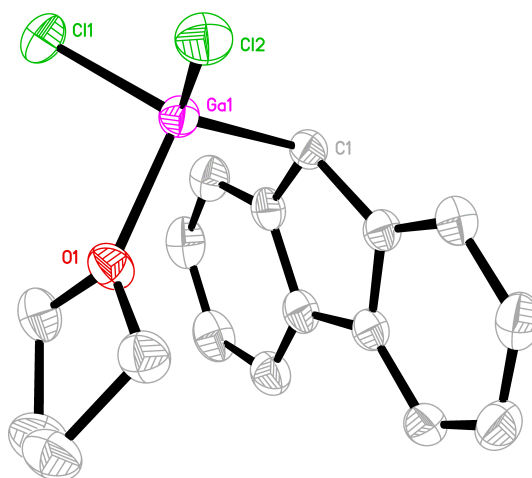


Figure 5.3: Displacement ellipsoid plot of **5.2**. Ellipsoids are drawn at the 50% probability level. Hydrogen atoms are omitted for clarity. Selected parameters (bond lengths in Å; bond angles in °): Ga1-C1 1.979(3), Ga1-O1 1.9584(18), Ga1-Cl1 2.1809(8), Ga1-Cl2 2.1657(8); Cl1-Ga1-Cl2 110.93(3), C1-Ga1-O1 105.10(9), Ga1-C1-C2 107.43(18).

As the synthesis of gallene precursors for strategies **A** and **B** were unsuccessful, efforts were then focussed on the synthesis of the precursor of strategy **C** (Figure 5.1). An *N*-heterocyclic carbene and DMAP were chosen as donor ligands, as they have different steric and electronic characteristics (pKa values for their conjugate acids: DMAP = 9.7; NHCs \approx 20;²⁸ percent buried volume of NHC = 33.9 to 38.4 %).²⁹ 1,3-diisopropyl-4,5-dimethylimidazol-2-ylidene (^{Me}IiPr),³⁰ was added to **5.1** at room temperature, immediately leading to the generation of a precipitate. **5.3** was obtained from the supernatant as a pale orange solid, which was identified as ^{Me}IiPr \rightarrow GaClFI₂Mes by spectroscopic and X-ray diffraction methods (Figure 5.4, Table 5.1). **5.3** crystallized in the P2₁/c space group; as the ^{Me}IiPr was added to the achiral gallate **5.1**, **5.3** was isolated as a racemic mixture, consistent with the centrosymmetric space group of the crystal structure. The ¹H and ¹³C{¹H} NMR spectra of **5.3** exhibited one set of signals for the ^{Me}IiPr and mesityl ligands, however, the benzo moieties of the fluorenyl group, being diastereotopic, each exhibited different signals in the ¹H and ¹³C NMR spectra of **5.3**. Compound **5.3** was found to slowly decompose upon exposure to ambient light in solution; however, attempts to generate significant quantities of the decomposition product to enable characterization were unsuccessful. Performing the synthesis of **5.3** in the absence of light and using volatile organic solvents, such as dichloromethane or diethyl ether in place of toluene, reduced the amount of decomposition observed (see Appendix D for additional details).

The reaction of DMAP with **5.1** resulted in the clean formation of a white solid, DMAP \rightarrow GaClFI₂Mes, **5.4** (Figure 5.5, Table 5.2), identified using multinuclear NMR spectroscopy, ESI-MS and X-ray crystallography. As with the NHC analogue, **5.4** crystallized in a centrosymmetric space group, consistent with the formation of a racemate.

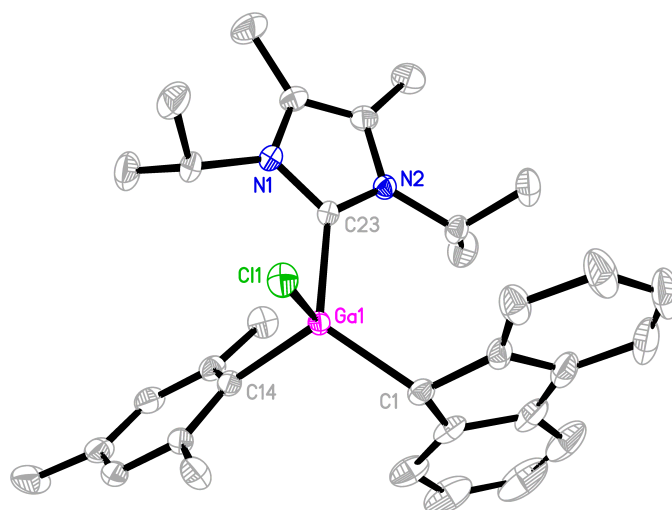


Figure 5.4: Displacement ellipsoid plot of **5.3**. Ellipsoids are drawn at the 50% probability level. Hydrogen atoms are omitted for clarity. Selected parameters (bond lengths in Å; bond angles in °): Ga1-C1 2.0254(12), Ga1-C14 2.0031(12), Ga1-C23 2.0551(13), Ga1-Cl1 2.2888(6); C14-Ga1-C1 113.63(5), C14-Ga1-C23 109.85(5), C1-Ga1-C23 120.12(4), C1-Ga1-Cl1 102.29(4), C23-Ga1-Cl1 98.99(3).

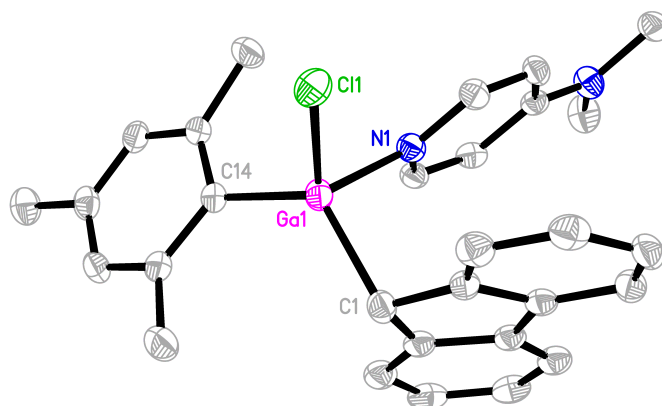
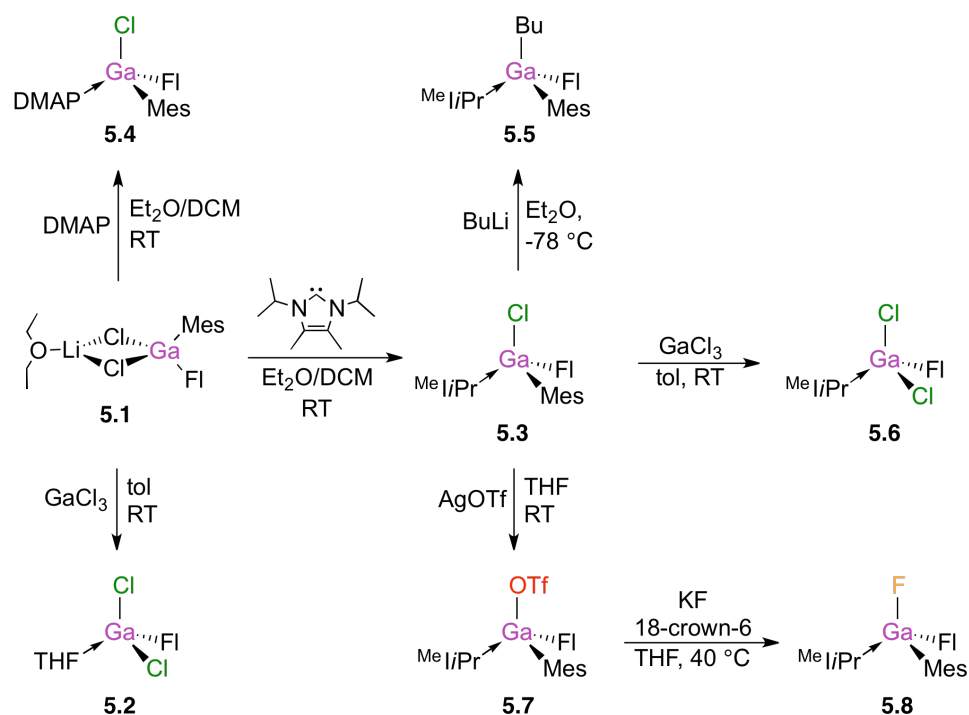


Figure 5.5: Displacement ellipsoid plot of **5.4**. Ellipsoids are drawn at the 50% probability level. Hydrogen atoms are omitted for clarity. Selected parameters (bond lengths in Å; bond angles in °): Ga1-C1 2.034(2), Ga1-C14 1.991(3), Ga1-N1 2.011(2), Ga1-Cl1 2.2325(7); C1-Ga1-C14 123.30(10), C1-Ga1-N1 99.09(9), C1-Ga1-Cl1 110.57(7), N1-Ga1-Cl1 100.74(6), C14-Ga1-Cl1 112.18(8).



Scheme 5.6: Synthesis of donor-stabilized organogallium compounds **5.1** to **5.8**.

An attempt was made to synthesize a gallene directly from the ^{Me}I₂Pr/chloride derivative **5.3** using organolithium reagents. The reaction of **5.3** with *t*BuLi gave a product that was deep red-orange in colour. All attempts at isolation and crystallization of the product were unsuccessful and the compound could not be identified on the basis of the ¹H and ¹³C NMR spectroscopic data or ESI-MS data. When BuLi was added to a solution of **5.3**, the pale yellow solution turned orange. Following workup, a pale orange solid was obtained and characterized using multinuclear NMR spectroscopy, ESI-MS, and X-ray crystallography (Figure 5.6, Table 5.1) The product was identified as ^{Me}I₂Pr→GaBuFIMes, **5.5**. Evidently, the less bulky alkyl lithium reagent acted preferentially as a nucleophile, rather than as a base.

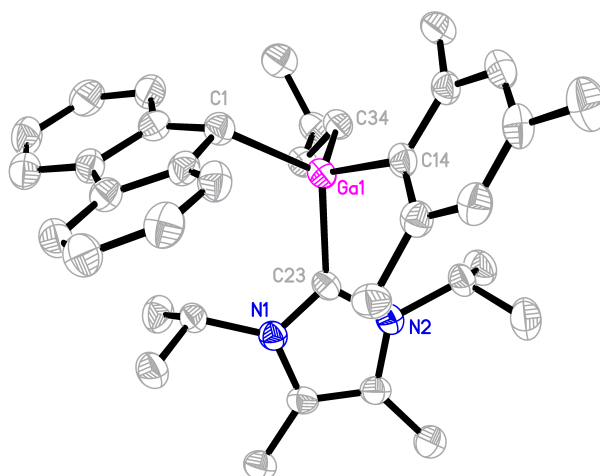


Figure 5.6: Displacement ellipsoid plot of **5.5**. Ellipsoids are drawn at the 50% probability level. Hydrogen atoms are omitted for clarity. Selected parameters (bond lengths in Å; bond angles in °): Ga1-C1 2.099(3), Ga1-C14 2.025(3), Ga1-C23 2.089(3), Ga1-C34 2.013(3); C23-Ga1-C1 119.87(11), C14-Ga1-C1 102.84(11), C34-Ga1-C1 108.47(12), C34-Ga1-C14 119.76(11), C34-Ga1-C23 100.79(11).

Abstraction of the chloride ligand from **5.3** was attempted using a strong Lewis acid to synthesize the $[\text{Me}^c\text{I}^i\text{Pr} \rightarrow \text{GaFlMes}]^+$ cation. With an electron deficient gallium centre, the hydrogen of the fluorenyl group was expected to be more acidic, and thus, its removal using a base was expected to be more facile. When **5.3** was reacted with GaCl_3 , a solid, **5.6**, was isolated. $[\text{GaCl}_4]^-$ was not detected in the ^{71}Ga NMR spectrum of **5.6**. X-ray quality crystals were obtained from a toluene solution of the product cooled to -20°C . **5.6** was identified as $\text{Me}^c\text{I}^i\text{Pr} \rightarrow \text{GaCl}_2\text{Fl}$ (Figure 5.7, Table 5.2). Although signals corresponding to an equivalent mesityl group were observed in the ^1H NMR spectrum of the crude reaction mixture, the mesityl ligand was not present in **5.6** and a mesityl-containing product was not isolated. As with **5.1**, the gallium-carbon bond of the mesityl group in **5.3** appears to be more labile than the gallium-chloride bond upon reaction with GaCl_3 . Other chloride abstraction reactions between **5.3** and numerous Lewis acids were attempted; however, the formation of the desired $[\text{Me}^c\text{I}^i\text{Pr} \rightarrow \text{GaFlMes}]^+$ cation was not successful.

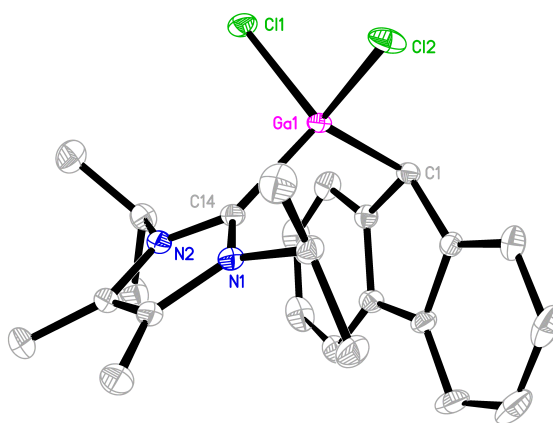


Figure 5.7: Displacement ellipsoid plot of **5.6**. Ellipsoids are drawn at the 50% probability level. Hydrogen atoms and the toluene solvent molecule are omitted for clarity. Selected parameters (bond lengths in Å; bond angles in °): Ga1-C1 2.0072(9), Ga1-C14 2.0422(8), Ga1-Cl1 2.2221(4), Ga1-Cl2 2.2234(5); Cl1-Ga1-Cl2 102.083(12), C1-Ga1-C14 113.75(3), Ga1-C1-C2 109.55(5).

The transformation of **5.3** to its fluoride derivative was then attempted (precursor for strategy C, Figure 5.1). Multiple fluorination reagents were explored: AgF, AgBF₄, KF (with and without 18-crown-6 as a co-reagent), CsF, and NMe₄F, all of which did not result in conversion of **5.3** to the fluoride analogue. Given the lack of success, the conversion of **5.3** to the triflate derivative was performed using AgOTf, resulting in the formation of ^{Me}IiPr→GaOTfFIMes, **5.7**, which was characterized using multinuclear NMR spectroscopy, ESI-MS and X-ray crystallography (Figure 5.8, Table 5.1).

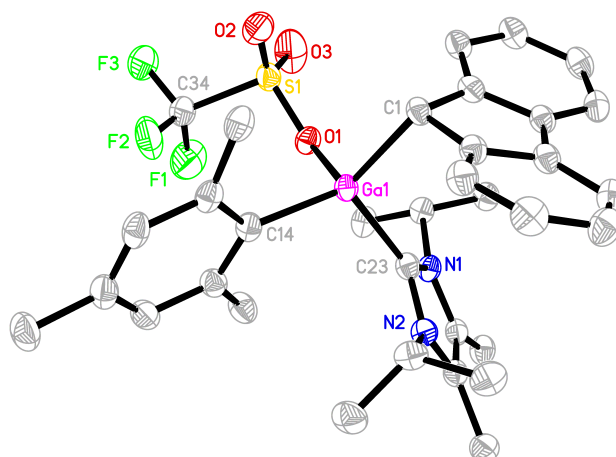


Figure 5.8: Displacement ellipsoid plot of **5.7**. Ellipsoids are drawn at the 50% probability level. Hydrogen atoms are omitted for clarity. Selected parameters (bond lengths in Å; bond angles in °): Ga1-C1 2.028(2), Ga1-C14 1.994(2), Ga1-C23 2.056(2), Ga1-O1 2.0004(17); O1-Ga1-C14 98.58(8), C1-Ga1-C14 128.48(10), O1-Ga1-C1 104.62(9), O1-Ga1-C23 100.05(8), C14-Ga1-C23 112.80(10), C1-Ga1-C23 107.54(10).

Similar to **5.3** and **5.5**, **5.7** crystallized in a centrosymmetric space group, consistent with a racemic mixture. The multinuclear NMR spectroscopic data of **5.7** exhibit many similar features to those of **5.3**, as two sets of signals attributable to the fluorenyl group and one set of signals for each of the mesityl and NHC ligands were observed in the ^1H and $^{13}\text{C}\{^1\text{H}\}$ NMR spectra of **5.7**. As with **5.3**, dehydrohalogenation of **5.7** using several bulky bases was carried out in an attempt to deprotonate the alpha carbon of the fluorenyl ligand. *t*BuLi, Li[N(SiMe₃)₂] and Li[NiPr₂] were utilized, but dehydrohalogenation was not observed by ^1H NMR spectroscopy. The inability to generate the gallene from the triflate derivative **5.7** may be due to the relative solubility of the LiOTf by-product in polar organic solvents in comparison to LiF, which is the by-product from fluoride-substituted derivatives (alkali metal triflates are recrystallized from polar organic solvents, i.e. acetone, versus 0.09 mM in THF at 24 °C for LiF).³¹ The low solubility of LiF is believed to be the driving force in the formation of germene **VII** (Scheme 5.4). Although the fluoride derivative of **5.3** could not be synthesized directly from the chloride, when a mixture of **5.7**, KF and 18-crown-6 suspended in THF was

heated to 40 °C, complete conversion to a new product was demonstrated by multinuclear NMR spectroscopy. An off-white solid was isolated and identified as $^{\text{Me}}\text{I}^{\text{Pr}}\rightarrow\text{GaFFIMes}$, **5.8**, using NMR spectroscopy, ESI-MS and X-ray crystallography (Figure 5.9, Table 5.3). Although many of the NMR spectral features of **5.8** were similar to those of the other $^{\text{Me}}\text{I}^{\text{Pr}}\rightarrow\text{GaXFIMes}$ complexes (**5.3**, **5.5** and **5.7**), two sets of signals attributed to the methine moiety of the $^{\text{Me}}\text{I}^{\text{Pr}}$ ligand were observed in both the ^1H and $^{13}\text{C}\{^1\text{H}\}$ NMR spectra of **5.8**. Both $^{13}\text{C}\{^{19}\text{F}\}$ and $^1\text{H}\{^{19}\text{F}\}$ NMR spectroscopic experiments were performed, which confirmed that both the methine carbon and hydrogen of the $^{\text{Me}}\text{I}^{\text{Pr}}$ are coupled to the fluoride. Thus, the signal for the methine hydrogen in the ^1H NMR spectrum of **5.8** is a doublet of septets due to $^5J_{\text{H-F}}$ and $^3J_{\text{H-H}}$ coupling, with coupling constants of 2 Hz and 7 Hz, respectively.

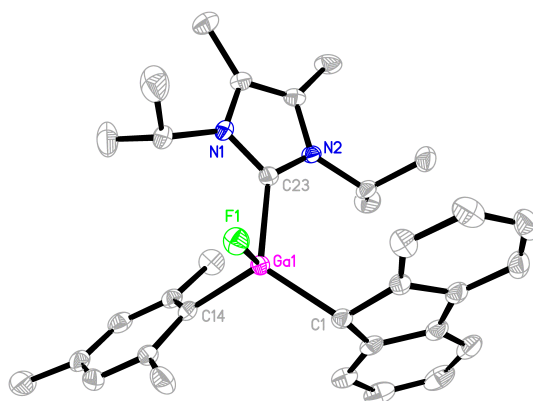


Figure 5.9: Displacement ellipsoid plot of **5.8**. Ellipsoids are drawn at the 50% probability level. Hydrogen atoms are omitted for clarity. Selected parameters (bond lengths in Å; bond angles in °): Ga1-C1 2.012(2), Ga1-C14 1.997(2), Ga1-C23 2.051(2), Ga1-F1 1.8443(14); C1-Ga1-C23 118.91(8), C14-Ga1-C23 110.57(9), C14-Ga1-C1 116.21(9), F1-Ga1-C1 101.35(8), F1-Ga1-C14 108.65(8), F1-Ga1-C23 98.51(7).

Similar to the NHC-stabilized derivatives, the exchange of the chloride ligand on the gallium centre of the DMAP stabilized **5.4** with a non-polarizable leaving group was performed to generate a gallene precursor analogous to the NHC derivative **5.8**. Reactions of **5.4** with AgF to fluorinate the gallium centre did not proceed cleanly, with

at least three products observed in the ^{19}F NMR spectrum. Reactions using KF and 18-crown-6 also did not result in the formation of the fluoride derivative of **5.4**. Similar to the NHC derivative, the conversion of the chloride to the triflate by reaction of **5.4** with AgOTf resulted in the formation of DMAP \rightarrow GaOTfFlMes, **5.9**, as elucidated using multinuclear NMR spectroscopy, ESI-MS and by X-ray crystallography (Figure 5.10, Table 5.2). Unlike the other derivatives of these compounds, **5.9** crystallized in the acentric space group Pn, however, both enantiomers were found in the asymmetric unit. Attempts to solve the structure in a centrosymmetric space group did not result in a suitable solution for refinement.

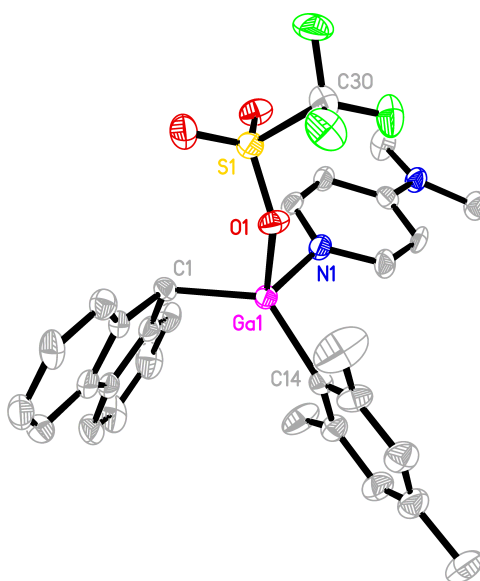


Figure 5.10: Displacement ellipsoid plot of **5.9**. Ellipsoids are drawn at the 50% probability level. Hydrogen atoms, the second formula unit and the dichloromethane solvent molecule are omitted for clarity. Selected parameters (bond lengths in Å; bond angles in °): Ga1-C1 2.005(5), Ga1-C14 1.978(6), Ga1-N1 1.993(5), Ga1-O1 2.004(4); C1-Ga1-C14 128.8(2), C1-Ga1-O1 100.8(2), C1-Ga1-N1 108.9(2), N1-Ga1-O1 97.3(2), N1-Ga1-C14 106.9(2); Ga2-C31 1.960(6), Ga2-C44 1.982(5), Ga2-N3 1.991(5), Ga2-O4 1.982(5); C31-Ga2-C44 130.9(2), C31-Ga2-O4 99.1(2), C31-Ga2-N3 108.8(4), N3-Ga2-O4 95.10(19), N3-Ga2-C44 107.7(2).

The conversion of **5.9** to its fluoride derivative was then performed. Reaction of **5.9** with KF and 18-crown-6 successfully yielded DMAP→GaFFIMes, **5.10**, which was characterized using multinuclear NMR spectroscopy, ESI-MS and X-ray crystallography (Figure 5.11, Table 5.2). Compound **5.10** crystallized in a centrosymmetric space group similar to all DMAP and ^{Me}IiPr complexes other than **5.9**. The synthesis of **5.10** (Scheme 5.7) provides another precursor for the synthesis of a gallium-carbon double bond (strategy C, Figure 5.1) and offers the opportunity to compare the reactivities of donor-stabilized organogallium fluorides **5.8** and **5.10**.

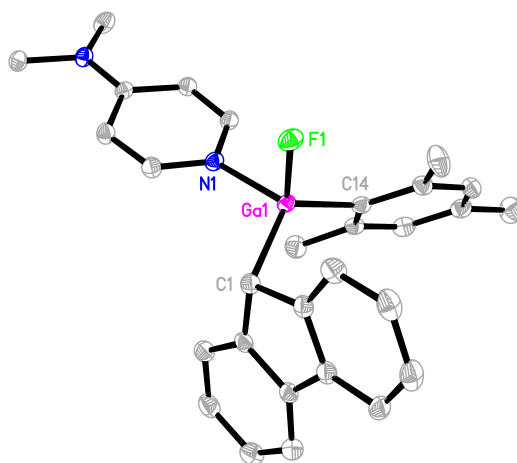
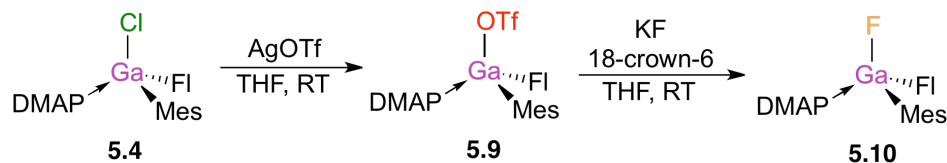


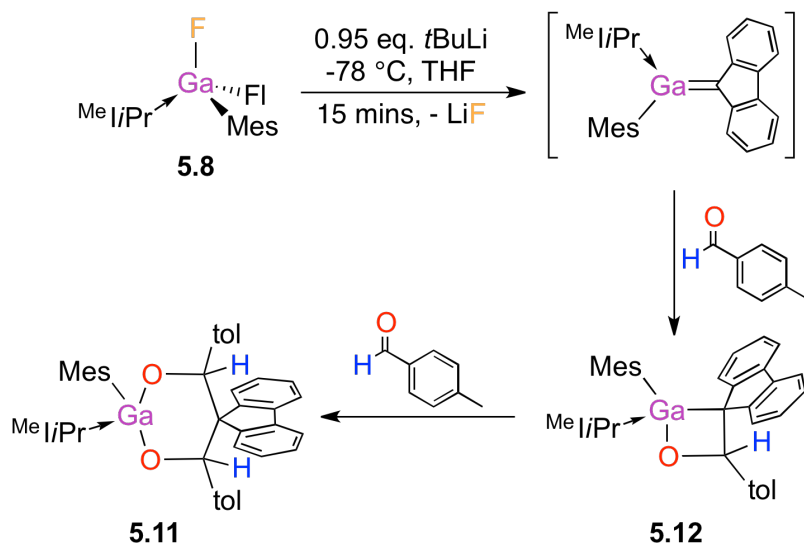
Figure 5.11: Displacement ellipsoid plot of **5.10**. Ellipsoids are drawn at the 50% probability level. Hydrogen atoms and the dichloromethane solvent molecule are omitted for clarity. Selected parameters (bond lengths in Å; bond angles in °): Ga1-C1 2.0139(19), Ga1-C14 1.9735(19), Ga1-F1 1.8226(12), Ga1-N1 2.0128(15); C1-Ga1-C14 124.19(7), C1-Ga1-F1 101.82(7), C1-Ga1-N1 108.50(7), N1-Ga1-F1 94.86(6), N1-Ga1-C14 109.37(7), C14-Ga1-F1 114.03(7).



Scheme 5.7: Synthesis of DMAP-stabilized organogallium compounds **5.4**, **5.9** and **5.10**.

5.2.2 Generation and Trapping of a Gallene

Reactions between *t*BuLi and the gallene precursors **5.8** and **5.10** were examined. **5.8** was cooled in a Dry Ice-acetone bath, and allowed to react with *t*BuLi in THF. Although the reaction mixture turned bright orange following the addition of the base, attempts to isolate the product were not successful. To provide evidence for the formation of an intermediate gallene, a trapping reagent was added to the solution in subsequent reactions (Scheme 5.8). Aldehydes were chosen as the trapping reagents due to their diagnostic ¹H NMR spectroscopic chemical shifts; aldehydic hydrogens have a resonance frequency around 10 ppm, whereas four-membered metallaoxetane products resonate between 4.3 ppm to 6.3 ppm for silene derivatives.³² For germenes, a similar downfield chemical shift has been observed for metallaoxetanes, where the reaction of germene **VII** (Scheme 5.4) with benzaldehyde gave a similar chemical shift to the silene-derived metallaoxetanes.³³



Scheme 5.8: Dehydrohalogenation of **5.8** to give gallene and subsequent trapping reactions products.

5.8 was allowed to react with *t*BuLi cooled in a Dry Ice-acetone bath, followed by the addition of tolualdehyde (Scheme 5.8). The initial deep orange colour that was generated after the addition of *t*BuLi dissipated slightly, giving a pale orange solution with a precipitate. Following warming to room temperature, some of the precipitate dissolved and the colour of the solution faded. After work up, the resultant residue was analyzed by ¹H NMR spectroscopy. The first feature that was evident from the ¹H NMR spectrum of the residue was the absence of a signal in the region expected for the fluorenyl hydrogen of the carbon bound to the gallium centre in **5.8**. Furthermore, three singlets at 6.38, 6.33 and 6.29 ppm were observed, in addition to a septet at 5.93 ppm, which was assigned to the methine hydrogen of the ^{Me}LiPr ligand. Unlike its Group 14 analogues, the product was unstable to chromatographic separation, leading to difficulty in the purification of the reaction products. However, crystallization yielded a compound which was isolated and analyzed using multinuclear and 2D NMR spectroscopy, and ESI-MS. The presence of two singlets at 6.35 and 6.65 ppm, the relative integrations of these signals to the septet assigned to the NHC moiety, and the observation of signals at *m/z* 779 and 795 in the ESI-MS, which correspond to a 2:1 adduct between a gallene and tolualdehyde with lithium and sodium cations, respectively, led to the assignment of the structure of **5.11** (Scheme 5.8). Accordingly, a correlation between the signal assigned to the *sp*³ hybridized carbon of the fluorenyl group and the two singlets at 6.35 and 6.65 ppm was observed in the ¹H-¹³C HMBC spectrum of **5.11**. The similarity in the intensity of the two correlations in the HMBC spectrum provides evidence for the regiochemistry of **5.11** as shown in Scheme 5.8, where both oxygen atoms of the activated tolualdehyde molecules are bound to the gallium centre. The assigned regiochemistry is also supported by the lack of correlation between these hydrogens and the carbenic and *ipso* carbons of the ^{Me}LiPr and mesityl ligands, respectively. Additionally, as the two formerly aldehydic hydrogens are chemically inequivalent, they must *trans* to one another, resulting in two different chemical environments. The structure of **5.11**, the *trans* orientation of the formerly aldehydic hydrogens and the regiochemistry of the product were confirmed by X-ray crystallography (Figure 5.12, Table 5.3).

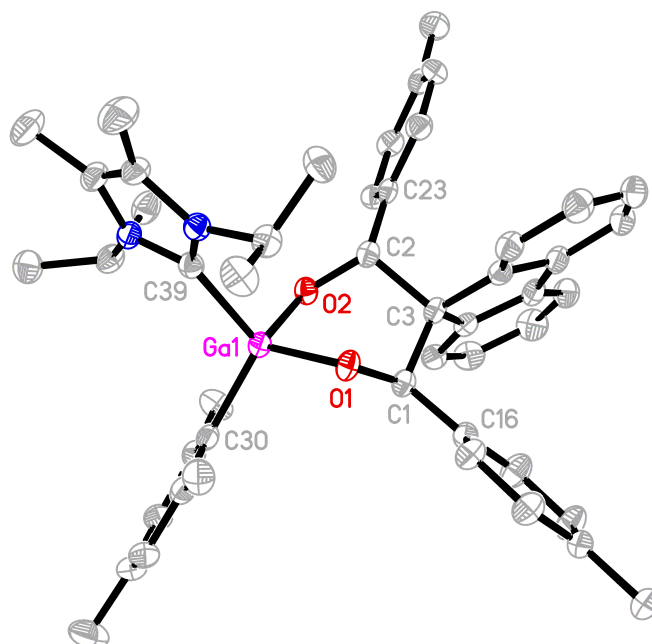
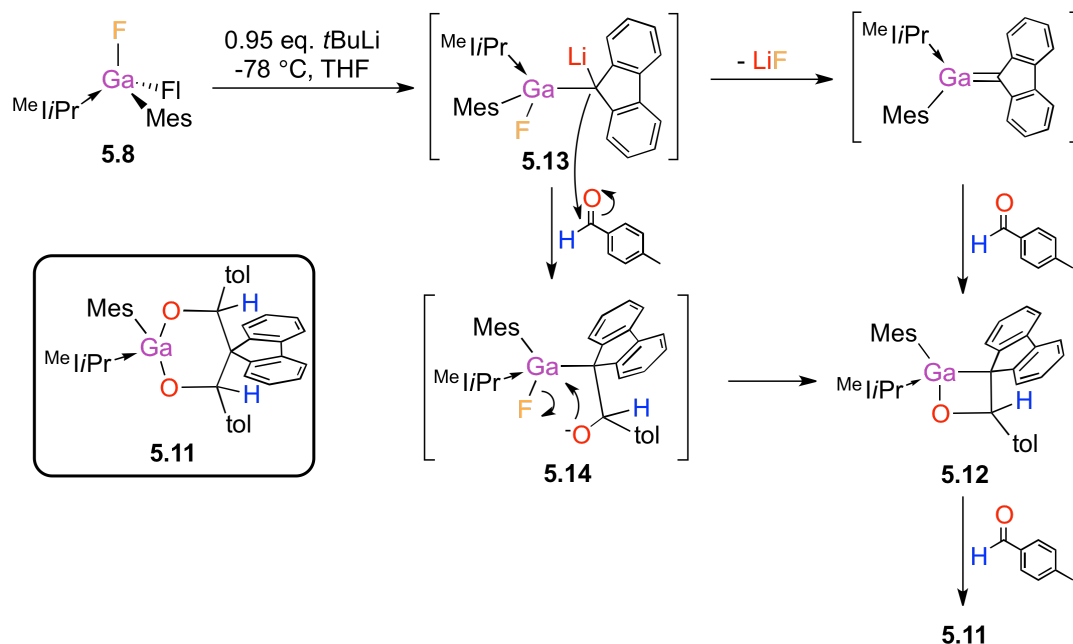


Figure 5.12: Displacement ellipsoid plot of **5.11**. Ellipsoids are drawn at the 50% probability level. Hydrogen atoms are omitted for clarity. Selected parameters (bond lengths in Å; bond angles in °): Ga1-O1 1.8677(15), Ga1-O2 1.8650(15), Ga1-C30 1.980(2), Ga1-C39 2.045(2), O1-C1 1.418(3), O2-C2 1.408 (3), C1-C3 1.569(3), C2-C31.593(3); O1-Ga1-O2 96.83(7), C1-O1-Ga1 106.22(12), C2-O2-Ga1 108.48(12), O1-C1-C3 111.19(17), O2-C2-C3 110.21(17), C1-C3-C2 107.26(17).

The mechanism for the formation of **5.11** is postulated to begin with initial addition of a molecule of tolualdehyde to an intermediate gallene that is generated through dehydrohalogenation. The second equivalent adds to the gallium-carbon bond of the four-membered cyclic intermediate **5.12**, giving **5.11** (Scheme 5.8, Scheme 5.9). Alternatively, as the solution was not warmed prior to the addition of the tolualdehyde, it is possible that the lithiated intermediate **5.13** could act as a nucleophile and attack a molecule of tolualdehyde at the carbonyl carbon. This would generate an open intermediate with a Ga-F bond, **5.14**, where the oxygen of the tolualdehyde attacks the gallium, displacing the fluoride, giving cycloadduct **5.12**, the same product observed for

an intermediate gallene. **5.12** then reacts with an additional equivalent of toluanaldehyde, giving **5.11** (Scheme 5.9).



Scheme 5.9: Two possible mechanisms for the formation of **5.11**.

The generation of a gallene derived from **5.10** was also attempted. When toluanaldehyde was added to the reaction mixture of **5.10** and *t*BuLi *in situ* in an identical procedure to that used to synthesize **5.11**, the ^1H NMR spectrum of the reaction mixture was inconclusive. The scale of the reaction was then increased; however, a product could not be isolated. A signal corresponding to the fluorenyl hydrogen of **5.10** was not observed in the ^1H NMR spectrum of the resultant residue. The inability to use chromatographic methods to separate and isolate the products of the reaction restricts the ability to characterize any products.

The isolation of cycloadduct **5.11** gives evidence in support of the formation of the gallene *in situ*, or that dehydrohalogenation of the donor-stabilized precursors is possible, as demonstrated by the deprotonation that occurred (Scheme 5.9). Additional work toward the isolation of adducts of the gallenes derived from **5.8** and **5.10** using

aldehydes and other trapping agents that allow for the facile separation of the products and isolation of the gallene itself will be the focus of future work.

5.3 Conclusions

We have demonstrated the facile synthesis and characterization of novel monomeric donor-stabilized organogallium complexes using $^{\text{Me}}\text{I}^{\text{Pr}}$ and DMAP as donor ligands. The complexes represent some of the first examples of organogallium(III) compounds stabilized by Lewis bases. Nucleophilic substitution at the gallium centre in **5.3** was performed using BuLi, demonstrating the ability of **5.3** to undergo substitution reactions with organic nucleophiles. Substitution of the chloride ligands of **5.3** and **5.4** for triflate groups, and subsequent fluorination resulted in the isolation of **5.8** and **5.10**, two potential precursors for the synthesis of a compound with a gallium-carbon double bond, a gallene. Both **5.8** and **5.10** were synthesized in relatively few steps from commercially available or easily synthesized starting materials. Dehydrohalogenation reactions of **5.8** and **5.10** were performed, and tolualdehyde was added as a trapping agent *in situ*, resulting in the isolation of **5.11**, a 2:1 adduct of the postulated gallene derived from **5.8** and two molecules of tolualdehyde. Compound **5.11** has a novel structure derived from the addition of a second equivalent of the aldehyde to an intermediate galloxetane, **5.12**. Future work toward the isolation of the parent gallenes to verify the reaction pathway and the synthesis of additional trapped gallene products will be performed.

5.4 Experimental

5.4.1 General Considerations

All manipulations were performed under an inert atmosphere of argon using Schlenk techniques or under an atmosphere of nitrogen in an MBraun glovebox unless otherwise stated. A freezer connected to the glovebox was used; although it was set to -20 °C, the actual temperature drifted between -10 °C and -20 °C. All solvents were purified using an Innovative Technologies 400-5 Solvent Purification System and were stored over activated 3 or 4 Å molecular sieves, unless otherwise stated. C_6D_6 and CDCl_3 were dried over activated 4 Å molecular sieves. All reagents were used as received from

Sigma-Aldrich, Alfa Aesar, Strem Chemicals, Gelest or Oakwood Chemicals. GaMes₃,^{27b} GaCl₂Mes,^{27a} 1,3-diisopropyl-4,5-dimethyl-2(3H)-imidazolethione,³⁴ and 1,3-diisopropyl-4,5-dimethylimidazole-2-ylidene (^{Me}iPr)³⁴ were synthesized according to literature procedures. NMR spectra were recorded on a Varian INOVA I600 (¹H 600 MHz; ¹³C 151 MHz; ¹⁹F 564 MHz; ⁷¹Ga 183 MHz) or a Bruker Avance III HD (¹H 400 MHz) spectrometer. Chemical shifts (δ) are reported in ppm and were internally referenced to the residual undeuterated solvent peaks for ¹H spectra (7.15 ppm for C₆D₅H, 7.25 ppm for CHCl₃ and 3.58 ppm for THF-*d*₈), and the deuterated solvent for ¹³C (128.00 ppm for C₆D₆, 77.00 for CDCl₃ and 67.21 ppm for THF-*d*₈). ¹⁹F NMR spectra were referenced to CFCl₃ (0.0 ppm) using the internal lock signal from the deuterated solvent and to Ga(NO₃)₃ (0.0 ppm) in D₂O for ⁷¹Ga spectra. Coupling constants (*J*) are reported in Hz and multiplicities are reported as singlet (s), doublet (d), triplet (t), quartet (q), septet, multiplet (m), broad (br) and overlapping (ov). All NMR assignments were confirmed using two-dimensional techniques (gCOSY, gHSQC, gHMBC). Electrospray ionization mass spectra (ESI-MS) were collected using a Bruker micrOTOF II spectrometer. Mass spectral data are reported in mass-to-charge units (*m/z*). Elemental analyses were performed by Laboratoire d'Analyse Élémentaire de l'Université de Montréal (Montréal, QC).

5.4.2 Synthesis of Lithium Dichlorofluorenylmesitylgallate, [Li(Et₂O)][GaCl₂FIMes], **5.1**

BuLi, 1.6 M in hexanes (22.5 mmol, 14.1 mL) was added dropwise to a stirring solution of fluorene (3.73 g, 22.5 mmol) dissolved in Et₂O (75 mL). The solution changed colour from colourless to deep red-orange. The solution was allowed to stir at room temperature for 4 hours, at which point it was added dropwise to a stirring solution of GaCl₂Mes (5.84 g, 22.5 mmol) dissolved in Et₂O (25 mL) cooled in a Dry Ice-acetone bath. The suspension changed colour from orange to green to off-white, with a precipitate forming after approximately 1 hour. The mixture was allowed to stir and then allowed to warm to room temperature over 18 hours, at which point the solvent was removed under reduced

pressure, yielding a yellow solid. The solid was washed with hexanes (3 x 15 mL), and the resulting pale yellow solid was dried under reduced pressure, yielding **5.1**. X-ray quality crystals were obtained from a saturated Et₂O solution at -20 °C.

Yield: 9.71 g of a pale yellow solid (85 %); mp: 150 – 160 °C (decomposition); ¹H NMR (600 MHz, THF-d₈, 298 K)³⁵ δ: 8.05 (d, *J* = 6 Hz, 2H, C₁H-FI), 7.73 (dd, *J* = 2 Hz, 7 Hz, 2H, C₄H-FI), 7.08 – 7.05 (m, 4H, C_{2,3}H-FI), 6.35 (s, 2H, CH-*m*-Mes), 4.27 (s, 1H, Ga-C₉H), 3.39 (q, *J* = 7 Hz, 4H, O-CH₂-CH₃), 2.01 (s, 3H, *p*-CH₃-Mes), 1.87 (s, 6H, *o*-CH₃-Mes), 1.12 (t, *J* = 7 Hz, 3H, O-CH₂-CH₃); ¹³C{¹H} NMR (151 MHz, THF-d₈, 298 K) δ: 150.38 (C₁₁-FI), 145.57 (*o*-C-Mes), 144.57 (Ga-C_{ipso}-Mes), 140.67 (C₁₀-FI), 136.02 (*p*-C-Mes), 127.39 (*m*-CH-Mes), 125.46 (C₃H-FI), 125.33 (C₁H-FI), 123.45 (C₂H-FI), 119.47 (C₄H-FI), 66.48 (O-CH₂-CH₃), 50.38 (Ga-C₉H), 25.43 (*o*-CH₃-Mes), 21.23 (*p*-CH₃-Mes), 15.84 (O-CH₂-CH₃); ⁷¹Ga{¹H} NMR (183 MHz, THF-d₈, 298 K) δ: no signal; LR ESI-TOF MS (*m/z*; negative ion): 339 ([⁶⁹Ga³⁵Cl₃(FI)]⁻); 423 ([⁶⁹Ga³⁵Cl₂FIMes]⁻); 853 [(Li[⁶⁹Ga³⁵Cl₂FIMes]₂)⁻]; HR ESI-TOF MS (*m/z*; negative ion): Calcd. for C₂₂H₂₀³⁵Cl₂⁶⁹Ga ([⁶⁹Ga³⁵Cl₂FIMes]⁻): 423.0198, Found: 423.0204; Satisfactory elemental analysis data could not be obtained presumably due to decomposition of **5.1** upon exposure to air or the experimental conditions.

5.4.3 Synthesis of Chloro(1,3-diisopropyl-4,5-dimethylimidazol-2-ylidene)fluorenylmesitylgallane, ^{Me}IiPr → GaClFIMes, **5.3**

A solution of ^{Me}IiPr (1.78 g, 9.88 mmol) dissolved in Et₂O (10 mL) was slowly added to a stirring suspension of **5.1** (5.00 g, 9.88 mmol) in Et₂O (50 mL) under the exclusion of light, giving an orange mother liquor and a white solid. The suspension was allowed to stir at room temperature for 18 hours, at which point the solid was removed by centrifugation. The white solid was washed with a mixture of Et₂O and DCM (1:2; 3 x 12 mL). The pale orange, decanted solutions were combined, and the solvent was removed under reduced pressure in the dark yielding a red-orange solid, **5.3**. A sample of the solid was dissolved in toluene (1 mL), filtered and placed in a vapour diffusion system with

Et₂O as the non-solvent. After cooling to -20 °C for several days, X-ray quality crystals formed.

Yield: 5.49 g of a red-orange powder (97 %); mp: 176 – 179 °C (decomposition); ¹H NMR (600 MHz, C₆D₆, 298 K)³⁵ δ: 8.78 (d, *J* = 8 Hz, 1H, C₁H-Fl), 7.88 (d, *J* = 7 Hz, 2H, C₄H-Fl or C₅H-Fl) 7.87 (d, *J* = 8 Hz, 2H C₄H-Fl or C₅H-Fl), 7.60 (d, *J* = 8 Hz, 1H, C₈H-Fl), 7.32 (td, *J* = 1 Hz, 7 Hz, 1H, C₂H-Fl), 7.28 (t, *J* = 7 Hz, 1H, C₃H-Fl), 7.23 (t, *J* = 7 Hz, 1H, C₆H-Fl), 7.09 (td, *J* = 1 Hz, 8 Hz, 1H, C₇H-Fl), 6.91 (s, 2H, CH-*m*-Mes), 4.83 (s, 1H, Ga-C₉H), 4.22 (septet, *J* = 7 Hz, 2H, (CH₃)₂CH-N), 2.44 (s, 6H, *o*-CH₃-Mes), 2.27 (s, 3H, *p*-CH₃-Mes), 1.29 (s, 6H, C=C-CH₃), 0.82 (d, *J* = 7 Hz, 6H, (CH₃)₂CH-N), 0.53 (d, *J* = 7 Hz, 6H, (CH₃)₂CH-N); ¹³C{¹H} NMR (151 MHz, C₆D₆, 298 K) δ: 167.84 (N-C-Ga), 150.28 (C₁₁-Fl), 149.06 (C₁₂-Fl), 145.03 (C₆-Mes), 144.79 (Ga-C_{ipso}-Mes), 140.25 (C₁₀-Fl), 139.79 (C₁₃-Fl), 137.08 (C_p-Mes), 128.47 (HC-Mes), 126.29 (N-C=C-N and C₂-Fl), 126.05 (C₇-Fl), 125.97 (C₁-Fl), 124.50 (C₈-Fl), 124.25 (C₃-Fl), 124.09 (C₆-Fl), 119.69 (C₄-Fl), 119.41 (C₅-Fl), 52.86 (N-CH-(CH₃)₂), 45.67 (Ga-C₉-Fl), 26.12 (*o*-CH₃-Mes), 21.28 (*p*-CH₃-Mes), 21.12 ((CH₃)₂CH-N), 20.46 ((CH₃)₂CH-N), 9.69 (C=C-CH₃); ⁷¹Ga{¹H} NMR (183 MHz, C₆D₆, 298 K) δ: no signal; LR ESI-TOF MS (*m/z*; positive ion): 533 ([^{Me}I₂Pr→⁶⁹GaFIMes]⁺); HR ESI-TOF MS (*m/z*; positive ion): Calcd. for C₃₃H₄₀⁶⁹GaN₂⁺ ([^{Me}I₂Pr→⁶⁹GaFIMes]⁺): 533.2447, Found: 533.2466; Satisfactory elemental analysis data could not be obtained, potentially due to decomposition of the compound or contamination of LiCl that is formed as a by-product during the synthesis of **5.3**.

5.4.4 Synthesis of Chloro(4-dimethylaminopyridine)fluorenylmesitylgallane, DMAP→GaCIFIMes, **5.4**

A solution of DMAP (0.48 g, 4.0 mmol) dissolved in DCM (5 mL) was added dropwise to a stirring suspension of **5.1** (2.0 g, 4.0 mmol) in DCM (10 mL). The pale yellow suspension became white within 30 minutes. The mixture was allowed to stir at room

temperature for 18 hours, at which point the suspension was centrifuged and the supernatant was decanted. The solid was washed with a 3:1 mixture of dichloromethane and Et₂O (5 mL x 2). The solvent was removed from the decanted solutions under reduced pressure yielding a white solid. THF, cooled to -20 °C, was added to the solid and the mixture was centrifuged and the THF was decanted. The solid was dried under reduced pressure yielding **5.4** as a white solid. X-ray quality crystals were obtained from a supersaturated solution of **5.4** in a mixture of THF and Et₂O (4:1) cooled to -20 °C.

Yield: 1.01 g of a white powder (50 %); mp: 234 – 236 °C; ¹H NMR (600 MHz, CDCl₃, 298 K) δ: 7.71 (d, *J* = 7 Hz, 1H, C₄H-FI), 7.70 (d, *J* = 8 Hz, 1H, C₃H-FI), 7.65 (d, *J* = 8 Hz, 1H, C₁H-FI), 7.53 (dd, *J* = 2 Hz, 7 Hz, 1H, C₈H-FI), 7.30 (d, 2H, *J* = 7 Hz, N-CH-CH), 7.22 (m, 3H, C₃H-FI, C₆H-FI, C₇H-FI), 7.16 (td, *J* = 1 Hz, 8 Hz, 1H, C₂H-FI), 6.77 (s, 2H, CH-*m*-Mes), 6.16 (d, *J* = 8 Hz, 2H, N-CH-CH), 4.47 (s, 1H, Ga-C₉H), 3.01 (s, 6H, N-(CH₃)₂), 2.25 (s, 3H, *p*-CH₃-Mes), 2.09 (s, 6H, *o*-CH₃-Mes); ¹³C{¹H} NMR (151 MHz, CDCl₃, 298 K) δ: 155.28 ((CH₃)₂N-C), 147.35 (C₁₁-FI), 147.31 (C₁₂-FI), 145.55 (N-CH-CH), 145.10 (C_o-Mes), 139.43 (C₁₃-FI), 139.19 (C₁₀-FI), 139.00 (Ga-C_{ipso}-Mes) 137.91 (C_p-Mes), 127.78 (HC-*m*-Mes), 125.80 (C₃-FI, C₆-FI, or C₇-FI), 125.39 (C₂-FI), 124.34 (C₃-FI, C₆-FI, or C₇-FI), 123.65 (C₈-FI), 123.56 (C₃-FI, C₆-FI, or C₇-FI), 123.46 (C₁-FI), 119.27 (C₄-FI), 118.98 (C₅-FI), 106.14 (N-CH-CH), 45.89 (Ga-C₉-FI), 39.29 ((CH₃)₂N), 24.93 and 24.84 (*o*-CH₃-Mes), 21.06 (*p*-CH₃-Mes); ⁷¹Ga{¹H} NMR (183 MHz, CDCl₃, 298 K) δ: no signal; LR ESI-TOF MS (*m/z*; positive ion): 353 ([⁶⁹GaFIMes]⁺); 475 ([DMAP→⁶⁹GaFIMes]⁺); LR ESI-TOF MS (*m/z*; negative ion): 425 ([⁶⁹Ga³⁵Cl₂FIMes]⁻); HR ESI-TOF MS (*m/z*; positive ion): Calcd. for C₂₉H₃₀⁶⁹GaN₂⁺ ([DMAP→⁶⁹GaFIMes]⁺): 475.1665, Found: 475.1655; Elemental analysis data calcd. (%) for DMAP→GaClFIMes (C₂₉H₃₀ClGa₂N₂): C, 68.06; H, 5.91; N, 5.47; S, 0.00; found C, 67.93; H, 6.25; N, 5.45; S, 0.00.

5.4.5 Synthesis of Butyl(1,3-diisopropyl-4,5-dimethylimidazol-2-ylidene)fluorenylmesitylgallane, ^{Me}l*i*Pr→GaBuFIMes, **5.5**

A solution of BuLi (0.53 mL, 0.84 mmol) in hexanes was added to a stirring solution of

5.3 (0.40 g, 0.70 mmol) dissolved in toluene/Et₂O (2:1; 10 mL) cooled in a Dry Ice-acetone bath. The solution was allowed to stir at that temperature for several hours, at which point the solution was allowed to warm to room temperature over 18 hours, leading to a colour change from yellow to orange. The volatiles were removed under reduced pressure. The residue was dissolved in toluene (3 mL), Et₂O (1 mL) was added, and the solution was cooled to -20 °C for 18 hours. After 18 hours, a powdered precipitate had formed. The precipitate was removed by centrifugation, and the supernatant was dried under reduced pressure. The residue was suspended in Et₂O (2 mL), and then the mixture was cooled to -20 °C for 18 hours. The resultant solid was collected by centrifugation and washed with hexanes (3 x 2 mL) to give an orange precipitate, **5.5**. Crystals suitable for X-ray crystallography were grown from a vapour diffusion experiment at -20 °C with toluene as the solvent and hexanes as the non-solvent.

Yield: 0.11 g of an orange powder (26 %, best yield); mp: 154 – 158 °C; ¹H NMR (600 MHz, C₆D₆, 298 K) δ: 8.06 (d, *J* = 7 Hz, 1H, C₈H-Fl), 8.03 (d, *J* = 7 Hz, 1H, C₅H-Fl), 8.00 (d, *J* = 8 Hz, 1H, C₄H-Fl), 7.38 (td, *J* = 1 Hz, 8 Hz, 1H, C₇H-Fl), 7.35 (t, *J* = 7 Hz, 1H, C₆H-Fl), 7.31 (d, *J* = 7 Hz, 1H, C₁H-Fl), 7.27 (t, *J* = 7 Hz, 1H, C₃H-Fl), 7.17 – 7.15 (ov. m, 1H, C₂H-Fl), 7.00 (s, 2H, CH-*m*-Mes), 4.76 (s, 1H, Ga-C₉H), 4.15 (septet, *J* = 7 Hz, 2H, (CH₃)₂CH-N), 2.38 (s, 6H, *o*-CH₃-Mes), 2.35 (s, 3H, *p*-CH₃-Mes), 1.63 – 1.56 (ov. m, 4H, Ga-CH₂-CH₂-CH₂-CH₃) 1.34 (s, 6H, C=C-CH₃), 1.12 (pseudo-td, *J* = 3 Hz, 13 Hz, 2H, Ga-CH₂-CH₂-CH₂-CH₃), 1.06 (t, *J* = 7 Hz, 3H, Ga-CH₂-CH₂-CH₂-CH₃), 0.75 (d, *J* = 7 Hz, 6H, (CH₃)₂CH-N), 0.71 (d, *J* = 7 Hz, 6H, (CH₃)₂CH-N); ¹³C {¹H} NMR (151 MHz, C₆D₆, 298 K) δ: 174.06 (N-C-Ga), 152.23 (C₁₂-Fl), 151.90 (C₁₁-Fl), 149.66 (Ga-C-Mes), 144.94 (C_o-Mes), 139.36 (C₁₃-Fl), 138.92 (C₁₀-Fl), 135.66 (C_p-Mes), 128.28 (*m*-Mes), 125.50 (N-C=C-N), 125.19 (C₇-Fl), 125.09 (C₂-Fl), 124.12 (C₈-Fl), 123.85 (C₁-Fl), 122.80 (C₆-Fl), 122.53 (C₃-Fl), 119.69 (C₅-Fl), 119.61 (C₄-Fl), 52.17 (N-CH-(CH₃)₂), 47.90 (Ga-C₉-Fl), 31.58 (Ga-CH₂-), 29.34 (Ga-CH₂-CH₂-), 26.36 (*o*-CH₃-Mes), 21.36 (*p*-CH₃-Mes), 21.03 ((CH₃)₂CH-N), 20.96 ((CH₃)₂CH-N), 17.63 (-CH₂-CH₃), 14.15 (-CH₂-CH₃), 9.79 (C=C-CH₃); ⁷¹Ga {¹H} NMR (183 MHz, C₆D₆, 298 K) δ: no signal; LR ESI-TOF MS (*m/z*; positive ion): 425 ([^{Me}IiPr → ⁶⁹GaBuMes]⁺); 533 ([^{Me}IiPr → ⁶⁹GaFlMes]⁺);

613 ($[\text{Me}^{\text{I}}\text{Pr} \rightarrow ^{69}\text{GaBuFlMes}]\text{Na}^+$); HR ESI-TOF MS (m/z ; positive ion): Calcd. for $\text{C}_{37}\text{H}_{49}^{69}\text{GaN}_2\text{Na}^+$ ($[\text{Me}^{\text{I}}\text{Pr} \rightarrow ^{69}\text{GaBuFlMes}]\text{Na}^+$): 613.3049, Found: 613.3057; Satisfactory elemental analysis data could not be obtained, potentially due to decomposition of the compound or contamination of LiCl that is formed as a by-product during the synthesis of **5.5**.

5.4.6 Synthesis of (1,3-diisopropyl-4,5-dimethylimidazol-2-ylidene)fluorenylmesityltrifluoromethanesulfonatogallane, $\text{Me}^{\text{I}}\text{Pr} \rightarrow \text{GaOTfFlMes}$, **5.7**

A solution of AgOTf (2.47 g, 9.63 mmol) dissolved in THF (10 mL) was added dropwise to a stirring solution of **5.3** (5.49 g, 9.63 mol) dissolved in THF (20 mL) in the dark, immediately resulting in the formation of a dark precipitate. The mixture was allowed to stir at room temperature for 4 hours, at which point the precipitate was separated by centrifugation and the supernatant was decanted. The precipitate was washed with THF (2 x 3 mL) and the mixture was centrifuged and separated each time. The washes were combined and the volatiles were removed under reduced pressure yielding an orange oil. The oil was triturated with toluene (2 mL) and a few drops of THF, giving **5.7** as an off-white solid. The solid was separated by centrifugation, washed with Et₂O (3 x 2 mL), and dried under reduced pressure. Hexanes (8 mL) were added to the combined solvent washes and the mixture was cooled to -20 °C, resulting in an off-white precipitate. The mother liquor was decanted, the precipitate was washed with Et₂O (3 x 2 mL) and dried under reduced pressure yielding more of **5.7**. The solvent was removed from the mother liquor under reduced pressure and the resultant oil was triturated with a mixture of THF, hexanes and Et₂O (1:1:0.5) multiple times, to yield additional **5.7**.

Yield: 3.27 g of an off-white powder (50 %); mp: 209 – 212 °C; ¹H NMR (600 MHz, C₆D₆, 298 K) δ : 8.29 (d, $J = 7$ Hz, 1H, C₁H-Fl), 7.76 (d, $J = 8$ Hz, 1H, C₄H-Fl), 7.75 (d, $J = 8$ Hz, 1H, C₅H-Fl), 7.71 (dd, $J = 1$ Hz, 7 Hz, 1H, C₈H-Fl), 7.33 (td, $J = 1$ Hz, 7 Hz, 1H, C₂H-Fl), 7.22 (t, $J = 8$ Hz, 1H, C₃H-Fl), 7.19 (tt, $J = 1$ Hz, 8 Hz, 1H, C₆H-Fl), 7.10 (td, J

= 1 Hz, 7 Hz, 1H, C₇H-Fl), 6.73 (s, 2H, CH-*m*-Mes), 4.83 (s, 1H, Ga-C9-H), 4.31 (septet, $J = 7$ Hz, 2H, (CH₃)₂CH-N), 2.14 (s, 3H, *p*-CH₃-Mes), 2.12 (br s, 6H, *o*-CH₃-Mes), 1.26 (s, 6H, C=C-CH₃), 0.85 (d, $J = 7$ Hz, 6H, (CH₃)₂CH-N), 0.63 (d, $J = 7$ Hz, 6H, (CH₃)₂CH-N); ¹³C{¹H} NMR (151 MHz, C₆D₆, 298 K) δ : 163.30 (N-C-Ga), 148.67 (C₁₁-Fl), 147.58 (C₁₂-Fl), 144.41 (C_o-Mes), 141.34 (Ga-C_{ipso}-Mes), 140.51 (C₁₀-Fl), 140.10 (C₁₃-Fl), 137.99 (C_p-Mes), 128.37 (HC-Mes), 127.39 (N-C=C-N), 126.63 (C₂-Fl), 126.36 (C₇-Fl), 125.26 (C₁-Fl), 124.81 (C₃-Fl), 124.73 (C₈-Fl, C₆-Fl), 120.57 (q, $J = 320$ Hz, ⁻O₃SCF₃), 119.98 (C₄-Fl), 119.74 (C₅-Fl), 53.39 (N-CH-(CH₃)₂), 45.67 (Ga-C₉-Fl), 24.98 (*o*-CH₃-Mes), 21.15 (*p*-CH₃-Mes, (CH₃)₂CH-N), 20.91 ((CH₃)₂CH-N), 9.80 (C=C-CH₃); ¹⁹F NMR (564 MHz, C₆D₆, 298 K): -77.20 (s, ⁻O₃SCF₃); ⁷¹Ga{¹H} NMR (183 MHz, C₆D₆, 298 K) δ : no signal; LR ESI-TOF MS (m/z ; positive ion): 353 ([^{Me}IiPr→⁶⁹GaFlMes]⁺); 533 ([^{Me}IiPr→⁶⁹GaFlMes]⁺); LR ESI-TOF MS (m/z ; negative ion): 149 ([CF₃SO₃]⁻); 831 ([^{Me}IiPr→⁶⁹GaOTfFlMes][OTf]⁻); HR ESI-TOF MS (m/z ; negative ion): Calcd. for C₃₅H₄₀F₆⁶⁹GaN₂O₆S₂⁻ ([^{Me}IiPr→⁶⁹GaOTfFlMes][OTf]⁻): 831.1488, Found: 831.1527; Elemental analysis data calcd. (%) for ^{Me}IiPr→GaOTfFlMes (C₃₄H₄₀F₃GaN₂O₃S): C, 59.75; H, 5.90; N, 4.10; S, 4.69; found C, 59.46; H, 5.97; N, 4.08; S, 4.50.

5.4.7 Synthesis of (1,3-diisopropyl-4,5-dimethylimidazol-2-ylidene)fluorenylfluoromesitylgallane, ^{Me}IiPr→GaFFlMes, **5.8**

A suspension of KF (0.251 g, 4.32 mmol) and 18-crown-6 (1.14 g, 4.32 mmol) in THF (10 mL) was added to a stirring solution of **5.7** (2.95 g, 4.32 mmol) dissolved in THF (15 mL). The solution was allowed to stir at 40 °C for 18 hours, at which point the mixture was filtered to remove debris from the Teflon sealing ring, and the solvent was removed from the filtrate under reduced pressure, yielding an oily yellow residue, which was suspended in toluene (7 mL) and filtered. The solvent was removed from the filtrate under reduced pressure yielding an orange oil. The oil was triturated with Et₂O (7 mL) to give an off-white solid. The mixture was cooled to -20 °C for 18 hours, at which point the mother liquor was decanted and the solid was washed with Et₂O (3 x 2 mL), dried under

reduced pressure to yield **5.8** as an off-white solid. X-ray quality crystals were grown from a saturated solution of **5.8** in a mixture of THF and pentane (1:2) at -20 °C

Yield: 1.31 g of an off-white powder (55 %); mp: 158 – 164 °C (decomposition); ¹H NMR (600 MHz, C₆D₆, 298 K) δ: 8.20 (dd, *J* = 2 Hz, 7 Hz, 1H, C₁H-FI), 7.92 (two ov. dd, *J* = 2 Hz, 4 Hz; 8 Hz, 2H, C₄H-FI and C₅H-FI), 7.82 (d, *J* = 8 Hz, 1H, C₈H-FI), 7.28 – 7.23 (m, 3H, C₂H-FI, C₃H-FI and C₆H-FI), 7.15 (td, *J* = 1 Hz, 8 Hz, 1H, C₇H-FI), 6.88 (s, 2H, CH-*m*-Mes), 4.80 (s, 1H, Ga-C₉H-FI), 4.47 (d of septets, *J* = 2 Hz, 7 Hz, 2H, (CH₃)₂CH-N), 2.40 (s, 6H, *o*-CH₃-Mes), 2.24 (s, 3H, *p*-CH₃-Mes), 1.33 (s, 6H, C=C-CH₃), 0.78 (d, *J* = 7 Hz, 6H, (CH₃)₂CH-N), 0.66 (d, *J* = 7 Hz, 6H, (CH₃)₂CH-N); ¹³C{¹H} NMR (151 MHz, C₆D₆, 298 K) δ: 167.91 (d, *J* = 20 Hz, N-C-Ga), 150.37 (C₁₁-FI), 149.71 (C₁₂-FI), 145.09 (d, *J* = 12 Hz, Ga-C_{ipso}-Mes), 144.98 (C_o-Mes), 140.10 (C₁₀-FI), 139.86 (C₁₃-FI), 136.89 (C_p-Mes), 128.28 (HC-Mes), 126.34 (N-C=C-N, C₃-FI), 126.15 (C₂-FI), 125.98 (C₇-FI), 125.13 (d, *J* = 3 Hz, C₁-FI), 124.27 (C₈-FI), 123.76 (C₃-FI and C₆-FI), 119.88 (C₄-FI), 119.53 (C₅-FI), 52.54 (d, *J* = 5 Hz, N-CH-(CH₃)₂), 45.12 (d, *J* = 15 Hz, Ga-C₉-FI), 25.12 (*o*-CH₃-Mes), 21.31 (*p*-CH₃-Mes), 21.11 ((CH₃)₂CH-N), 21.03 ((CH₃)₂CH-N), 9.75 (C=C-CH₃); ¹⁹F NMR (564 MHz, C₆D₆, 298 K): -185.3 (s, Ga-F); ⁷¹Ga{¹H} NMR (183 MHz, C₆D₆, 298 K) δ: no signal; LR ESI-TOF MS (*m/z*; positive ion): 395 ([⁶⁹GaFFIMes]Na⁺); 533 ([^{Me}IiPr→⁶⁹GaFIMes]⁺); 575 ([^{Me}IiPr→⁶⁹GaFFIMes]Na⁺); 1127 ([^{Me}IiPr→⁶⁹GaFFIMes]₂Na⁺): HR ESI-TOF MS (*m/z*; positive ion): Calcd. for C₃₃H₄₀F⁶⁹GaN₂Na⁺ ([^{Me}IiPr→⁶⁹GaFFIMes]Na⁺): 575.2323, Found: 575.2329; Satisfactory elemental analysis data could not be obtained, potentially due to decomposition of the compound or contamination with [K(18-crown-6)][OTf] that is formed as a by-product during the synthesis of **5.8**.

5.4.8 Synthesis of (4-dimethylaminopyridine)fluorenylmesityltrifluoromethanesulfonategallane, DMAP→GaOTfFIMes, **5.9**

A solution of AgOTf (0.78 g, 3.1 mmol) dissolved in THF (5 mL) was added dropwise to

a stirring solution of **5.4** (1.56 g, 3.1 mmol) dissolved in THF (15 mL) in the absence of light. The formation of a white precipitate occurred immediately. The resulting mixture was allowed to stir at room temperature in the dark for 18 hours, at which point the solution was decanted from the red-brown precipitate by centrifugation. The solvent was removed under reduced pressure, yielding an off-white solid. The solid was dissolved in DCM (7 mL) and the solution was filtered to remove any additional particulates. Et₂O (7 mL) was added to the filtrate, and the solution was cooled to -20 °C for 18 hours. A white precipitate formed and was isolated by decantation of the mother liquor and triturating the precipitate with Et₂O (3 x 3 mL). The solid was dried yielding pure **5.9**. X-ray quality crystals were obtained from a saturated solution of **5.9** dissolved in a 1:2 mixture of DCM and Et₂O and cooled to -20 °C.

Yield: 1.26 g of a white powder (70 %); mp: 203 – 206 °C; ¹H NMR (600 MHz, CDCl₃, 298 K) δ: 7.81 (d, *J* = 8 Hz, 2H, C₄H-FI, C₅H-FI), 7.58 (br m, 2H, C₁H-FI, C₈H-FI), 7.53 (d, *J* = 7 Hz, 2H, N-CH-CH), 7.28 (t, *J* = 7 Hz, 2H, C₂H-FI, C₇H-FI), 7.23 (t, *J* = 8 Hz, 2H, C₃H-FI, C₆H-FI), 6.72 (s, 2H, CH-*m*-Mes), 6.40 (d, *J* = 8 Hz, 2H, N-CH-CH), 4.70 (s, 1H, Ga-C₉H), 3.10 (s, 6H, N-(CH₃)₂), 2.23 (s, 3H, *p*-CH₃-Mes), 1.89 (s, 6H, *o*-CH₃-Mes); ¹³C {¹H} NMR (151 MHz, CDCl₃, 298 K) δ: 155.81 ((CH₃)₂N-C), 145.97 (N-CH-CH), 145.70 (C₁₁-FI or C₁₂-FI), 145.25 (C₁₁-FI or C₁₂-FI), 139.64 (C₁₀-FI and C₁₃-FI), 139.23 (Ga-C_{ipso}-Mes), 138.86 (C_o-Mes), 134.69 (C_p-Mes) 127.76 (HC-*m*-Mes), 125.20 (C₃-FI, C₆-FI), 124.49 (C₂-FI, C₇-FI), 123.83 (C₁-FI, C₈-FI), 119.67 (C₄-FI, C₅-FI), 119.41 (q, *J* = 318 Hz, ⁻O₃SCF₃), 106.77 (N-CH-CH), 43.42 (Ga-C₉-FI), 39.43 ((CH₃)₂N), 24.49 (*o*-CH₃-Mes), 21.03 (*p*-CH₃-Mes); ¹⁹F NMR (564, CDCl₃, 298 K) δ: -77.8 (-OSO₂CF₃); ⁷¹Ga {¹H} NMR (183 MHz, CDCl₃, 298 K) δ: no signal; LR ESI-TOF MS (*m/z*; positive ion): 353 ([⁶⁹GaFIMes]⁺); 475 ([DMAP→⁶⁹GaFIMes]⁺); HR ESI-TOF MS (*m/z*; positive ion): Calcd. for C₂₉H₃₀⁶⁹GaN₂⁺ ([DMAP→⁶⁹GaFIMes]): 475.1665, Found: 475.1649; Elemental analysis data calcd. (%) for DMAP→GaOTfFIMes (C₃₀H₃₀F₃GaN₂O₃S): C, 57.62; H, 4.84; N, 4.48; S, 5.13; found C, 56.64; H, 4.74; N, 4.44; S, 5.83.

5.4.9 Synthesis of (4-dimethylaminopyridine)fluorenylfluoromesitylgallane, DMAP→GaFFIMes, **5.10**

A suspension of KF (0.12 g, 2.0 mmol) and 18-crown-6 (0.53 g, 2.0 mmol) in THF (8 mL) was added to a stirring solution of **5.9** (1.26 g, 2.0 mmol) dissolved in THF (10 mL). The suspension was allowed to stir for 18 hours, at which point the solid was removed by centrifugation and washed once with THF (2 mL). The decanted solutions were dried under reduced pressure yielding an off-white residue. The residue was dissolved in toluene (8 mL) and filtered to remove any undissolved salts. The solvent was removed under reduced pressure, and the resultant solid was suspended in DCM (6 mL) and filtered once more to remove any additional particulates. Et₂O (4 mL) was added and the mixture was cooled to -20 °C for 18 hours, at which point an off-white precipitate had formed. The solvent was decanted, and the precipitate was washed with Et₂O (3 x 3 mL) and dried under reduced pressure yielding **5.10**. X-ray quality crystals were obtained from a saturated solution of **5.10** in a 1:2 mixture of DCM and Et₂O, at -20 °C.

Yield: 0.43 g of an off-white powder (43 %); mp: 161 – 163 °C; ¹H NMR (600 MHz, CDCl₃, 298 K) δ: 7.85 (d, *J* = 8 Hz, 2H, C₄H-FI and C₅H-FI), 7.57 (br m, 1H, C₁H-FI), 7.43 (br m, 3H, C₈H-FI and N-CH-CH), 7.24 (t, *J* = 8 Hz, 2H, C₃H-FI and C₆H-FI), 7.18 (br m, 2H, C₂H-FI and C₇H-FI), 6.73 (s, 2H, CH-*m*-Mes), 6.29 (d, *J* = 5 Hz, 2H, N-CH-CH), 4.44 (s, 1H, Ga-C₉H), 3.00 (s, 6H, N-(CH₃)₂), 2.24 (s, 3H, *p*-CH₃-Mes), 1.99 (s, 6H, *o*-CH₃-Mes); ¹³C{¹H} NMR (151 MHz, CDCl₃, 298 K) δ: 155.47 ((CH₃)₂N-C), 147.76 (C₁₁-FI or C₁₂-FI), 146.08 (N-CH-CH), 145.52 (C₁₁-FI or C₁₂-FI), 139.20 (br. s, C_o-Mes, C₁₃-FI and C₁₀-FI), 138.61 (d, *J* = 15 Hz, Ga-C_{ipso}-Mes), 137.80 (C_p-Mes), 127.15 (HC-*m*-Mes), 125.67 (C₂-FI and C₇-FI), 123.68 (C₁-FI and C₈-FI), 123.45 (C₃-FI and C₆-FI), 119.36 (C₄-FI and C₄-FI), 106.50 (N-CH-CH), 44.09 (d, *J* = 16 Hz, Ga-C₉-FI), 39.26 ((CH₃)₂N), 24.44 (*o*-CH₃-Mes), 21.04 (*p*-CH₃-Mes); ¹⁹F NMR (564 MHz, CDCl₃, 298 K) δ: -183.04 (Ga-F); ⁷¹Ga{¹H} NMR (183 MHz, CDCl₃, 298 K) δ: no signal; LR ESI-TOF MS (*m/z*; positive ion): 353 ([⁶⁹GaFIMes]⁺); 375 ([DMAP→⁶⁹GaFFI]⁺); 395

([GaFFIMes]Na⁺); 475 ([DMAP→⁶⁹GaFIMes]⁺); 517 ([DMAP→⁶⁹GaFFIMes]Na⁺); 617 ([DMAP→⁶⁹GaFFIMes] [DMAP-H]⁺); LR ESI-TOF MS (*m/z*; negative ion): 391 ([⁶⁹GaF₂FIMes]⁻); HR ESI-TOF MS (*m/z*; positive ion): Calcd. for C₃₆H₄₁F⁶⁹GaN₄⁺ ([DMAP→⁶⁹GaFFIMes][DMAP-H]⁺): 617.2571, Found: 617.2564; Calcd. for C₂₉H₃₀F⁶⁹GaN₂Na⁺ ([DMAP→⁶⁹GaFFIMes]Na⁺): 517.1547, Found: 517.1560; Elemental analysis data calcd. (%) for DMAP→GaFFIMes[CH₂Cl₂]_{0.4} (C_{29.4}H_{30.8}Cl_{0.8}F⁶⁹GaN₂): C, 66.72; H, 5.87; N, 5.29; S, 0.00; found C, 65.84; H, 6.49; N, 5.35; S, 0.00 (CH₂Cl₂ was used as the crystallization solvent and co-crystallized with **5.10**, and its ratio is supported by the relative integration in the ¹H NMR spectrum).

5.4.10 Synthesis of **5.11**

*t*BuLi (0.21 mL, 0.36 mmol), 1.7 M in hexanes, was added to a stirring solution of **5.8** (0.20 g, 0.38 mmol) dissolved in THF (3 mL) cooled in a Dry Ice-acetone bath. The resultant orange solution was allowed to stir for 20 minutes, at which point a solution of tolualdehyde (0.043 g, 0.36 mmol) in THF (3 mL) was added dropwise. The orange suspension was stirred for another 20 minutes, at which point the cooling bath was removed. The reaction mixture was allowed to warm to room temperature over 40 minutes, after which time the initial precipitate had dissolved and the colour of the mixture had darkened. The solvent was removed under reduced pressure, and toluene (5 mL) was added. The suspension was filtered, hexanes (2 mL) were added to the filtrate and the solution was cooled to -20 °C for 18 hours, during which time a tan coloured precipitate formed. The mother liquor was decanted, the precipitate was washed with hexanes (3 x 1 mL), dried, suspended in benzene (3 mL) and filtered. The solvent was removed from the filtrate under reduced pressure, yielding **5.11** as a beige solid. Another batch of **5.11** was obtained from the mother liquor after adding additional hexanes (2 mL) and cooling the mixture to -20 °C for 18 hours. X-ray quality single crystals were obtained from the slow diffusion of the solvent from a solution of **5.11** dissolved in THF into toluene cooled to -20 °C.

Yield: 0.040 g of a tan solid; ^1H NMR (600 MHz, CDCl_3 , 298 K)³⁵ δ : 8.42 (d, $J = 8$ Hz, 1H, $\text{C}_1\text{H-FI}$), 8.30 (d, $J = 7$ Hz, 1H, $\text{C}_8\text{H-FI}$), 7.30 (td, $J = 8$ Hz, 1 Hz, 1H, $\text{C}_7\text{H-FI}$), 7.27 (dt, $J = 8$ Hz, 1 Hz, 1H, $\text{C}_5\text{H-FI}$), 7.25 (dt, $J = 7$ Hz, 1 Hz, 1H, $\text{C}_4\text{H-FI}$), 7.21 (td, $J = 8$ Hz, 1 Hz, 1H, $\text{C}_2\text{H-FI}$), 7.16 – 7.13 (m, 4H, $\text{CH-}o\text{-Tol}$), 7.10 (td, $J = 7$ Hz, 1 Hz, 1H, $\text{C}_6\text{H-FI}$), 7.07 (td, $J = 8$ Hz, 1 Hz, 1H, $\text{C}_3\text{H-FI}$), 6.95 (s, 2H, $\text{CH-}m\text{-Mes}$), 6.70 (d, $J = 8$ Hz, 2H, $\text{CH-}m\text{-Tol}$), 6.66 (d, $J = 8$ Hz, 2H, $\text{CH-}m\text{-Tol}$), 6.62 (s, 1H, O-CH-Tol), 6.35 (s, 1H, O-CH-Tol), 5.95 (septet, $J = 7$ Hz, 2H, $(\text{CH}_3)_2\text{CH-N}$), 2.94 (s, 6H, $o\text{-CH}_3\text{-Mes}$), 2.25 (s, 3H, $p\text{-CH}_3\text{-Mes}$), 1.82 (s, 3H, $p\text{-CH}_3\text{-Tol}$), 1.81 (s, 3H, $p\text{-CH}_3\text{-Tol}$), 1.44 (s, 6H, $\text{C}=\text{C-CH}_3$), 1.26 (d, $J = 7$ Hz, 6H, $(\text{CH}_3)_2\text{CH-N}$), 0.99 (d, $J = 7$ Hz, 6H, $(\text{CH}_3)_2\text{CH-N}$); $^{13}\text{C}\{^1\text{H}\}$ NMR (151 MHz, CDCl_3 , 298 K) δ : 165.68 (N-C-Ga), 149.66 ($\text{C}_{13}\text{-FI}$), 149.31 ($\text{C}_{10}\text{-FI}$), 145.78 ($\text{C}_o\text{-Mes}$), 142.99 (Ga- $\text{C}_{ipso}\text{-Tol}$), 142.63 (Ga- $\text{C}_{ipso}\text{-Tol}$), 142.52 ($\text{C}_{12}\text{-FI}$), 141.79 ($\text{C}_{11}\text{-FI}$), 140.43 (Ga- $\text{C}_{ipso}\text{-Mes}$), 137.40 ($\text{C}_p\text{-Mes}$), 134.20 ($\text{C}_p\text{-Tol}$), 134.16 ($\text{C}_p\text{-Tol}$), 128.53 ($\text{CH-}o\text{-Tol}$), 128.29 ($\text{CH-}o\text{-Tol}$), 127.38 ($\text{CH-}m\text{-Tol}$), 127.16 ($\text{CH-}m\text{-Tol}$), 127.08 ($\text{C}_2\text{-FI}$), 126.83 ($\text{C}_1\text{-FI}$), 126.55 ($\text{C}_3\text{-FI}$), 126.45 ($\text{C}_6\text{-FI}$), 126.25 ($\text{C}_8\text{-FI}$), 125.50 ($\text{C}_7\text{-FI}$), 119.70 ($\text{C}_5\text{-FI}$), 119.34 ($\text{C}_4\text{-FI}$), 81.67 (O-CH-Tol), 80.58 (O-CH-Tol), 69.37 (Ga- $\text{C}_9\text{-FI}$), 52.41 (N-CH- $(\text{CH}_3)_2$), 24.66 ($o\text{-CH}_3\text{-Mes}$), 22.05 ($(\text{CH}_3)_2\text{CH-N}$), 21.83 ($(\text{CH}_3)_2\text{CH-N}$), 21.31 ($p\text{-CH}_3\text{-Mes}$), 20.94 ($p\text{-CH}_3\text{-Tol}$), 9.81 ($\text{C}=\text{C-CH}_3$; $^{71}\text{Ga}\{^1\text{H}\}$ NMR (183 MHz, CDCl_3 , 298 K) δ : no signal; LR ESI-TOF MS (m/z ; positive ion): 533 ($[\text{Me}_6\text{IiPr} \rightarrow ^{69}\text{GaFI}(\text{Mes})]^+$); 653 ($[\text{Me}_6\text{IiPr} \rightarrow ^{69}\text{GaFI}(\text{Mes}(\text{O-CH-Tol}))\text{H}^+$); 779 ($[\text{Me}_6\text{IiPr} \rightarrow ^{69}\text{GaFI}(\text{Mes}(\text{O-CH-Tol})_2)\text{Li}^+$); 795 ($[\text{Me}_6\text{IiPr} \rightarrow ^{69}\text{GaFI}(\text{Mes}(\text{O-CH-Tol})_2)\text{Na}^+$); HR ESI-TOF MS (m/z ; positive ion): Calcd. for $\text{C}_{41}\text{H}_{48}^{69}\text{GaN}_2\text{O}^+$ ($[\text{Me}_6\text{IiPr} \rightarrow ^{69}\text{GaFI}(\text{Mes}(\text{O-CH-Tol}))\text{H}^+$): 653.3022, Found: 653.3050; Calcd. for $\text{C}_{49}\text{H}_{55}^{69}\text{GaLiN}_2\text{O}_2^+$ ($[\text{Me}_6\text{IiPr} \rightarrow ^{69}\text{GaFI}(\text{Mes}(\text{O-CH-Tol})_2)\text{Li}^+$): 779.3679, Found: 779.3712; Calcd. for $\text{C}_{49}\text{H}_{55}^{69}\text{GaN}_2\text{NaO}_2^+$ ($[\text{Me}_6\text{IiPr} \rightarrow ^{69}\text{GaFI}(\text{Mes}(\text{O-CH-Tol})_2)\text{Na}^+$): 795.3417, Found: 795.3454; Satisfactory elemental analysis data could not be reliably obtained, potentially due to decomposition of the compound.

5.4.11 X-ray Crystallography

5.4.11.1 General Considerations

Data Collection and Processing: The samples were mounted on a MiTeGen polyimide micromount with a small amount of Paratone N oil. All X-ray measurements were made on a Bruker Kappa Axis Apex2 or a Nonius Bruker KappaCCD Apex2 diffractometer at a temperature of 110 – 117 K. The frame integration was performed using SAINT.³⁶ The resulting raw data was scaled and absorption corrected using a multi-scan averaging of symmetry equivalent data using SADABS³⁷ or TWINABS.³⁸

Structure Solution and Refinement: The structures were solved by using a dual space methodology using the SHELXT program.³⁹ All non-hydrogen atoms were obtained from the initial solution. The hydrogen atoms were introduced at idealized positions and were allowed to ride on the parent atom. The structural model was fit to the data using full matrix least-squares based on F^2 . The calculated structure factors included corrections for anomalous dispersion from the usual tabulation. The structures were refined using the SHELXL-2014 program from the Shelx suite of crystallographic software.⁴⁰ Graphic plots were produced using the XP program from the SHELXTL suite.⁴¹

5.4.11.2 X-ray Crystallographic Data

Table 5.1: Selected crystallographic details for compounds **5.1**, **5.3**, **5.5** and **5.7**.

	5.1 •Et ₂ O	5.3	5.5	5.7
Formula	C ₂₂ H ₁₉ Cl ₂ GaLi• (Et ₂ O) ₂	C ₃₃ H ₄₀ ClGaN ₂	C ₃₇ H ₄₉ GaN ₂	C ₃₄ H ₄₀ F ₃ GaN ₂ O ₃ S
M _r (g mol ⁻¹)	580.18	569.84	591.50	683.46
Crystal size (mm)	0.165 x 0.110 x 0.086	0.412 x 0.097 x 0.084	0.176 x 0.161 0.057	0.181 x 0.112 x 0.069
Crystal colour/habit	Colourless prism	Colourless needle	Orange plate	Colourless prism
Crystal system		monoclinic		
Space group	P 2 ₁ /n	P 2 ₁ /c		P 2 ₁ /n
T (K)		110		
<i>a</i> (Å)	10.880(3)	10.349(3)	11.363(3)	8.9347(9)
<i>b</i> (Å)	21.813(5)	19.788(7)	19.068(4)	37.412(4)

	5.1•Et₂O	5.3	5.5	5.7
<i>c</i> (Å)	25.601(7)	18.093(6)	15.329(3)	9.9287(11)
α (°)	90	90	90	90
β (°)	90.49	102.522(6)	106.710(8)	103.962(6)
γ (°)	90	90	90	90
<i>V</i> (Å ³)	6076(3)	3617(2)	3181.3(12)	3220.8(6)
<i>Z</i>	8	4	4	4
F(000)	2432	1200	1264	1424
ρ (g cm ⁻¹)	1.269	1.046	1.235	1.409
λ (Å)	1.54178 (Cu K α)	0.71073 (Mo K α)	1.54178 (Cu K α)	
μ (cm ⁻¹)	3.029	0.854	1.370	2.235
Diffractometer type	Nonius Bruker KappaCCD Apex2	Bruker Kappa Axis Apex2	Nonius Bruker KappaCCD Apex2	
Max 2 θ (°)	134.632	67.738	133.964	135.508
Measd fraction of data	0.923	0.995	0.970	0.980
Reflns measd	36447	203079	30380	23084
Unique reflns	10050	14521	5508	5706
R_{merge}	0.0768	0.0580	0.0748	0.0319
Reflns in refinement	100500	14521	5508	5706
Number of params	710	339	366	402
R_1	0.0538	0.0338	0.0436	0.0401
wR_2	0.1260	0.0848	0.1032	0.1048
R_1 (all data)	0.0907	0.0553	0.0641	0.0447
wR_2 (all data)	0.1445	0.0933	0.1151	0.1079
GOF	1.019	1.020	1.019	1.042
Min/max peak heights on final ΔF map (e Å ⁻¹)	-0.597, 0.603	-0.340, 0.548	-0.273, 0.390	-0.359, 0.674

Table 5.2: Selected crystallographic details for compounds **5.2**, **5.4**, **5.6** and **5.9**.

	5.2	5.6•C₇H₈	5.4	5.9
Formula	C ₁₇ H ₁₇ Cl ₂ GaO	C ₃₁ H ₃₇ Cl ₂ GaN ₂	C ₂₉ H ₃₀ ClGa ₂ N ₂	C ₃₀ H ₃₀ F ₃ GaN ₂ O ₃ S
M_r (g mol ⁻¹)	377.92	578.24	511.72	625.34
Crystal size (mm)	0.177 × 0.126 × 0.089	0.479 × 0.317 × 0.256	0.149 × 0.123 × 0.046	0.241 × 0.102 × 0.052

	5.2	5.6•C ₇ H ₈	5.4	5.9
Crystal colour/habit	colourless prism	colourless prism	colourless prism	colourless plate
Crystal system			monoclinic	
Space group	P 2 ₁ /n	P 2 ₁ /n	P 2 ₁ /c	P n
T (K)	110	112	110	117
a (Å)	7.6614(11)	9.7797(17)	10.5325(19)	17.289(11)
b (Å)	16.740(3)	18.221(5)	15.445(2)	9.933(6)
c (Å)	12.604(2)	16.058(4)	16.207(3)	21.053(14)
α (°)	90	90	90	90
β (°)	90.236(8)	93.681(7)	107.144(8)	112.993(14)
γ (°)	90	90	90	90
V (Å ³)	1616.5(5)	2855.5(11)	2519.4(8)	3328(4)
Z	4	4	4	4
F(000)	768	1208	1064	1288
ρ (g cm ⁻³)	1.553	1.345	1.349	1.248
λ (Å)	1.54178 (Cu Kα)	0.71073 (Mo Kα)	1.54178 (Cu Kα)	0.71073 (Mo Kα)
μ (cm ⁻¹)	5.323	1.173	2.604	0.936
Diffraction type	Nonius Bruker KappaCCD Apex2	Bruker Kappa Axis Apex2	Nonius Bruker KappaCCD Apex2	Bruker Kappa Axis Apex2
Max 2θ (°)	128.9	82.53	128.662	56.694
Measd fraction of data	0.988	0.997	0.987	0.999
Reflns measd	16212	165575	27680	71230
Unique reflns	2681	19039	4169	16467
R _{merge}	0.0408	0.0357	0.0484	0.0644
Reflns in refinement	2681	19039	4169	16467
Number of params	190	328	303	731
R ₁	0.0302	0.0317	0.0332	0.0493
wR ₂	0.0753	0.0765	0.0766	0.1011
R ₁ (all data)	0.0356	0.0504	0.0456	0.0773
wR ₂ (all data)	0.0782	0.0820	0.0825	0.1103
GOF	1.084	1.038	1.033	1.037
Min/max peak heights on final ΔF map (e Å ⁻¹)	-0.382, 0.411	-0.575, 0.568	-0.383, 0.290	-0.367, 0.623

Table 5.3: Selected crystallographic details for compounds **5.8**, **5.10** and **5.11**.

	5.8	5.10 •CH ₂ Cl ₂	5.11
Formula	C ₃₃ H ₄₀ FGaN ₂	C ₃₀ H ₃₂ Cl ₂ FGaN ₂	C ₄₉ H ₅₅ GaN ₂ O ₂
M _r (g mol ⁻¹)	553.39	580.19	773.67
Crystal size (mm)	0.134 x 0.080 x 0.065	0.419 × 0.063 × 0.035	0.213 × 0.180 × 0.105
Crystal colour/habit	colourless prism	colourless needle	colourless prism
Crystal system		monoclinic	
Space group	P 2 ₁ /c		P 2 ₁ /n
T (K)		110	
a (Å)	10.506(4)	9.093(3)	11.472(3)
b (Å)	19.721(11)	33.588(12)	18.590(3)
c (Å)	18.108(9)	9.421(4)	20.025(4)
α (°)	90	90	90
β (°)	105.353(12)	107.129(16)	106.321(11)
γ (°)	90	90	90
V (Å ³)	3618(3)	2749.8(18)	4098.7(15)
Z	4	4	4
F(000)	1168	1200	1640
ρ (g cm ⁻³)	1.016	1.401	1.254
λ (Å)	0.71073 (Mo Kα)		1.54178 (Cu Kα)
μ (cm ⁻¹)	0.784	1.224	1.228
Diffractometer type	Bruker Kappa Axis Apex2		Nonius Bruker KappaCCD Apex2
Max 2θ (°)	56.806	66.338	132.694
Measd fraction of data	0.998	0.998	0.972
Reflns measd	85713	66693	53665
Unique reflns	8995	10480	7007
R _{merge}	0.0880	0.0711	0.0782
Reflns in refinement	8995	10480	7007
Number of params	339	330	494
R ₁	0.0403	0.0462	0.0374
wR ₂	0.0961	0.0904	0.0882
R ₁ (all data)	0.0678	0.0799	0.0511
wR ₂ (all data)	0.1066	0.1004	0.0945
GOF	1.030	1.023	1.043

	5.8	5.10•CH₂Cl₂	5.11
Min/max peak heights on final ΔF map (e \AA^{-1})	-0.439, 0.355	-0.746, 0.771	-0.401, 0.388

Where: $R_1 = \Sigma(|F_o| - |F_c|) / \Sigma F_o$; $wR_2 = [\Sigma(w(F_o^2 - F_c^2)^2) / \Sigma(wF_o^4)]^{1/2}$; $GOF = [\Sigma(w(F_o^2 - F_c^2)^2) / (\text{No. of reflns.} - \text{No. of params.})]^{1/2}$

5.4.12 Additional Details

Specific details for the synthesis of **5.2** and **5.6**, as well as additional X-ray crystallographic details and multinuclear NMR spectroscopic data are presented in Appendix D.

5.5 References

- [1] Power, P.P. *Nature* **2010**, *463*, 171-177.
- [2] Some examples of Ga(I) complexes that undergo small molecule activation and catalysis: a) Jones, C.; Mills, D.P.; Rose, R.P. *J. Organomet. Chem.* **2006**, *691*, 3060-3064; b) Seifert, A.; Scheid, D.; Linti, G.; Zessin, T. *Chem. Eur. J.* **2009**, *15*, 12114-12120; c) Ganesamoorthy, C.; Bläser, D.; Wölper, C.; Schulz, S. *Organometallics* **2015**, *34*, 2991-2996; d) Lichtenthaler, M.R.; Higelin, A.; Kraft, A.; Hughes, S.; Steffani, A.; Plattner, D.A.; Slattery, J.M.; Krossing, I. *Organometallics* **2013**, *32*, 6725-6735; e) Qin, B.; Schneider, U. *J. Am. Chem. Soc.* **2016**, *138*, 13119-13122.
- [3] An example of a gallium(I) with a strongly donating ligand, GaNacNac^{Dipp}: Hardman, N.J.; Eichler, B.E.; Power, P.P. *Chem. Commun.* **2000**, 1991-1992.
- [4] One of the first reports of a digallium compound with formal multiple bond character: He, X.; Bartlett, R.A.; Olmstead, M.M.; Ruhlandt-Senge, K.; Sturgeon, B.E.; Power, P.P. *Angew. Chem., Int. Ed. Engl.* **1993**, *32*, 717-719.

- [5] Other reports of gallium-gallium multiple bonds: a) Li, X.-W.; Pennington, W.T.; Robinson, G.H. *J. Am. Chem. Soc.* **1995**, *117*, 7578-7579; b) Li, X.-W.; Xie, Y.; Schreiner, P.R.; Gripper, K.D.; Crittendon, R.C.; Campana, C.F.; Schaefer, H.F.; Robinson, G.H. *Organometallics* **1996**, *15*, 3798-3803.
- [6] a) Hardman, N.J.; Wright, R.J.; Phillips, A.D.; Power, P.P. *Angew. Chem., Int. Ed.* **2002**, *41*, 2842-2844; b) Hardman, N.J.; Wright, R.J.; Phillips, A.D.; Power, P.P. *J. Am. Chem. Soc.* **2003**, *125*, 2667-2679; c) Zhu, Z.; Fisher, R.C.; Ellis, B.D.; Rivard, E.; Merrill, W.A.; Olmstead, M.M.; Power, P.P.; Guo, J.D.; Nagase, S.; Pu, L. *Chem. Eur. J.* **2009**, *15*, 5263-5272; d) Moilanen, J.; Power, P.P.; Tuononen, H.M. *Inorg. Chem.* **2010**, *49*, 10992-11000
- [7] Su, J.; Li, X.-W.; Crittendon, R.C.; Robinson, G.H. *J. Am. Chem. Soc.* **1997**, *119*, 5471-5472.
- [8] Zhu, Z.; Wang, X.; Peng, Y.; Lei, H.; Fettinger, J.C.; Rivard, R.; Power, P.P. *Angew. Chem., Int. Ed.* **2009**, *48*, 2031-2034.
- [9] a) Zhu, Z.; Wang, X.; Olmstead, M.M.; Power, P.P. *Angew. Chem., Int. Ed.* **2009**, *48*, 2027-2030; b) Caputo, C.A.; Zhu, Z.; Brown, Z.D.; Fettinger, J.C.; Power, P.P. *Chem. Commun.* **2011**, *47*, 7506-7508; c) Caputo, C.A.; Guo, J.-D.; Nagase, S.; Fettinger, J.C.; Power, P.P. *J. Am. Chem. Soc.* **2012**, *134*, 7155-7164; d) Caputo, C.A.; Koivistoinen, J.; Moilanen, J.; Boynton, J.N.; Tuononen, H.M.; Power, P.P. *J. Am. Chem. Soc.* **2013**, *135*, 1952-1960.
- [10] a) Wright, R.J.; Brynda, M.; Fettinger, J.C.; Betzer, A.R.; Power, P.P. *J. Am. Chem. Soc.* **2006**, *128*, 12498-12509; b) Zhu, Z.; Wright, R.J.; Brown, Z.D.; Fox, A.R.; Phillips, A.D.; Richards, A.F.; Olmstead, M.M.; Power, P.P. *Organometallics* **2009**, *28*, 2512-2519; c) Serrano, O.; Hoppe, E.; Power, P.P. *J. Clust. Sci.* **2010**, *21*, 449-460; d) McCrea-Hendrick, M.L.; Caputo, C.A.; Roberts, C.J.; Fettinger, J.C.; Tuononen, H.M.; Power, P.P. *Organometallics* **2016**, *35*, 579-586.
- [11] Examples of Group 14 and Group 15 multiply bonded systems: a) Stender, M.; Phillips, A.D.; Wright, R.J.; Power, P.P. *Angew. Chem., Int. Ed.* **2002**, *41*, 1785-1787;

- b) Yoshifuji, M.; Shima, I.; Inamoto, N.; Hirotsu, K.; Higuchi, T. *J. Am. Chem. Soc.* **1981**, *103*, 4587-4589.
- [12] Spikes, G.H.; Fettinger, J.C.; Power, P.P. *J. Am. Chem. Soc.* **2005**, *127*, 12232-12233.
- [13] a) Stender, M.; Phillips, A.D.; Power, P.P. *Chem. Commun.* **2002**, 1312-1313; b) Cui, C.; Olmstead, M.M.; Power, P.P. *J. Am. Chem. Soc.* **2004**, *126*, 5062-5063; c) Peng, Y.; Ellis, B.D.; Wang, X.; Fettinger, J.C.; Power, P.P. *Science* **2009**, *325*, 1668-1670.
- [14] a) Brook, A.G.; Abdesaken, F.; Gutekunst, B.; Gutekunst, G.; Kallury, R.K. *J. Chem. Soc., Chem. Commun.* **1981**, 191-192; b) Brook, A.G.; Nyburg, S.C.; Abdesaken, F.; Gutekunst, B.; Gutekunst, G.; Kallury, R.K.M.R.; Poon, Y.C.; Chang, Y.-M.; Wong-Ng, W. *J. Am. Chem. Soc.* **1982**, *104*, 5667-5672.
- [15] a) Meyer, H.; Baum, G.; Massa, W.; Berndt, A. *Angew. Chem., Int. Ed. Engl.* **1987**, *26*, 798-799; b) Berndt, A.; Meyer, H.; Baum, G.; Massa, W.; Berger, S. *Pure & Appl. Chem.* **1987**, *59*, 1011-1014; c) Couret, C.; Escudié, J.; Satgé, J.; Lazraq, M. *J. Am. Chem. Soc.* **1987**, *109*, 4411-4412; d) Lazraq, M.; Escudié, J.; Couret, C.; Satgé, J.; Dräger, M.; Dammel, R. *Angew. Chem., Int. Ed. Engl.* **1988**, *27*, 828-829.
- [16] a) Meyer, H.; Baum, G.; Massa, W.; Berger, S.; Berndt, A. *Angew. Chem., Int. Ed. Engl.* **1987**, *26*, 546-548; b) Anselme, G.; Ranaivonjatovo, H.; Escudié, J.; Couret, C.; Satgé, J. *Organometallics* **1992**, *11*, 2748-2750.
- [17] Reviews of silene, germene and stannene chemistry: a) Escudié, J.; Couret, C.; Ranaivonjatovo, H. *Coord. Chem. Rev.* **1998**, *178-180*, 565-592; b) Milnes, K.K.; Pavelka, L.C.; Baines, K.M. *Chem. Soc. Rev.* **2016**, *45*, 1019-1035; c) Ottosson, H.; Steel, P.G. *Chem. Eur. J.* **2005**, *12*, 1576-1585; d) Baines, K.M.; Samuel, M.S. Product Subclass 2: Silenes. In *Science of Synthesis, 4: Category 1, Organometallics*; Fleming, I., Ed.; Georg Thieme Verlag: Stuttgart, 2002; e) Takeda, N.; Tokitoh, N.; Okazaki, R. Product Subclass 6: Germenes. In *Science of Synthesis, 5: Category 1, Organometallics*; Moloney, M.G., Ed.; Georg Thieme Verlag: Stuttgart, 2003; f) Mizuhata, Y.; Tokitoh, N.

Stannenes, distannenes, and stannynes. In *Tin Chemistry*; Davies, A.G.; Gielen, M.; Pannell, K.H.; Tiekink, E.R., Eds.; John Wiley & Sons: Chichester, 2008; pp 177-200.

[18] a) Mathey, F. *Angew. Chem., Int. Ed.* **2003**, *42*, 1578-1604; b) Bates, J.I.; Dugal-Tessier, J.; Gates, D.P. *Dalton Trans.* **2010**, *39*, 3151-3159.

[19] Weber, L. *Chem. Ber.* **1996**, *129*, 367-379.

[20] a) Pavelka, L.C.; Milnes, K.K.; Baines, K.M. *Chem Mater.* **2008**, *20*, 5948-5950;

b) Pavelka, L.C.; Holder, S.J.; Baines, K.M. *Chem. Commun.* **2008**, 2346-2348; c)

Tsang, C.-W.; Yam, M.; Gates, D.P. *J. Am. Chem. Soc.* **2003**, *125*, 1480-1481.

[21] Tashkandi, N.Y.; Parsons, F.; Guo, J.; Baines, K.M. *Angew. Chem., Int. Ed.* **2015**, *54*, 1612-1615.

[22] a) Klusik, H.; Berndt, A. *Angew. Chem., Int. Ed. Engl.* **1983**, *22*, 877-878; b)

Frenking, G.; Schaefer III, H.F. *Chem. Phys. Lett.* **1984**, *109*, 521-524; c) Glaser, B.;

Nöth, H. *Angew. Chem., Int. Ed. Engl.* **1985**, *24*, 416-417; d) Olmstead, M.M.; Power,

P.P.; Weese, K.J.; Doedens, R.J. *J. Am. Chem. Soc.* **1987**, *109*, 2542-2544; e) Tapper,

A.; Schmitz, T.; Paetzold, P. *Chem. Ber.* **1989**, *122*, 595-601; f) Paetzold, P.; Englert,

U.; Finger, R.; Schmitz, T.; Tapper, A.; Ziembinski, R. *Z. Anorg. Allg. Chem.* **2004**, *630*, 508-518.

[23] a) Li, X.-W.; Su, J.; Robinson, G.H. *Chem. Commun.* **1996**, 2683-2684; b)

Baker, R.J.; Jones, C. *Appl. Organometal. Chem.* **2003**, *17*, 807-808; c) Stasch, A.;

Singh, S.; Roesky, H.W.; Noltemeyer, M.; Schmidt, H.-G. *Eur. J. Inorg. Chem.* **2004**,

4052-4055; d) Marion, N.; Escudero-Adán, E.C.; Benet-Buchholz, J.; Stevens, E.D.;

Fensterbank, L.; Malacria, M.; Nolan, S.P. *Organometallics* **2007**, *26*, 3256-3259; e)

Alexander, S.G.; Cole, M.L.; Furfari, S.K.; Kloth, M. *Dalton Trans.* **2009**, 2909-2911;

f) Cole, M.L.; Furfari, S.K.; Kloth, M. *J. Organomet. Chem.* **2009**, *694*, 2934-2940; g)

El-Hellani, A.; Monot, J.; Guillot, R.; Bour, C.; Gandon, V. *Inorg. Chem.* **2013**, *52*, 506-

514; h) Tang, S.; Monot, J.; El-Hellani, A.; Michelet, B.; Guillot, R.; Bour, C.; Gandon,

V. *Chem. Eur. J.* **2012**, *18*, 10239-10243; i) Bour, C.; Monot, J.; Tang, S.; Guillot, R.;

- Farjon, J.; Gandon, V. *Organometallics* **2014**, *33*, 594-599; j) Swarnakar, A.K.; Ferguson, M.J.; McDonald, R.; Rivard, E. *Dalton Trans.* **2017**, *46*, 1406-1412.
- [24] a) Schmidbaur, H.; Nogai, S.D. *Z. Anorg. Allg. Chem.* **2004**, *630*, 2218-2225; b) Timoshkin, A.Y.; Bodensteiner, M.; Sevastianova, T.N.; Lisovenko, A.S.; Davydova, E.I.; Scheer, M.; Graßl, C.; Butlak, A.V. *Inorg. Chem.* **2012**, *51*, 11602-11611; c) Vasko, P.; Kinnunen, V.; Moilanen, J.O.; Roemmele, T.L.; Boéré, R.T.; Konu, J.; Tuononen, H.M. *Dalton Trans.* **2015**, *44*, 18247-18259.
- [25] Escudie, J.; Couret, C.; Satge, J.; Andrianarison, M.; Andriamizaka, J.-D. *J. Am. Chem. Soc.* **1985**, *107*, 3378-3379.
- [26] Allan, C.J.; Reinhold, C.R.W.; Pavelka, L.C.; Baines, K.M. *Organometallics* **2011**, *30*, 3010-3017.
- [27] Literature reports of gallium-mesityl compounds: a) Beachley, Jr., O.T.; Churchill, M.R.; Pazik, J.C.; Ziller, J.W. *Organometallics* **1987**, *6*, 2088-2093; b) Beachley, Jr., O.T.; Churchill, M.R.; Pazik, J.C.; Ziller, J.W. *Organometallics* **1986**, *5*, 1814-1817; c) Petrie, M.A.; Power, P.P.; Dias, H.V.R.; Ruhlandt-Senge, K.; Waggoner, K.M.; Wehmschulte, R.J. *Organometallics* **1993**, *12*, 1086-1093; d) Neumüller, B.; Gahlmann, F. *Z. Anorg. Allg. Chem.* **1992**, *612*, 123-129; e) Neumüller, B.; Gahlmann, F. *Angew. Chem., Int. Ed.* **1993**, *32*, 1701-1702; f) Quillian, B.; Wei, P.; Wannere, C.S.; Schleyer, P.v.R.; Robinson, G.H. *J. Am. Chem. Soc.* **2009**, *131*, 3168-3169.
- [28] a) Barlow, B.C.; Burgess, I.J. *Langmuir* **2007**, *23*, 1555-1563; b) Higgins, E.M.; Sherwood, J.A.; Lindsay, A.G.; Armstrong, J.; Massey, R.S.; Alder, R.W.; O'Donoghue, A.M.C. *Chem. Commun.* **2011**, *47*, 1559-1561.
- [29] Clavier, H.; Nolan, S.P. *Chem. Commun.* **2010**, *46*, 841-861.
- [30] a) Rugar, P.A.; Staroverov, V.N.; Ragona, P.J.; Baines, K.M. *J. Am. Chem. Soc.* **2007**, *129*, 15138-15139; b) Ellis, B.D.; Dyker, C.A.; Decken, A.; Macdonald, C.L.B. *Chem. Commun.* **2005**, 1965-1967.
- [31] a) Gebreyesus, M.A.; Purusthatham, Y.; Kumar, J.S. *Heliyon* **2016**, *2*, article e00134; b) Wynn, D.A.; Roth, M.M.; Pollard, B.D. *Talanta* **1984**, *31*, 1036-1040.

- [32] a) Delpon-Lacaze, G.; de Battisti, C.; Couret, C. *J. Organomet. Chem.* **1996**, *514*, 59-66; b) Schmohl, K.; Reinke, H.; Oehme, H. *Eur. J. Inorg. Chem.* **2001**, 481-489; c) Milnes, K.K.; Baines, K.M. *Organometallics* **2007**, *26*, 2392-2401.
- [33] Lazraq, M.; Couret, C.; Escudie, J.; Satgé, J.; Dräger, M. *Organometallics* **1991**, *10*, 1771-1778.
- [34] Kuhn, N.; Kratz, T. *Synthesis* **1993**, *6*, 561-562.
- [35] Note: C₁ is assigned to the carbon of the fluorenyl group with the most deshielded hydrogen nucleus, and follows the customary numbering system for this group.
- [36] Bruker-AXS, SAINT version 2013.8, **2013**, Bruker-AXS, Madison, WI 53711, USA.
- [37] Bruker-AXS, SADABS version 2012.1, **2012**, Bruker-AXS, Madison, WI 53711, USA.
- [38] Bruker-AXS, TWINABS version 2012.1, **2012**, Bruker-AXS, Madison, WI 53711, USA
- [39] Sheldrick, G. M., *Acta Cryst.* **2015**, *A71*, 3-8.
- [40] Sheldrick, G. M., *Acta Cryst.* **2015**, *C71*, 3-8.
- [41] Bruker-AXS, XP version 2013.1, **2013**, Bruker-AXS, Madison, WI 53711, USA.

Chapter 6

6 Summary, Conclusions and Future Work

6.1 Summary and Conclusions

The work presented herein addresses the primary goals of the thesis: the synthesis of novel gallium compounds from commercially available or easily synthesized ligands, the characterization of new gallium complexes by computational and innovative experimental techniques, and the exploration of the reactivity of the novel gallium compounds. All of the identified objectives of the thesis are related to the generation of new main group compounds for the activation of small molecules and catalysis.

The synthesis of $[\text{Ga}_3\text{Cl}_4(\text{crypt-222})][\text{GaCl}_4]$, **2.1**, and $[\text{Ga}_2\text{Cl}_2(\text{crypt-222})][\text{OTf}]_2$, **2.2**, revealed the ability of the commercially available cryptand[2.2.2] ligand to complex multiple gallium centres within the cavity of the macrocycle. The $[\text{Ga}_3\text{Cl}_4]^+$ (**2.1**) and $[\text{Ga}_2\text{Cl}_2]^{2+}$ (**2.2**) cores represent the first bimetallic complexes using cryptand[2.2.2] as a stabilizing ligand. The multi-centred gallium cations exhibit vastly different coordination modes compared to germanium(II) and tin(II) complexes of cryptand[2.2.2]. The germanium(II) complex was found to have a naked dication within the macrocycle, whereas two different structures were observed for tin(II) complexes of cryptand[2.2.2]: a naked tin(II) dication similar to germanium(II) when triflate was used as a counteranion, and a tin(II) with a strongly bound halide ligand when tin(II) halides were employed as starting materials.¹ The coordination chemistry of low valent main group cations using macrocyclic ethers such as cryptand[2.2.2] resulted in the generation of novel molecular structures, adding to the small library of ligand-stabilized multi-centred low valent gallium cations that have been reported in the literature.²

The results of the XPS and XAS studies of the experimental chemical states of **2.1**, **2.2**, $[\text{Ga}_2\text{I}_2(\text{crypt-222})][\text{GaI}_4]_{1.75}[\text{OTf}]_{0.25}$ (**3.1**) and other known gallium compounds led to two main conclusions: widely accessible XPS instruments allow for the facile

experimental determination of the electronic environment of the gallium centre in molecular compounds, and XAS experiments are of sufficiently high resolution to enable the deconvolution of signals arising from different gallium centres in a multi-valent or multi-centred species. When gallium(II) and gallium(III) compounds were analyzed by XPS using Wagner plots, their assigned oxidation numbers generally corresponded to their experimentally determined chemical state, although slight variations were observed. The gallium-cryptand species **2.1**, **2.2** and **3.1** were shown to have an intermediate chemical state most similar to those of gallium(II) species. When gallium(I) species were analyzed using XPS, a range of empirical chemical states were observed which were highly dependent on the nature of the ligand used to stabilize the gallium(I) centre. For example, the macrocycle-stabilized gallium(I) cation [Ga(prismand)][OTf] was found to have a chemical state similar to gallium(II)/gallium(III) species based on its location on the Wagner plot, allowing for the [Ga(prismand)]⁺ cation to be described as electron deficient at gallium. The location of the electron deficient gallium(I) compounds on the Wagner plot is counter to what is often thought of for gallium(I) species, as they are presumed, with a lone pair at gallium, to be electron rich. Our study has revealed the stark differences between cationic gallium(I) species and neutral or anionic gallium(I) species with covalently-bound ligands, such as GaNacNac^{Dipp}, where the ligand drastically influences the electronic environment and reactivity of a main group complex. We have demonstrated that XPS experimental data can be invaluable in the prediction and rationalization of the reactivity of main group complexes.

In instances where multiple gallium centres are present in one complex, such as in **2.1**, **2.2**, Ga₂Cl₄ ([Ga][GaCl₄]) and [Ga(prismand)][GaCl₄], the resolution of the XPS instrument was not sufficient to observe multiple signals from the different sites. When XAS experiments were performed on these complexes, resolution of the signals was achieved. In addition to observing energy differences depending on the gallium sites, the fine structure of the absorption spectra of the complexes gave detailed information about the electronic environment and bonding when analyzed in conjunction with computational work. The XAS data also provided some information regarding the nature

of the interactions between the cation and anion in $[\text{Ga}][\text{GaCl}_4]$ and $[\text{Ga}(\text{prismand})][\text{GaCl}_4]$; there is significant charge transfer between the gallium(I) cation and tetrachlorogallate anion in the former, however in the latter, the presence of the macrocyclic ligand effectively sequesters the gallium(I) cation from the anion and there is minimal interaction. While the XAS spectrum of **2.2** demonstrated a single type of gallium centre (Ga(II)) with significant core-ligand interactions, **2.1** was more difficult to analyze, as significant electron motility and delocalization within the $[\text{Ga}_3\text{Cl}_4]^+$ cationic core contributed to an overall electronic environment similar to the gallium(II) centres in **2.2**, supporting the conclusions from the XPS data.

The low valent gallium macrocyclic ether-stabilized salt, **4.1**, was readily synthesized from $[\text{Ga}][\text{GaCl}_4]$ and 12-crown-4. Due to the presence of the reactive $[\text{GaCl}_4]^-$ anion, an anion exchange was performed to give **4.3** with a weakly coordinating borate anion. **4.3** was analyzed using XPS and, similar to the $[\text{Ga}(\text{prismand})]^+$ cation, the $[\text{Ga}(12\text{-crown-4})]^+$ cation was found to be electrophilic in nature, again reinforcing that gallium(I) compounds can be isolated with a range of chemical states. In addition, **4.1** and **4.3** were found to be stable to donor solvents, a characteristic that is rare among gallium(I) compounds.³ The synthesis of Cp^*Ga , **4.4**, and **4.5** from **4.3** demonstrated the utility of this macrocycle-stabilized gallium(I) cation as an efficient source of gallium(I). This crown ether-stabilized gallium(I) starting material offers new possibilities in the synthesis of novel gallium(I) complexes that may exhibit unique electronic and structural properties, leading to unprecedented reactivity.

Compounds containing main group element-carbon double bonds exist for nearly all Group 14 and Group 15 elements; however, a compound with a boron-carbon double bond is the only example from Group 13. Therefore, the synthesis of a compound with a gallium-carbon double bond, a gallene, was targeted.⁴ A donor stabilization strategy was employed using an NHC and DMAP as donor ligands,⁵ and the syntheses of two gallene precursors, **5.8** and **5.10** were achieved. **5.8** and **5.10** were subsequently reacted with a strong base to form the desired gallene; the isolation of cycloadduct **5.11** using

tolualdehyde as a trapping agent gave evidence supporting the generation of an intermediate gallene. Our report is the first example of a gallium-carbon doubly bonded species which undergoes a unique reaction where two equivalents of tolualdehyde add to the gallene. Further work is required to verify that **5.11** formed as a result of an intermediate gallene. The synthetic pathway provides a promising route to stabilize monomeric, neutral organogallium compounds that can be selectively substituted with various organic and halide ligands.

The work outlined throughout this thesis describes not only the synthesis and reactivity of new gallium containing species, but also the use of spectroscopic techniques that are rarely employed for molecular systems. The chemistry described herein may facilitate the discovery of new gallium species that are capable of activating small molecules or as catalysts. We have demonstrated that XPS and XAS can be used to identify appropriate avenues of reactivity to explore. The results contribute to an understanding of the coordination and organometallic chemistry of gallium compounds, while also igniting a discussion about the value of assigned oxidation numbers as the only gauge of the chemical state of novel main group species. The study also provides a new, readily accessible and well defined gallium(I) starting material for the synthetic chemist's toolbox.

6.2 Future Work

6.2.1 Utilizing XPS for Other Main Group Elements

Recent work in our group has focussed on using solid-state NMR spectroscopic techniques for chemical state determination of germanium and tin compounds.^{1b,6} The work presented in Chapter 3 has the same goal, however, XPS was used. There are many draw backs to using solid-state NMR spectroscopy for oxidation number determination, such as the breadth of signals, especially for quadrupolar nuclei. Thus, using XPS to study the experimental chemical state of germanium and tin compounds could allow for the more facile characterization of the electronic environments of Group 14 complexes. As with the XPS study of gallium complexes, there may be significant variability in the

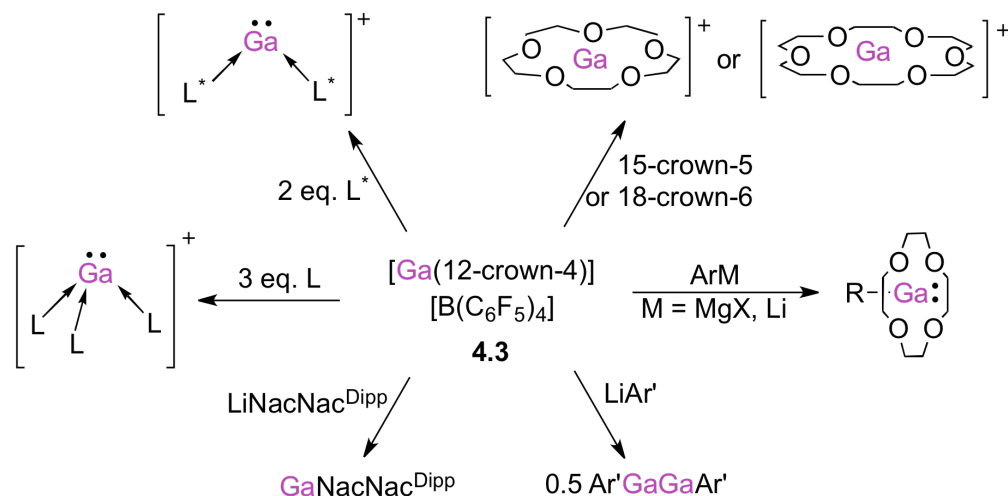
chemical state of compounds with the same oxidation number. Additionally, a comparison of the conclusions drawn from the SSNMR and XPS data sets for germanium and tin compounds will facilitate further analysis and interpretation. Conversely, SSNMR techniques could also be compared to the XPS and XAS data reported in Chapter 3 by performing ^{71}Ga SSNMR spectroscopy on gallium compounds, achieving a similar outcome.

The XPS spectra of additional gallium complexes, in particular those that undergo small molecule activation or catalysis, should be recorded and analyzed to determine whether the chemical state as determined by XPS can provide insights into the reactivity observed.

6.2.2 The Use of $[\text{Ga}(12\text{-crown-4})]^+$ as a Widely Applicable Source of Gallium(I)

While **4.3** has been shown to be a clean, donor solvent-stable starting material for gallium(I) compounds, additional examples are needed to illustrate the scope of the chemistry and the effectiveness of **4.3** as a starting material. The reaction of **4.3** with strong electron donors, such as NHCs (L and L^* , where L^* is a bulky donor ligand; Scheme 6.1) may lead to the synthesis of novel gallium(I) complexes. The addition of moderately bulky aryl groups to **4.3** (ArM , Scheme 6.1) may lead to a 12-crown-4 stabilized organogallium(I) complex. The 12-crown-4 ligand in $\text{ArGa}(12\text{-crown-4})$ (Scheme 6.1) may act as an additional stabilizing ligand for a substituted, neutral gallium(I) species and prevent oligomerization. $\text{ArGa}(12\text{-crown-4})$ may exhibit enhanced reactivity due to increased electron density at gallium as a result of the covalently bound organic ligand. The syntheses of useful gallium(I) compounds, such as $\text{GaNaCNac}^{\text{Dipp}}$,⁷ $\text{Ar}'\text{GaGaAr}'^8$ and the larger scale synthesis of Cp^*Ga^9 should be performed to demonstrate the versatility of **4.3** as a source of gallium(I). Furthermore, a detailed comparison of the new and the literature methods should be carried out to determine which methods are most efficient (Scheme 6.1). A facile method for the removal of the crown ether that is formed as a by-product of these reactions will also be required.

Reactions of **4.3** with tributyl- and triphenylphosphine oxide produced oils as products that were contaminated with free crown ether, which was difficult to separate. The removal of the crown ether may be possible through vacuum distillation or complexation of the free macrocycle using a lithium salt, resulting in the precipitation of [Li(12-crown-4)][X].



Scheme 6.1: Reactivity of **4.3** with donor and organic ligands.

The synthesis of salts with different counteranions for the [Ga(12-crown-4)]⁺ cation should be explored. The perfluorinated borate salt ([Ph₃C][B(C₆F₅)₄]) used to generate [(Et₃Si)₂(μ-H)][B(C₆F₅)₄], which was then reacted with **4.1** to give **4.3** ([Ga(12-crown-4)][B(C₆F₅)₄]), is moderately expensive. Despite numerous reactions with large excesses of NaBPh₄ and NMe₄BPh₄, and attempts to remove the [GaCl₄]⁻ anion using cheaper electrophilic reagents such as TMSOTf, Ph₃SiOTf and [Ph₃C]⁺, none have been successful to date. Identification of a more cost effective alternative would make the [Ga(12-crown-4)]⁺ cation become a more widely used gallium(I) synthon.

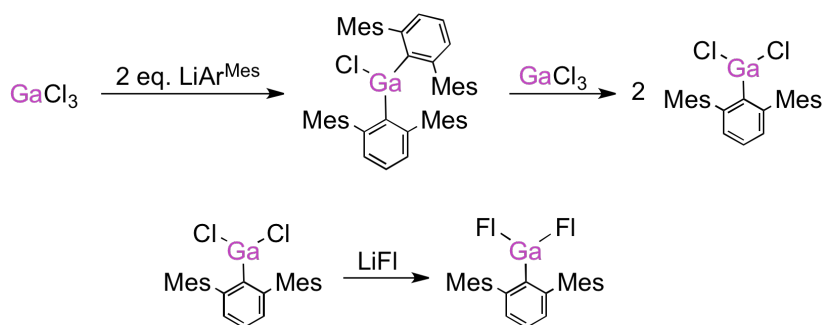
The synthesis of 15-crown-5 and 18-crown-6 complexes of gallium(I) and their reactivity should be examined (Scheme 6.1). The reactivity of [Ga(15-crown-5)]⁺ and [Ga(18-crown-6)]⁺ cations is expected to be greater than that of the 12-crown-4 analogue due to the additional electron density at the gallium centre. Synthesis of a [Ga(15-crown-

5)]⁺ cation from Ga₂Cl₄ and 15-crown-5 was attempted and, although spectroscopic data suggested that the gallium(I) cation formed, upon dissolution of the product in acetonitrile, numerous products were observed by ¹H NMR spectroscopy. Two compounds were characterized by X-ray crystallography and were postulated to arise from the reaction between the [Ga(15-crown-5)]⁺ cation and the [GaCl₄]⁻ anion (Appendix C). The increased reactivity of the [Ga(15-crown-5)]⁺ cation toward the tetrachlorogallate anion in comparison to the 12-crown-4 derivative suggests that the reactivity of gallium(I) complexes with larger crown ethers as ligands may be increased to the point where significant activation of small molecules could occur. Thus, the synthesis of [Ga(15-crown-5)]⁺ and [Ga(18-crown-6)]⁺ salts with an innocent anion and the reactivity of these complexes should be explored as potential catalysts. The electron density at the gallium(I) cation in the 15-crown-5 and 18-crown-6 cations should be assessed using XPS. Comparison of the reactivity of the cations to the XPS data and the calculated HOMO-LUMO gap of the three gallium(I) cations should also be performed to determine what insights these techniques may offer.

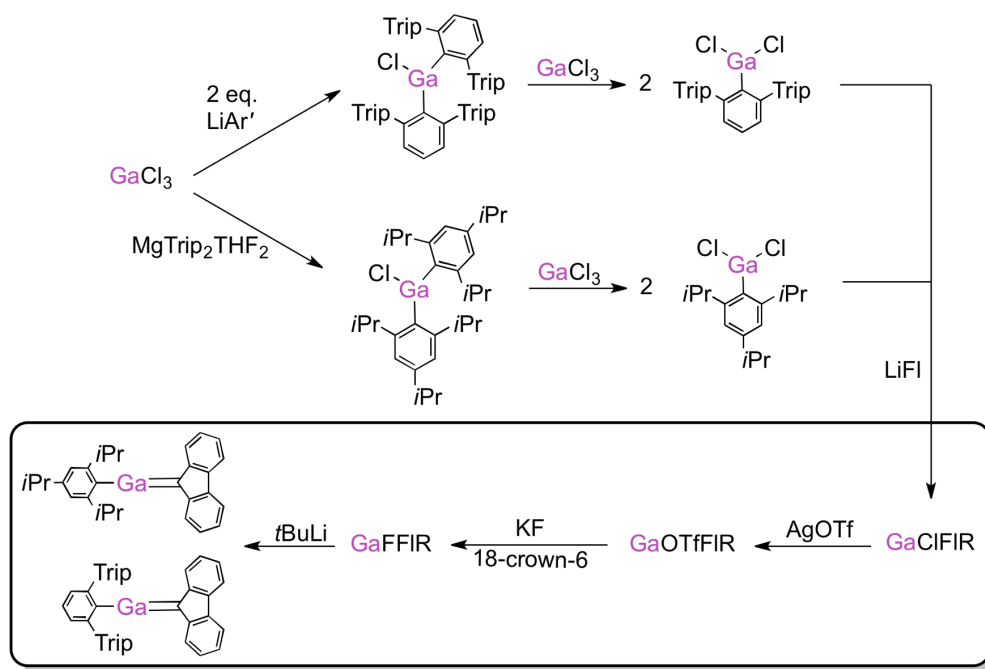
6.2.3 The Use of Bulkier Ligands for the Synthesis of Gallenes

Our synthetic route to the gallene utilized a donor ligand to stabilize the monomeric, neutral organogallium species. An alternate method can be envisioned which takes advantage of steric, rather than electronic, stabilization. Dichloro-2,6-dimesitylphenylgallane (Ar^{*}GaCl₂) was identified as a promising starting material in this regard. As the reported synthesis of Ar^{*}GaCl₂¹⁰ produces the dichloride in very low yield, a new synthetic route to Ar^{*}GaCl₂, utilizing a redistribution reaction similar to that used in the synthesis of GaCl₂Mes,¹¹ was devised (Appendix D). (Ar^{*})₂GaCl¹² and GaCl₃ were reacted to give Ar^{*}GaCl₂ in high yield. However, the reaction of Ar^{*}GaCl₂ with LiFl gave the difluorenylated product, Ar^{*}GaFl₂, as a minor component of the resultant mixture, as determined by ¹H NMR spectroscopy and an X-ray crystallographic structure of poor quality (Scheme 6.2). Thus, the synthesis of organogallium(III) starting materials possessing various bulky aryl ligands should be performed: dichloro-2,6-bis(2,4,6-triisopropylphenyl)phenylgallane (Ar'^{*}GaCl₂)¹³ and dichloro-2,4,6-triisopropylgallane

(TripGaCl₂)¹⁴ are two examples with different steric demand at the gallium centre. If Ar'^{*}GaCl₂ or TripGaCl₂ resulted in the desired non-donor stabilized RGaClFI complex upon reaction with LiFI (Scheme 6.3), the RGaClFI complex could be converted to its triflate and subsequently its fluoride derivative, giving a gallene precursor utilizing steric stabilization. Generation of the gallene and comparing its reactivity to the donor-stabilized examples should be performed in future work.



Scheme 6.2: Synthesis of Ar^{*}GaCl₂ and its reaction with LiFI.



Scheme 6.3: Synthesis of substituted phenyl gallium dichlorides and the pathway to two sterically stabilized gallenes.

The work presented in this thesis is expected to impact the Group 13 community, and can be easily expanded to other elements such as germanium and tin in the case of the XPS work, to the synthesis of novel gallium(I) complexes using the $[\text{Ga}(12\text{-crown-}4)]^+$ cation as a synthon and the synthesis of isolable gallenes using steric stabilization. Although no examples of small molecule activation or catalysis using low valent gallium complexes were demonstrated in the experimental results of this thesis, much of the work can be considered as foundational and fundamental; the synthetic work with the gallium(I)-crown ether complexes and the spectroscopic results using XPS could be directly utilized in the directed synthesis of new catalytic gallium(I) species. The chemistry of gallium and low valent forms of the Group 13 elements can, in the words of A.J. Downs, be described as “erratic”;¹⁵ although that may not be evident throughout this thesis, I can attest to the fact that many hypotheses turn out to be false, often in the most frustrating yet elegant ways.

6.3 References

- [1] a) Rugar, P.A.; Staroverov, V.N.; Baines, K.M. *Science* **2008**, *322*, 1360-1363; b) Avery, J.C.; Hanson, M.A.; Herber, R.H.; Bladek, K.J.; Rugar, P.A.; Nowik, I.; Huang, Y.; Baines, K.M. *Inorg. Chem.* **2012**, *51*, 7307-7316.
- [2] a) Linti, G.; Zessin, T. *Dalton Trans.* **2011**, *40*, 5591-5598; b) Kuchta, M.C.; Bonanno, J.B.; Parkin, G. *J. Am. Chem. Soc.* **1996**, *118*, 10914-10915; c) Malbrecht, B.J.; Dube, J.W.; Willans, M.J.; Ragogna, P.J. *Inorg. Chem.* **2014**, *53*, 9644-9656.
- [3] Two examples: a) Schmidt, E.S.; Schier, A.; Schmidbaur, H. *J. Chem. Soc., Dalton Trans.* **2001**, 505-507; b) Kunze, A.; Gleiter, R.; Bethle, S.; Rominger, F. *Organometallics* **2006**, *25*, 4787-4791.
- [4] Couret, C.; Escudie, J.; Satge, J.; Lazraq, M. *J. Am. Chem. Soc.* **1987**, *109*, 4411-4412.
- [5] Glaser, B.; Nöth, H. *Angew. Chem., Int. Ed. Engl.* **1985**, *24*, 416-417.

- [6] a) Hanson, M.A.; Sutrisno, A.; Terskikh, V.V.; Baines, K.M.; Huang, Y. *Chem. Eur. J.* **2012**, *18*, 13770-13779; b) Hanson, M.A.; Terskikh, V.V.; Baines, K.M.; Huang, Y. *Inorg. Chem.* **2014**, *53*, 7377-7388.
- [7] Hardman, N.J.; Eichler, B.E.; Power, P.P. *Chem. Commun.* **2000**, 1991-1992.
- [8] a) Hardman, N.J.; Wright, R.J.; Phillips, A.D.; Power, P.P. *Angew. Chem. Int. Ed.* **2002**, *41*, 2842-2844; b) Hardman, N.J.; Wright, R.J.; Phillips, A.D.; Power, P.P. *J. Am. Chem. Soc.* **2003**, *125*, 2667-2679.
- [9] Loos, D.; Schnöckel, H. *J. Organomet. Chem.* **1993**, *463*, 37-40.
- [10] Crittendon, R.C.; Li, X.-W.; Su, J.; Robinson, G.H. *Organometallics* **1997**, *16*, 2443-2447.
- [11] Beachley, Jr., O.T.; Churchill, M.R.; Pazik, J.C.; Ziller, J.W. *Organometallics* **1987**, *6*, 2088-2093.
- [12] Li, X.-W.; Pennington, W.T.; Robinson, G.H. *Organometallics* **1995**, *14*, 2109-2111.
- [13] Reported synthesis of $\text{Ar}'\text{GaCl}_2$; depending on the success of initial reactions, redistribution from $(\text{Ar}')_2\text{GaCl}$ and GaCl_3 would be attempted: Twamley, B.; Power, P.P. *Chem. Commun.* **1999**, 1805-1806.
- [14] Reported synthesis of Trip_2GaCl : Petrie, M.A.; Power, P.P.; Rasika Dias, H.V.; Ruhlandt-Senge, K.; Waggoner, K.M.; Wehmschulte, R.J. *Organometallics* **1993**, *12*, 1086-1093.
- [15] Downs, A.J. Chemistry of the Group 13 metals: some themes and variations. In *Chemistry of Aluminium, Gallium, Indium and Thallium*; Downs, A.J., Ed.; Blackie Academic & Professional: Glasgow, 1993; p 12.

Appendices

Appendix A: Supplementary Information for Chapter 2

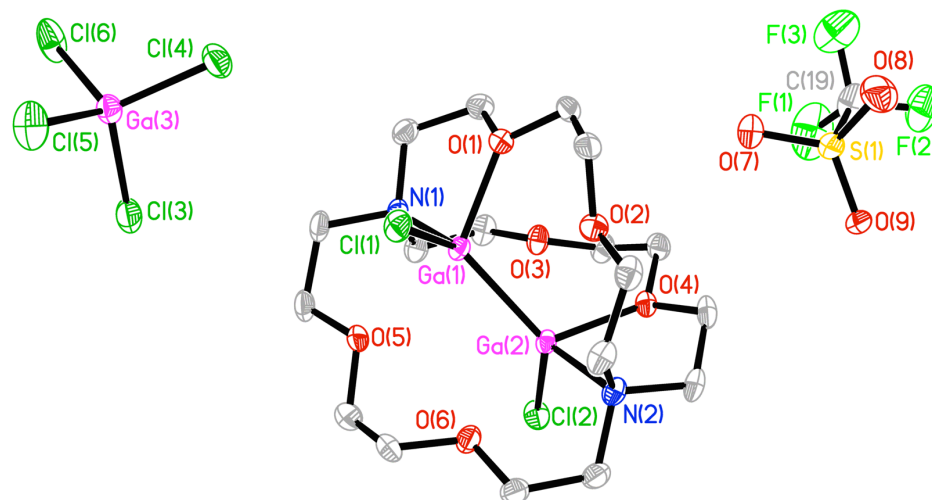


Figure A.1: Displacement ellipsoid plot of **2.2a**. Ellipsoids are drawn at 50% probability level and anion disorder, solvent, and hydrogen atoms are omitted for clarity.

Table A.1: Bond lengths, angles and torsions around the gallium centres in **2.2a**.

Parameter	Ga(1)	Ga(2)
Ga-Ga	2.3787(7) Å	
Ga-Cl	2.1786(9) Å	2.1876(8) Å
Ga-N	2.046(2) Å	2.072(2) Å
Ga-O	2.0858(18) Å	2.0963(17) Å
O-Ga-N	82.18(8)°	81.34(8)°
O-Ga-Cl	92.35(6)°	92.74(5)°
O-Ga-Ga	114.87(4)°	114.94(5)°
N-Ga-Cl	107.92(6)°	108.77(6)°
N-Ga-Ga	118.96(7)°	120.34(6)°
Cl-Ga-Ga	127.66(3)°	125.79(3)°
O-Ga-Ga-O	-6.62(9)°	

Table A.2: Crystallographic details for **2.2a**.

2.2a	
Formula	C ₁₉ H ₃₆ Cl ₆ F ₃ Ga ₃ N ₂ O ₉ S•C ₆ H ₆
FW (g/mol)	1025.52
Crystal Size (mm)	0.194 x 0.158 x 0.046
Crystal Colour/Habit	colourless plate
Crystal System	triclinic
Space Group	P -1
Temperature, K	110
<i>a</i> , Å	12.120(4)
<i>b</i> , Å	13.199(3)
<i>c</i> , Å	14.943(4)
α , °	68.818(9)
β , °	84.757(10)
γ , °	65.916(7)
<i>V</i> , Å ³	2030.6(10)
<i>Z</i>	2
F(000)	1032
ρ (g/cm)	1.677
λ , Å	0.71073 (MoK α)
μ , cm ⁻¹	2.482
Diffractometer Type	Bruker Kappa Axis Apex2
Max 2 θ for Data Collection, °	63.216
Measd Fraction of Data	0.997
No. Rflns Measd	78739
Unique Rflns Measd	13398
<i>R</i> _{merge}	0.0597
No. Rflns in Refinement	13398
<i>R</i> ₁	0.0439
w <i>R</i> ₂	0.0919
<i>R</i> ₁ (all data)	0.0902
w <i>R</i> ₂ (all data)	0.1059
GOF	1.026
Min, Max Peak Heights on final ΔF map (e/Å)	-0.854, 0.760

Where: $R_1 = \Sigma(|F_o| - |F_c|) / \Sigma F_o$; $wR_2 = [\Sigma(w(F_o^2 - F_c^2)^2) / \Sigma(w F_o^4)]^{1/2}$; $GOF = [\Sigma(w(F_o^2 - F_c^2)^2) / (\text{No. of reflns.} - \text{No. of params.})]^{1/2}$

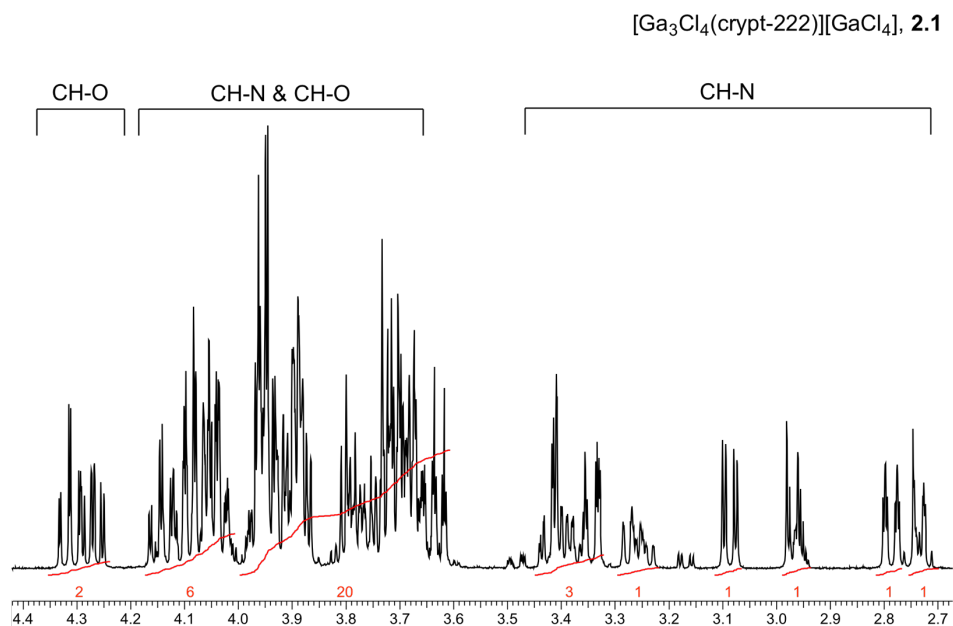


Figure A.2: ¹H NMR spectrum of **2.1** in CD₃CN at 600 MHz.

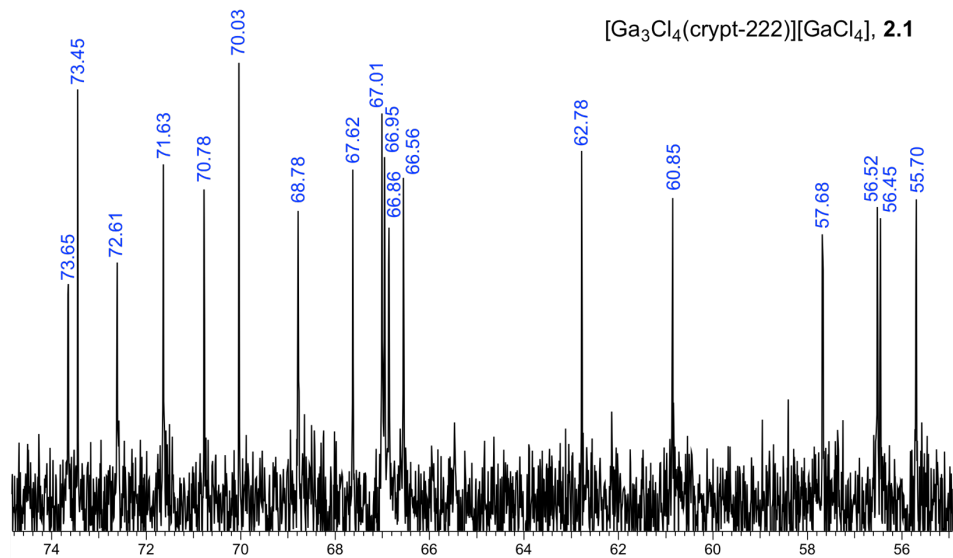


Figure A.3: ¹³C{¹H} NMR spectrum of **2.1** in CD₃CN at 151 MHz.

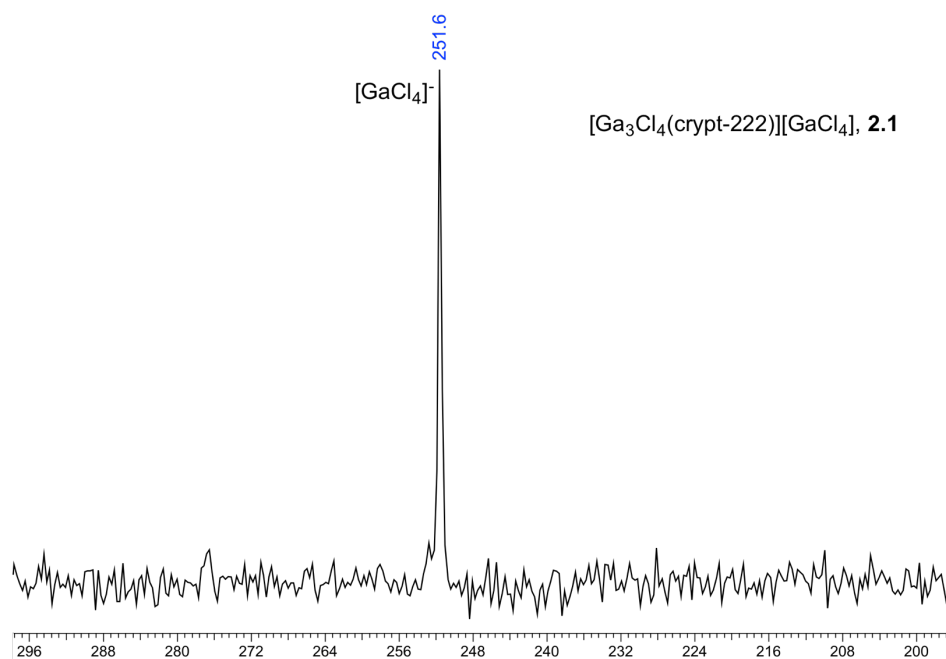


Figure A.4: $^{71}\text{Ga}\{^1\text{H}\}$ NMR spectrum of **2.1** in CD_3CN at 183 MHz.

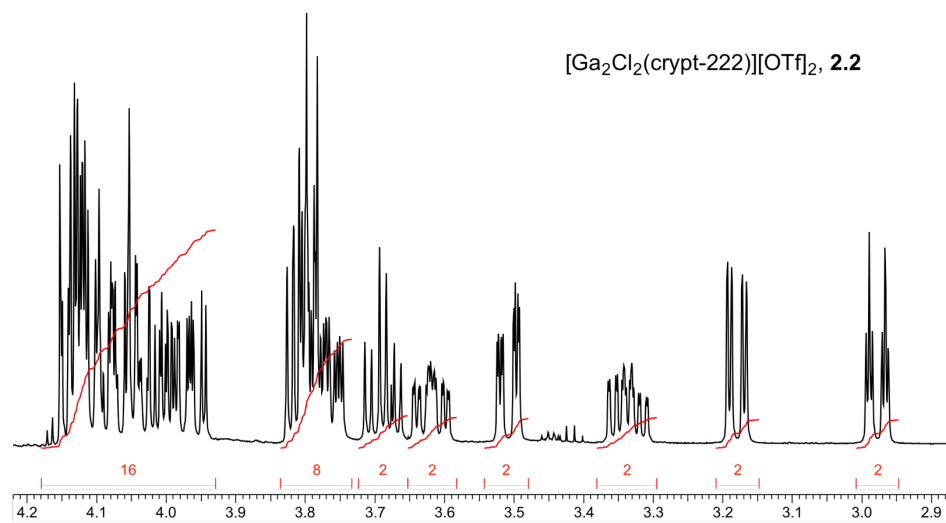


Figure A.5: ^1H NMR spectrum of **2.2** in CD_3CN at 600 MHz.

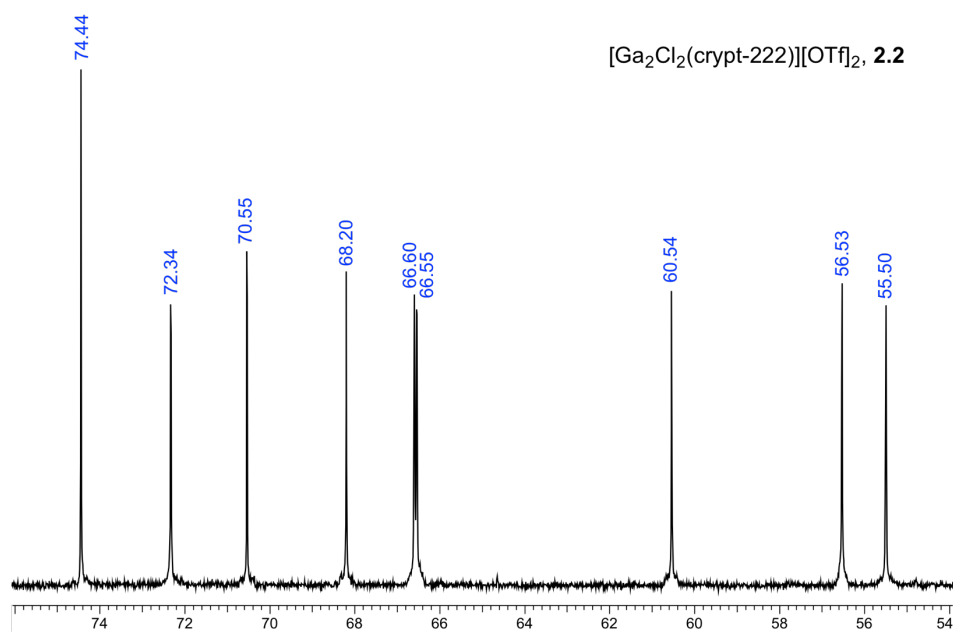


Figure A.6: $^{13}\text{C}\{^1\text{H}\}$ NMR spectrum of **2.2** in CD_3CN at 151 MHz. The triflate signal was omitted for clarity.

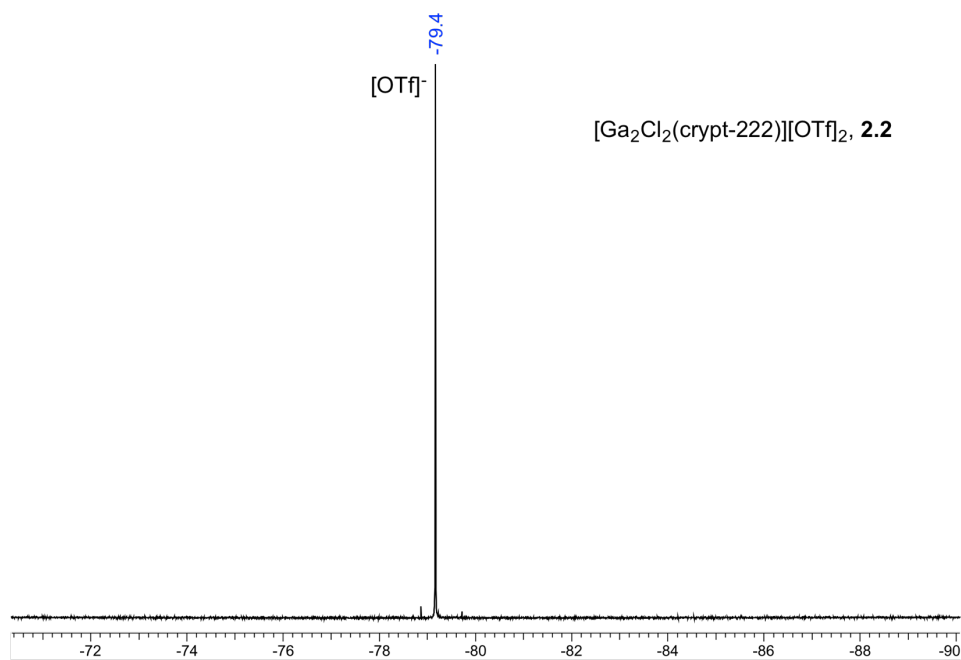


Figure A.7: ^{19}F NMR spectrum of **2.2** in CD_3CN at 376 MHz.

Appendix B: Supplementary Information for Chapter 3

Table A.3: Tabulated survey scans for all compounds studied by XPS.

Compound	Atomic Percentage (%)													
	C	N	O	F	Na	Mg	Si	S	Cl	K	Ca	Ga	Br	I
2.1	56.5	-	19.1	0.3	-	-	-	-	14.3	-	-	9.5	-	0.4
2.2	50.3	-	21.7	7.2	-	-	-	-	12.1	-	-	8.6	-	-
3.1	57.1	-	23.9	9.6	-	-	-	2.6	-	-	-	2.3	-	4.5
3.2	90.3	3.5	2.2	-	-	-	-	-	0.3	-	-	3.1	-	0.6
3.3	65.5	-	18.1	1.3	-	-	0.3	-	2.7	8.9	-	2.2	-	0.9
3.4	50.3	-	25.0	15.8	-	-	1.8	5.0	-	-	-	2.0	-	0.1
3.5	51.7	-	19.0	-	-	-	-	-	19.9	-	-	9.5	-	-
3.6	68.7	-	15.1	-	-	-	-	-	-	-	-	6.5	-	9.7
3.7	85.1	-	8.3	-	-	-	-	-	-	-	-	3.5	-	3.1
3.8	41.9	-	17.0	5.6	0.4	-	-	-	21.8	-	-	13.4	-	-
3.9	67.5	-	10.0	1.4	0.2	-	-	-	-	-	-	6.9	12.6	1.3
3.10	53.4	-	10.2	-	-	-	-	-	-	-	-	8.2	-	28.3
3.11	42.6	-	20.3	3.6	-	0.6	-	-	19.7	-	0.6	12.2	-	0.3
3.12	34.9	-	10.0	42.4	-	-	-	-	7.8	-	-	4.9	-	-
3.13	55.1	-	16.0	18.3	-	-	-	-	-	-	-	4.2	-	6.4
3.17	8.7	-	55.5	-	-	-	-	-	0.2	-	-	35.5	-	-

Note: Varying levels of contamination were observed for most of the samples analyzed. Common contaminants were found to be iodine, oxygen, carbon, and fluorine. The source of the iodine is postulated to come from cross-contamination arising from the vacuum chamber of the XPS instrument, as it was not only observed in samples related to this study, but in other data from unrelated work. Carbon and oxygen arise from the adhesive tape used in sample preparation. Alternatively, the oxygen could have been a result of possible oxidation of the samples. Despite the use of an argon filled glovebox for sample preparation and introduction to the XPS instrument, the sensitivity of the gallium compounds to oxygen and water could have led to some oxidation on the surface of some samples, causing oxygen contamination, however, because of the strict anaerobic conditions employed, this was assumed to be negligible. Any additional carbon and oxygen contamination could be resulting from excess solvent present in the samples, due to incomplete drying. The presence of fluorine in the survey spectra is likely a result of the fluoropolymer lining in the sample vial caps, which were used for synthesis and transportation of the samples. Overall, none of the contaminants were believed to interfere with any of the results of this study, as the gallium signals were used for characterization and assignment for all compounds, of which there was no contamination source.

Table A.4: Auger parameters and relevant shifts for compounds analyzed using Ga 2p_{3/2} binding energy.

Compound	Auger Parameter, α' (eV)	ΔE_B (eV)	ΔE_K (eV)	Relaxation Shift, $\Delta\alpha'$ (eV)	Final State Shift, ΔR (eV)	Initial State Shift, $\Delta\varepsilon$ (eV)
Ga_(m) (meas)	2184.50	-	-	-	-	-
Ga_(m) (lit)	2184.88	-	-	-	-	-
3.2	2180.60	1.01	-4.91	-3.90	-1.95	0.94

Compound	Auger Parameter, α' (eV)	ΔE_B (eV)	ΔE_K (eV)	Relaxation Shift, $\Delta\alpha'$ (eV)	Final State Shift, ΔR (eV)	Initial State Shift, $\Delta\varepsilon$ (eV)
3.3	2180.86	1.76	-6.40	-4.64	-2.32	0.56
3.4	2180.96	2.82	-7.36	-3.54	-1.77	-1.05
3.5	2180.25	2.37	-6.62	-4.25	-2.13	-0.25
3.6	2180.49	1.87	-5.88	-4.01	-2.01	0.14
3.7	2181.34	1.84	-5.00	-3.16	-1.58	-0.26
3.8	2179.94	3.36	-7.92	-4.56	-2.28	-1.08
3.9	2180.62	2.96	-6.84	-3.88	-1.94	-1.02
3.10	2181.40	2.68	-5.78	-3.10	-1.55	-1.13
3.11	2180.26	3.61	-7.85	-4.24	-2.12	-1.49
3.12	2179.97	3.05	-7.58	-4.53	-2.27	-0.79
3.13	2180.70	2.23	-6.03	-3.80	-1.90	-0.33
3.16	2183.30	0.41	-1.61	-1.20	-0.60	0.19
3.17 (meas)	2180.40	1.31	-5.41	-4.10	-2.05	0.74
3.17 (lit)	2180.25	0.96	-5.16	-4.25	-2.13	1.22
2.1	2180.15	2.02	-6.37	-4.35	-2.18	0.16
2.2	2180.19	2.08	-6.39	-4.31	-2.16	0.08
3.1	2180.81	2.41	-6.10	-3.69	-1.85	-0.57

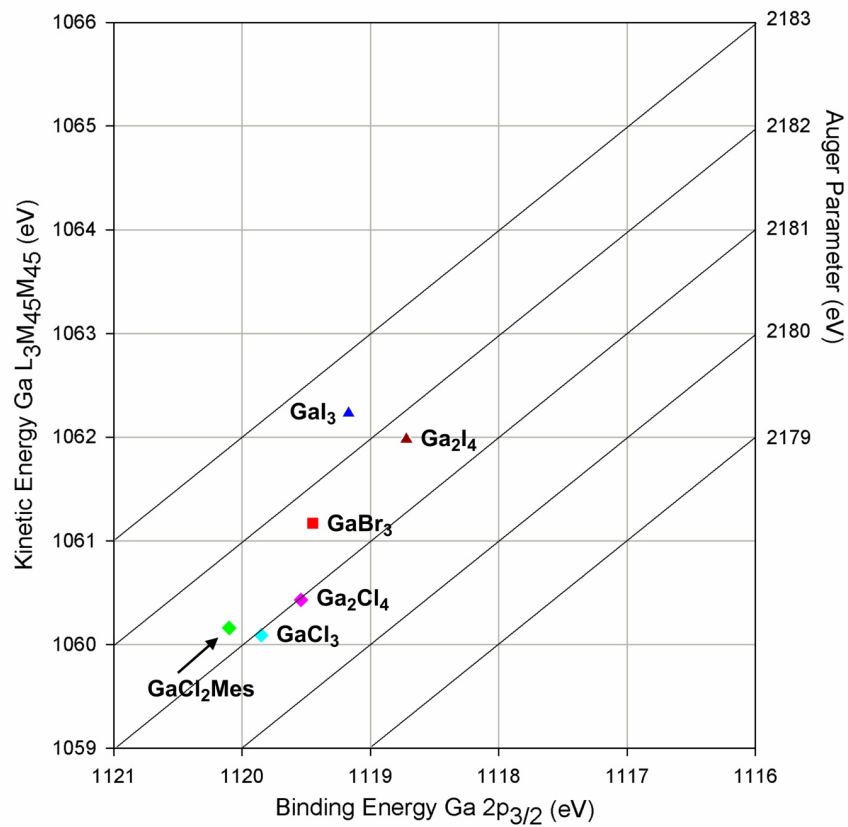


Figure A.8: Wagner plot of gallium halides using Ga 2p_{3/2} binding energy. Symbol legend: diamond = chloride ligands; square = bromide ligands; triangle = iodide ligands.

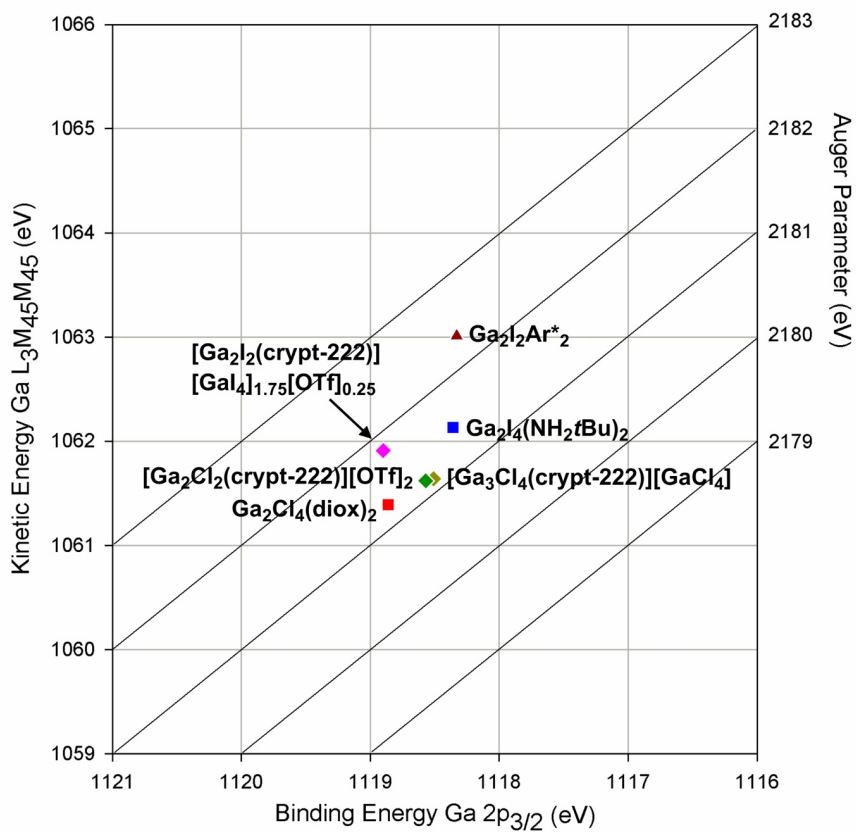


Figure A.9: Wagner plot of Ga-Ga compounds using Ga 2p_{3/2} binding energy. Symbol legend: diamond = synthesized gallium-cryptand complexes; square = chloride and iodide ligands and O/N donors; triangle = iodide and terphenyl ligands.

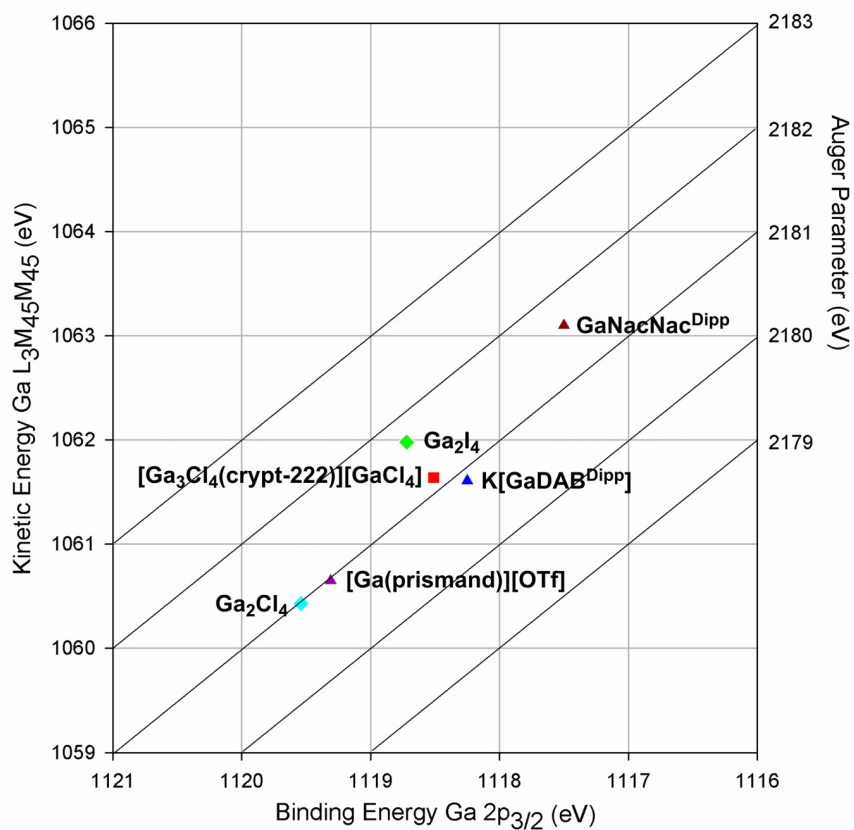


Figure A.10: Wagner plot of Ga(I) compounds using Ga 2p_{3/2} binding energy. Symbol legend: diamond = halide ligands; square = chloride ligands and O/N donors; triangle = organic ligands.

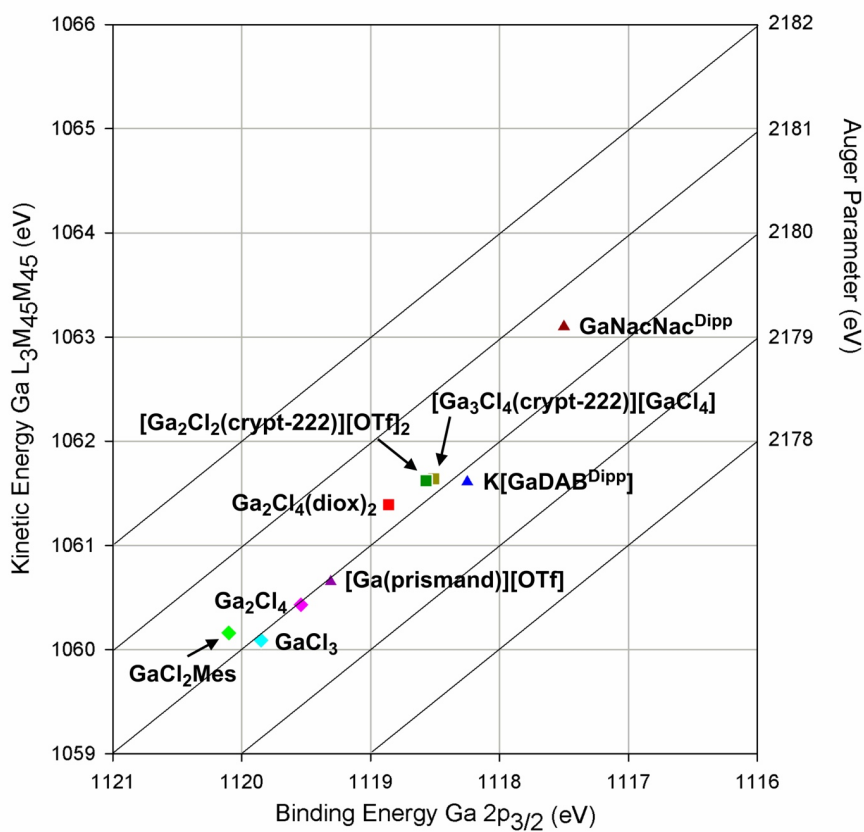


Figure A.11: Wagner plot of gallium-chloride and gallium-nitrogen compounds using Ga 2p_{3/2} binding energy. Symbol legend: diamond = Ga(III); square = Ga(II); triangle = Ga(I).

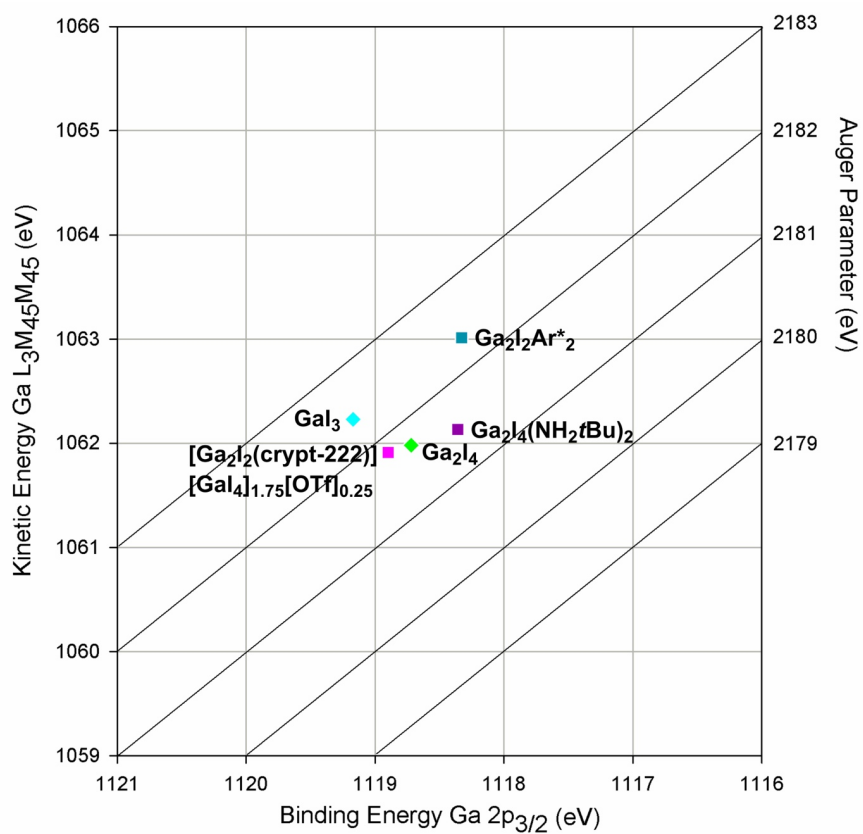


Figure A.12: Wagner plot of gallium-iodide compounds using Ga 2p_{3/2} binding energy. Symbol legend: diamond = Ga(III); square = Ga(II).

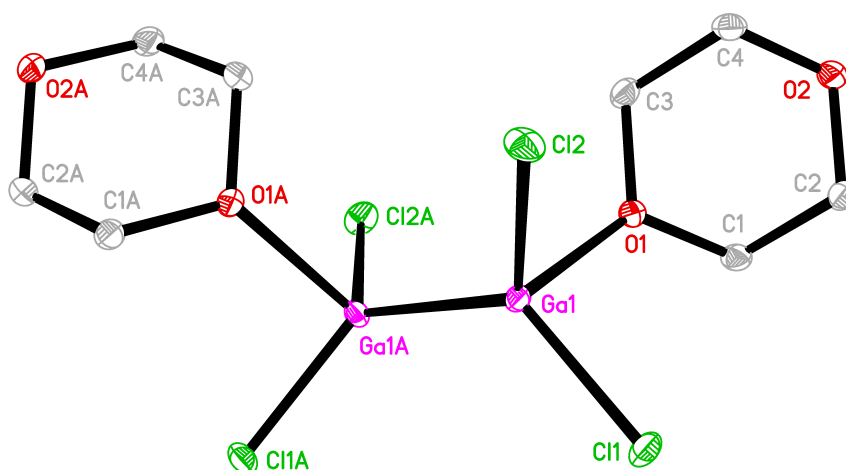


Figure A.13: Displacement ellipsoid plot of $\text{Ga}_2\text{Cl}_4(1,4\text{-dioxane})_2$ showing naming and numbering scheme. Ellipsoids are drawn at the 50% probability level and hydrogen atoms are omitted for clarity. Selected parameters (bond lengths in Å, angles in °): Ga1-Cl1 2.1837(9), Ga-Cl2 2.1937(9), Ga1-O1 2.1432(9), Ga1-Ga1 2.3911(17), Ga1-O2B 2.631(1); O1-Ga1-Cl1 95.23(4), O1-Ga1-Cl2 94.50(4), O1-Ga1-Ga1-98.52(4), Cl1-Ga1-Cl2 111.44(4), O1-Ga1-O2B 179.86(4).

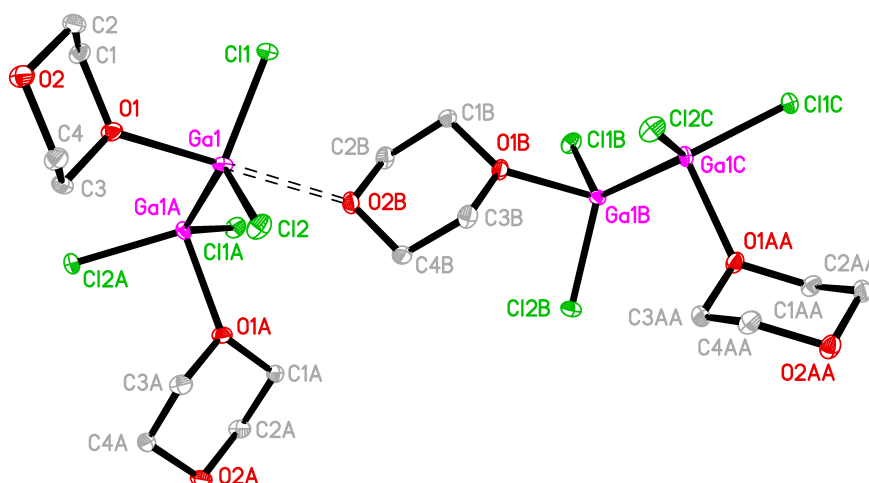


Figure A.14: Displacement ellipsoid plot of $\text{Ga}_2\text{Cl}_4(1,4\text{-dioxane})_2$ showing naming and numbering scheme and the bridging structure between formula units. Ellipsoids are drawn at the 50% probability level and hydrogen atoms are omitted for clarity.

Table A.5: Crystallographic details for Ga₂Cl₄(1,4-dioxane)₂.

Formula	C ₈ H ₁₆ Cl ₄ Ga ₂ O ₄
FW (g/mol)	457.45
Crystal Size (mm)	0.436 x 0.179 x 0.151
Crystal Colour/Habit	colourless prism
Crystal System	orthorhombic
Space Group	Fddd
Temperature, K	110
<i>a</i> , Å	16.316(4)
<i>b</i> , Å	16.503(4)
<i>c</i> , Å	22.551(5)
α , °	90
β , °	90
γ , °	90
<i>V</i> , Å ³	6072(2)
<i>Z</i>	16
F(000)	3616
ρ (g/cm ³)	2.002
λ , Å	0.71073 (MoK α)
μ , cm ⁻¹	4.254
Diffractometer Type	Bruker Kappa Axis Apex2
Max 2 θ for Data Collection, °	90.746
Measd Fraction of Data	0.995
No. Rflns Measd	81045
Unique Rflns Measd	6192
R_{merge}	0.0320
No. Rflns in Refinement	6192
R_1	0.0154
wR_2	0.0334
R_1 (all data)	0.0196
wR_2 (all data)	0.0343
GOF	1.041
Min, Max Peak Heights on final ΔF map (e/Å)	-0.363, 0.642

Where: $R_1 = \Sigma(|F_o| - |F_c|) / \Sigma F_o$; $wR_2 = [\Sigma(w(F_o^2 - F_c^2)^2) / \Sigma(wF_o^4)]^{1/2}$; $GOF = [\Sigma(w(F_o^2 - F_c^2)^2) / (\text{No. of reflns.} - \text{No. of params.})]^{1/2}$

Crystallographic Details

Data Collection and Processing: The sample was mounted on a MiTeGen polyimide micromount with a small amount of Paratone N oil. The unit cell dimensions were determined from a symmetry constrained fit of 9821 reflections with $6.16^\circ < 2\theta < 89.92^\circ$. The data collection strategy was a number of ϕ and ω scans which collected data up to 90.746° (2θ). The frame integration was performed using SAINT.¹ The resulting raw data were scaled and absorption corrected using a multi-scan averaging of symmetry equivalent data using SADABS.²

Structure Solution and Refinement: The structure was solved by using a dual space methodology using the SHELXT program.³ All non-hydrogen atoms were obtained from the initial solution. The hydrogen atoms were found in the difference map and were allowed to refine isotropically. Ga(1) was found to be disordered, flipping below the plane of Cl(1), Cl(2) and Ga(1a). The occupancy of the major component was found to refine to a normalized occupancy of 0.857(10). In addition, the disorder was found to exhibit high degrees of correlation between several of the Ga(1) and Ga(1)' parameters, leading to the occupancy value of the disorder to be constrained at the above value. The structural model was fit to the data using full matrix least-squares based on F^2 . The calculated structure factors included corrections for anomalous dispersion from the usual tabulation. The structure was refined using the SHELXL-2014 program from the SHELXTL suite of crystallographic software.⁴ Graphic plots were produced using the XP program suite.⁵

References

- [1] Bruker-AXS, SAINT version 2013.8, **2013**, Bruker-AXS, Madison, WI 53711, USA.
- [2] Bruker-AXS, SADABS version 2012.1, **2012**, Bruker-AXS, Madison, WI 53711, USA.
- [3] G. M. Sheldrick, *Acta Cryst.* 2015, **A71**, 3.

- [4] G. M. Sheldrick, *Acta Cryst.* 2015, **C71**, 3
- [5] Bruker-AXS, XP version 2013.1, **2013**, Bruker-AXS, Madison, WI 53711, USA.

Appendix C: Supplementary Information for Chapter 4

Additional Experimental Details

Isolation of Single Crystals of Na[GaCl₃Ph], 4.2

A solution of NaBPh₄ (0.061 g, 0.18 mmol) dissolved in toluene (2 mL) was added to a stirring solution of Ga₂Cl₄ (0.050 g, 0.18 mmol) dissolved in toluene (2 mL). The solution was allowed to stir at room temperature for 2 hours, during which time the formation of a grey precipitate was observed. The mixture was centrifuged, the supernatant was decanted and cooled to -20 °C for several days, after which time X-ray quality single crystals of **4.2** had formed.

Isolation of Single Crystals of [GaCl₂(15-crown-5)][GaCl₄] and [Ga₂Cl₃(15-crown-5)(CH₃CN)]₂[Ga₂Cl₆]

A solution of Ga₂Cl₄ (0.50 g, 1.8 mmol) dissolved in benzene (7 mL) was added dropwise to a stirring solution of 15-crown-5 (0.39 g, 1.8 mmol) dissolved in benzene (3 mL). The solution turned red with the addition of each drop but the colour dissipated after several seconds. Following the addition, the resultant solution was allowed to stir at room temperature for 18 hours at which point an off-white precipitate had formed. The volatiles were removed under reduced pressure, and the solid was suspended in THF (5 mL). The solution was filtered, and the solvent was removed under reduced pressure, yielding an oily residue. The oil was dissolved in a minimal amount of THF (2 mL), and when left to stand at room temperature, X-ray quality single crystals of [Ga₂Cl₃(15-crown-5)(CH₃CN)]₂[Ga₂Cl₆] were obtained. Alternatively, when the oil was dissolved in a minimal amount of ACN (1 mL), Et₂O (2 mL) was added, the solution was filtered, and crystals of [GaCl₂(15-crown-5)][GaCl₄] were obtained after cooling to -20 °C for 24 hours. The major product of this reaction is postulated to be [Ga(15-crown-5)][GaCl₄] based on ESI-MS data ($m/z = 289$, positive ion) and a signal in the ⁷¹Ga NMR spectrum at -536 ppm, however, this product could not be isolated without the presence of the two crystallized impurities and single crystals of [Ga(15-crown-5)][GaCl₄] could not be

obtained. As an example, after the recrystallization of bulk product, each of the products was observed in the ^1H NMR spectrum.

Crude reaction mixture: ^1H NMR (CD_3CN , 600 MHz, 298 K) δ : 4.23 (m, [-O-CHH-CHH-O-] from $[\text{Ga}_2\text{Cl}_3(15\text{-crown-5})(\text{CH}_3\text{CN})]^+$), 4.02 (s, [-O-CH₂-CH₂-O-] from $[\text{GaCl}_2(15\text{-crown-5})]^+$), 3.97 (m, [-O-CHH-CHH-O-] from $[\text{Ga}_2\text{Cl}_3(15\text{-crown-5})(\text{CH}_3\text{CN})]^+$), 3.70 (s, [-O-CH₂-CH₂-O-] from $[\text{Ga}(15\text{-crown-5})]^+$); ^{71}Ga NMR (CD_3CN , 183 MHz, 298 K) δ : 251.2 ($[\text{GaCl}_4]^-$), -536.5 ($[\text{Ga}(15\text{-crown-5})]^+$); Product distribution (^1H NMR): $[\text{Ga}(15\text{-crown-5})]^+ : [\text{GaCl}_2(15\text{-crown-5})]^+ : [\text{Ga}_2\text{Cl}_3(15\text{-crown-5})(\text{CH}_3\text{CN})]^+$, 1 : 0.14 : 0.08.

Recrystallized product: ^1H NMR (CD_3CN , 600 MHz, 298 K) δ : 4.24 (m, [-O-CHH-CHH-O-] from $[\text{Ga}_2\text{Cl}_3(15\text{-crown-5})(\text{CH}_3\text{CN})]^+$), 4.02 (s, [-O-CH₂-CH₂-O-] from $[\text{GaCl}_2(15\text{-crown-5})]^+$), 3.96 (m, [-O-CHH-CHH-O-] from $[\text{Ga}_2\text{Cl}_3(15\text{-crown-5})(\text{CH}_3\text{CN})]^+$), 3.74 (s, [-O-CH₂-CH₂-O-] from $[\text{Ga}(15\text{-crown-5})]^+$); ^{71}Ga NMR (CD_3CN , 183 MHz, 298 K) δ : 251.2 ($[\text{GaCl}_4]^-$), -536.5 ($[\text{Ga}(15\text{-crown-5})]^+$); Product distribution (^1H NMR): $[\text{Ga}(15\text{-crown-5})]^+ : [\text{GaCl}_2(15\text{-crown-5})]^+ : [\text{Ga}_2\text{Cl}_3(15\text{-crown-5})(\text{CH}_3\text{CN})]^+$, 1 : 0.05 : 0.06.

Crystallographic Data

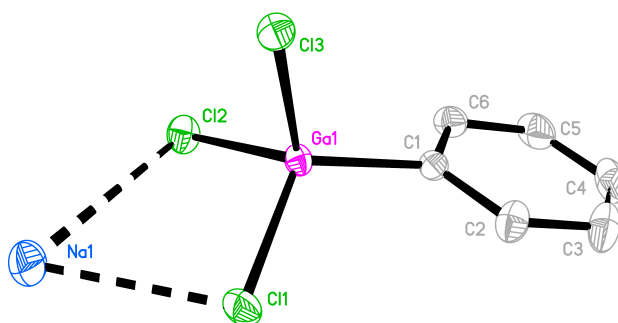


Figure A.15: Displacement ellipsoid plot of **4.2**. Ellipsoids are drawn at the 50% probability level and hydrogen atoms are omitted for clarity. Selected bond lengths and angles (\AA , $^\circ$): Ga1-C1 1.9445(11), Ga1-Cl1 2.2188(5), Ga1-Cl2 2.2068(5), Ga1-Cl3 2.2438(6), Na1-Cl1 2.8108(8), Na1-Cl2 3.2106(10); Cl1-Ga1-Cl2 102.91(2), Cl1-Ga1-Cl3 100.45(2).

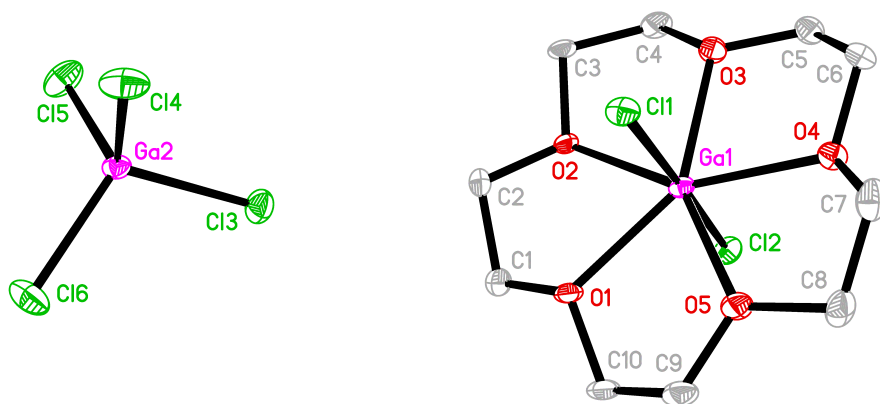


Figure A.16: Displacement ellipsoid plot of $[\text{GaCl}_2(15\text{-crown-5})][\text{GaCl}_4]$. Ellipsoids are drawn at the 50% probability level and hydrogen atoms are omitted for clarity.

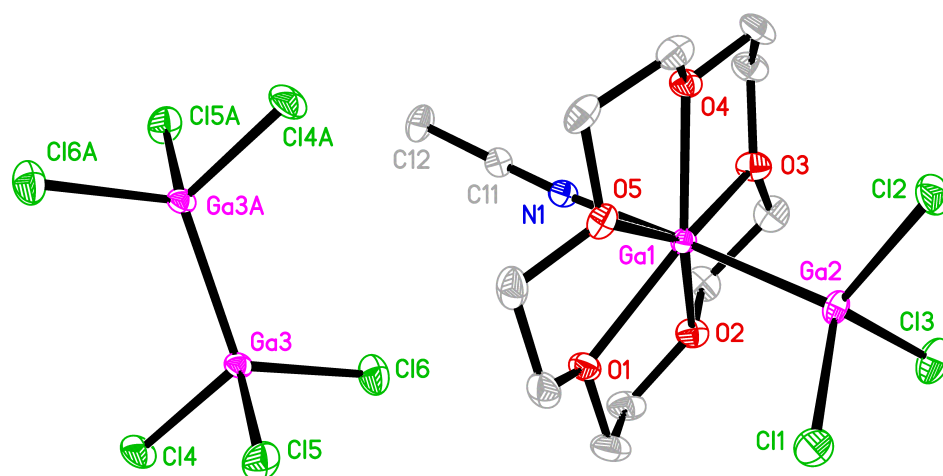


Figure A.17: Displacement ellipsoid plot of $[\text{Ga}_2\text{Cl}_3(15\text{-crown-5})(\text{CH}_3\text{CN})]_2[\text{Ga}_2\text{Cl}_6]$. Ellipsoids are drawn at the 50% probability level and hydrogen atoms are omitted for clarity.

Table A.6: Selected crystallographic data for **4.2**, [GaCl₂(15-crown-5)][GaCl₄],
[Ga₂Cl₃(15-crown-5)(CH₃CN)][Ga₂Cl₆].

	4.2	[GaCl₂(15-crown-5)] [GaCl₄]	[Ga₂Cl₃(15-crown-5)(CH₃CN)]₂ [Ga₂Cl₆]
Formula	C ₆ H ₅ Cl ₃ GaNa	C ₁₀ H ₂₀ Cl ₆ Ga ₂ O ₅	C ₁₄ H ₂₆ Cl ₆ Ga ₃ N ₂ O ₅
M _r (g mol ⁻¹)	276.16	572.40	724.23
Crystal Colour and Habit	colourless needle	colourless prism	colourless plate
Crystal System	orthorhombic	orthorhombic	monoclinic
Space Group	P c c n	P n m a	C 2/c
Temperature, K	110	110	110
<i>a</i> , Å	11.812(4)	11.2123(16)	39.795(15)
<i>b</i> , Å	23.738(8)	32.861(6)	8.527(3)
<i>c</i> , Å	6.9110(17)	16.363(2)	17.116(6)
α, °	90	90	90
β, °	90	90	112.354(14)
γ, °	90	90	90
V, Å ³	1937.8(10)	6028.9(16)	5371(3)
Z	8	12	8
F(000)	1072	3408	2872
ρ (g/cm ³)	1.893	1.892	1.791
λ, Å	0.71073 (MoKα)	1.54178 (CuKα)	0.71073 (MoKα)
μ, (cm ⁻¹)	3.642	10.798	3.611
No. of refl. meas.	77081	57628	93618
Unique refl. meas.	5482	5107	10723
R _{merge}	0.0459	0.0817	0.0730
No. of refl. incld in refinm.	5482	5107	10723
No. of params. in least-squares	120	322	283
R ₁	0.0247	0.0383	0.0437
wR ₂	0.0493	0.0952	0.0938
R ₁ (all data)	0.0392	0.0423	0.0697
wR ₂ (all data)	0.0535	0.0978	0.1029
GOF	1.021	1.065	1.036

Where: $R_1 = \Sigma(|F_o| - |F_c|) / \Sigma F_o$; $wR_2 = [\Sigma(w(F_o^2 - F_c^2)^2) / \Sigma(wF_o^4)]^{1/2}$; $GOF = [\Sigma(w(F_o^2 - F_c^2)^2) / (\text{No. of reflns.} - \text{No. of params.})]^{1/2}$

Crystallographic Details

Data Collection and Processing. The samples were mounted on a MiTeGen polyimide micromount with a small amount of Paratone N oil. All X-ray measurements were made on a Bruker Kappa Axis Apex2 (MoK α) or a Nonius Bruker KappaCCD Apex2 (CuK α) diffractometer at a temperature of 110 K. The frame integration was performed using SAINT.¹ The resulting raw data were scaled and absorption corrected using a multi-scan averaging of symmetry equivalent data using SADABS.²

Structure Solution and Refinement. The structure was solved by using a dual space methodology using the SHELXT program.³ All non-hydrogen atoms were obtained from the initial solution. The hydrogen atoms were introduced at idealized positions and were allowed to refine isotropically for **4.2**, and were allowed to ride for [GaCl₂(15-crown-5)][GaCl₄] and [Ga₂Cl₃(15-crown-5)(CH₃CN)][Ga₂Cl₆]. For [GaCl₂(15-crown-5)][GaCl₄], the second formula unit was found to sit on a centre of symmetry, and therefore only half of the second unit was found to be in the asymmetric unit. For [Ga₂Cl₃(15-crown-5)(CH₃CN)][Ga₂Cl₆], it was found during refinement that the second weight value was abnormally large. Upon further analysis, it was found that the sample appeared to be twinned, although a suitable secondary domain could not be found and adequately refined. As the sample was determined to be an impurity, the structure was refined without accounting for any twinning. In addition, Cl3 was found to be disordered, as two positions for this atom could be found in the difference map. The disorder was modelled and was found to refine to a normalized occupancy of 0.912(15) for the major component. The structural model was fit to the data using full matrix least-squares based on F^2 . The calculated structure factors included corrections for anomalous dispersion from the usual tabulation. The structure was refined using the SHELXL-2014 program from the SHELXTL suite of crystallographic software.⁴ Graphic plots were produced using the XP program suite.⁵

Spectroscopic Data

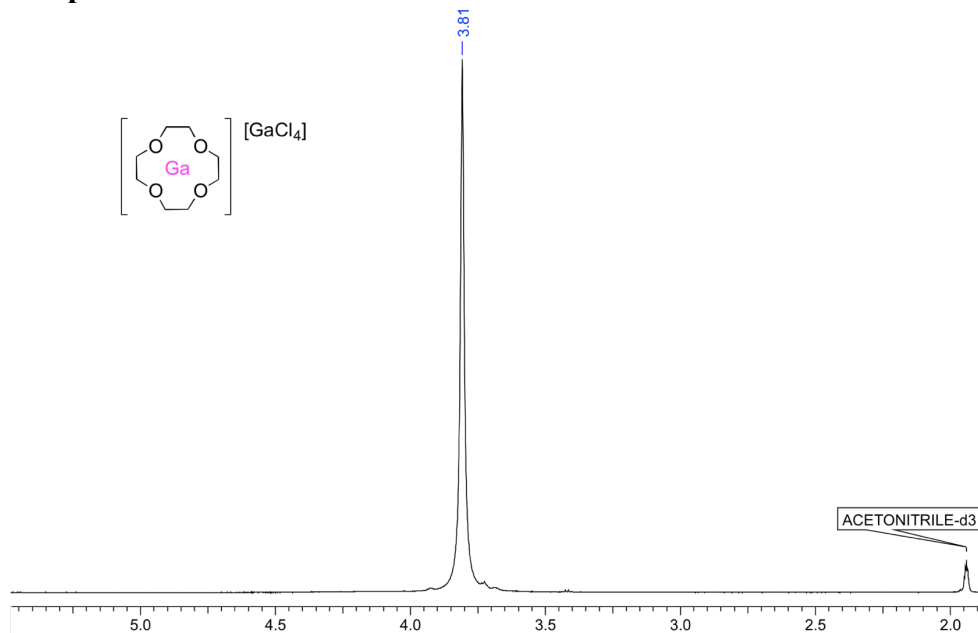


Figure A.18 : 1H NMR spectrum of **4.1** in CD_3CN at 600 MHz.

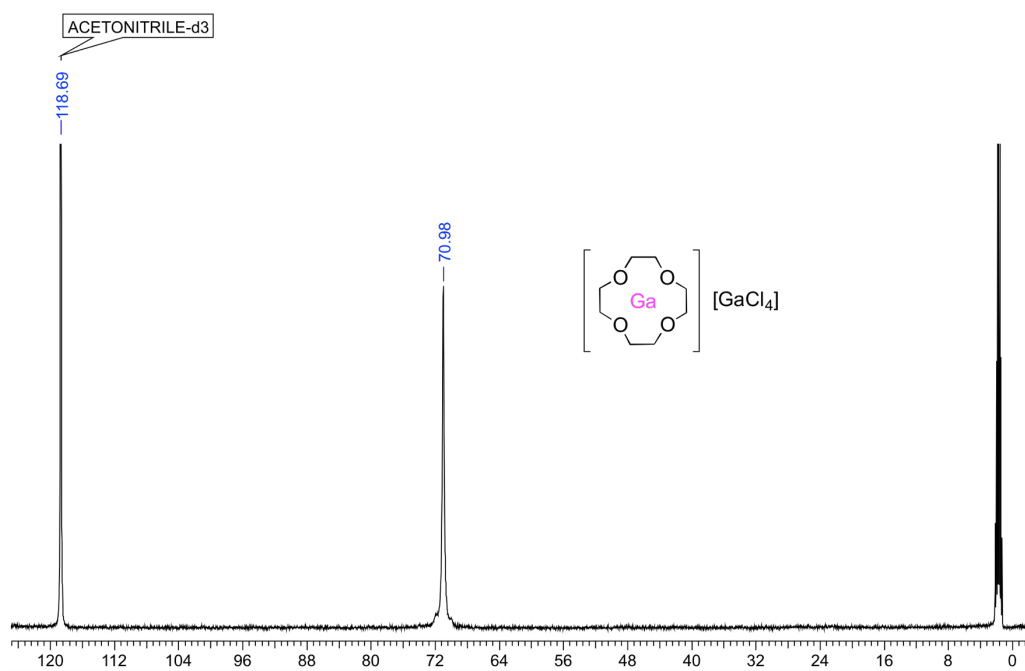


Figure A.19: $^{13}C\{^1H\}$ NMR spectrum of **4.1** in CD_3CN at 151 MHz.

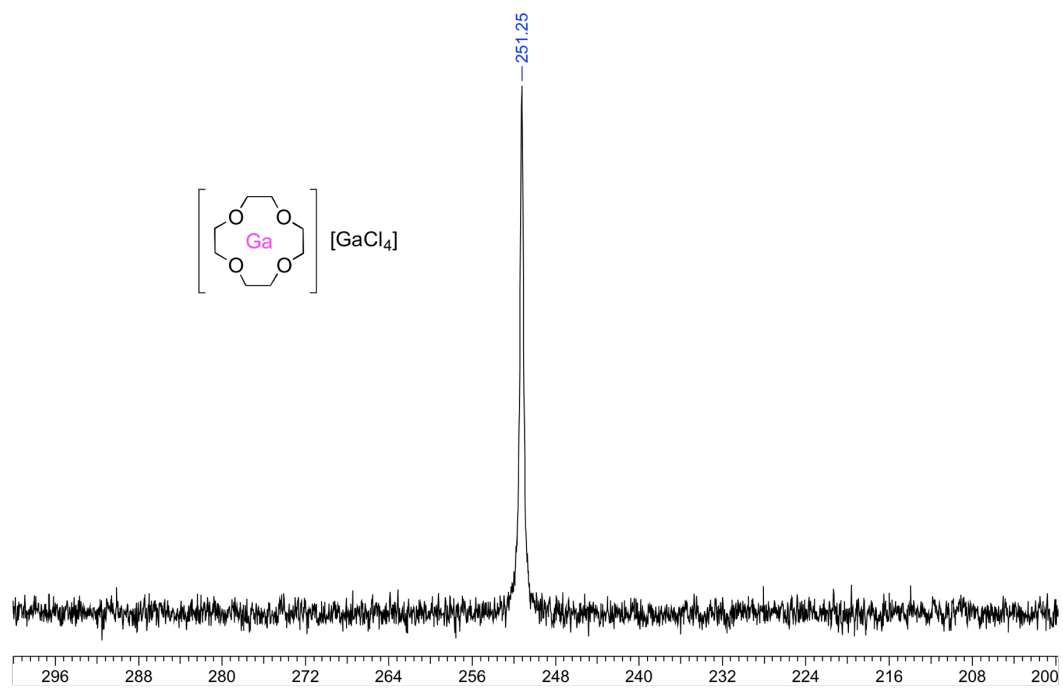


Figure A.20: $^{71}\text{Ga}\{^1\text{H}\}$ NMR spectrum of **4.1** in CD_3CN at 183 MHz.

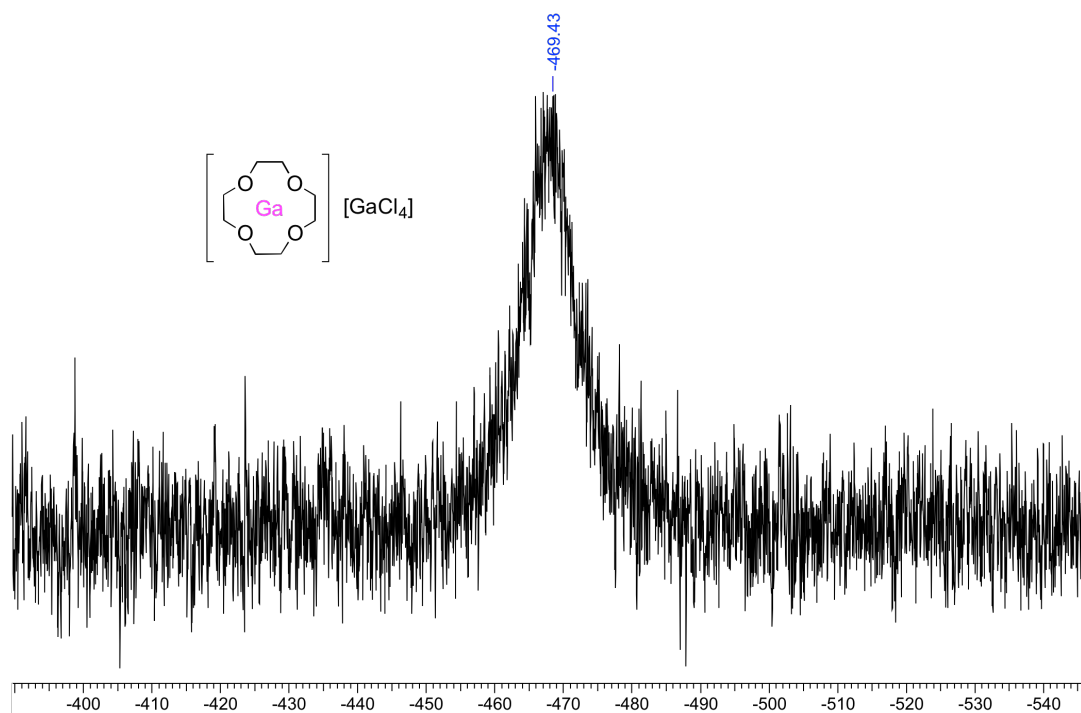


Figure A.21: $^{71}\text{Ga}\{^1\text{H}\}$ NMR spectrum of **4.1** in CD_3CN at 183 MHz.

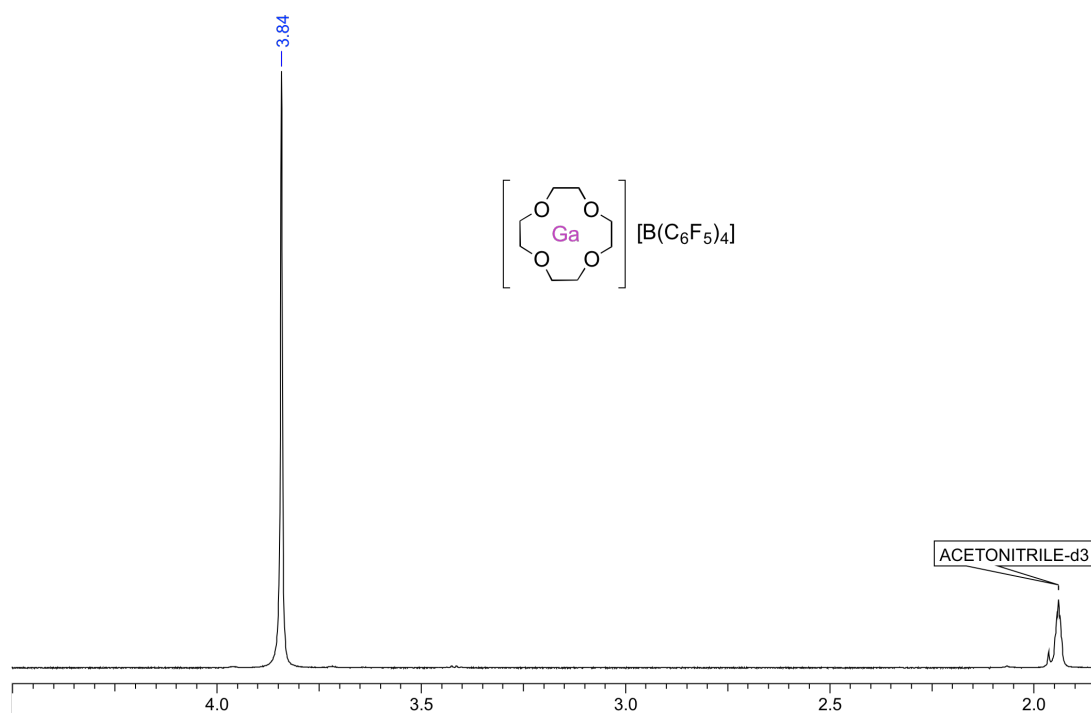


Figure A.22: 1H NMR spectrum of **4.3** in CD_3CN at 600 MHz.

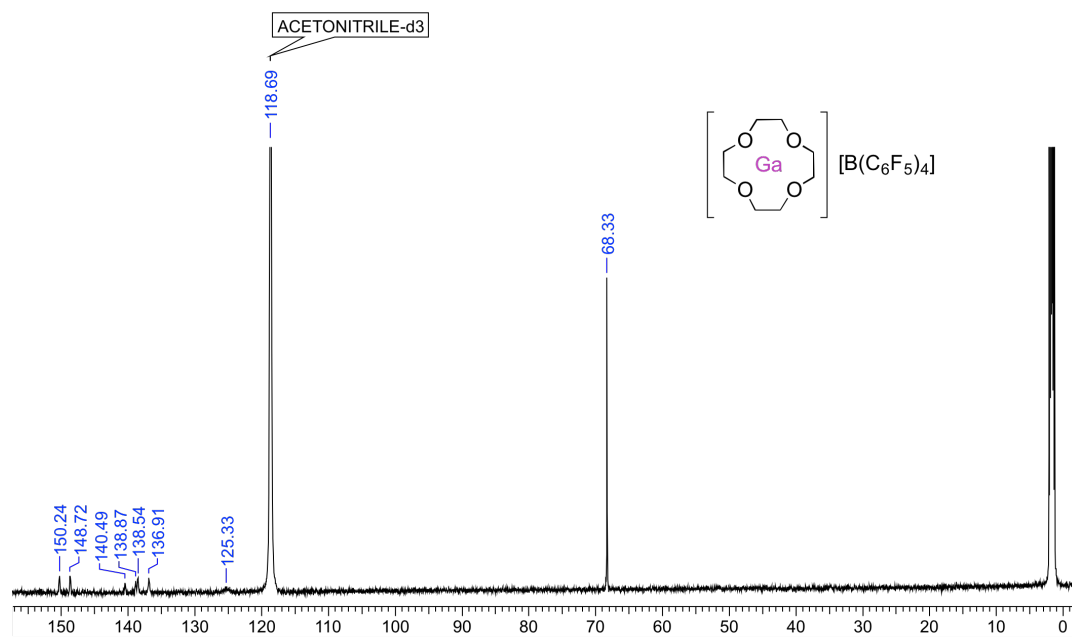


Figure A.23: $^{13}C\{^1H\}$ NMR spectrum of **4.3** in CD_3CN at 151 MHz.

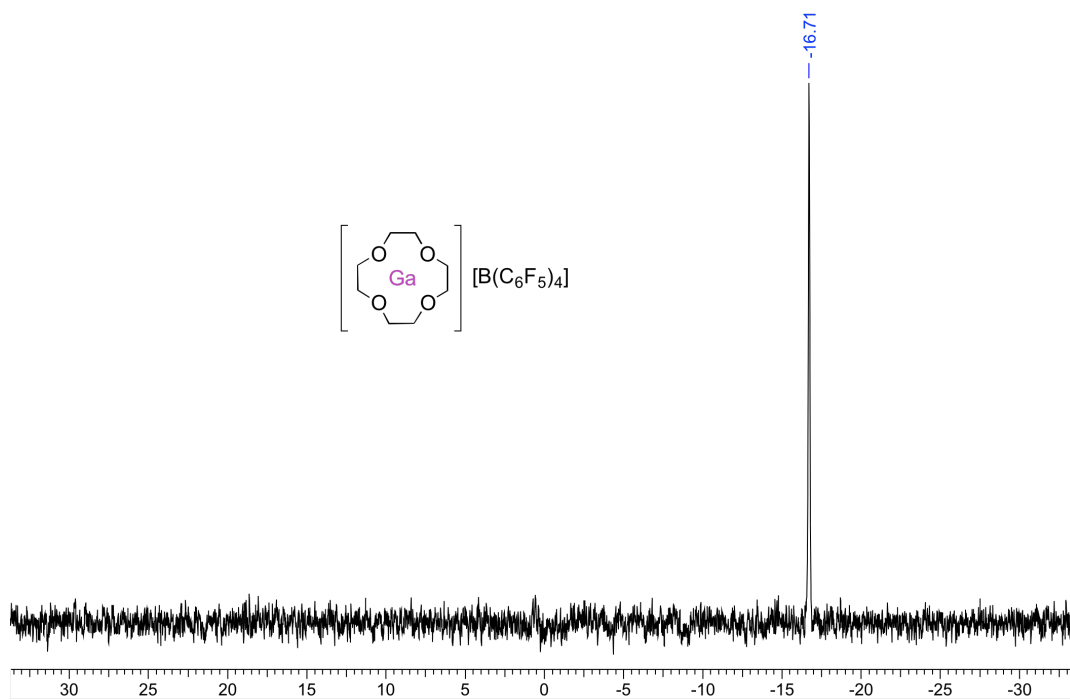


Figure A.24: $^{11}\text{B}\{^1\text{H}\}$ NMR spectrum of 4.3 in CD_3CN at 193 MHz.

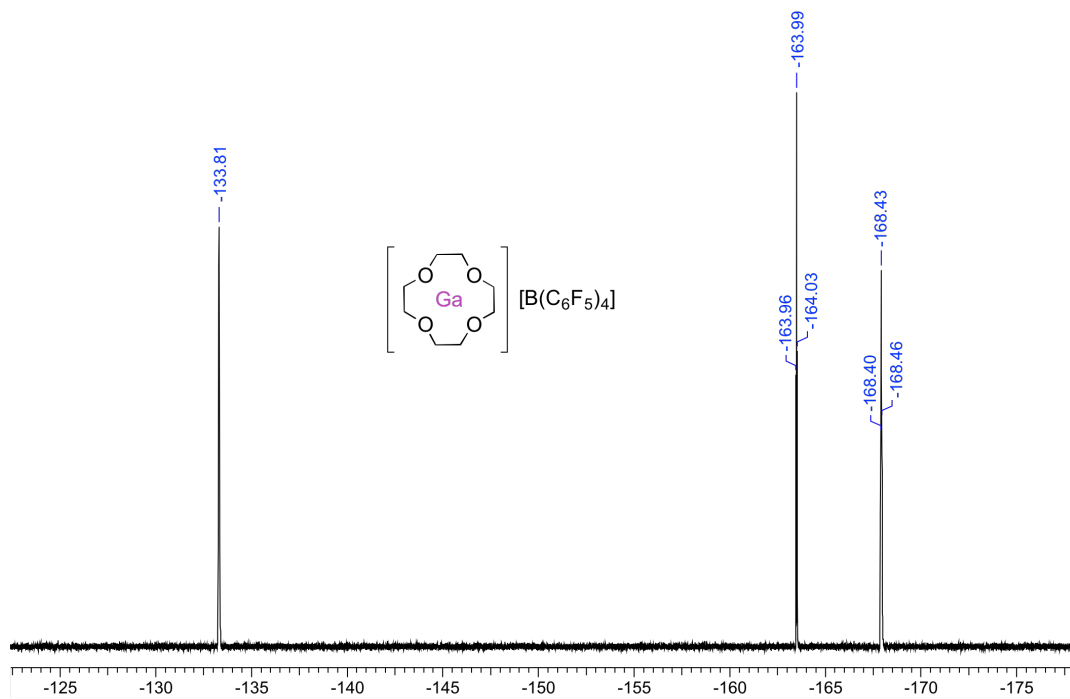


Figure A.25: ^{19}F NMR spectrum of 4.3 in CD_3CN at 564 MHz.

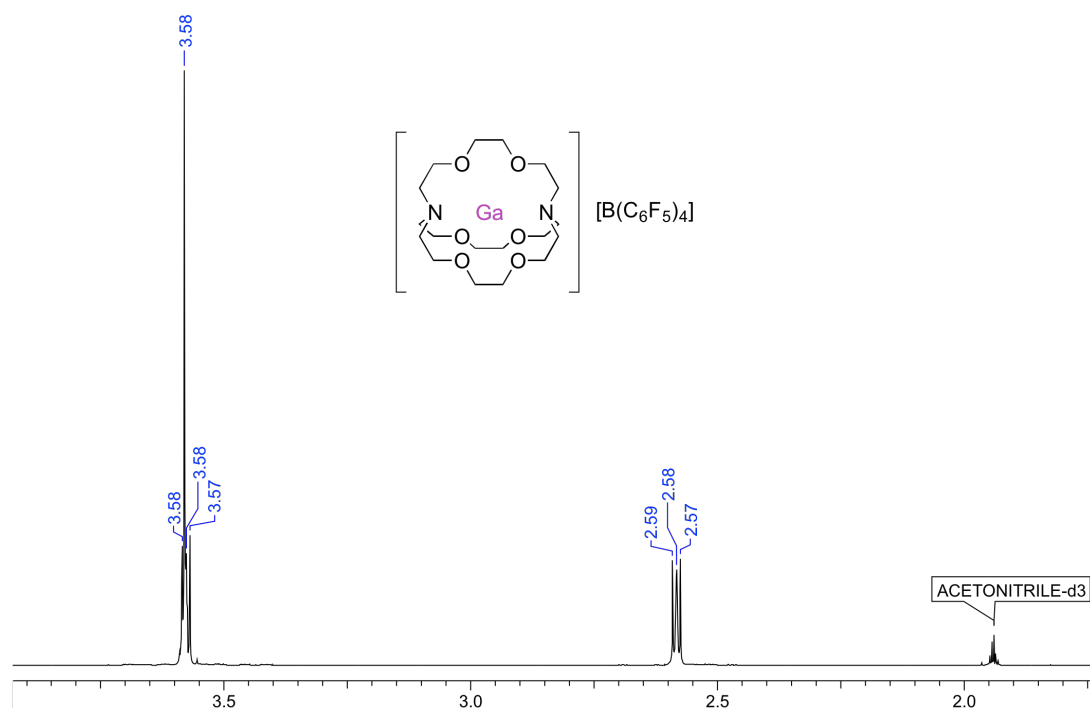


Figure A.26: ^1H NMR spectrum of **4.4** in CD_3CN at 600 MHz.

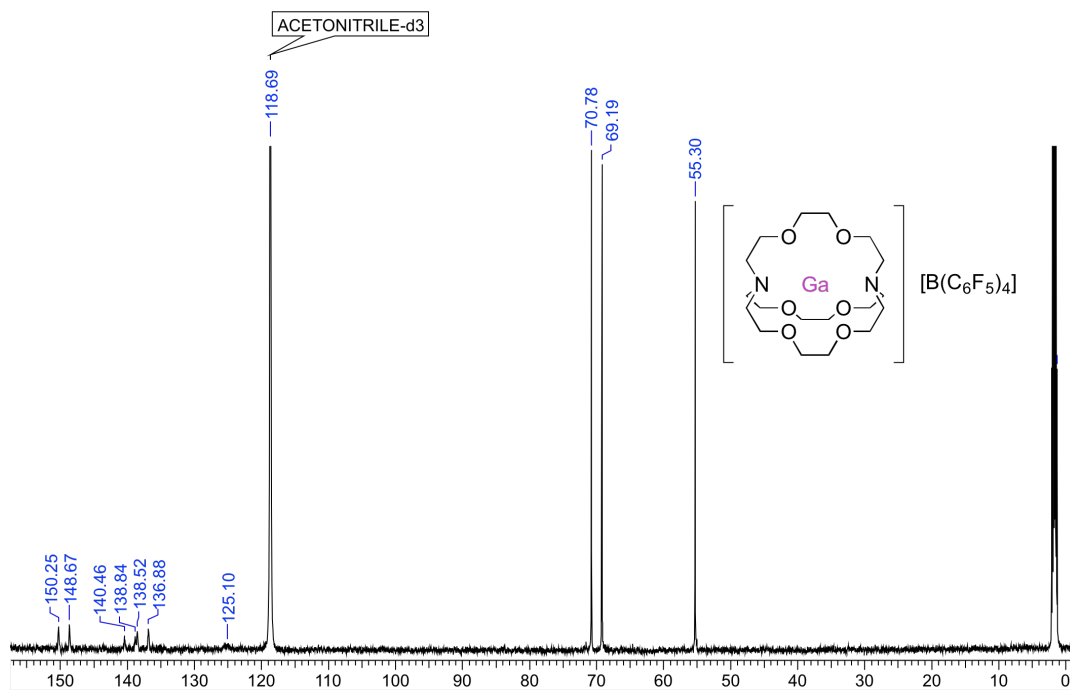


Figure A.27: $^{13}\text{C}\{^1\text{H}\}$ NMR spectrum of **4.4** in CD_3CN at 151 MHz.

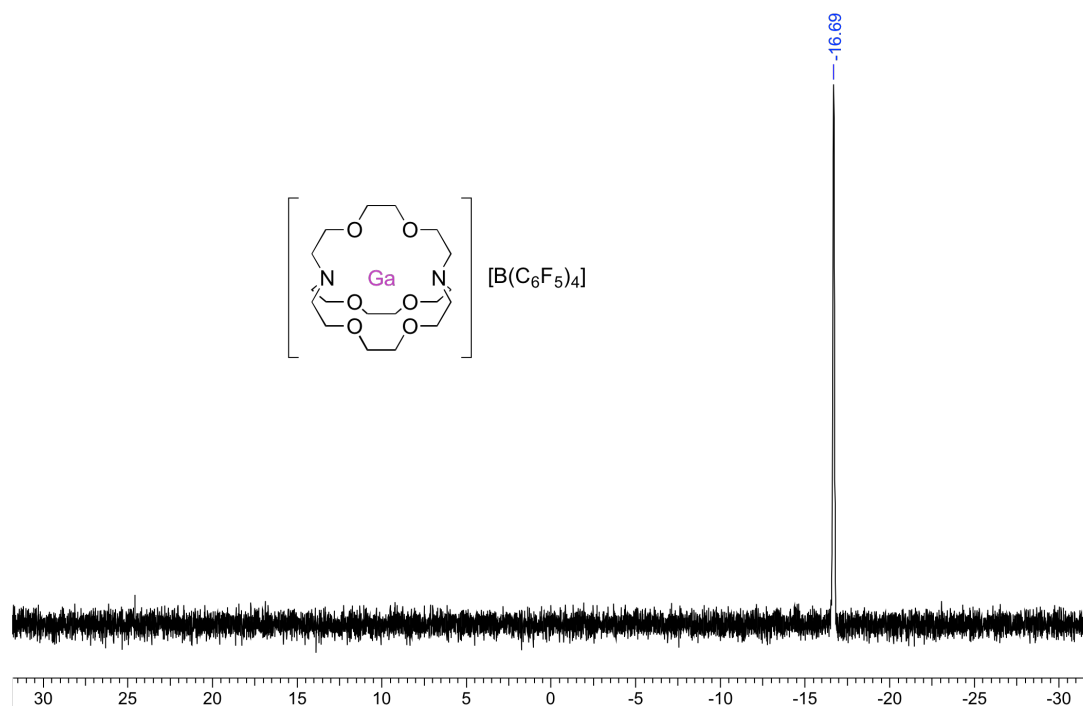


Figure A.28: $^{11}\text{B}\{^1\text{H}\}$ NMR spectrum of 4.4 in CD_3CN at 193 MHz.

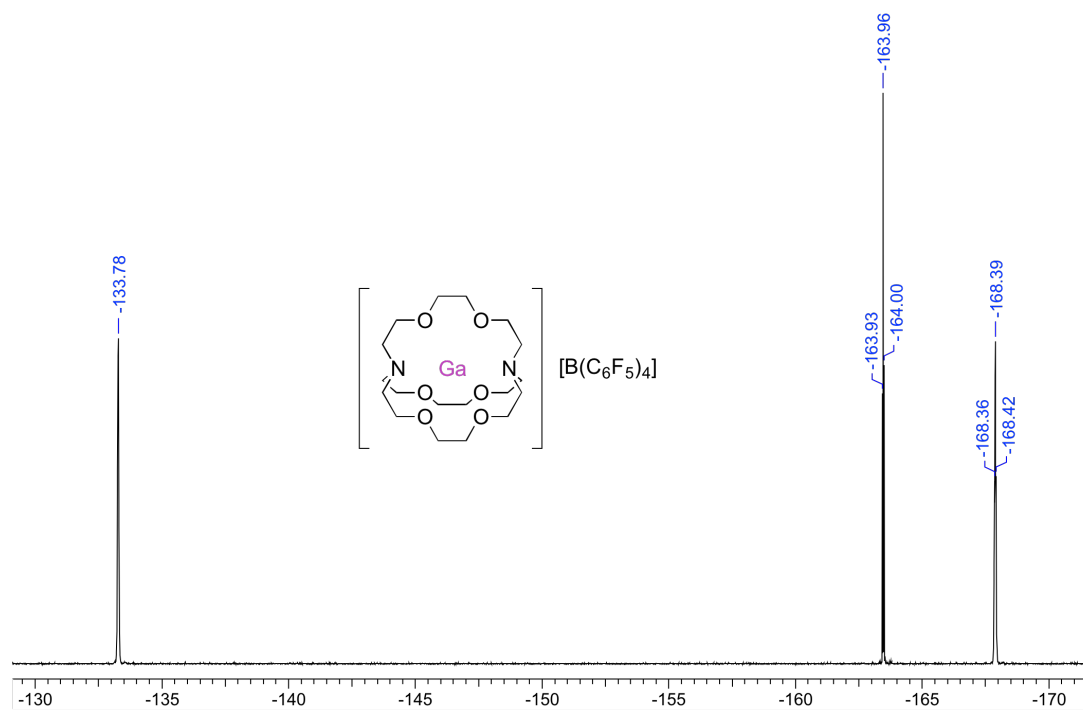


Figure A.29: ^{19}F NMR spectrum of 4.4 in CD_3CN at 564 MHz.

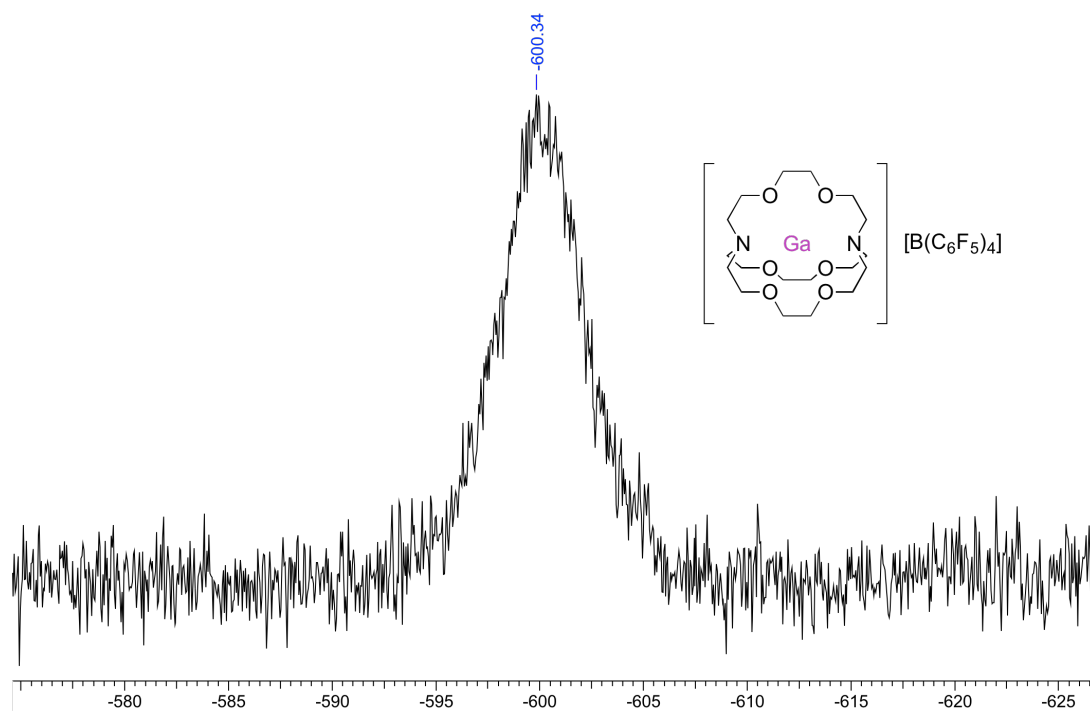


Figure A.30: $^{71}\text{Ga}\{^1\text{H}\}$ NMR spectrum of **4.4** in CD_3CN at 183 MHz.

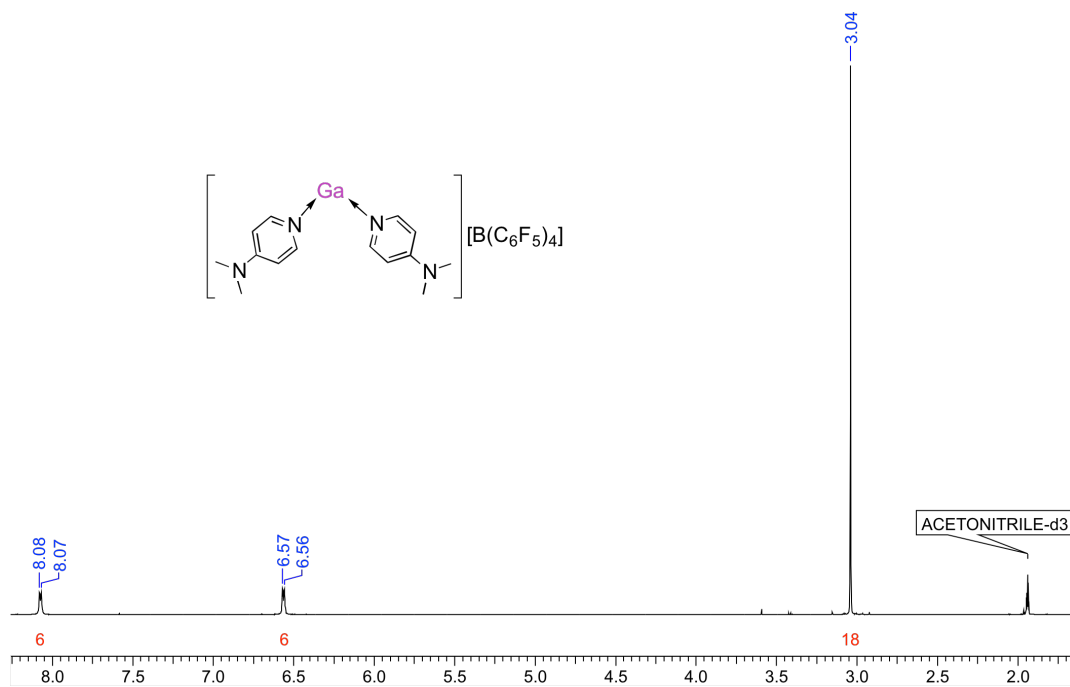


Figure A.31: ^1H NMR spectrum of **4.5** in CD_3CN at 600 MHz.

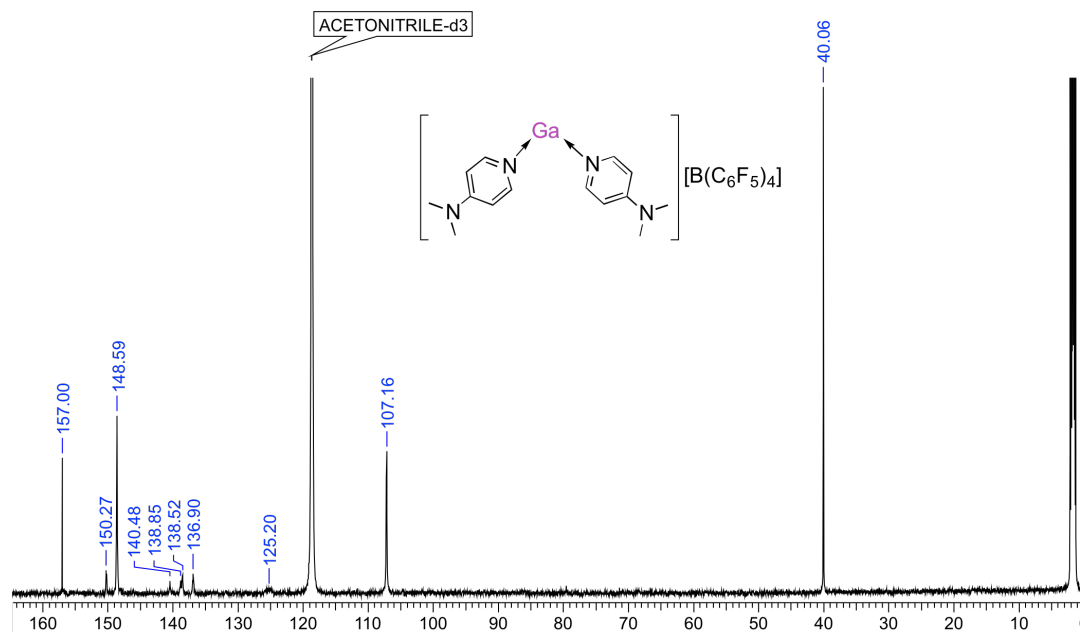


Figure A.32: $^{13}\text{C}\{^1\text{H}\}$ NMR spectrum of **4.5** in CD_3CN at 151 MHz.

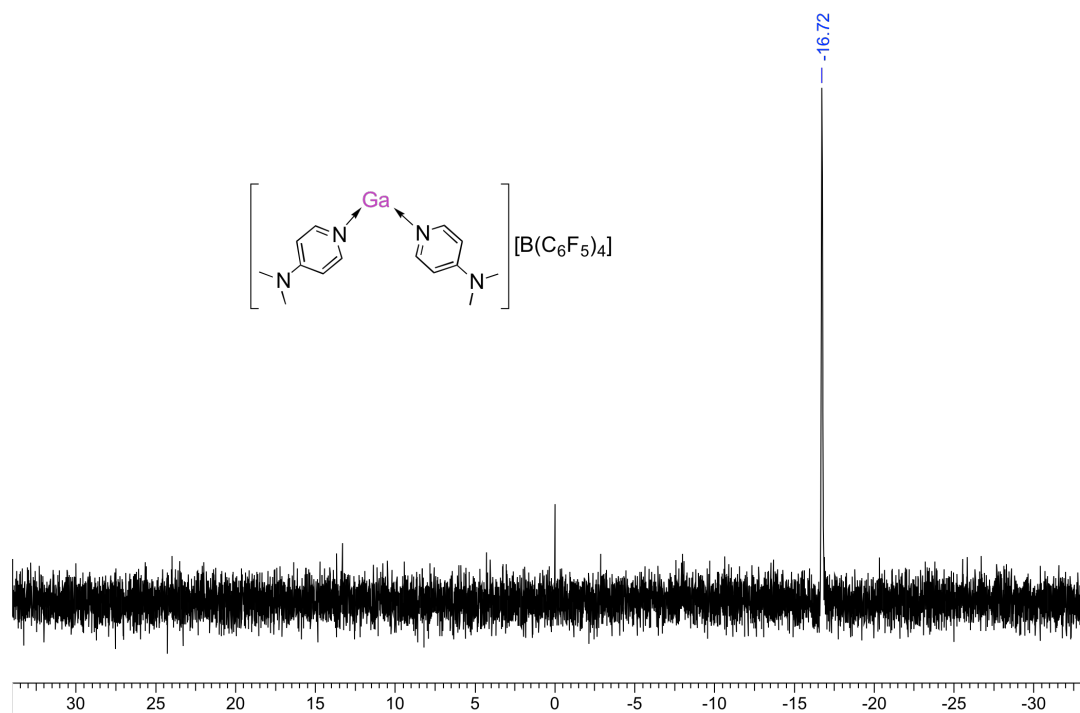


Figure A.33: $^{11}\text{B}\{^1\text{H}\}$ NMR spectrum of **4.5** in CD_3CN at 193 MHz.

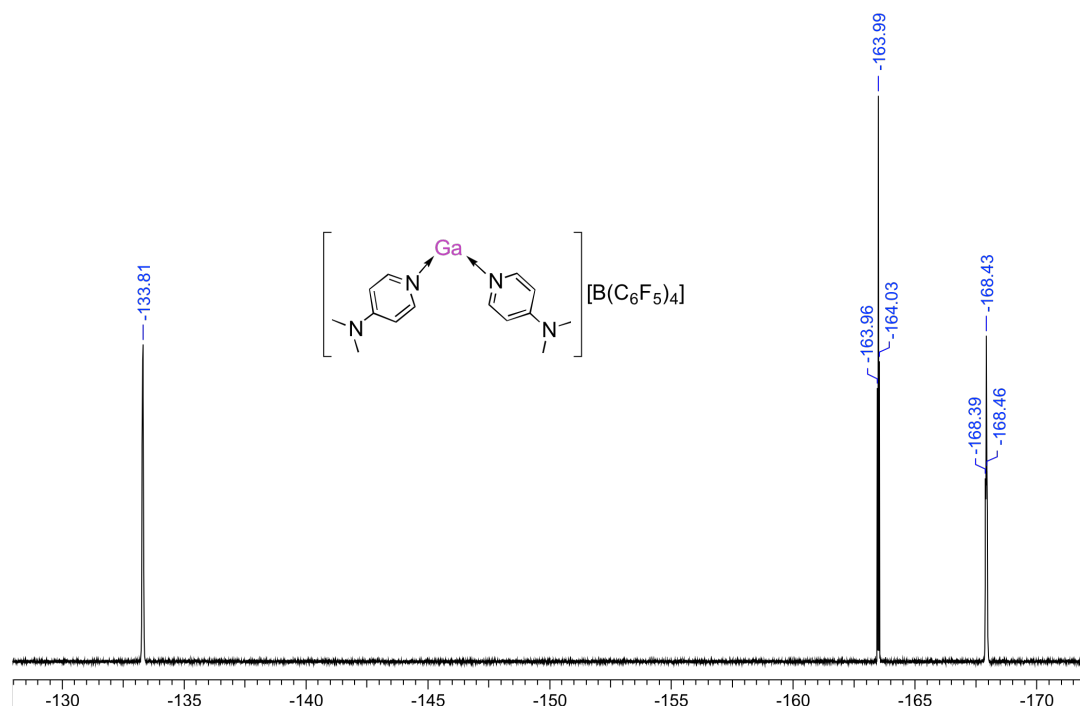


Figure A.34: ^{19}F NMR spectrum of **4.5** in CD_3CN at 564 MHz.

References

- [1] Bruker-AXS, SAINT version 2013.8, **2013**, Bruker-AXS, Madison, WI 53711, USA.
- [2] Bruker-AXS, SADABS version 2012.1, **2012**, Bruker-AXS, Madison, WI 53711, USA.
- [3] Sheldrick, G.M. *Acta Cryst.* **2015**, *A71*, 3-8.
- [4] Sheldrick, G.M. *Acta Cryst.* **2015**, *C71*, 3-8.
- [5] Bruker-AXS, XP version 2013.1, **2013**, Bruker-AXS, Madison, WI 53711, USA.

Appendix D: Supplementary Information for Chapter 5

Additional Experimental Details

Notes for the Synthesis of **5.3**

Although the synthesis of **5.1** remained high yielding at large scale, its solubility in Et₂O was found to be quite low and therefore the reaction solvent to synthesize **5.3** was changed to toluene. As toluene has a much higher boiling point than ether and the reaction was done at a much larger scale, the reaction mixture was exposed to light for a significantly longer time than previous attempts. This led to a colour change of the mixture from pale yellow to purple. Spectroscopically, the major product remained unchanged, but several impurities were detected in the ¹H NMR spectrum at low relative intensities. The conversion of **5.3** to this highly coloured was found to be very slow, despite the intense colour of the mixture. Attempts to purposely generate the impurity proved difficult due to the slow rate of conversion. Despite the light sensitivity, when the reaction and extraction solvents were changed to Et₂O and dichloromethane and the reaction mixture was protected from ambient light, **5.3** could be isolated in good yield and purity.

In addition to the light sensitivity of **5.3**, the large scale conversion of **5.3** to the triflate derivative **5.7** proved difficult, as an oil was obtained from many reaction mixtures. This was initially attributed to residual amounts of the purple impurity that formed from **5.3**, however, performing the transformation from **5.1** to **5.7** *in situ* and changing the reaction solvent did not aid in the isolation of **5.7** as a solid. A solution was found, as **5.7** could be formed in good yields when the reaction of AgOTf and **5.3** was allowed to stir for only 4 hours. Although an oil was initially obtained after separating the silver salts, pure, crystalline **5.7** was isolated through multiple triturations and recrystallizations, giving several batches of clean **5.7**.

Isolation of X-ray Quality Crystals of **5.2**, THF→GaCl₂Fl

A solution of GaCl₃ (0.17 g, 0.99 mmol) dissolved in toluene (2 mL) was added dropwise to a stirring solution of **5.1** (0.50 g, 0.99 mmol) dissolved in toluene (5 mL). The solution was allowed to stir at room temperature for 18 hours, at which point the solvent was removed under pressure, yielding a yellow oil. The oil was dissolved in THF (2 mL), and Et₂O (2 mL) was added to the solution in an attempt to grow X-ray quality crystals. Although unsuccessful, the solvent was removed under reduced pressure, yielding a yellow oil. The oil was left standing at room temperature for several days, at which point X-ray quality crystals of **5.2** had formed.

Isolation of X-ray Quality Crystals of **5.6**, NHC→GaCl₂Fl

A solution of GaCl₃ (0.17 g, 0.97 mmol) dissolved in benzene (2 mL) was added dropwise to a stirring solution of **5.3** (0.55 g, 0.97 mmol) dissolved in benzene (3 mL). The original pale orange colour of the solution dissipated within an hour. The mixture was allowed to stir at room temperature for approximately 6 hours, at which point the solvent was removed under reduced pressure. The residue was triturated with benzene (3 mL), the suspension was centrifuged and the supernatant was decanted. The precipitate was extracted using DCM (2 mL) and the solvent was removed under reduced pressure yielding a solid. The solid was dissolved in toluene (3 mL) and the solution was cooled to -20 °C, yielding X-ray quality crystals of **5.6**.

¹H NMR (600 MHz, CDCl₃, 298 K) δ: 8.05 (dd, *J* = 3 Hz, 8 Hz, 2H, Fl), 7.85 (dd, *J* = 3 Hz, 6 Hz, 2H, Fl), 7.32 – 7.29 (m, 4H, Fl), 4.40 (s, 1H, Ga-C₉H), 4.31 (septet, *J* = 7 Hz, 2H, N-CH-(CH₃)₂), 2.04 (s, 6H, C=C-CH₃), 0.97 (d, *J* = 7 Hz, 12H, N-CH-(CH₃)₂).

Synthesis of Tetramethylammonium Chlorotrimesitylgallate, [NMe₄][GaClMes₃]

A solution of GaMes₃ (0.50 g, 1.2 mmol) dissolved in a 1:1 mixture of CH₃CN and THF (3 mL) was added dropwise to a stirring solution of NMe₄Cl (0.13 g, 1.2 mmol) dissolved in CH₃CN (3 mL). A flocculent precipitate formed after approximately 20 minutes, and the mixture was allowed to stir for 18 hours. The solvent was removed under reduced pressure, and the solid was suspended in THF (5 mL). The mixture was centrifuged, and

the supernatant was removed. The precipitate was washed with THF (3 x 3 mL) and was dried under reduced pressure yielding a white solid, $[\text{NMe}_4][\text{GaClMes}_3]$. Crystals suitable for X-ray diffraction experiments were grown from a saturated solution of in CH_3CN cooled to $-20\text{ }^\circ\text{C}$.

Yield: (57 %); mp: $261 - 265\text{ }^\circ\text{C}$ (decomposition); ^1H NMR (600 MHz, CD_3CN , 298 K) δ : 6.61 (s, 6H, *m*-CH), 3.09 (s, 12H, $[\text{N}(\text{CH}_3)_4]^+$), 2.24 (s, 18H, *o*-CH₃), 2.17 (s, 9H, *p*-CH₃); $^{13}\text{C}\{^1\text{H}\}$ NMR (151 MHz, CD_3CN , 298 K) δ : 155.12 (Ga-C), 146.38 (*o*-C-CH₃), 135.62 (*m*-CH), 128.08 (*p*-C-CH₃), 56.55 ($[\text{N}(\text{CH}_3)_4]^+$), 26.27 (*o*-CH₃), 21.46 (*p*-CH₃); $^{71}\text{Ga}\{^1\text{H}\}$ NMR (183 MHz, CD_3CN , 298 K) δ : no signal; LR ESI-TOF MS (*m/z*; negative ion): 377 ($[\text{Ga}^{35}\text{Cl}_2\text{Mes}_2]^-$), 461 ($[\text{Ga}^{35}\text{ClMes}_3]^-$); HR ESI-TOF MS (*m/z*; negative ion): Calcd. for $[\text{C}_{27}\text{H}_{33}^{35}\text{Cl}^{69}\text{Ga}]^-$: 461.1527, Found: 461.1519; Elemental analysis data could not be obtained for $[\text{NMe}_4][\text{GaClMes}_3]$ due to residual contamination of the NMe_4Cl salt.

Alternative Synthesis of Dichloro-2,6-dimesitylphenylgallane, Ar^*GaCl_2

Ar^*_2GaCl was synthesized according to literature procedures.¹ A solution of GaCl_3 dissolved in toluene was added to one equivalent of Ar^*_2GaCl as a stirring solution dissolved in toluene. The mixture was allowed to stir for approximately 24 hours, at which point the solvent was removed under reduced pressure, yielding a brown solid, Ar^*GaCl_2 . X-ray quality crystals were obtained from concentrating a solution of Ar^*GaCl_2 in toluene under reduced pressure.

Crystallographic Data

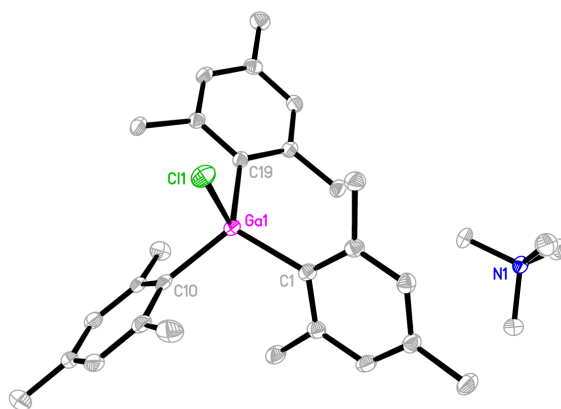


Figure A.35: Displacement ellipsoid plot of $[\text{NMe}_4][\text{GaClMes}_3]$. Ellipsoids are drawn at the 50% probability level and hydrogen atoms are omitted for clarity. Selected bond lengths and angles (\AA , $^\circ$): Ga1-C1 2.0360(18), Ga1-C10 2.0361(18), Ga1-C19 2.0371(18), Ga1-Cl1 2.3536(6); Cl1-Ga1-C1 104.56(5), Cl1-Ga1-C10 102.05(5), Cl1-Ga1-C19 99.38(5).

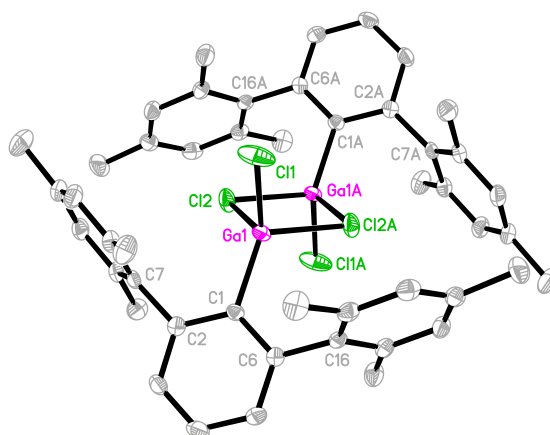


Figure A.36: Displacement ellipsoid plot of Ar^*GaCl_2 . Ellipsoids are drawn at the 50% probability level and hydrogen atoms are omitted for clarity. Selected bond lengths and angles (\AA , $^\circ$): Ga1-C1 1.946(2), Ga1-Cl1 2.1571(7), Ga1-Cl2 2.3142(6), Ga1A-Cl2 2.3146(7); C1-Ga1-Cl1 126.93(6), C1-Ga1-Cl2 112.38(6), Cl1-Ga1-Cl2 103.61(3), Cl2-Ga1-Cl2A 87.95(2), Ga1-Cl2-Ga1A 92.05(2).

Table A.7: Selected crystallographic data for [NMe₄][GaClMes₃] and Ar*GaCl₂.

Formula	C ₃₃ H ₄₈ ClGaN ₂	C _{27.50} H ₂₉ Cl ₂ Ga
M _r (g mol ⁻¹)	577.90	500.13
Crystal size (mm)	0.233 x 0.143 x 0.082	0.323 x 0.155 x 0.144
Crystal colour/habit	Colourless prism	Colourless prism
Crystal system	Monoclinic	Triclinic
Space group	P 2 ₁ /n	P -1
T (K)		110
<i>a</i> (Å)	16.896(2)	9.0822(16)
<i>b</i> (Å)	9.0381(18)	11.6960(20)
<i>c</i> (Å)	20.516(3)	12.6067(18)
α (°)	90	108.192(8)
β (°)	93.044(10)	95.285(8)
γ (°)	90	103.282(7)
V (Å ³)	3128.5(8)	1218.6(4)
Z	4	2
F(000)	1232	518
ρ (g cm ⁻³)	1.227	1.363
λ (Å)		1.54178 (Cu Kα)
μ (cm ⁻¹)	2.145	3.637
Diffractometer type	Nonius Bruker KappaCCD Apex2	
Max 2θ (°)	127.52	128.326
Measd fraction of data	0.992	0.962
Reflns measd	34437	23675
Unique reflns	5125	3912
R _{merge}	0.0355	0.0268
Reflns in refinement	5125	3912
Number of params	344	290
R ₁	0.0287	0.0289
wR ₂	0.0712	0.0767
R ₁ (all data)	0.0323	0.0305
wR ₂ (all data)	0.0735	0.0786
GOF	1.043	1.072
Min/max peak heights on final ΔF map (e Å ⁻¹)	-0.574, 0.701	-0.586, 0.690

Where: $R_1 = \Sigma(|F_o| - |F_c|) / \Sigma F_o$; $wR_2 = [\Sigma(w(F_o^2 - F_c^2)^2) / \Sigma(wF_o^4)]^{1/2}$; $GOF = [\Sigma(w(F_o^2 - F_c^2)^2) / (\text{No. of reflns.} - \text{No. of params.})]^{1/2}$

Crystallographic Details

Data Collection and Processing. The samples were mounted on a MiTeGen polyimide micromount with a small amount of Paratone N oil. The data collection strategy was a number of ω and φ scans. The frame integration was performed using SAINT.² The resulting raw data was scaled and absorption corrected using a multi-scan averaging of symmetry equivalent data using SADABS.³

Structure Solution and Refinement. The structures were solved by using a dual space methodology using the SHELXT program.⁴ All non-hydrogen atoms were obtained from the initial solution. The hydrogen atoms were introduced at idealized positions and were allowed to ride on the parent atom. For Ar^{*}GaCl₂, a molecule of toluene was found to be disordered about an inversion center, and was refined using a number of restraints. The structural model was fit to the data using full matrix least-squares based on F^2 . The calculated structure factors included corrections for anomalous dispersion from the usual tabulation. The structure was refined using the SHELXL-2014 program from the SHELXTL suite of crystallographic software.⁵ Graphic plots were produced using the XP program suite.⁶

Additional Crystallographic Details

5.1•Et₂O, [Li(Et₂O)][GaCl₂FIMes]•Et₂O

For **5.1**, multiple regions of disorder were found within the asymmetric unit. Flipping of the terminal methyl group of one of the ether molecules bound to Li1 was found to refine to a normalized occupancy value of 0.532(14) for C24A. Disorder of the CH₂ in the other ether molecule bound to Li1 was found to refine to a normalized occupancy value of 0.56(3) for C27A. Both ether molecules of the other molecule in the asymmetric unit were more heavily disordered, and refined to normalized occupancy values of 0.571(10) for C23C, C25C and C26C, and 0.741(10) for C27C and C28C.

5.3, NHC→GaCIFIMes

For **5.3**, two regions of solvent disorder were observed in the asymmetric unit. The first was located on the (0.5, 0.5, 0.5) special position, which corresponded to a disordered ether solvent molecule, with the oxygen located on the inversion centre. The second was a disordered toluene molecule centred at an inversion centre, with additional electron density stretching in two directions. Attempts at refining the disordered solvent molecules were unsuccessful. The SQUEEZE⁷ procedure featured in the PLATON program⁸ was then used to remove the areas of electron density. No other significant residual peaks were observed in the difference map following the application of the SQUEEZE program.

5.7, NHC→GaOTfFIMes

For **5.7**, the initial indexing indicated the sample crystal was a non-merohedral twin. The twin law was determined to be:

```
Twin Law, Sample 1 of 1
Transforms h1.1(1)->h1.2(2)
-1.00026 0.00129 -0.43334
-0.02247 -0.99999 -0.01004
0.00125 -0.00036 1.00027
```

which corresponds to an approximately -179.8° rotation about the [100] vector in reciprocal space. The data demonstrated that the minor component of the twin refined to a normalized occupancy value of 0.01271(18). Due to the small size of the secondary domain, the larger R_1 value obtained when including all the data, and increased noise observed in the difference map, the structural model was refined using only data from the dominant component of the twin.

5.8, NHC→GaFFIMes

For **5.8**, the asymmetric unit demonstrated two regions of disorder, postulated to be two molecules of disordered toluene, which were located in the difference map. They were located around and on inversion centres, respectively. While a model was initially

determined for the first molecule, upon anisotropic refinement, the model was not stable, even after the introduction of numerous restraints. A model was not able to be generated for the second molecule that was located on the inversion centre. The data were then subject to the SQUEEZE procedure,⁷ as implemented in the PLATON program.⁸

5.9, DMAP→GaOTfFIMes

For **5.9**, upon obtaining the solution, it was discovered that similar to other compounds of this type, the structure was of a racemic mixture. Unlike other examples, the presence of disordered dichloromethane solvent molecules did not allow the compound to crystallize in a centrosymmetric space group. As such, the Flack parameter for the structure in the Pn space group was found to be very close to 0.50 (0.49) due to the presence of both enantiomers in the asymmetric unit. In addition, the disordered dichloromethane solvent molecules could not be refined by a reasonable model, and the data were subject to the SQUEEZE⁷ procedure, as implemented in the PLATON program.⁸

Spectroscopic Data

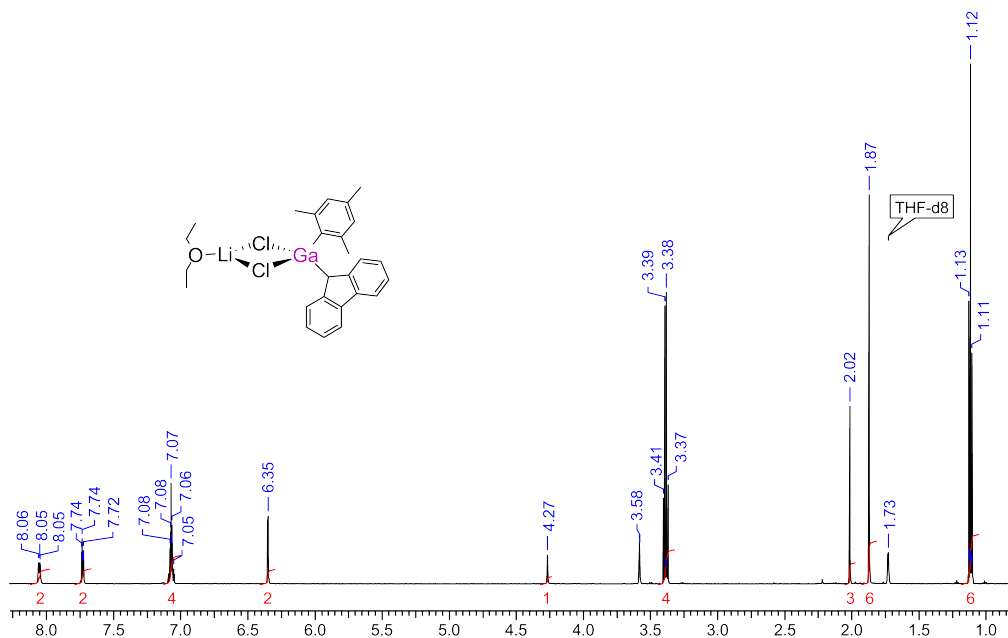


Figure A.37: ¹H NMR spectrum of **5.1** in THF-*d*₈ at 600 MHz.

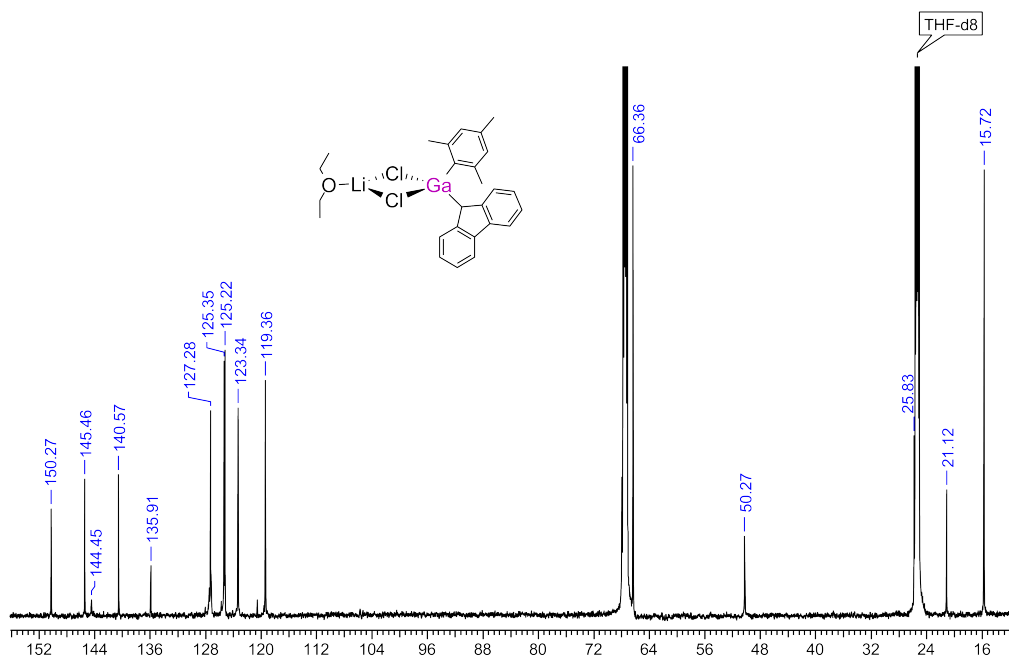


Figure A.38: $^{13}\text{C}\{^1\text{H}\}$ NMR spectrum of **5.1** in $\text{THF-}d_8$ at 151 MHz.

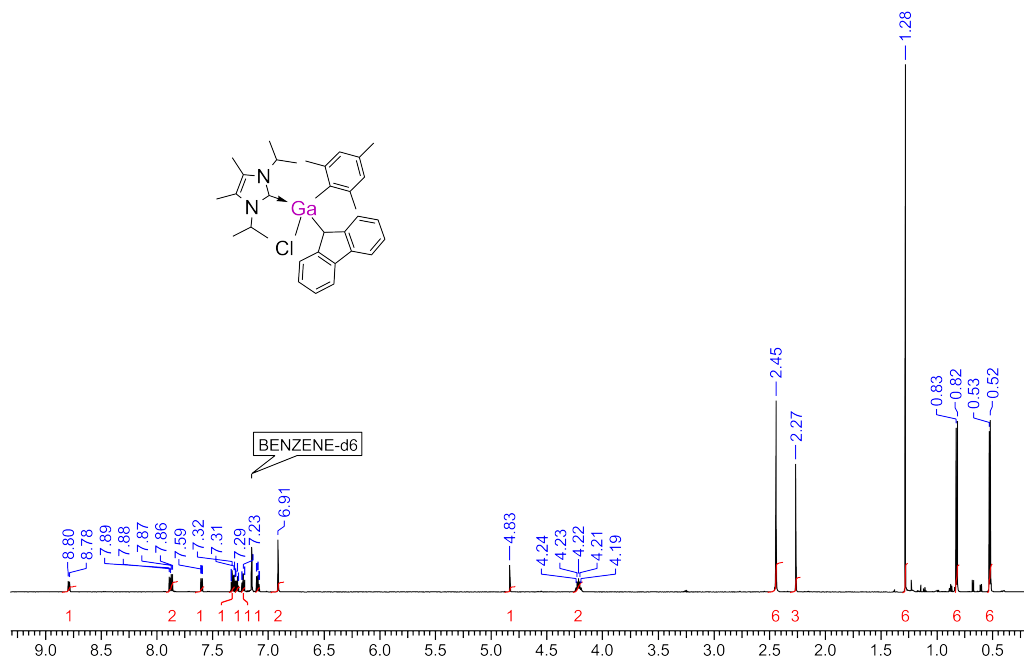


Figure A.39: ^1H NMR spectrum of **5.3** in C_6D_6 at 600 MHz.

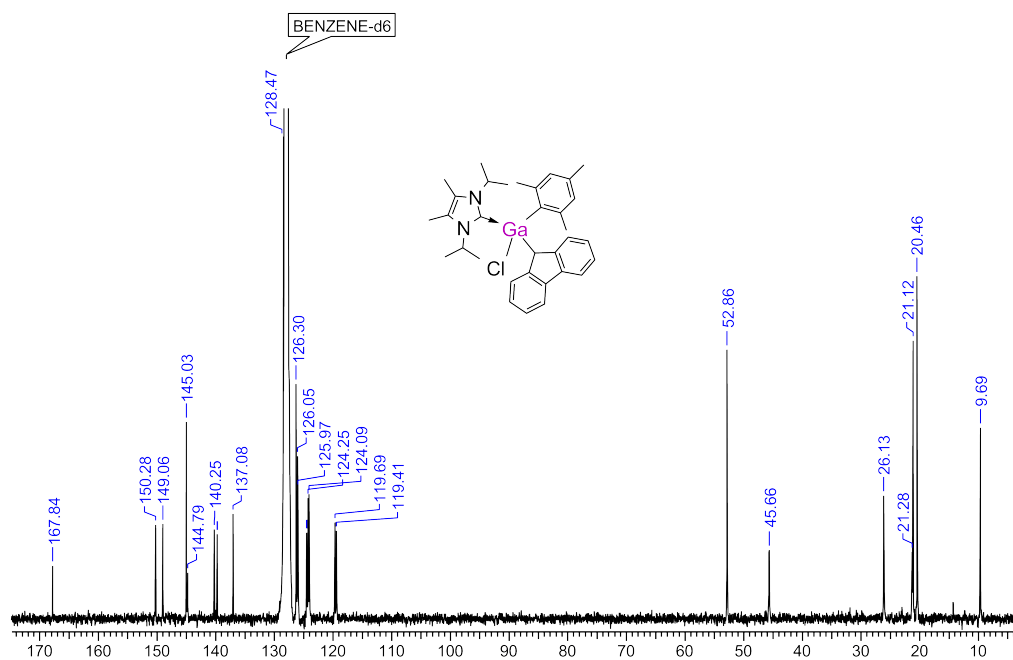


Figure A.40: $^{13}\text{C}\{^1\text{H}\}$ NMR spectrum of **5.3** in C_6D_6 at 151 MHz.

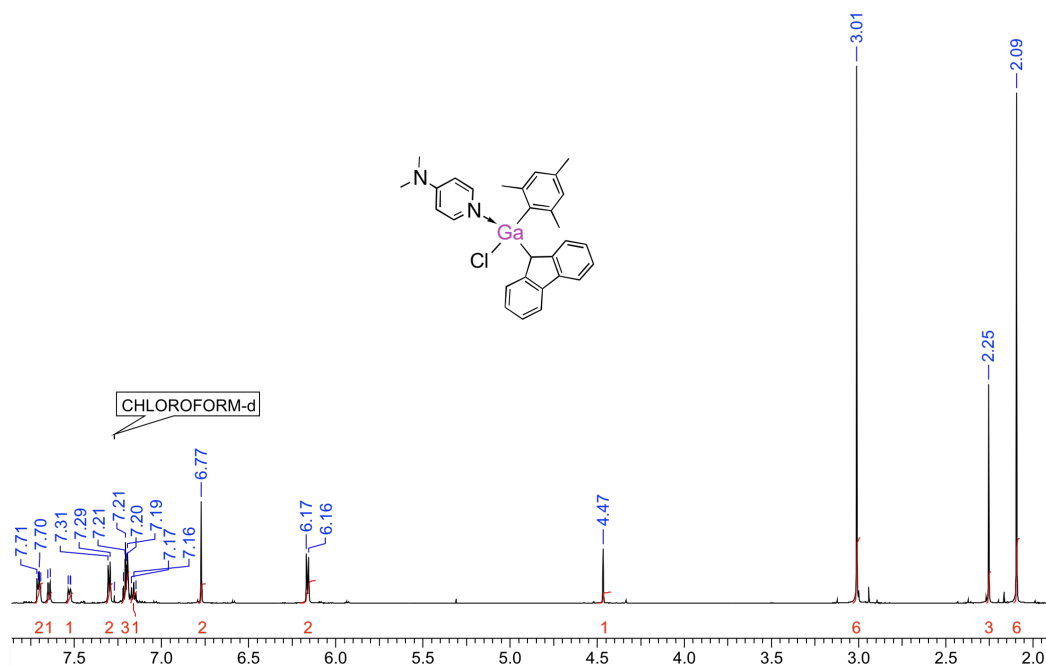


Figure A.41: ^1H NMR spectrum of **5.4** in CDCl_3 at 600 MHz.

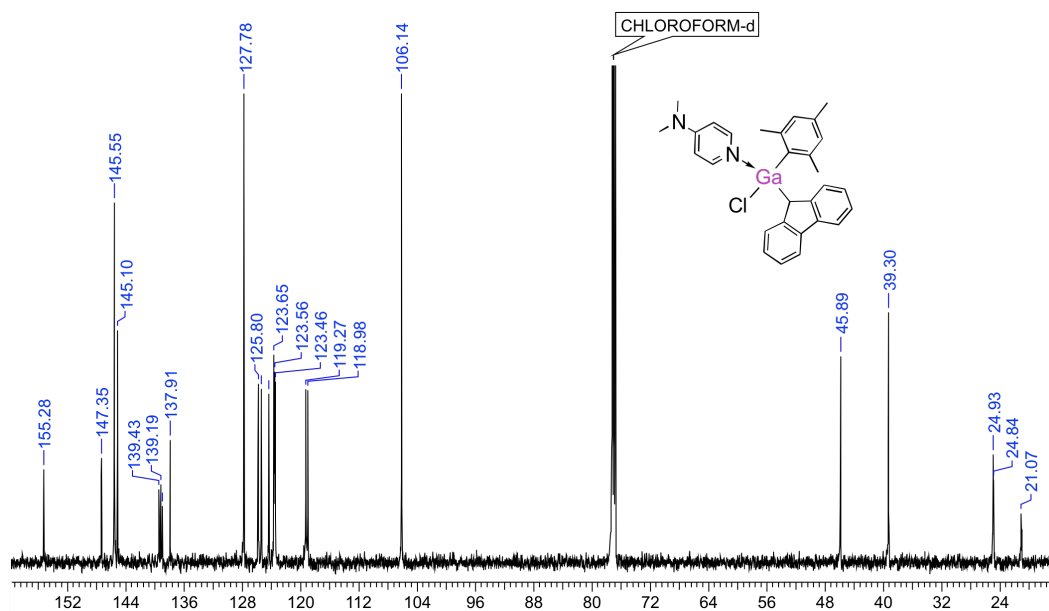


Figure A.42: $^{13}\text{C}\{^1\text{H}\}$ NMR spectrum of **5.4** in CDCl_3 at 151 MHz.

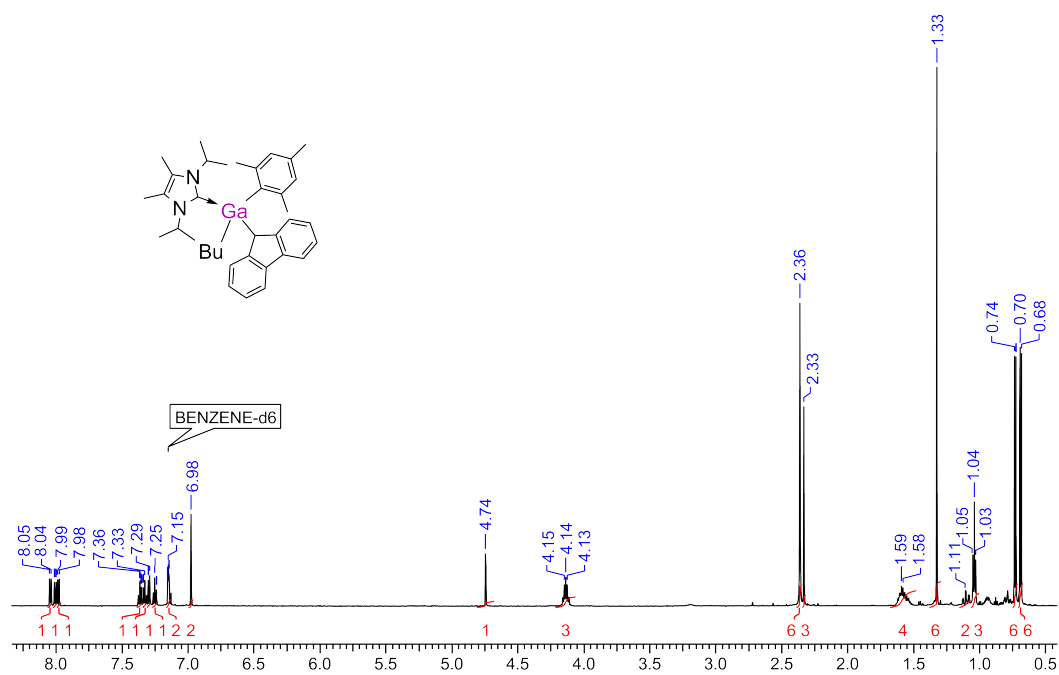


Figure A.43: ^1H NMR spectrum of **5.5** in C_6D_6 at 600 MHz.

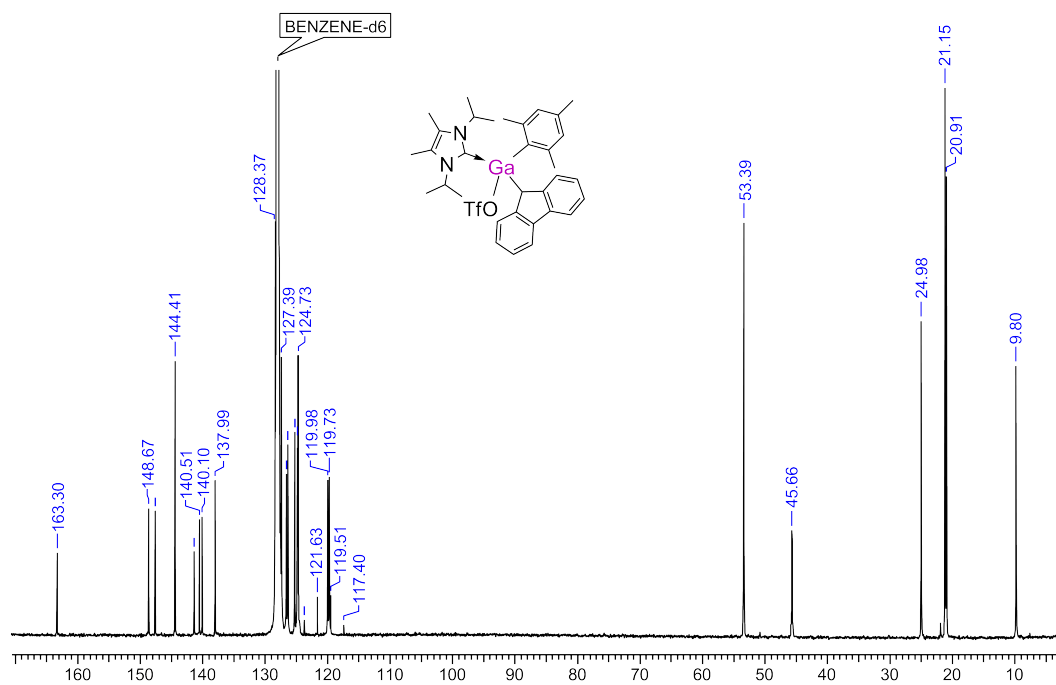


Figure A.46: $^{13}\text{C}\{^1\text{H}\}$ NMR spectrum of **5.7** in C_6D_6 at 151 MHz.

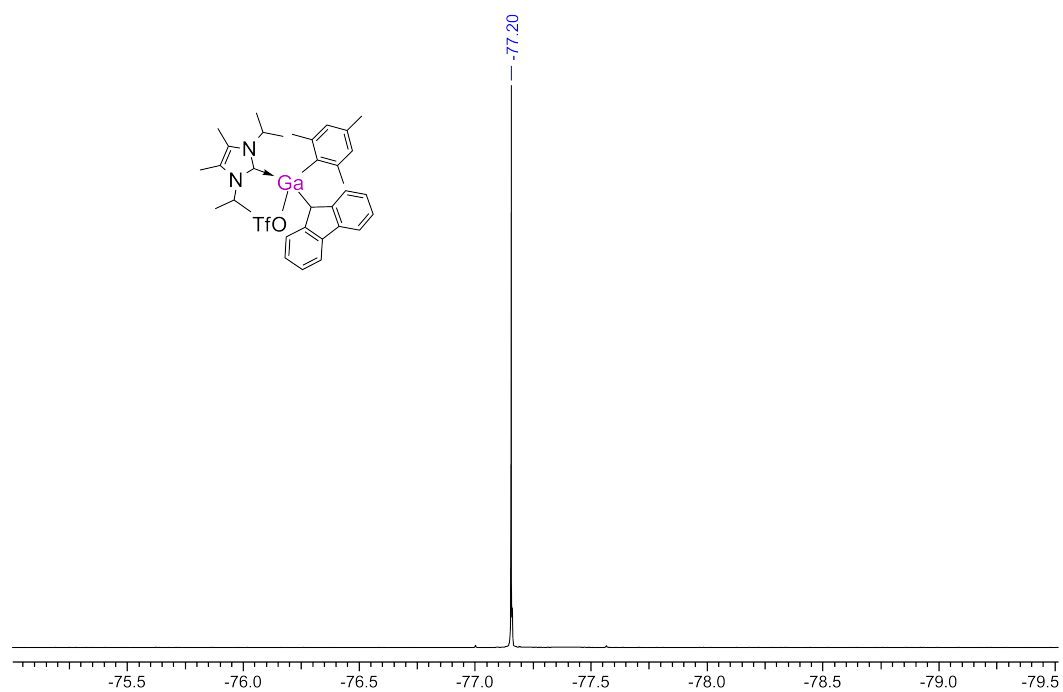


Figure A.47: ^{19}F NMR spectrum of **5.7** in C_6D_6 at 564 MHz.

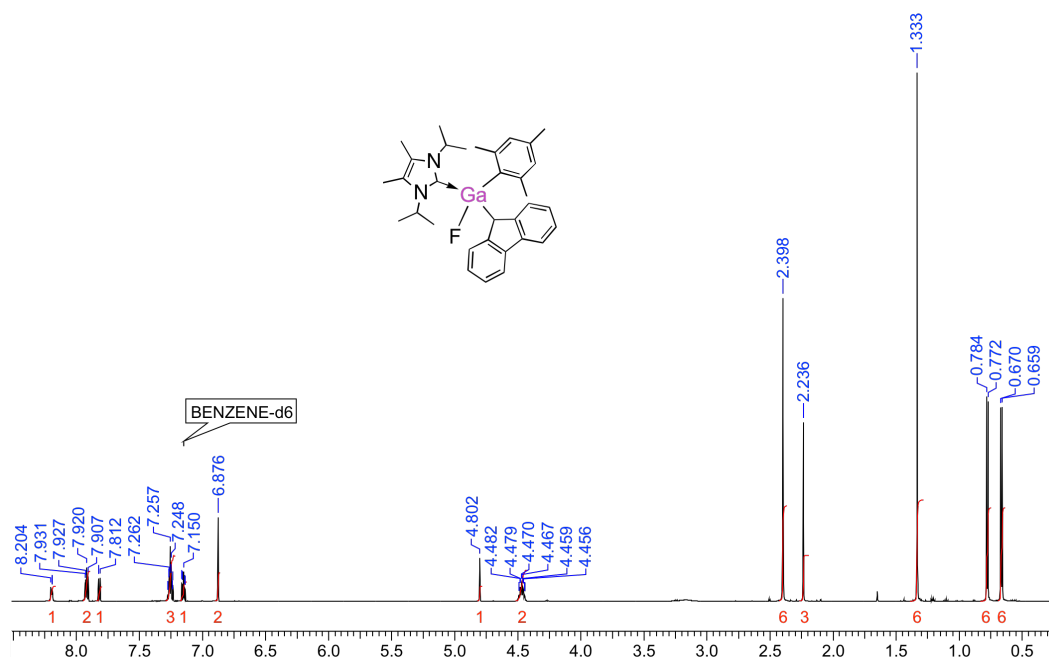


Figure A.48: ^1H NMR spectrum of **5.8** in C_6D_6 at 600 MHz.

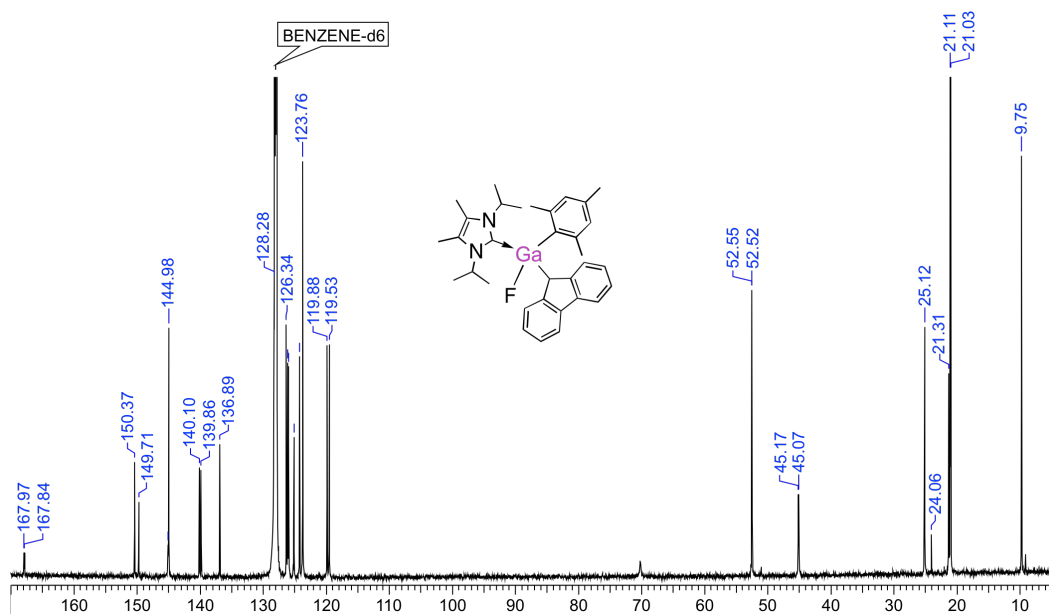


Figure A.49: $^{13}\text{C}\{^1\text{H}\}$ NMR spectrum of **5.8** in C_6D_6 at 151 MHz.

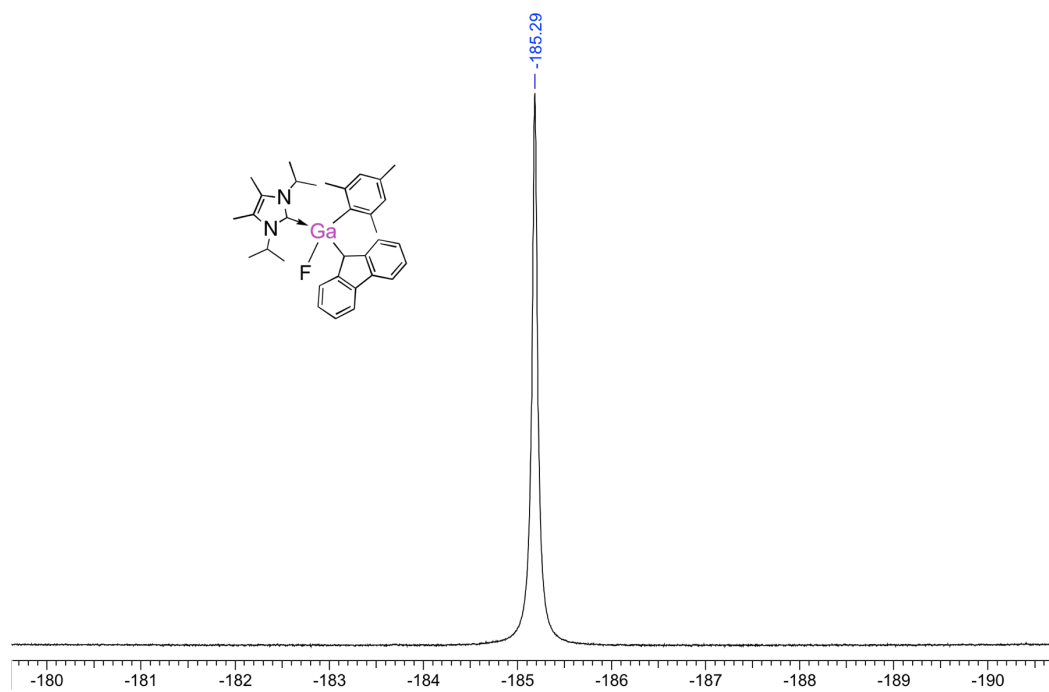


Figure A.50: ^{19}F NMR spectrum of **5.8** in C_6D_6 at 564 MHz.

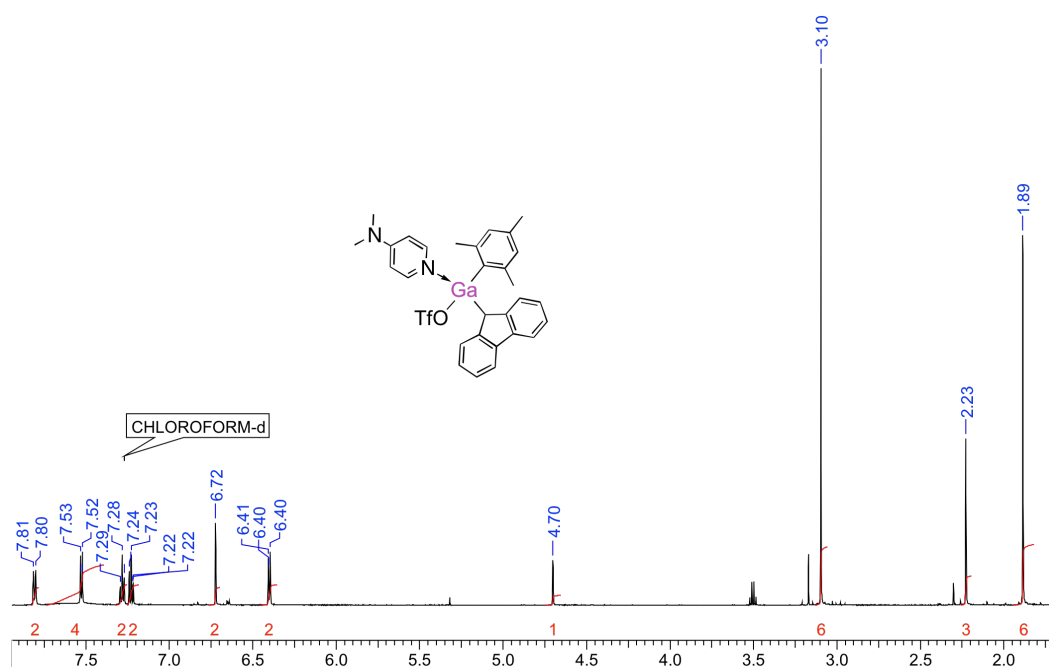


Figure A.51: ^1H NMR spectrum of **5.9** in CDCl_3 at 600 MHz.

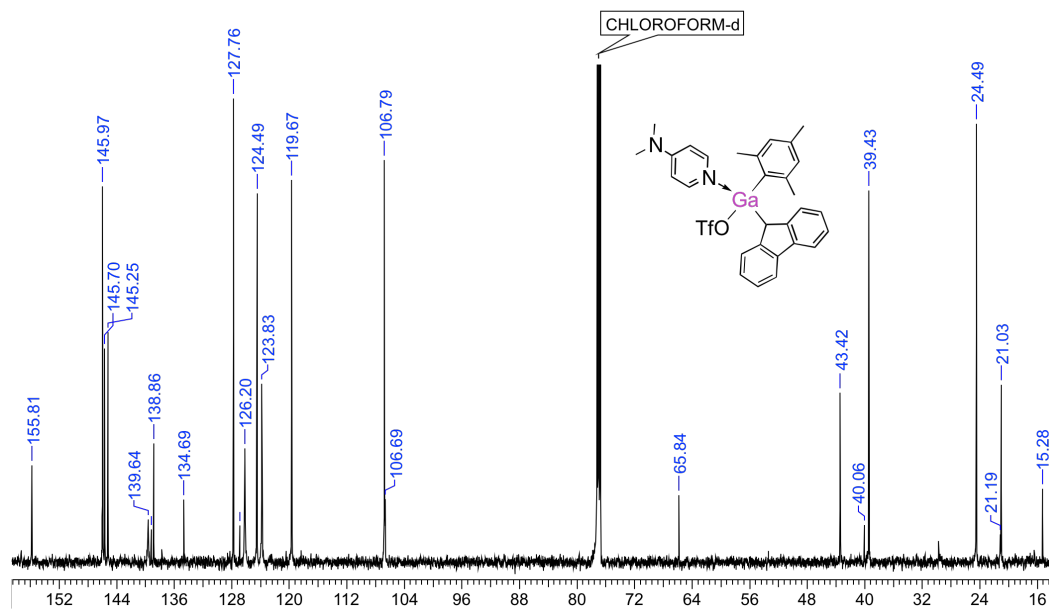


Figure A.52: $^{13}\text{C}\{^1\text{H}\}$ NMR spectrum of **5.9** in CDCl_3 at 151 MHz.

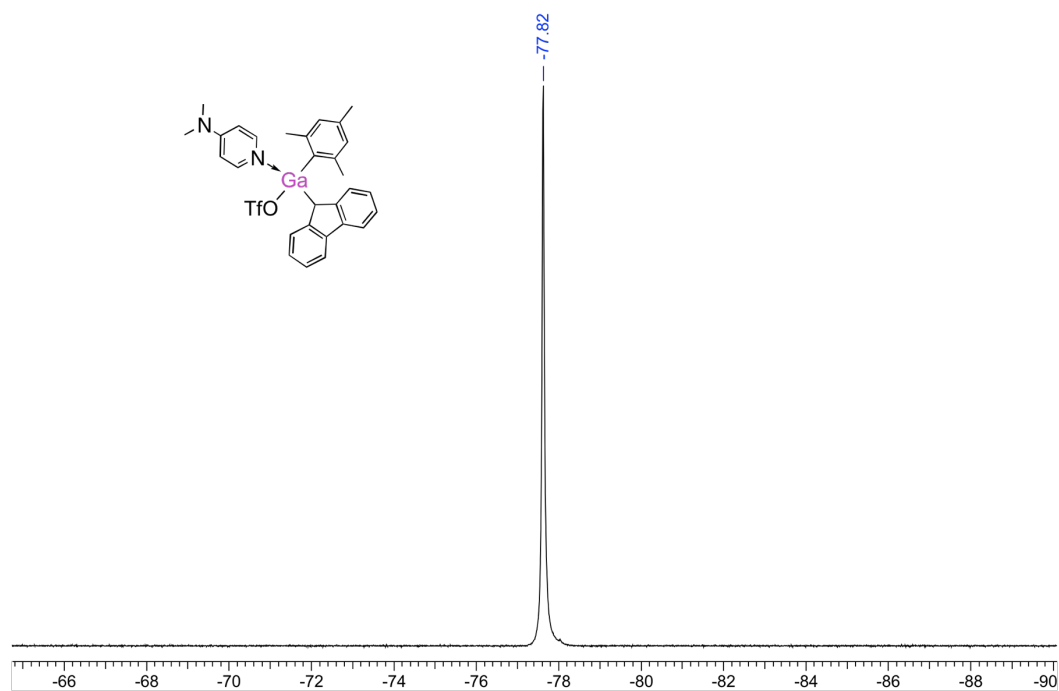


Figure A.53: ^{19}F NMR spectrum of **5.9** in CDCl_3 at 564 MHz.

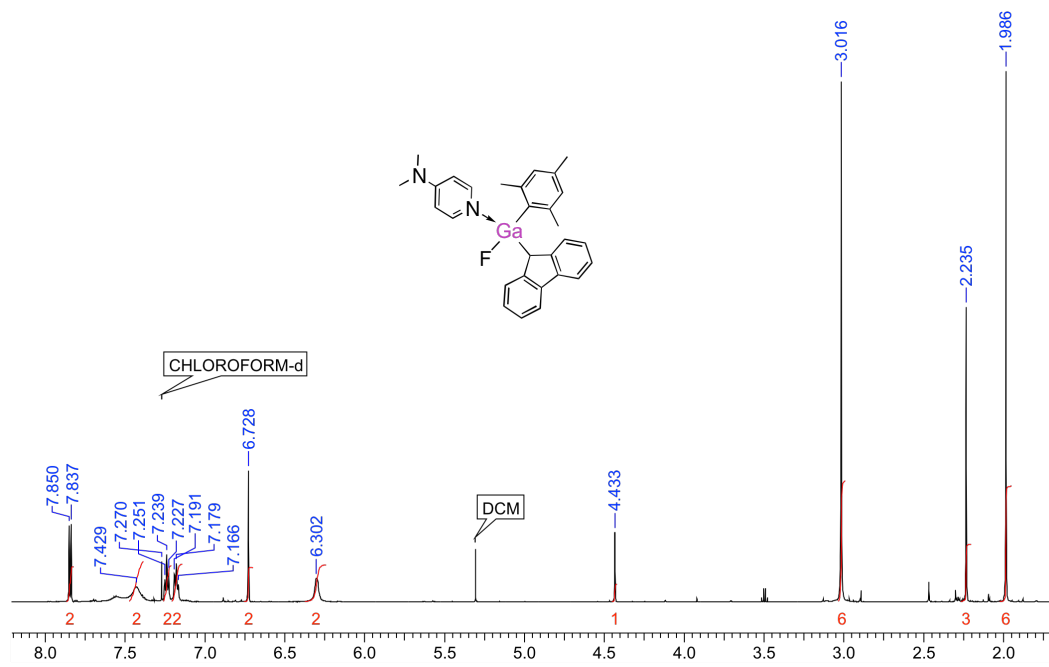


Figure A.54: ^1H NMR spectrum of 5.10 in CDCl_3 at 600 MHz.

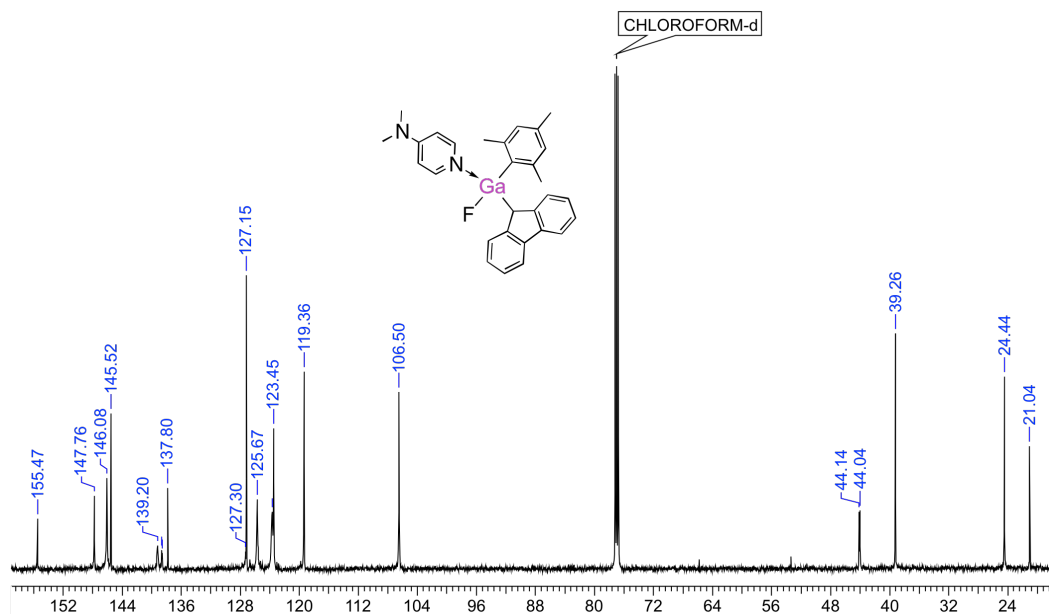


Figure A.55: $^{13}\text{C}\{^1\text{H}\}$ NMR spectrum of 5.10 in CDCl_3 at 151 MHz.

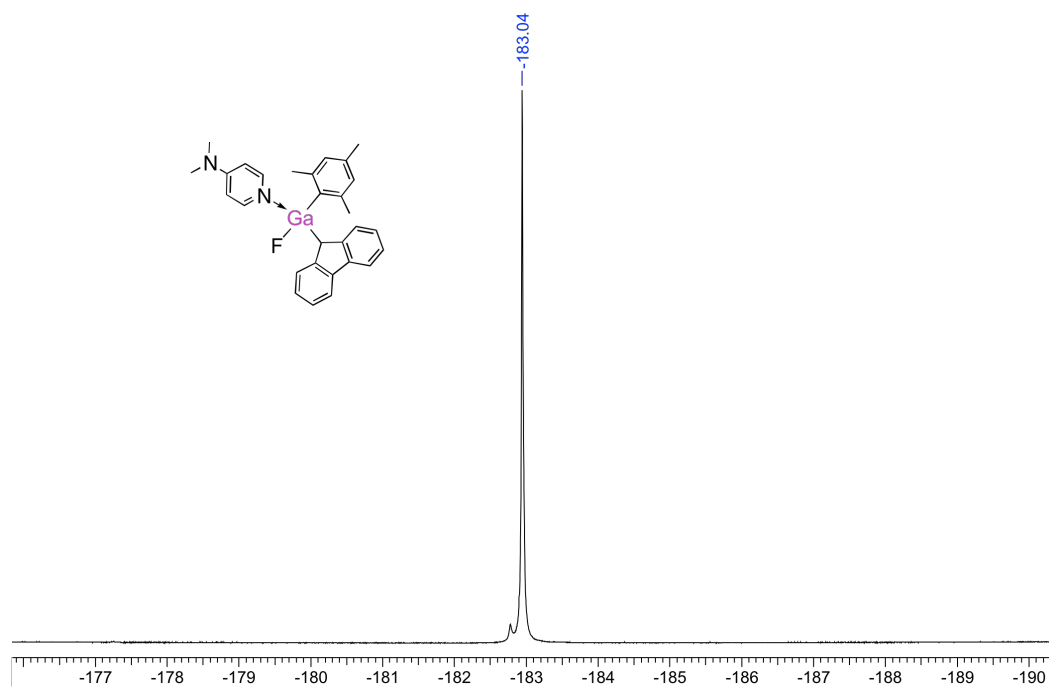


Figure A.56: ^{19}F NMR spectrum of **5.10** in CDCl_3 at 564 MHz.

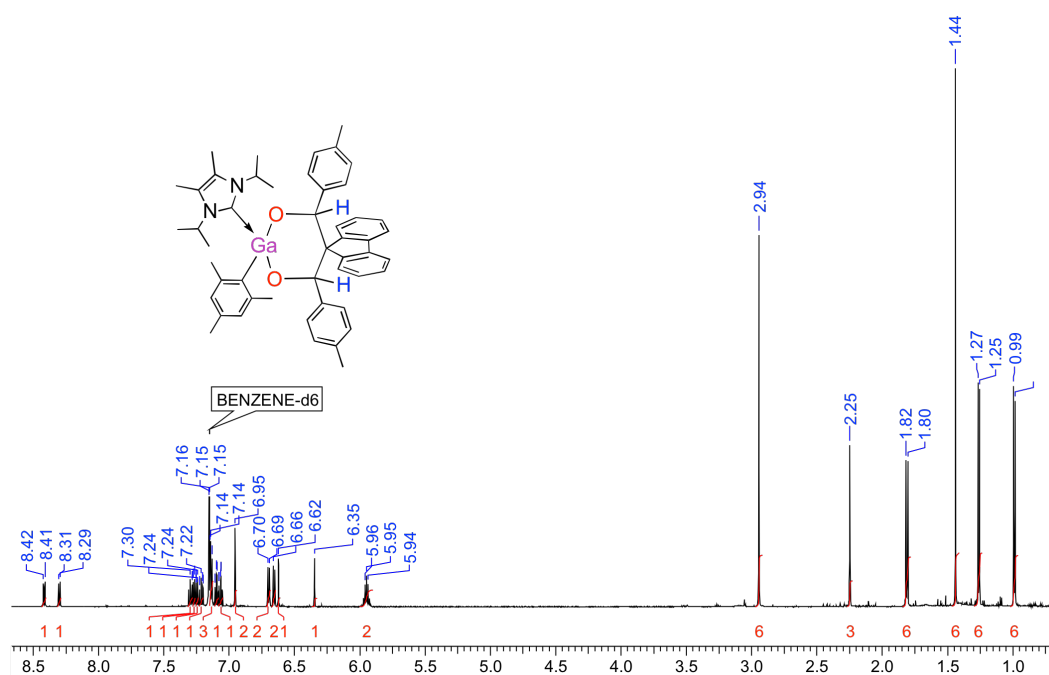


Figure A.57: ^1H NMR spectrum of **5.11** in C_6D_6 at 600 MHz.

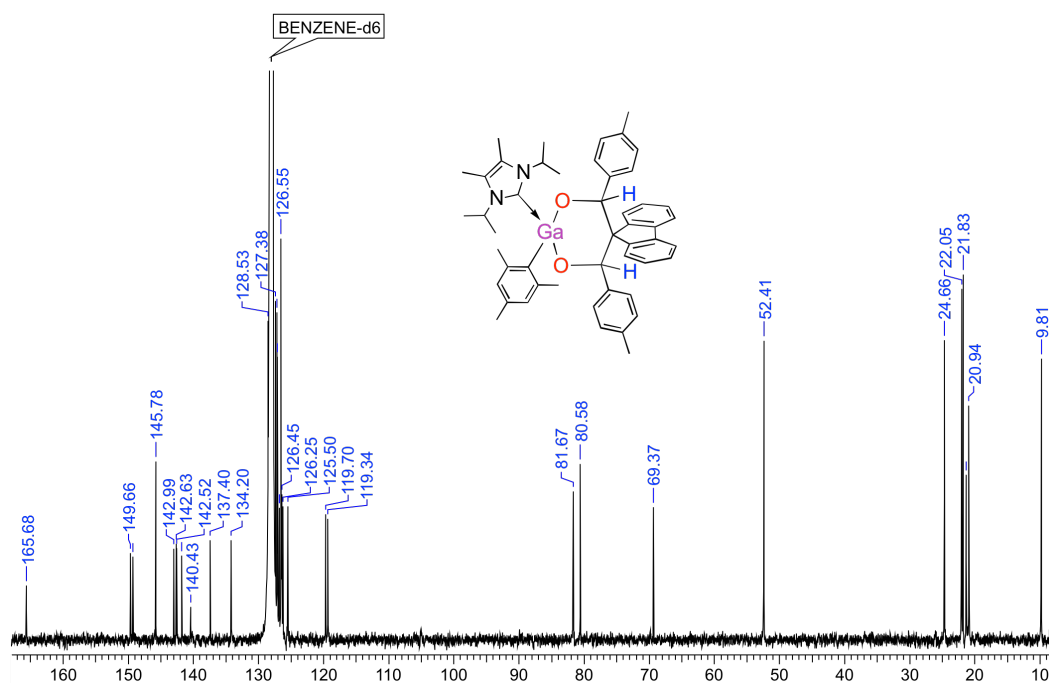


Figure A.58: $^{13}\text{C}\{^1\text{H}\}$ NMR spectrum of **5.11** in C_6D_6 at 151 MHz.

References

- [1] Li, X.-W.; Pennington, W.T.; Robinson, G.H. *Organometallics* **1995**, *14*, 2109-2111.
- [2] Bruker-AXS, SAINT version 2013.8, **2013**, Bruker-AXS, Madison, WI 53711, USA.
- [3] Bruker-AXS, SADABS version 2012.1, **2012**, Bruker-AXS, Madison, WI 53711, USA.
- [4] Sheldrick, G.M. *Acta Cryst.* **2015**, *A71*, 3-8.
- [5] Sheldrick, G.M. *Acta Cryst.* **2015**, *C71*, 3-8.
- [6] Bruker-AXS, XP version 2013.1, **2013**, Bruker-AXS, Madison, WI 53711, USA.
- [7] van der Sluis, P.; Spek, A.L. *Acta Cryst.* **1990**, *A46*, 194-201.
- [8] Spek, A. L. *J. Appl. Cryst.* **2003**, *36*, 7-13.

Appendix E: Copyrighted Material and Permissions

Chapter 2 – John Wiley and Sons License Agreement

JOHN WILEY AND SONS LICENSE

TERMS AND CONDITIONS

Aug 23, 2017

This Agreement between Mr. Jeremy Bourque ("You") and John Wiley and Sons ("John Wiley and Sons") consists of your license details and the terms and conditions provided by John Wiley and Sons and Copyright Clearance Center.

License Number	4174820442283
License date	Aug 23, 2017
Licensed Content Publisher	John Wiley and Sons
Licensed Content Publication	Chemistry - A European Journal
Licensed Content Title	Synthesis and Characterization of Cationic Low-Valent Gallium Complexes of Cryptand[2.2.2]
Licensed Content Author	Jeremy L. Bourque,Paul D. Boyle,Kim M. Baines
Licensed Content Date	Jun 3, 2015
Licensed Content Pages	7
Type of use	Dissertation/Thesis
Requestor type	Author of this Wiley article
Format	Print and electronic
Portion	Full article
Will you be translating?	No
Title of your thesis / dissertation	Coordination and Organometallic Chemistry of Novel Gallium Complexes: Synthesis, Reactivity and Spectroscopy
Expected completion date	Aug 2017
Expected size (number of pages)	270
Requestor Location	Mr. Jeremy Bourque Department of Chemistry Western University 1151 Richmond St London, ON N6A 5B7 Canada Attn: Mr. Jeremy Bourque
Publisher Tax ID	EU826007151
Billing Type	Invoice
Billing Address	Mr. Jeremy Bourque Department of Chemistry Western University

1151 Richmond St
London, ON N6A 5B7
Canada
Attn: Mr. Jeremy Bourque
0.00 CAD

Total
Terms and Conditions

TERMS AND CONDITIONS

This copyrighted material is owned by or exclusively licensed to John Wiley & Sons, Inc. or one of its group companies (each a "Wiley Company") or handled on behalf of a society with which a Wiley Company has exclusive publishing rights in relation to a particular work (collectively "WILEY"). By clicking "accept" in connection with completing this licensing transaction, you agree that the following terms and conditions apply to this transaction (along with the billing and payment terms and conditions established by the Copyright Clearance Center Inc., ("CCC's Billing and Payment terms and conditions"), at the time that you opened your RightsLink account (these are available at any time at <http://myaccount.copyright.com>).

Terms and Conditions

The materials you have requested permission to reproduce or reuse (the "Wiley Materials") are protected by copyright.

You are hereby granted a personal, non-exclusive, non-sub licensable (on a stand-alone basis), non-transferable, worldwide, limited license to reproduce the Wiley Materials for the purpose specified in the licensing process. This license, and any CONTENT (PDF or image file) purchased as part of your order, is for a one-time use only and limited to any maximum distribution number specified in the license. The first instance of republication or reuse granted by this license must be completed within two years of the date of the grant of this license (although copies prepared before the end date may be distributed thereafter). The Wiley Materials shall not be used in any other manner or for any other purpose, beyond what is granted in the license. Permission is granted subject to an appropriate acknowledgement given to the author, title of the material/book/journal and the publisher. You shall also duplicate the copyright notice that appears in the Wiley publication in your use of the Wiley Material. Permission is also granted on the understanding that nowhere in the text is a previously published source acknowledged for all or part of this Wiley Material. Any third party content is expressly excluded from this permission.

With respect to the Wiley Materials, all rights are reserved. Except as expressly granted by the terms of the license, no part of the Wiley Materials may be copied, modified, adapted (except for minor reformatting required by the new Publication), translated, reproduced, transferred or distributed, in any form or by any means, and no derivative works may be made based on the Wiley Materials without the prior permission of the respective copyright owner. For STM Signatory Publishers clearing permission under the

terms of the STM Permissions Guidelines only, the terms of the license are extended to include subsequent editions and for editions in other languages, provided such editions are for the work as a whole in situ and does not involve the separate exploitation of the permitted figures or extracts, You may not alter, remove or suppress in any manner any copyright, trademark or other notices displayed by the Wiley Materials. You may not license, rent, sell, loan, lease, pledge, offer as security, transfer or assign the Wiley Materials on a stand-alone basis, or any of the rights granted to you hereunder to any other person.

The Wiley Materials and all of the intellectual property rights therein shall at all times remain the exclusive property of John Wiley & Sons Inc, the Wiley Companies, or their respective licensors, and your interest therein is only that of having possession of and the right to reproduce the Wiley Materials pursuant to Section 2 herein during the continuance of this Agreement. You agree that you own no right, title or interest in or to the Wiley Materials or any of the intellectual property rights therein. You shall have no rights hereunder other than the license as provided for above in Section 2. No right, license or interest to any trademark, trade name, service mark or other branding ("Marks") of WILEY or its licensors is granted hereunder, and you agree that you shall not assert any such right, license or interest with respect thereto

NEITHER WILEY NOR ITS LICENSORS MAKES ANY WARRANTY OR REPRESENTATION OF ANY KIND TO YOU OR ANY THIRD PARTY, EXPRESS, IMPLIED OR STATUTORY, WITH RESPECT TO THE MATERIALS OR THE ACCURACY OF ANY INFORMATION CONTAINED IN THE MATERIALS, INCLUDING, WITHOUT LIMITATION, ANY IMPLIED WARRANTY OF MERCHANTABILITY, ACCURACY, SATISFACTORY QUALITY, FITNESS FOR A PARTICULAR PURPOSE, USABILITY, INTEGRATION OR NON-INFRINGEMENT AND ALL SUCH WARRANTIES ARE HEREBY EXCLUDED BY WILEY AND ITS LICENSORS AND WAIVED BY YOU.

WILEY shall have the right to terminate this Agreement immediately upon breach of this Agreement by you.

You shall indemnify, defend and hold harmless WILEY, its Licensors and their respective directors, officers, agents and employees, from and against any actual or threatened claims, demands, causes of action or proceedings arising from any breach of this Agreement by you.

IN NO EVENT SHALL WILEY OR ITS LICENSORS BE LIABLE TO YOU OR ANY OTHER PARTY OR ANY OTHER PERSON OR ENTITY FOR ANY SPECIAL, CONSEQUENTIAL, INCIDENTAL, INDIRECT, EXEMPLARY OR PUNITIVE DAMAGES, HOWEVER CAUSED, ARISING OUT OF OR IN CONNECTION WITH THE DOWNLOADING, PROVISIONING, VIEWING OR USE OF THE MATERIALS REGARDLESS OF THE FORM OF ACTION, WHETHER FOR BREACH OF

CONTRACT, BREACH OF WARRANTY, TORT, NEGLIGENCE, INFRINGEMENT OR OTHERWISE (INCLUDING, WITHOUT LIMITATION, DAMAGES BASED ON LOSS OF PROFITS, DATA, FILES, USE, BUSINESS OPPORTUNITY OR CLAIMS OF THIRD PARTIES), AND WHETHER OR NOT THE PARTY HAS BEEN ADVISED OF THE POSSIBILITY OF SUCH DAMAGES. THIS LIMITATION SHALL APPLY NOTWITHSTANDING ANY FAILURE OF ESSENTIAL PURPOSE OF ANY LIMITED REMEDY PROVIDED HEREIN.

Should any provision of this Agreement be held by a court of competent jurisdiction to be illegal, invalid, or unenforceable, that provision shall be deemed amended to achieve as nearly as possible the same economic effect as the original provision, and the legality, validity and enforceability of the remaining provisions of this Agreement shall not be affected or impaired thereby.

The failure of either party to enforce any term or condition of this Agreement shall not constitute a waiver of either party's right to enforce each and every term and condition of this Agreement. No breach under this agreement shall be deemed waived or excused by either party unless such waiver or consent is in writing signed by the party granting such waiver or consent. The waiver by or consent of a party to a breach of any provision of this Agreement shall not operate or be construed as a waiver of or consent to any other or subsequent breach by such other party.

This Agreement may not be assigned (including by operation of law or otherwise) by you without WILEY's prior written consent.

Any fee required for this permission shall be non-refundable after thirty (30) days from receipt by the CCC.

These terms and conditions together with CCC's Billing and Payment terms and conditions (which are incorporated herein) form the entire agreement between you and WILEY concerning this licensing transaction and (in the absence of fraud) supersedes all prior agreements and representations of the parties, oral or written. This Agreement may not be amended except in writing signed by both parties. This Agreement shall be binding upon and inure to the benefit of the parties' successors, legal representatives, and authorized assigns.

In the event of any conflict between your obligations established by these terms and conditions and those established by CCC's Billing and Payment terms and conditions, these terms and conditions shall prevail.

WILEY expressly reserves all rights not specifically granted in the combination of (i) the license details provided by you and accepted in the course of this licensing transaction, (ii) these terms and conditions and (iii) CCC's Billing and Payment terms and conditions.

This Agreement will be void if the Type of Use, Format, Circulation, or Requestor Type was misrepresented during the licensing process.

This Agreement shall be governed by and construed in accordance with the laws of the State of New York, USA, without regards to such state's conflict of law rules. Any legal action, suit or proceeding arising out of or relating to these Terms and Conditions or the breach thereof shall be instituted in a court of competent jurisdiction in New York County in the State of New York in the United States of America and each party hereby consents and submits to the personal jurisdiction of such court, waives any objection to venue in such court and consents to service of process by registered or certified mail, return receipt requested, at the last known address of such party.

WILEY OPEN ACCESS TERMS AND CONDITIONS

Wiley Publishes Open Access Articles in fully Open Access Journals and in Subscription journals offering Online Open. Although most of the fully Open Access journals publish open access articles under the terms of the Creative Commons Attribution (CC BY) License only, the subscription journals and a few of the Open Access Journals offer a choice of Creative Commons Licenses. The license type is clearly identified on the article.

The Creative Commons Attribution License

The Creative Commons Attribution License (CC-BY) allows users to copy, distribute and transmit an article, adapt the article and make commercial use of the article. The CC-BY license permits commercial and non-

Creative Commons Attribution Non-Commercial License

The Creative Commons Attribution Non-Commercial (CC-BY-NC) License permits use, distribution and reproduction in any medium, provided the original work is properly cited and is not used for commercial purposes.(see below)

Creative Commons Attribution-Non-Commercial-NoDerivs License

The Creative Commons Attribution Non-Commercial-NoDerivs License (CC-BY-NC-ND) permits use, distribution and reproduction in any medium, provided the original work is properly cited, is not used for commercial purposes and no modifications or adaptations are made. (see below)

Use by commercial "for-profit" organizations

Use of Wiley Open Access articles for commercial, promotional, or marketing purposes requires further explicit permission from Wiley and will be subject to a fee.

Further details can be found on Wiley Online Library

<http://olabout.wiley.com/WileyCDA/Section/id-410895.html>

Other Terms and Conditions:

v1.10 Last updated September 2015

Questions? customercare@copyright.com or +1-855-239-3415 (toll free in the US) or +1-978-646-2777.

Chapter 3 – Royal Society of Chemistry Reproduction Permissions

“Chemical state determination of molecular gallium compounds using XPS”

J. L. Bourque, M. C. Biesinger and K. M. Baines, *Dalton Trans.*, 2016, **45**, 7678

DOI: 10.1039/C6DT00771F

If you are not the author of this article and you wish to reproduce material from it in a third party non-RSC publication you must [formally request permission](#) using RightsLink. Go to our [Instructions for using RightsLink page](#) for details.

Authors contributing to RSC publications (journal articles, books or book chapters) do not need to formally request permission to reproduce material contained in this article provided that the correct acknowledgement is given with the reproduced material.

Reproduced from the above reference with permission from The Royal Society of Chemistry.

If you are the author of this article you do not need to formally request permission to reproduce figures, diagrams etc. contained in this article in third party publications or in a thesis or dissertation provided that the correct acknowledgement is given with the reproduced material.

If you are the author of this article you still need to obtain permission to reproduce the whole article in a third party publication with the exception of reproduction of the whole article in a thesis or dissertation.

Information about reproducing material from RSC articles with different licences is available on our [Permission Requests page](#).

Chapter 3 – American Chemical Society’s Policy on Theses and Dissertations

If your university requires you to obtain permission, you must use the RightsLink permission system.

See RightsLink instructions at <http://pubs.acs.org/page/copyright/permissions.html>.

This is regarding request for permission to include your paper(s) or portions of text from your paper(s) in your thesis. Permission is now automatically granted; please pay special attention to the implications paragraph below. The Copyright Subcommittee of the Joint Board/Council Committees on Publications approved the following:

Copyright permission for published and submitted material from theses and dissertations ACS extends blanket permission to students to include in their theses and dissertations their own articles, or portions thereof, that have been published in ACS journals or submitted to ACS journals for publication, provided that the ACS copyright credit line is noted on the appropriate page(s).

Publishing implications of electronic publication of theses and dissertation material
Students and their mentors should be aware that posting of theses and dissertation material on the Web prior to submission of material from that thesis or dissertation to an ACS journal may affect publication in that journal. Whether Web posting is considered prior publication may be evaluated on a case-by-case basis by the journal’s editor. If an ACS journal editor considers Web posting to be “prior publication”, the paper will not be accepted for publication in that journal. If you intend to submit your unpublished paper to ACS for publication, check with the appropriate editor prior to posting your manuscript electronically.

Reuse/Republication of the Entire Work in Theses or Collections: Authors may reuse all or part of the Submitted, Accepted or Published Work in a thesis or dissertation that the author writes and is required to submit to satisfy the criteria of degree-granting institutions. Such reuse is permitted subject to the ACS’ “Ethical Guidelines to Publication of Chemical Research” (<http://pubs.acs.org/page/policy/ethics/index.html>); the author should secure written confirmation (via letter or email) from the respective ACS journal editor(s) to avoid potential conflicts with journal prior publication*/embargo policies. Appropriate citation of the Published Work must be made. If the thesis or dissertation to be published is in electronic format, a direct link to the Published Work must also be included using the ACS Articles on Request author-directed link – see <http://pubs.acs.org/page/policy/articlesonrequest/index.html>

* Prior publication policies of ACS journals are posted on the ACS website at

<http://pubs.acs.org/page/policy/prior/index.html>

If your paper has not yet been published by ACS, please print the following credit line on the first page of your article: "Reproduced (or 'Reproduced in part') with permission from [JOURNAL NAME], in press (or 'submitted for publication'). Unpublished work copyright [CURRENT YEAR] American Chemical Society." Include appropriate information.

If your paper has already been published by ACS and you want to include the text or portions of the text in your thesis/dissertation, please print the ACS copyright credit line on the first page of your article: "Reproduced (or 'Reproduced in part') with permission from [FULL REFERENCE CITATION.] Copyright [YEAR] American Chemical Society." Include appropriate information.

Submission to a Dissertation Distributor: If you plan to submit your thesis to UMI or to another dissertation distributor, you should not include the unpublished ACS paper in your thesis if the thesis will be disseminated electronically, until ACS has published your paper. After publication of the paper by ACS, you may release the entire thesis (not the individual ACS article by itself) for electronic dissemination through the distributor; ACS's copyright credit line should be printed on the first page of the ACS paper.

Appendix F: Curriculum Vitae

Jeremy Bourque

EDUCATION

University of Western Ontario, London, ON	
Ph.D student in Inorganic Chemistry	2013 – 2017
Supervisor: Dr. Kim M. Baines	
“Coordination and Organometallic Chemistry of Novel Gallium Compounds: Synthesis, Reactivity and Spectroscopy”	
Mount Allison University, Sackville, NB	
Bachelor of Science, Honours in Chemistry	2009 - 2013
Supervisor: Dr. Stephen A. Westcott	
Concentration in Organometallic and Boron Chemistry	

AWARDS AND SCHOLARSHIPS

Western University Doctoral Excellence Research Award	2015-2017
O'Brien Foundation Scholarship	2015
NSERC CGS D Award	2014 - 2017
Western University Ontario Graduate Scholarship – QEII (Declined)	2014
NSERC CGS M Award	2013 - 2014
Western University Ontario Graduate Scholarship (Declined)	2013
Western Science Doctoral Scholarship (Declined)	2013
Mount Allison University Chemistry Departmental Award	2013
NSERC USRA	2012 & 2013
Murray Sears Departmental Award	2011
Mount Allison University Dean's List	2009 - 2013
John F. & Eula M. Baugh Scholarship	2009 - 2013
Mount Allison University Entrance Scholarship	2009 - 2013
Dr. R. Fitch Memorial Scholarship	2009
Peter E. Cook Scholarship	2009
Emily B. Wood Memorial Scholarship	2009
Governor General's Academic Medal (Bronze)	2009
UNB Beaverbrook Scholars Award (Declined)	2009

PUBLICATIONS

Journal Articles

- “Reactivity of Sulfonyl-Containing Compounds with Ditetrelenes” Tashkandi, N.Y.; Bourque, J.L.; Baines, K.M. *Dalton Trans.* **2017**, accepted.
- “Beyond Oxidation States: Distinguishing Chemical States of Gallium in Compounds with Multiple Gallium Centres” Yang, L.; Bourque, J.L.; McLeod, J.A.; Shen, P.; Baines, K.M.; Liu, L. *Inorg. Chem.* **2017**, *56*, 2985-2991.
- “The Addition of Isocyanides to Tetramesityldigermene: A Comparison of the Reactivity between Surface and Molecular Digermenes” Tashkandi, N.Y.; Cook, E.E.; Bourque, J.L.; Baines, K.M. *Chem. Eur. J.* **2016**, *22*, 14006-14012.
- “Chemical State Determination of Molecular Gallium Compounds Using XPS” Bourque, J.L.; Biesinger, M.C.; Baines, K.M. *Dalton Trans.* **2016**, *45*, 7678-7696.
- “Synthesis and Characterization of Cationic Low-Valent Gallium Complexes of Cryptand[2.2.2]” Bourque, J.L.; Boyle, P.D.; Baines, K.M. *Chem. Eur. J.* **2015**, *21*, 9790-9796.
- “Synthesis and Reactivity of Novel Boranes Derived from Bulky Salicylaldimines: The Molecular Structure of a Maltolato Compound” Bourque, J.L.; Geier, S.J.; Vogels, C.M.; Decken, A.; Westcott, S.A. *Crystals* **2015**, *5*, 91-99.
- “Addition of Boranes to (E)-(n⁵-C₅H₅)₂ZrCl(CH=CHPh)” Ferland, P.; Prosser, K.E.; Bourque, J.L.; Edwards, I.C.; Hamilton, N.S.; Joyce, L.E.; Finniss, M.C.; Yorke, S.R.; Vogels, C.M.; Fontaine, F.-G.; Decken, A.; Westcott, S.A. *Cent. J. Eur. Chem.* **2013**, *11*, 811-816.

Data Reports

- “(tert-Butyl isocyanide-κC)trichloridogallium(III)” Bourque, J.L.; Tashkandi, N.Y.; Baines, K.M. *IUCrData* **2016**, *1*, x160389.
- “Tetramethylammonium trifluoromethanesulfonate” Bourque, J.L.; Baines, K.M. *IUCrData* **2016**, *1*, x160370.

CONFERENCE ABSTRACTS AND SUBMISSIONS

- “Beyond Oxidation Numbers: Using X-ray Spectroscopy to Determine the Chemical States of Novel Gallium Compounds.” **J.L. Bourque**, R.A. Nanni, M.C. Biesinger, L. Yang, J.A. McLeod, L. Liu, K.M. Baines (Oral Presentation). Main Group Transformations and Catalysis Symposium, 100th Canadian Chemistry Conference and Exhibition, Toronto, ON, June 2017.
- “Synthesis of a Gallene, a Gallium-Carbon Double Bond.” **J.L. Bourque**, K.M. Baines (Oral Presentation). 49th Inorganic Discussion Weekend, Hamilton, ON, November 2016.
- “In Pursuit of a Gallium-Carbon Double Bond.” **J.L. Bourque**, K.M. Baines (Poster Presentation). Boron in the Americas XV, Kingston, ON, June 2016.

"In Pursuit of a Gallium-Carbon Double Bond." **J.L. Bourque**, K.M. Baines (Oral Presentation). Main Group Symposium, 99th Canadian Chemistry Conference and Exhibition, Halifax, NS, June 2016.

"Synthesis and Characterization of Cationic Low Valent Gallium Complexes of Cryptand-222." **J.L. Bourque**, M.C. Biesinger, P.D. Boyle, K.M. Baines (Oral Presentation). 98th Canadian Chemistry Conference and Exhibition, Ottawa, ON, June 2015.

"Synthesis and Reactivity of Novel Low Valent Cationic Gallium Complexes." **J.L. Bourque**, K.M. Baines (Oral Presentation). 47th Inorganic Discussion Weekend, Montreal, QC, November 2014.

"Synthesis and Reactivity of Cationic and Low Valent Gallium(II) Compounds." **J.L. Bourque**, K.M. Baines (Poster Presentation). 19th International Symposium on Homogeneous Catalysis, Ottawa, ON, July 2014.

"Synthesis and Reactivity of a Novel Bulky Gernylborane Derived from a Salicylaldamine." **J.L. Bourque**, S.J. Geier, C.M. Vogels, A. Decken, S.A. Westcott (Flash and Poster Presentation). 14th International Conference on the Coordination and Organometallic Chemistry of Germanium, Tin and Lead, Baddeck, NS, July 2013.

"Synthesis and Reactivity of a Novel Bulky Borane Derived from a Salicylaldimine." **J.L. Bourque**, C.M. Vogels, A. Decken, S.A. Westcott (Poster Presentation). 96th Canadian Chemistry Conference and Exhibition, Quebec City, QC, May 2013.

"Synthesis and Reactivity of a Novel Bulky Borane Derived from a Salicylaldimine." **J.L. Bourque**, C.M. Vogels, A. Decken, S.A. Westcott (Poster Presentation). Atlantic Inorganic Discussion Weekend 2013, Moncton, NB, March 2013.

EXPERIMENTAL TECHNIQUES

Specific Techniques

X-ray Crystallography

Fully trained operator in the Western University Department of Chemistry's X-ray crystallography facility, managed by Dr. Paul Boyle. Experienced in sample preparation, structure solution and refinement using Bruker Kappa Axis Apex2 and Nonius Bruker KappaCCD Apex2 diffractometers and the SHELX program suite. Experience with disordered and non-merohedral twinned structure refinements. Personal structures, as well as many other structures for other research group members have been processed. Experienced in molecular graphics using NRCVAX and XP, packing and statistical bond length analysis using Mercury, and CIF file editing using text editors and enCIFer software. Powder X-ray diffraction measurements have been performed on an INEL CPS Powder diffractometer.

Computational Chemistry

Experience in performing computational studies on main group compounds. Calculations have been performed on the SHARCNET cluster. Geometry optimization and frequency

calculations, as well as molecular orbital and population analysis, including NBO methods, have been performed using Gaussian 09. Experienced with mechanistic and transition state computations.

NMR Spectroscopy

Significant experience in the collection and interpretation of solution multinuclear NMR spectra, specifically both one- and two-dimensional techniques, including data collection for quadrupolar nuclei.

General Laboratory and Spectroscopic Techniques

Experienced in using MBraun glove boxes technology, MBraun and Innovative Technology Solvent Purification Systems, Schlenk techniques, Varian MercuryPlus NMR spectrometers, Varian INOVA NMR spectrometers, JEOL JMN-ECS400 Spectrometer, Varian Cary UV-Vis Spectrometer, Thermo Nicolet FT-IR 200 Spectrometer, Thermo Nicolet iS5 FT-IR Spectrometer and CEM Microwave Reactors.

Computing Skills

Experienced with Windows operating systems, Mac OS X operating systems, Linux workstations, APEX 2 Bruker crystallographic software, the SHELX crystallographic software suite, Delta NMR software, Varian VNMRJ, MestReNova, ACD Labs, Gaussian 09, GaussView 03, ChemBioOffice 12, CEM Synergy, Maple, and Microsoft Office.

RELEVANT COURSEWORK

Graduate courses, University of Western Ontario, London, ON

- X-ray Crystallography
- Computational Chemistry
- Advanced NMR Spectroscopy
- Solid-State NMR Spectroscopy
- Catalysis

RESEARCH EXPERIENCE

Graduate Student Research Assistant, Baines Group

2013 - Present

Western University, London, ON

Performed experiential research involving the synthesis and reactivity of low valent gallium cations stabilized by macrocyclic ligands and novel organometallic gallium compounds, under the supervision of Dr. Kim M. Baines.

Research Assistant, Barclay Group

2013

Mount Allison University, Sackville, NB

Conducted experimental research under the supervision of Dr. L. Ross C. Barclay examining the reaction kinetics of the autoxidation of linoleic acid and deuterium labeled linoleic acid using free radical initiators and various antioxidants.

Undergraduate Research Assistant, Westcott Lab

2011 - 2013

Mount Allison University, Sackville, NB

Conducted experimental research in Dr. Steve Westcott's laboratory investigating the synthesis, reactivity and biological activity of novel boranes derived from salicylaldehydes of adamantylamine and their reactions with transition metal complexes and unsaturated organic compounds. The new molecules were characterized by numerous analytical methods. This work was performed towards an Honours degree in Chemistry. Previous work examined the synthesis and reactivity of novel thio- and selenoboranes with transition metal complexes and unsaturated organic compounds. Further research was conducted into the addition of hydro- and diboranes to oximes.

Volunteer Teaching Assistant, Westcott Lab **2011 - 2013**
Mount Allison University, Sackville, NB

Volunteered in Dr. Steve Westcott's laboratory training undergraduate students in experimental research, where students gained experience in the synthesis and characterization of Schiff base ligands and their complexes with transition metals using a variety of analytical techniques.

Volunteer Research Assistant, Westcott Lab **2010 - 2011**
Mount Allison University, Sackville, NB

Conducted volunteer experimental research in Dr. Steve Westcott's laboratory investigating the synthesis and biological reactivity of novel Schiff-base compounds derived from long chain amines. New compounds were characterized using a number of analytical techniques.

WORK EXPERIENCE

Teaching Assistant, Department of Chemistry **2013 - Present**
Western University, London, ON

Employed as a graduate teaching assistant by the Department of Chemistry at Western University. Responsibilities included acting as a demonstrator and supervisor for undergraduate students in a laboratory setting; evaluating their in-lab performance, written and oral work; and invigilating midterm tests and final exams. These duties were performed for Transition Metal Chemistry and Introductory Chemistry for Engineers courses.

Laboratory Assistant, Dept. of Chemistry & Biochemistry **2010 - 2013**
Mount Allison University, Sackville, NB

Employed as a laboratory and teaching assistant by the Mount Allison University Chemistry and Biochemistry Department. Invigilated midterm exams, evaluated laboratory assignments, and acted as a demonstrator in undergraduate teaching labs. Performed these tasks for a wide range of courses: Introductory Chemistry I and II, Introductory Biochemistry, Thermodynamics, Coordination Chemistry, Organometallics and Analytical Chemistry I.

Teaching Assistant, Dept. of Physics **2010 - 2011**
Mount Allison University, Sackville, NB

Employed as teaching, laboratory and setup assistant by the Mount Allison University Physics Department. Invigilated midterm exams, evaluated laboratory assignments and

performed duties as a demonstrator during laboratory periods. These tasks were performed for: Introductory Physics I and II, Physics for the Life Sciences.

VOLUNTEER EXPERIENCE

Substitute Lecturer, Third Year Spectroscopy Course **January – February 2016**
University of Western Ontario, London, ON

Performed duties as a lecturer for 10 hours of lecture time teaching introductory concepts about infrared spectroscopy, mass spectrometry and nuclear magnetic resonance spectroscopy. Developed lecture material including practice problems for IR and NMR spectroscopies and lecture slides/notes, responded to student questions and facilitated assignment distribution and collection. Was well received by students and supervisor (K.M. Baines) and received positive evaluations

Workshop Instructor and Volunteer, Canadian Chemistry Olympiad **March - May 2016**
University of Western Ontario, London, ON

Participated in the organization of the Canadian Chemistry Olympiad Final Competition to be held at the University of Western Ontario, from May 26th to 31st, 2016. Organized portions of the schedule, as well as composed and delivered workshops to the participants, as well as preparing practice problems, exam questions and grading completed examinations. The laboratory sessions were also compiled, organized the participation of other graduate students to help in the supervision of the students, as well as composed the laboratory exam questions. Also participated in the evaluation and marking of the students' performance and written work.

Student Representative, Visiting Speakers Committee **2014 - Present**
University of Western Ontario, London, ON

Facilitated the process of choosing student nominated visiting speakers to visit the Department of Chemistry. Organized and scheduled the visit of two speakers per academic year, including lodging, meetings with both faculty and students and meals.

VP Academic, Chemistry & Biochemistry Society Executive **2011 - 2013**
Mount Allison University, Sackville, NB

Performed various duties such as general organization and promotion of the department to the campus, the organization and direction of a departmental tutoring service, and the executive representative on the student academic advising committee conducted by the Department of Chemistry and Biochemistry.

AFFILIATIONS

American Chemical Society (2011 - Present)
Canadian Society of Chemistry (2012 - Present)
SHARCNET (2014 – Present)